Activation of Hypoxia Inducible Factor pathway for neuroprotection in *in vitro* models of ischaemic stroke

Ayesha Singh

A thesis submitted for the degree of Doctor of Philosophy

June 2022

Keele University

Contents

Abstract

Ischaemic stroke is the most common form of stroke, accounting for appropriate 87% of all strokes. Reperfusion is the only immediate treatment option following ischaemic stroke, however, this option is only applicable to a small percentage of patients. There is an urgent need for intervention to delay or reduce the impact of ischaemia after the stroke. Neuroprotection seeks to restrict injury to the brain parenchyma following an ischaemic insult.

Hypoxia-inducible factors (HIF), is a protein regulated by cellular oxygen tension in mammals. HIF-1 regulates hypoxia inducible genes such as erythropoietin (EPO) and vascular endothelial growth factor (VEGF). HIF levels in cells and tissue are tightly controlled by HIF prolyl hydroxylases (PHDs). Pharmacological inhibition of PHD will lead to HIF signalling pathway activation, thus upregulating hundreds of HIF downstream genes.

This study aimed to characterize the effectiveness and underlying mechanism of action of neuroprotective strategies in hypoxic / ischaemic preconditioning with a novel class of PHD inhibitors, as well as by astrocyte conditioned media (ACM) using an *in vitro* model of ischaemic stroke.

Cerebral ischaemia was modelled *in vitro* by omission of glucose alone (GD), omission of oxygen alone (OD), and simultaneous omission of glucose and oxygen (OGD) in PC12 cells, primary rat neurons, and astrocytes. Both PC12 cells and

primary neurons had similar sensitivities towards OD and OGD. Primary astrocytes were more resistant to OD and OGD insults compared to primary neurons. GD, OD, and OGD altered the HIF1α and HIF2α in all these cells. Preconditioning with sub-lethal OD and OGD was protective in PC12 cells, primary neurons, and primary astrocytes against subsequent severe OGD (0.3% O_2) insults.

The effects of a novel class of PHD inhibitors such as FG4592 and Bayer 85-3934 were applied in the ischaemic tolerant model in PC12 cells and primary neurons along with a non-specific PHD inhibitor such as Dimethyloxalylglycine (DMOG). These PHD inhibitors upregulated HIF1α in normoxia (ambient air) and promoted autophagy. Preconditioning with the clinical PHD inhibitors followed by reversion was protective in PC12 cells and primary neurons against subsequent severe OGD insults by reducing cell death. In addition, the effects of astrocyte hypoxia / ischaemia preconditioning on primary neuronal cultures following OGD were studied. ACM from 6h OGD protected neurons from subsequent OGD damage while ACM from 24 h OGD further damaged the neurons following OGD.

In conclusion, preconditioning strategies that activate HIF1α, HIF2α and / or autophagy were protective in the *in vitro* model of ischaemic tolerance. The PHD inhibitors possess capabilities to stabilise HIF1α and induced autophagy and are neuroprotective in the cellular models of ischaemic tolerance. Overall, all the interventions explored activated either HIF1α, HIF2α, and / or autophagy in the cells. The link between HIF activation, autophagy, and ischaemic tolerance warrants further investigation.

Acknowledgments

Foremost, I would like to express my sincere and heartfelt gratitude and appreciation to my supervisors, Dr. Ruoli Chen and Dr. Stuart Jenkins, whose immense knowledge, continuous support, motivation, continuous advice, and guidance helped me in all the times of research. With their vision, they have inspired me to do this research and it was a great privilege to work with them. I am very grateful for the extensive feedback they have provided on my thesis. I would like to thank Professor Christopher J Schofield and his group at Oxford University for providing me with the novel PHD inhibitors and giving me invaluable feedback during this research.

I would like to extend my gratitude to my advisor Dr. Michael Evans for his supportive comments. I would like to thank Professor Paul Horrocks and Keele University ACORN fund for the support awarded to me to help me pursue this research. I owe a big thank you to Dr. James Wilson who had taught me the methodology to carry out this research, and Dr. David Morgan for his feedback on my research and for generously letting me use gene primers and equipment for my research. I would like to sincerely thank Dr. Anthony Curtis and Dr. Clare Hoskins who have let me use several equipments in their laboratories for my research. I would also thank Dr. Helen Price for providing me access and training to use the ultracentrifuge. I would like to thank Dr. Mirna Mourtada for allowing me to use the flow cytometer in her lab. I would also like to thank Atieme Joseph Ogbolosingha, who has been a great friend and motivated me throughout my research. Every time I was about to give up, he inspired me to keep repeating and trying again. I would also

like to thank, Oliver Chow and Alexander Gunn for their help and invaluable ideas during their summer internship.

I would like to extend my special thanks to all the School of Life sciences staff, especially Chris Bain, Jayne Bromley, and Nigel Bowers. I would also like to thank all the School of Pharmacy staff for their support and my special thanks to Mark Arrowsmith for providing me the resources to help me during my research.

I am extremely grateful to my parents for their love, prayers, care, and sacrifices, without which I would not be able to accomplish all this. I would also like to thank my brother for his valuable insight on my research and long-distance support.

Publications and conferences

Publications

i. PATABENDIGE, A., SINGH, A., JENKINS, S., SEN, J. and CHEN, R., 2021. Astrocyte Activation in Neurovascular Damage and Repair Following Ischaemic Stroke. *International journal of molecular sciences,* **22**(8), pp. 4280.

ii. SINGH, A., CHOW, O., JENKINS, S., ZHU, L., ROSE, E., ASTBURY, K. and CHEN, R., 2021. Characterizing Ischaemic Tolerance in Rat Pheochromocytoma (PC12) Cells and Primary Rat Neurons. *Neuroscience,* **453**, pp. 17-31.

iii. SINGH, A., WILSON, J.W., SCHOFIELD, C.J. and CHEN, R., 2020. Hypoxia-inducible factor (HIF) prolyl hydroxylase inhibitors induce autophagy and have a protective effect in an in-vitro ischaemia model. *Scientific reports,* **10**(1), pp. 1597.

iv. CHEN, R., LAI, U.H., ZHU, L., SINGH, A., AHMED, M. and FORSYTH, N.R., 2018. Reactive Oxygen Species Formation in the Brain at Different Oxygen Levels: The Role of Hypoxia Inducible Factors. *Frontiers in cell and developmental biology,* **6**, pp. 132.

v. GUNN, A., SINGH, A., DIAO, A. and CHEN, R., 2018. Pharmacological Modulation of Autophagy for Neuroprotection in Ischaemic Stroke. *Journal of experimental stroke & translational medicine,* **11**(1).

Conferences

i. Fourth UK Preclinical Stroke Symposium (2019) (Oral presentation). SINGH, A; CHEN, R. Pharmacological inhibition of hypoxia-inducible factor prolyl hydroxylases (HIF-PHDs) induces tolerance in an in-vitro model of ischaemic stroke

ii. Physiology (2019). SINGH, A; CHEN, R; JENKINS, S (Oral presentation). Ischaemic preconditioning induced tolerance in primary rat neurones and astrocytes

iii. ISTM symposium (2019) (Oral presentation). SINGH, A. Characterising pharmacologically induced ischaemic tolerance in an in-vitro model

iv. Europhysiology (2018) (Poster). SINGH, A; CHEN, R. Ischaemic preconditioning induced tolerance in PC12 cells.

v. ISTM symposium (2018) (Poster / turbo talk). SINGH, A. Neuroprotection in PC12 cells following ischaemic preconditioning-induced tolerance

List of Figures

List of Tables

List of Abbreviations

2-ME2	2-methyoxyestradiol
2-OG	2-oxoglutarate
7-AAD	7-amino-actinomycin D
ACEI	Angiotensin-converting enzyme inhibitors
ACM	Astrocyte conditioned medium
AF	Atrial fibrillation
AJ	Adherens junctions
AMPA	α-amino-3-hydroxy-5-methyl-4-isoxazolepropionic acid
APAF-1	Apoptotic protease activating factors
AQP-4	Aquaporin-4
ARBs	Angiotensin II Type 1 Receptor Blockers
ARNT	Aryl hydrocarbon receptor nuclear translocator
ASPA	Animals Scientific Procedures Act
ATP	Adenosine 5’-triphosphate
AWERB	Animal Welfare and Ethical Review Board
Bax	Bcl-2-associated-X
BBB	Blood-brain barrier
BCA	Bicinchoninic acid
BCCAO	Bilateral common carotid artery occlusion

Bcl-2	B-cell lymphoma 2
Bcl-xL	B-cell lymphoma-extra large
BDNF	Brain-derived neurotropic factor
bFGF	Basic fibroblast growth factor
bHLH-PAS	Basic-helix-loop-helix- PER-ARNT-SIM BNDF
Bid	BH3 interacting domain
BNIP3	Bcl-2 / adenovirus EIB 19kDa-interacting protein 3
BSA	Bovine serum albumin
Ca^{2+}	Calcium ion
CAMs	Cell adhesion molecules
CBF	Cerebral blood flow
CBP	CREB-binding protein
cDNA	Complementary deoxyribonucleic acid
CKD	Chronic kidney disease
Cl^-	Chloride ion
CNS	Central nervous system
$CoCl_2$	Cobalt chloride
C-TAD	C-terminal TAD
CX3CR1	Fractalkine receptor chemokine (C-X3-C motif) receptor 1
CXCR4	Chemokine-receptor type-4

D609	Tricyclodecan-9-yl-xanthogenate
DAPI	4’6-diamidino-2-phenylindole dihydrochloride
DFO	Desferrioxamine
DHB	3,4-dihydroxybenzoic acid
DIV	Days *in vitro*
DMEM	Dulbecco’s Modified Eagle’s Medium
DMOG	Dimethyloxalylglycine
DMSO	Dimethyl sulfoxide
DNA	Deoxyribonucleic acid
DNAse	Deoxyribonuclease
dNTP	deoxynucleoside triphosphates
D-PBS	Dulbecco’s Phosphate-buffered saline
EBSS	Earl’s balanced salt solution
EGF	Epidermal growth factor
eNOS	endothelial nitric oxide synthase
EPO	Erythropoietin
EVs	Extracellular vesicles
FACS	Fluorescence-activated cell sorting
FBS	Fetal bovine serum
FDA	Food and drug administration

FIH	Factor inhibiting HIF
FITC	Fluorescein isothiocyanate
GABA	Gamma aminobutyric acid
G-CSF	Granulocyte-colony stimulating factor
GD	Glucose deprivation
GDNF	Glial-cell derived neurotropic factor
GD-PC	Glucose deprivation preconditioning
GFAP	Glial fibrillary acidic protein
GLUT1	Glucose transporter 1
GLUT3	Glucose transporter 3
GSH	Glutathione
HBSS	Hank’s balanced salt solution
HCA	Homocysteic acid
HIF-1	Hypoxia inducible factor-1
HPC	Hypoxic preconditioning
HS	Horse serum
I / R	Ischaemia / reperfusion
IF	Immunofluorescence
IFNγ	Interferon γ
IGF	Insulin growth factor

IL-10	Interleukin-10
IL-13	Interleukin-13
IL-1b	Interleukin-1b
IL-1β	Interleukin 1β
IL-4	Interleukin 4
IL-6	Interleukin-6
IPC	Ischaemic preconditioning
JAM	Junctional adhesion molecule
K^+	Potassium ion
KO	Knock-out
LC3	Microtubule associated light chain protein 3
LC-MS	Liquid chromatography-mass spectrometry
LDH	Lactate dehydrogenase
LDL	Low density lipoprotein
MAP-1	Mitogen-activated protein
MAP2	Microtubule associated protein 2
MCAO	Middle cerebral artery occlusion
MMPs	Matrix mettaloproteinases
MPTP	Mitochondrial permeability transition pore
mRNA	Messenger ribonucleic acid

mTOR	Mechanistic target of rapamycin
MTT	3-(4,5-dimethylthiazol-2-yl)-2,5-diphenyltetrazolium bromide)
Na^+	Sodium ion
NADH	Nicotinamide adenine dinucleotide
NADPH	Nicotinamide adenine dinucleotide phosphate
NEMO	Nuclear factor-κb essential modulator
NF-κB	Nuclear factor Kappa B
NGF	Nerve growth factor
NIX	Nip-like protein X
NMDA	N-methyl-D-aspartate
nNOS	Neuronal nitric-oxide synthase
NO	Nitric oxide
Nrf2	Nuclear erythroid factor 2
NT	Neurotransmitter
NT-3	Neurotrophin 3
N-TAD	N-terminal TAD
NVU	Neurovascular unit
Nx	Normoxia
OD	Oxygen deprivation
ODD	Oxygen-dependent degradation

OD-PC	Oxygen deprivation preconditioning
OGD	Oxygen-glucose deprivation
OGD-PC	Oxygen glucose deprivation preconditioning
PARP	Poly ADP ribose polymerase
PBS	Phosphate-buffered saline
PBS-T	Phosphate-buffered saline – Tween
PC	Preconditioning
PDK-1	Pyruvate Dehydrogenase Kinase 1
PDL	Poly-D-lysine
PFA	Paraformaldehyde
PFKFB1	6-phosphofructo-2-kinase / fructose-2,6-biphosphatase 1
PFKFB3	6-phosphofructo-2-kinase / fructose-2,6-biphosphatase 3
PHD	Propyl-4-hydroxylase
PI3K / Akt	phosphatidylinositol-3 kinase / protein kinase B
Pmaip1	Phorbol-12-Myristate-13-Acetate-Induced Protein 1
PMSF	phenylmethylsulfonyl fluoride
PS	Penicillin / Streptomycin
PS	Phosphatidylserine
qRT-PCR	Quantitative real-time polymerase chain reaction
Rcf	Relative centrifugal force

rhEPO	Recombinant human EPO
RIPA	radio-immuno precipitation assay
RIPC	Remote ischaemic preconditioning
RNS	Reactive nitrogen species
ROS	Reactive oxygen species
RT	reverse transcriptase
rTPA	recombinant tissue plasminogen activator
SDF-1	Stromal derived factor-1
SDS	Sodium dodecyl sulphate
SDS-PAGE	Sodium dodecyl sulphate polyacrylamide gel electrophoresis
SRC	Steroid-receptor co-activator
STAT3	Signal transducers and activators of transcription
SVZ	Sub ventricular zone
TBS	Tris-buffered saline
TBS-T	Tris buffered saline – Tween
TCA	Tricarboxylic acid cycle
TGFα	Transforming growth factor α
TGFβ	Transforming growth factor β
TIA	Transient ischaemic attack
TJ	Tight junctions

TNFα	Tumour necrosis factor-α
Tuj1	Class III beta tubulin
VEGF	Vascular endothelial growth factor
VHL	Von Hippel-Lindau
εPKC	ε protein kinase C

Chapter 1:

Introduction

1.1 Overview of stroke

1.1.1 Incidence of stroke

Stroke is a major cause of morbidity and mortality around the world with around 15 million incidences occurring every year (Lopez *et al.,* 2001). Around 100,000 strokes occur in the UK each year, with a stroke occurring every 5 minutes, and nearly 60,000 deaths due to stroke every year (SSNAP, 2021). Between 1990 and 2010, stroke incidence has reduced by a quarter in the UK due to improvement in stroke prevention management and by increasing awareness among the people about the importance of healthy living. Almost two-thirds of stroke survivors in the UK leave the hospital with a disability and remain dependent on others for daily tasks (SSNAP, 2021). Stroke leads to an increase in economic burden, costing the NHS UK about £26 billion per annum, despite this the stroke research in the UK is underfunded in comparison to research in diseases with similar economic burdens such as cancer and infectious disease (Patel *et al.,* 2020).

1.1.2 Definition and classification of stroke

World Health Organisation defines stroke as “rapidly developing clinical signs of focal or global disturbance of cerebral function lasting more than 24 h or leading to death, with no apparent cause other than that of the vascular origin”. Transient ischaemic attacks (TIAs) have similar clinical features but symptoms resolve within 24 h. TIA also does not result in any pathological changes. A TIA is usually considered as a warning sign of stroke or other cardiovascular complications. Around 15 to 30% of cerebral infarctions are preceded by TIA (Easton *et al.,* 2009). The common symptoms seen during an occurrence of stroke are described in Table 1.1.

Table 1.1 Common symptoms of stroke

- Sudden onset of weakness or numbness of the face, arm or leg
- A sudden decrease in the level of consciousness
- Facial droop
- Confusion
- Aphasia
- Dysarthria
- Visual field deficit (difficulty seeing with one or both eyes)
- Hemisensory deficits
- Ataxia
- Difficult walking
- Dizziness
- Severe headache and vertigo
- Nausea or vomiting

Reference: Kothari *et al.,* 1997

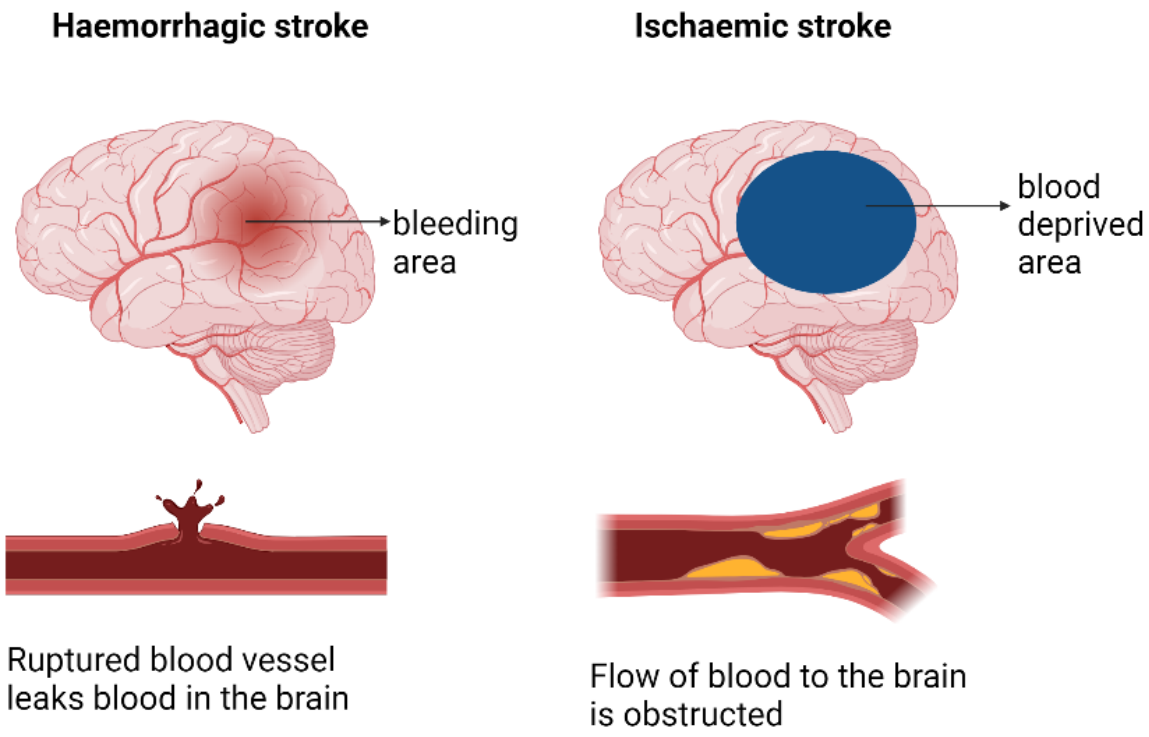

Figure 1.1. Representation of different types of stroke. Stroke is classified into ischaemic stroke and haemorrhagic stroke. Ischaemic stroke involves the blockage of an artery in or leading to the brain. Haemorrhagic stroke involves the rupture of a blood vessel resulting in bleeding in or on the surface of the brain (Image produced using Biorender).

As shown in Figure 1.1, stroke is widely classified into haemorrhagic stroke and ischaemic stroke (Hisham and Bayraktutan, 2013). Haemorrhagic stroke accounts for around 15% of all strokes and involves rupture of a cerebral artery within (intracerebral haemorrhage) or on the surface of the brain (subarachnoid haemorrhage) (Hisham and Bayraktutan, 2013). Haemorrhagic strokes are generally more severe and are associated with a higher rate of mortality as compared to that of ischaemic strokes (Andersen *et al.,* 2009). Ischaemic strokes are more common,

accounting for 85% of all strokes. Ischaemic stroke involves the occlusion of a cerebral artery that leads to a blockage of oxygen and blood supply into the brain. Ischaemic stroke is divided into thrombotic and embolic strokes (Grau *et al.,* 2001). A thrombotic stroke occurs as a result of the formation of thrombus in the artery in or leading to the brain. Thrombotic strokes usually occur as a result of atherosclerosis. As shown in Figure 1.2, atherosclerotic plaques develop when the endothelium of blood vessels gets damaged due to factors such as hypertension or hypercholesterolemia leading to the accumulation of substances such as cholesterol, fat, and cellular debris at the site of damage (Hisham and Bayraktutan, 2013). Thrombotic strokes can be further categorized into lacunar and non-lacunar strokes (Hisham and Bayraktutan, 2013). Lacunar strokes are small infarcts observed in deep cerebral white matter, basal ganglia, and pons (Hisham and Bayraktutan, 2013). Embolic stroke occurs due to an embolus that breaks loose and travels to the brain through the bloodstream resulting in occlusion of a small cerebral artery. Common causes of emboli include atrial fibrillation (AF), endocarditis, or mitral stenosis (Hisham and Bayraktutan, 2013). It has also been observed that longstanding hypertension accounts for the majority of haemorrhagic strokes. Cerebral amyloid angiopathy is another common cause of haemorrhagic strokes (Grysiewicz *et al*., 2008). The common aetiologies in ischaemic stroke include atherothrombotic vasculopathy such as macroangiopathy and microangiopathy; non-atherosclerotic angiopathy such as arterial dissection; cerebral vasculitis; cardiac or transcardiac embolism; coagulopathies and hematologic disorders such as thrombocytopenia (Kristensen *et al*., 1997; Grau *et al*., 2001).

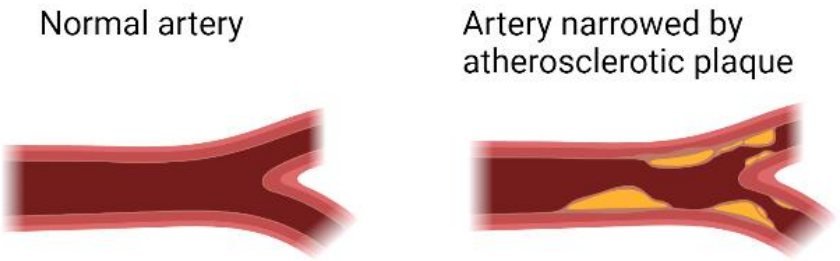

Figure 1.2. Atherosclerotic plaque. Damage to the endothelium initiates an inflammatory response leading to the formation of a plaque in the wall of the blood vessels. This leads to narrowing of the blood vessels resulting in restricted blood flow (Image produced using Biorender).

1.1.3 Risk factors

Table 1.2 shows the various modifiable and non-modifiable risk factors of stroke (Jauch *et al*., 2013; Hisham and Bayraktutan, 2013). Age is the most important risk factor of stroke; studies have shown that increasing age increases the risk of stroke and two-thirds of all strokes occur in those aged over 65 years. (Andersen *et al*., 2009). Stroke is also seen to be more common in men than women before 65 years of age. After 65 years of age, women are more prone to stroke than men mainly due to menopause and longer life span (Lee *et al*., 2011). Hispanics and blacks have a higher risk of death and disability following stroke partly due to higher blood pressure (Grau *et al*., 2001; Thrift *et al*., 2017). Hypertension is a risk factor for both ischaemic and haemorrhagic stroke. Additionally hypercholesterolemia, migraine, previous TIA, AF, and heart disease favour ischaemic stroke instead of haemorrhagic stroke. High alcohol intake and smoking are more commonly associated with the risk of haemorrhagic stroke. Studies have also shown that light or moderate alcohol consumption is protective in ischaemic stroke whereas high alcohol consumption elevated the risk of ischaemic stroke (Grysiewicz *et al*., 2008; Andersen *et al*., 2009).

Primary care management of the common risks has shown to have a potential effect in reducing the risk of stroke (Lee *et al.,* 2011). These changes particularly corresponded with a marked increase in primary care prescriptions of primary and secondary cardiovascular prevention therapies (Lee *et al*., 2011)

Table 1.2. Risk factors of ischaemic stroke

Non - modifiable risks	Modifiable risks
➢ Age ➢ Race ➢ Sex ➢ Ethnicity ➢ Migraine ➢ Fibromuscular dysplasia ➢ Family history of stroke or TIAs	➢ Hypertension ➢ Diabetes mellitus ➢ Cardiac diseases such as atrial fibrillation, valvular disease, heart failure, mitral stenosis, structural anomalies, for example, patent foramen ovale, and atrial and ventricular enlargement ➢ Hypercholesterolemia ➢ TIAs ➢ Carotid stenosis ➢ Hyperhomocysteinemia ➢ Lifestyle issues: Excessive alcohol intake, tobacco use, illicit drug use, physical inactivity ➢ Obesity ➢ Oral contraceptive use / postmenopausal hormone use ➢ Sickle cell diseases

References: Jauch *et al*., 2013; Hisham and Bayraktutan, 2013)

1.2 Pathophysiology of stroke

1.2.1 Energy failure and excitotoxicity

The brain is the most metabolically active organ in the body requiring about 15-20% of total resting cardiac output to provide energy for its metabolism (Prabal *et al*., 2010). The brain capacity to store energy is limited and it relies on the continuous blood supply to deliver the essential nutrients for its function (Prabal *et al*., 2010). As shown in Figure 1.3, cerebral ischaemia leads to a reduction in cerebral blood flow (CBF), causing functional and metabolic deficits. The reduction of CBF depletes oxygen and glucose resulting in rapid failure of mitochondria leading to a decrease or depletion in cellular ATP (adenosine 5'-triphosphate) levels (Dirnagl *et al.,* 1999). Also, the lack of oxygen results in anaerobic glycolysis of glucose for the production of energy, which results in accumulation of lactate, further resulting in ATP depletion (Strandgaard and Paulson., 1989). The loss of ATP leads to loss of function of sodium-potassium adenosine triphosphatase (Na^+ / K^+ -ATPase) pump and calcium-hydrogen adenosine triphosphatase (Ca^{+2} / H^+ ATPase) pump deteriorating the ion gradient. An increase in intracellular levels of Na^+, $Ca^{2+,}$ and Cl^- result in swelling and depolarisation of neurons and glial cells (Kintner *et al.,* 2007; Olney *et al.,* 1986; Rothman, 1985).

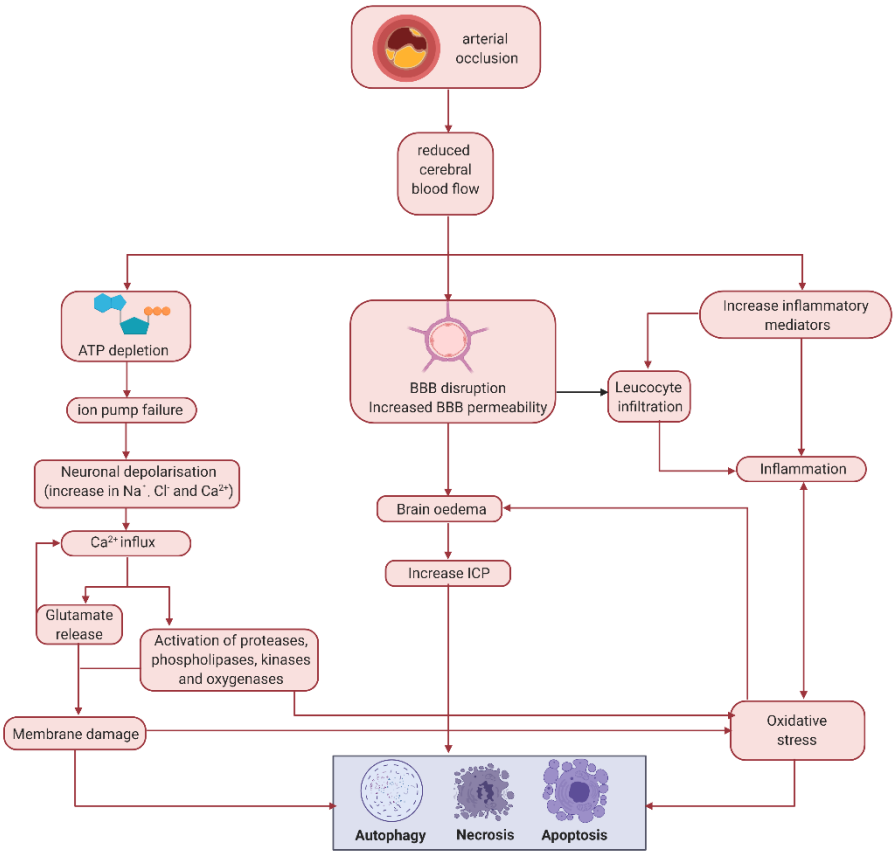

Figure 1.3. The major events that occur after arterial occlusion. Following a cerebral arterial occlusion, there is reduced blood flow in a brain region resulting in energy failure. Energy failure causes ion dyshomeostasis (intracellular levels of Na^{+}, $Ca^{+2,}$ and Cl^{-} ions rise), BBB disruption, and an increase in inflammatory mediators. Glutamate release in extracellular spaces further exacerbates membrane damage. Ca^{+2} overload, membrane damage, and inflammation result in oxidative stress. Cytotoxic substances and inflammatory responses result in necrosis, autophagy, or apoptosis of cells (Image produced using Biorender).

This, in turn, results in the activation of somatodendritic and presynaptic voltage-dependent and ligand-gated calcium channels. Ca^{2+} influx results in the activation of various Ca^{2+} dependent enzymes such as protein kinase C, phospholipase A2, phospholipase C, cyclooxygenase, nitric oxide synthase, and various other proteases (Durukan and Tatlisumak, 2007). Subsequently, excitatory neurotransmitters (NTs) are released spontaneously into extracellular spaces (Rothman, 1985). Glutamate is the major excitatory NT in the central nervous system (CNS) and it is primarily released during ischaemic injury (Durukan and Tatlisumak, 2007). Under physiological conditions, glutamate plays an important role in learning and memory and glutamate released from astrocytes synchronizes the activity of hippocampal neurons. In normal synaptic communication, neurons release glutamate from the presynaptic terminals of axons into the synaptic cleft. Glutamate accumulated in the extracellular space activates glutamate receptors on the surface of post-synaptic terminals. The extracellular levels of glutamate are closely regulated to maintain optimal neuronal excitation and restrain excitotoxicity. Glutamate homeostasis largely relies on astrocytic transporter that clears glutamate from synaptic cleft during physiological conditions (Dessi *et al.,* 1994; Chen *et al.,* 1999). During ischaemia, the dysfunction of glutamatergic transmission results in increased glutamate levels resulting in neuronal excitotoxicity. At the same time, energy-dependent processes such as presynaptic reuptake of excitatory amino acids are impeded, further increasing the accumulation of glutamate in the extracellular space (Dirnagl *et al*., 1999). Accumulation of glutamate in extracellular spaces results in the over activation of glutamate receptors on nearby post-synaptic neurons. Glutamate commonly leads to the activation of ionotropic receptors such as N-methyl-D-aspartate (NMDA), α-amino-3-hydroxy-5-methyl-4-isoxazole propionic acid (AMPA),

kainate receptors, and metabotropic glutamate receptors. Activation of ionotropic receptors allows rapid influx of Ca^{2+} and Na^{+} ions into neurons resulting in Ca^{2+} overload and excitotoxicity (Durukan and Tatlisumak, 2007). The rise in intracellular Ca^{2+} is harmful to neurons and initiates a series of injurious events such as generation of free radicals and leukotrienes, irreversible mitochondrial damage, activation of proteolytic enzymes that degrade proteins, membrane and nucleic acids and inflammation. These events lead to neuronal death through necrosis, autophagy, or apoptosis (Dirnagl *et al*., 1999). Additionally, water passively follows the ion influx resulting in cytotoxic oedema (Dirnagl *et al*., 1999). This affects perfusion of brain tissue and may also lead to an increase in intracranial pressure (Dirnagl *et al*., 1999).

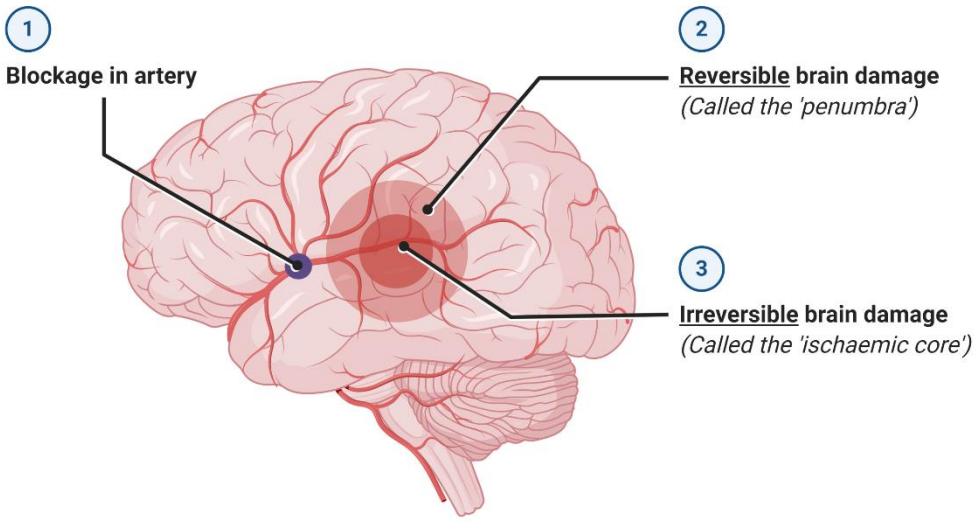

Figure 1.4. Different regions of the cerebrovascular tissue during ischaemia. A blockage in a cerebral artery results in reduced blood supply. The ischaemic core is the region with minimal perfusion resulting in irreversible damage. The region surrounding the ischaemic core is the penumbra where there is intermediate blood flow and the damage can be reversed upon timely reperfusion (Image produced using Biorender).

As shown in Figure 1.4, tissue undergoing ischaemia is categorized into two layers: the ischaemic core and penumbra. The ischaemic core is a region of profound or complete loss in CBF leading to irreversible tissue damage because neuronal and glial cells undergo necrosis. The tissue at the periphery of the core is known as the penumbra. Penumbra has a less severe reduction in CBF and the neurons are dysfunctional but the area is structurally intact. Penumbral tissue is undergoing either necrosis or apoptosis and can be recovered by immediate reperfusion (Dirnagl *et al*., 1999; Prabal *et al*., 2010). CBF thresholds for ischaemic core (<12 mL / 100g / minute) and penumbra (12-22 mL / 100g / minute) were described by Lindsay Symon and colleagues in 1970 using a baboon model of focal cerebral ischaemia (Steven *et al.,* 2011). The main aim of stroke therapeutics is to salvage most of the penumbral region during ischaemia (Dirnagl *et al*., 1999).

1.2.2 Peri-infarct depolarisations

Per-infarct depolarisations (Figure 1.5) are secondary mechanisms that contribute to the expansion of ischaemic lesion. In the ischaemic core (Figure.1.4), the cell can undergo anoxic depolarisation and never repolarise. In the penumbra, cells can repolarize but at the expense of more energy. The same cells can depolarise again in response to an increase in glutamate and K^+ levels in the extracellular space (Dirnagl *et al.,* 1999). Repetitive depolarisations are known as peri-infarct depolarisation and have been demonstrated in mouse, rat, and cat models of stroke. They occur with a frequency of several events per hour and can be seen for up to 8 h (Dirnagl *et al.,* 1999).

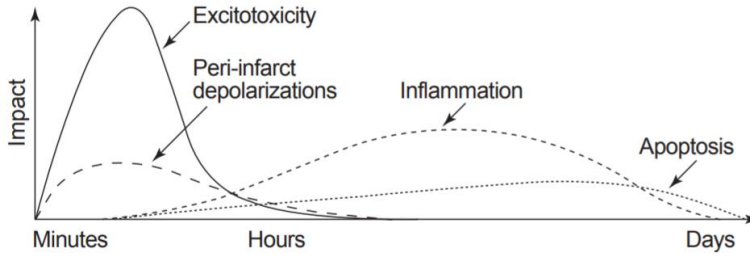

Figure 1.5. Profile summarizing major pathogenic mechanisms underlying focal cerebral ischaemia. During early onset of ischaemia, excitotoxic mechanisms damage the neurons and glial cells. This also additionally triggers events such as peri-infarct depolarisations and later on mechanisms such as inflammation and apoptosis occur (Adapted from Dirnagl *et al.,* 1999) (Image produced using Biorender).

1.2.3 Oxidative stress

Oxidative stress has been implicated as an important mediator of tissue damage after cerebral ischaemia. Free radicals such as superoxide, hydrogen peroxide, and hydroxyl radicals are generated via several mechanisms. The primary source of ROS (reactive oxygen species) during ischaemic stroke is the mitochondria (Woodruff *et al.*, 2011). ROS mediates the disruption of inner mitochondrial membrane and oxidation of proteins involved in the electron transport chain. Partly due to the formation of a mitochondrial permeability transition pore (MPTP), the mitochondrial membrane becomes leaky resulting in termination of ATP production, and ROS burst into the cytoplasm. Cytochrome C is released from the mitochondria triggering apoptosis (Dirnagl *et al*., 1999). The activation of cyclooxygenase and lipooxygenases also generate ROS that results in lipid peroxidation and membrane damage (Dirnagl *et al*., 1999). Following reperfusion, ROS can also be generated by activated microglia and infiltrating peripheral leucocytes via NADPH (Nicotinamide

adenine dinucleotide phosphate) oxidase system (Woodruff *et al.,* 2011). ROS serve as important signalling molecules that trigger apoptosis and inflammation (Woodruff *et al.*, 2011). Additionally, nitric oxide (NO) synthesized by Ca^{2+}-dependent enzyme neuronal nitric oxide synthase (nNOS) reacts with superoxide anion forming highly reactive peroxynitrite that promotes tissue damage (Dirnagl *et al*., 1999). A wide range of cellular effects induced by RNS (reactive nitrogen species) and ROS include inactivation of enzymes, protein denaturation, lipid peroxidation, and damage to the cytoskeleton and DNA (deoxyribonucleic acid). They also increase BBB permeability through activation of matrix metalloproteinase 9 (MMP9) resulting in vasogenic oedema (Woodruff *et al.,* 2011).

1.2.4 Ischaemia-reperfusion injury

Rapid reperfusion can reduce the size of infarct by recovery of penumbra and improve the overall clinical outcomes (Zoppo and Hallenback, 2000). Often paradoxically, restoration of vascular supply to the brain following ischaemia can result in “ischaemia-reperfusion (I / R) injury”, which significantly worsens the functional outcomes of stroke (Nour *et al*., 2013). The main mechanisms resulting in I / R injury include oxidative stress, leucocyte infiltration, platelet activation, complement activation, hyperperfusion, and BBB disruption (Pan *et al*., 2007). During I / R injury, a major source of ROS production is the mitochondria (Nour *et al*., 2013). I / R induces post-translational modification of oxidative phosphorylation proteins, which increases MMPs (matrix mettaloproteinases) resulting in excessive ROS generation (Lin *et al*., 2016). Another key source is NADPH oxidase, a key component of electron transport chain in the plasma membrane that generates free radicals by transferring an electron to molecular oxygen (Lin *et al*., 2016). Leucocytes play a key role in I / R injury. During I / R, activated leucocytes interact

with endothelial cells followed by BBB disruption, through the release of neutrophil-derived oxidants and proteolytic enzymes (Pan *et al*., 2007). Leucocytes in turn extravasate from capillaries and infiltrate brain tissue releasing cytokines that mediate inflammation, which eventually results in deterioration of penumbra (Lin *et al*., 2016). Leucocytes along with red blood cells and platelets during reperfusion can plug capillaries, resulting in obstruction of blood flow via the “no-reflow” phenomenon (Khatri *et al.,* 2012; Lin *et al*., 2016). Activated platelets also release various mediators resulting in vasospasm and exacerbation of oxidative stress and inflammation (Lin *et al*., 2016). Complement activation also results in the formation of several inflammatory mediators further amplifying inflammation (Lin *et al*., 2016).

1.2.5 Neuroglial interaction during ischaemic stroke

Astrocytes are the key targets for considering the relationship between cerebral vasculature and neurons. Astrocytes are the most abundant cells in the brain and almost all vascular endothelial cells in the brain are surrounded by foot processes of astrocytes and interact with neurons through astrocytes (Ozaki *et al*., 2019). Astrocytes' cellular processes enwrap synaptic terminals and modulate neuronal activity (Becerra-Calixto and Gomez, 2017). Astrocytes are the major homeostatic cell type in the CNS, fulfilling many important roles in healthy and injured brain (Figure 1.6). Astrocytes maintain homeostasis, promote synthesis and removal of NTs, store glycogen, provide antioxidant defense, and regulate synaptic activity by producing various cytokines, chemokines, growth factors, and metabolites (Becerra-Calixto and Gomez, 2017). Various studies have reported dual roles of astrocytes during and post ischaemia. Unlike neurons, astrocytes are less vulnerable to glutamate excitotoxicity, however acute ischaemia triggers the release of cytokines such as transforming growth factor α (TGFα) resulting in the formation of

astrogliosis. Astrogliosis displays cellular hypertrophy, proliferation, and increased expression of glial fibrillary acidic protein (GFAP) (George *et al.,* 2011). Within a few days post ischaemia, a glia scar is formed around the ischaemic core mainly generated by astrogliosis. The role of the glial scar is controversial, as during recovery it may obstruct axonal regeneration and reduce functional outcome. Whereas on the other hand, it also secludes viable tissue from the injury site and protects surrounding area from harmful substances in the ischaemic core (Becerra-Calixto and Gomez, 2017). Neurons and astrocytes have different but complementary metabolic profiles. Astrocytes are reported to have the ability to support energy needs of neurons. Astrocytes present a high glycolytic rate (upregulation of phosphofructose-2-kinase / fructose-2, 6-bisphosphate 3 (Pfkfb3)) (Becerra-Calixto and Gomez, 2017). Astrocytes also have glycogen stores that may provide energy during ischaemia but also can aggravate brain damage due to lactic acidosis (Rossi *et al.,* 2007). Astrocytes have also been reported to produce pro-inflammatory cytokines such as interleukins (IL6, IL10, and IL1β), interferon γ and TGFβ (transforming growth factor β), which have multiple roles in both neurodegeneration and protection (George *et al.,* 2011). In the acute phase of ischaemic stroke, astrocytic gap junctions remain open allowing substances to diffuse from dying cells to surrounding cells, resulting in the expansion of ischaemic lesion. However, inter-astrocytic gap junctional communication also decreases neuronal vulnerability to oxidative stress by mechanisms involving stabilisation of Ca^{2+} homeostasis and dissipation of oxidative stress (Rossi *et al.,* 2007; George *et al.,* 2011). In the normal brain tissue, astrocytes produce antioxidants such as glutathione and these molecules may enhance neuron survival and protect astrocyte function after ischaemic stroke (Rossi *et al.,* 2007). Astrocytes have been reported to

be neuroprotective as they can limit lesion extension via anti-excitotoxicity effects such as uptake of excess glutamate, sequester free iron, production of neurotrophic factors, and promotion of angiogenesis, neurogenesis, synaptogenesis, and axonal remodelling aiding recovery (Becerra-Calixto and Gomez, 2017). Figure 1.6 summarizes the key roles of astrocytes in physiological conditions and ischaemic stroke.

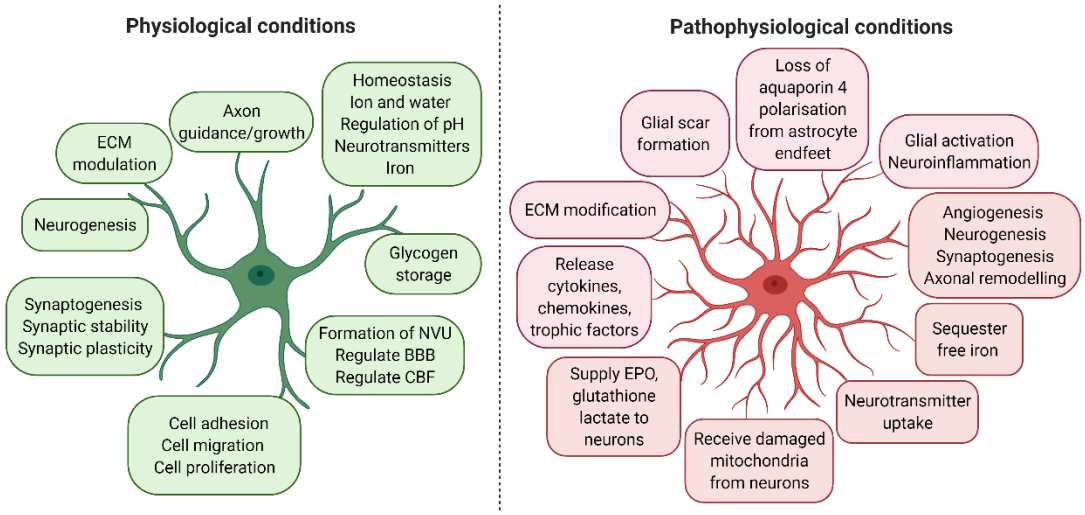

Figure 1.6. Key roles of astrocytes in physiological conditions and ischaemic stroke. The diverse functions of astrocytes during physiological and pathophysiological conditions. Astrocytes have several important roles in the healthy and diseased brain. They are the main housekeeping cells of the brain, and can exert either protective or detrimental effects on neurons during pathophysiological conditions. Astrocytes are essential for the development and maintenance of the BBB, homeostasis of the brain microenvironment, CBF regulation, NT uptake, synaptogenesis, neurogenesis and release of neurotrophic factors and energy supply to neurons. Astrocytes also play a major role during pathophysiological conditions. Neuronal survival heavily depends on astrocytes. For example, neurons do not survive if neighbouring astrocytes are lost during an ischaemic stroke. Cerebral ischaemia leads astrocytes to change their morphology and function, causing astrocytes to become reactive, thereby producing several pro-inflammatory modulators and participating in glial scar formation. Their neuroprotective roles include clearing glutamate from synaptic regions, secretion of neurotrophic factors and promotion of angiogenesis, neurogenesis, synaptogenesis and axonal remodelling (Image produced using Biorender).

1.2.6 Neuroinflammation

During ischaemia, activation of transcription factors results in increased protein levels of inflammatory mediators such as TNFα (tumour necrosis factor-α), IL1β, and platelet-activating factors (Dirnagl *et al*., 1999) and expression of endothelial cell adhesion molecules (CAMs) at the vascular endothelium (Woodruff *et al.*, 2011). CAMs mediate the interaction between vascular endothelium and leucocytes promoting leukocyte recruitment (Prabal *et al*., 2010). Neutrophils transmigrate into the brain parenchyma within few hours after reperfusion, followed by macrophages and monocytes within a few days (Dirnagl *et al*., 1999). Microvascular obstruction by neutrophils can worsen the degree of ischaemia and production of toxic mediators by inflammatory cells**,** and injured neurons such as cytokines, prostanoids, superoxide, and NO can amplify tissue injury (Durukan and Tatlisumak, 2007).

Microglia plays a major role in brain inflammation after a stroke (Woodruff *et al.,* 2011). Microglia are mononuclear phagocytes that constitute around 10% of total brain cells. The activation of microglia is controlled via neuronal-glia crosstalk via CX3CL1 / CX3CR1 (Fractalkine receptor chemokine (C-X3-C motif) receptor 1) signalling pathways**,** and ischaemic stroke elicits activation of microglia by impairing this crosstalk (Patel *et al.,* 2013). Upon activation, microglia produce a wide range of pro- and anti-inflammatory mediators. Microglia are rapidly activated within a few minutes during the acute phase of ischaemia. In ischaemic core, the activation is triggered by excitotoxic signal whereas in the peri-infarct region, activation of microglia is triggered by damaged associated molecular patterns (DAMPs), eliciting a strong inflammatory response (Guruswamy and Elali, 2017). Upon activation, microglia change their phenotype by adopting different morphologies that are tightly

associated with the spatial structural change. Microglia can be detected in three distinct morphologies; in the peri-infarct region, either microglia with enlarged cell body and short ramification or amoeboid cell structure with rare ramification are detected, whereas round-shaped representing the highly activated form of microglia are detected nearby the ischaemic core (Patel *et al.,*2013; Guruswamy and Elali, 2017). Upon activation, microglia become polarized adopting different phenotypes ranging between activated M1 phenotype that is pro-inflammatory and activated M2 phenotype that is anti-inflammatory (Figure 1.7). The cell surface markers specific to the M1 phenotype include CD16, CD32, CD80, CD86, CD40, iNOS, MHCII, and FcγR. The cell surface markers specific to the M2 phenotype include Arg-1, CD68, Fizz1, Ym1, CD206, and Dectin-1. M1 microglia release a variety of pro-inflammatory factors such as TNFα, IL1β, and IL6 exacerbating the inflammatory response. It also causes oxidative stress by stimulating the release of ROS as well as excessive production of NO via inducible nitric oxide synthase (iNOS) resulting in the generation of RNS. M2 are reported to improve brain repair and regeneration as they release anti-inflammatory factors such as IL4, IL10, IL13, TGFβ. M2 phenotype secretes neurotrophic factors such as insulin growth factor 1 (IGF1), brain-derived neurotrophic factor (BDNF), TGFβ, and neuronal growth factor (NGF). Acute ischaemic insults trigger the generation of M2 reparative microglia, but in sub-acute and chronic phase microglia polarisation shifts towards M1 destructive phenotype (Patel *et al.,* 2013).

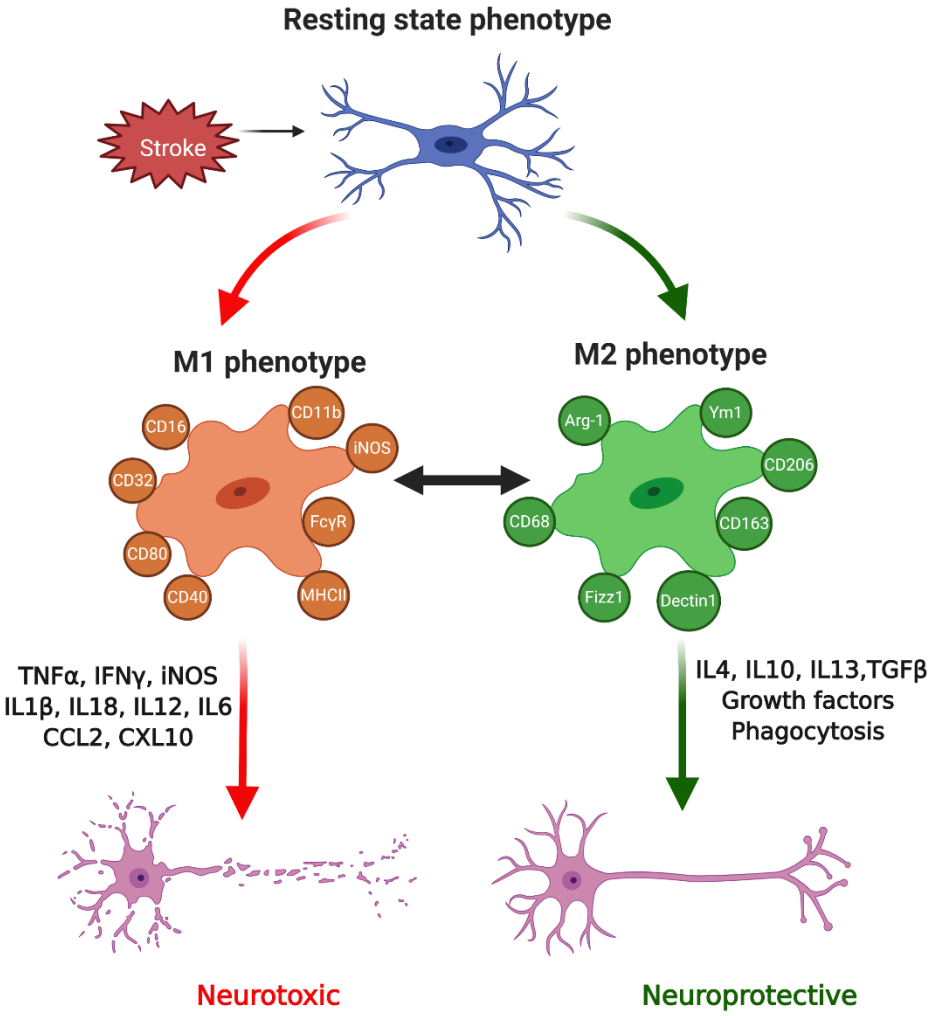

Figure 1.7. Represents phenotypes of microglia. Resting-state microglia in the physiological state are responsible for surveillance, microenvironment homeostasis, maintaining neuronal plasticity, and circuit shaping. Upon activation by stroke, microglia become polarized adopting different phenotypes ranging between activated M1 phenotype that is pro-inflammatory and activated M2 phenotype that is anti-inflammatory (Adapted from Patel et al.,2013) (Image produced using Biorender).

1.2.7 BBB disruption

The BBB is critical for maintaining homeostasis in the brain. BBB is a structural and biochemical barrier between peripheral blood circulation and CNS. BBB anatomy is comprised of neurons, astrocytes, endothelium, pericytes and perivascular space that constitute a neurovascular unit (NVU) (Figure 1.8). The concept of the NVU was formalized in 2001 by the Stroke Progress Review Group of the National Institute of Neurological Disorders and Stroke (NINDS, 2019). The concept of NVU emphasizes that each cell of the NVU plays an essential role in maintaining the BBB integrity. All the cells in the NVU are closely interrelated to maintain brain homeostasis, regulate blood flow, modulate exchange across the BBB, contribute to immune responses, and provide trophic support to the brain. The cells interacting with neurons are equally affected by ischaemic stroke and engage in complex and cell-specific signalling cascades (Ozaki *et al*., 2019; Posada-Duque *et al*., 2014).

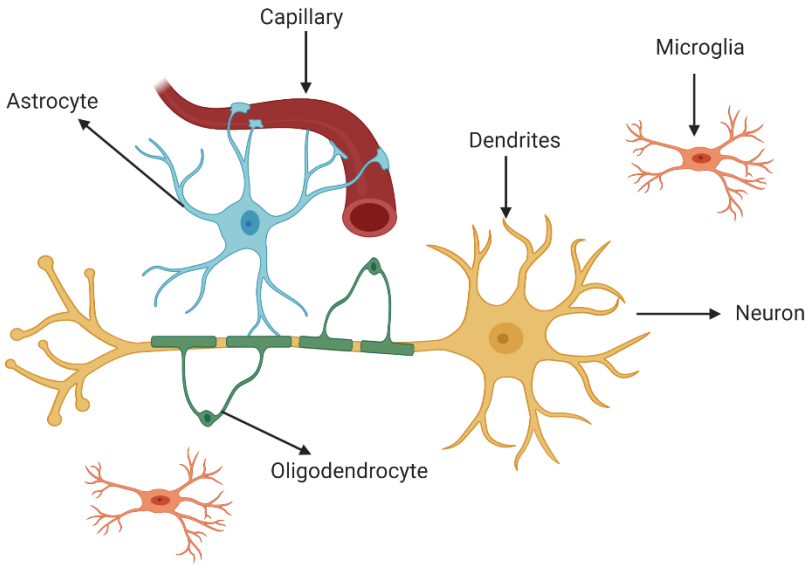

Figure 1.8. Neurovascular unit (NVU). The NVU consists of neurons, glial cells (astrocytes, oligodendrocytes, microglia), and endothelial cells. The cells are closely related to maintain brain homeostasis, regulate blood flow, modulate exchange across the BBB, contribute to immune responses, and provide trophic support to the brain (Image produced using Biorender).

BBB functions are mainly controlled by the tight and adherens junctional protein complexes. As seen in Figure 1.9, endothelial cells lining the BBB have more extensive tight junctions to limit the flux of hydrophilic molecules across the BBB. The tight junctions consist of three membrane proteins known as claudin, occludin, and junction adhesion molecules as well as cytoplasmic accessory proteins such as ZO-1, ZO-2, ZO-3 and others (Ballabh *et al.,* 2004). Under normal conditions, BBB prevents the extravasation of cells, solute, ions and molecules. However, BBB disruption can lead to change in paracellular and transcellular permeability and extravasation of leucocytes into the brain tissue. This in turn contributes to cytotoxic oedema. During ischaemic injury, mechanical damage of vasculature and toxic

damage due to inflammatory mediators and free radicals cause loss of structural integrity of vascular endothelium and brain tissue. The major contributory factor is the release of MMPs that lead to the destruction of the basal lamina. All these together cause the disruption of the BBB resulting in cerebral oedema, influx of toxic substances, inflammation, and haemorrhagic transformation (Zoppo and Hallenback, 2000).

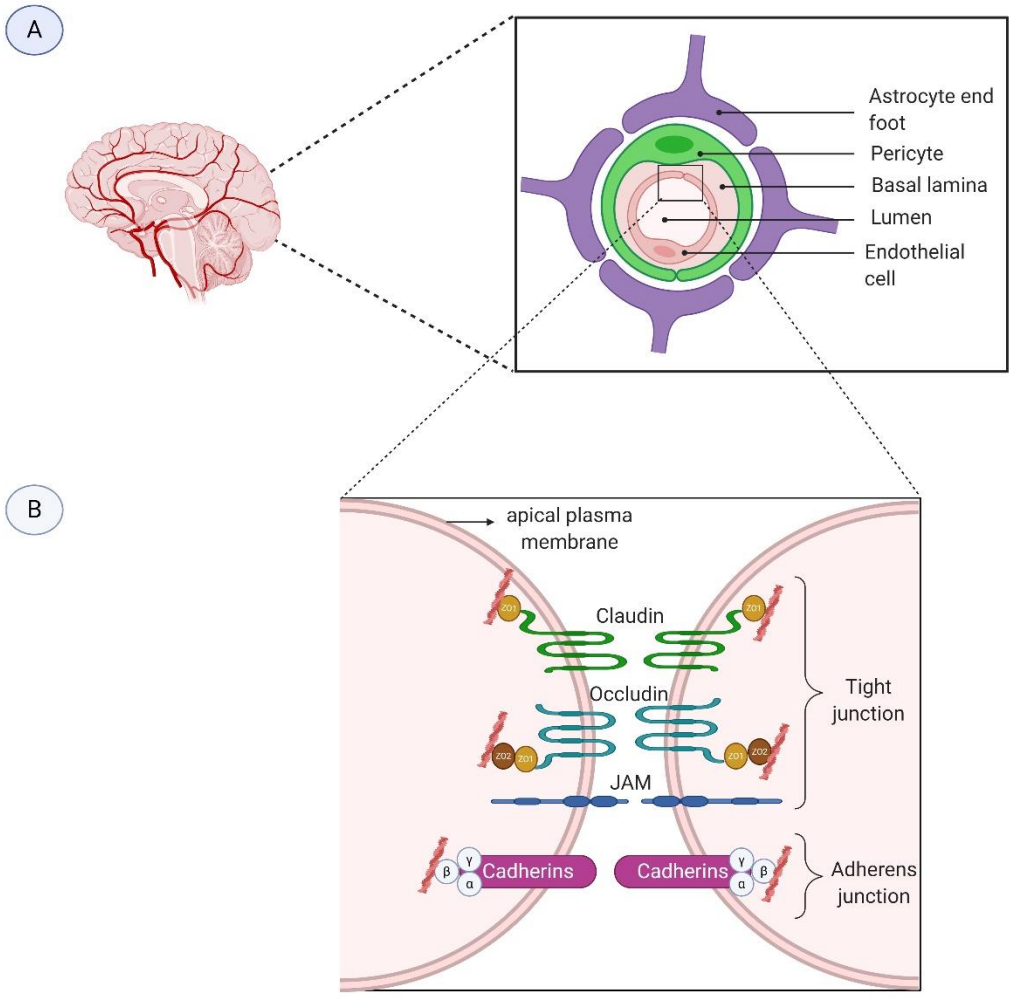

Figure 1.9. The structure of the blood-brain barrier (BBB). (A) Schematic drawing of the transverse section of BBB. The BBB is composed of endothelial cells, capillary basement membrane in which pericytes are embedded, and astrocyte end-feet ensheathing the blood vessels. (B) Magnified structure of the junctions on the BBB. The BBB comprises tight junction (TJ) and adherens junction (AJ). The TJ consists of three integral membrane proteins known as claudins, occludin, and junctional adhesion molecule (JAM) and cytoplasmic proteins such as ZO-1, ZO-2, ZO-3 and others that link membrane protein to actin. AJ consists of membrane protein cadherin that joins the actin cytoskeleton via intermediary proteins to form adhesive contact between cells (Image produced using Biorender).

1.2.8 Necrotic, apoptotic and autophagic cell death

Cell death during ischaemic stroke is widely classified into necrosis, apoptosis, and more recently autophagy (Broughton *et al.*, 2009). Figure 1.10 illustrates a diagrammatic comparison between necrosis and apoptosis. Necrosis is the predominant mechanism for cell death that follows acute, permanent vascular occlusion (Dirnagl *et al*., 1999). On the onset of acute brain ischaemia, dramatic blood flow reduction results in necrotic cell death in the ischaemic core. When cells die by necrosis, they release more glutamate and toxins into the extracellular environment affecting the surrounding neurons and glial cells (Broughton *et al.,* 2009). Necrotic cells become oedematous, cytoskeleton breaks down resulting in disruption of the plasma membrane, thus releasing the intracellular content. (Durukan and Tatlisumak, 2007).

Apoptosis is an energy-consuming process, so reperfusion could potentiate apoptosis by restoring cellular energy (Durukan and Tatlisumak, 2007). Apoptosis results in DNA fragmentation, degradation of cytoskeletal and nuclear proteins, cross-linking of proteins, the formation of apoptotic bodies, and expression of ligands for phagocytic cell receptors (Radak *et al.,* 2017). As a result, apoptotic cells are rapidly cleared by phagocytosis without eliciting an inflammatory reaction (Durukan and Tatlisumak, 2007). Apoptosis is triggered by several processes including excitotoxicity, free-radical formation, inflammation, mitochondrial, and DNA damage (Durukan and Tatlisumak, 2007). Several mediators facilitate cross-communication between apoptotic cell death pathways such as the calpains, cathepsin B, nitric oxide, and poly-ADP-ribose-polymerase (PARP) (Durukan and Tatlisumak, 2007). Following ischaemia, caspase-mediated apoptosis occurs in response to pro-

apoptotic signals such as upregulation of Bcl-2 associated X (Bax), BH3-interacting domain death agonist (Bid) and downregulation of anti-apoptotic Bcl-2 family proteins B-cell lymphoma 2 (Bcl-2) and B-cell lymphoma extra-large (Bcl-xL) (Broughton *et al.,* 2009). Activated caspase-3 cleaves nuclear DNA repair enzymes and structural proteins such as laminin, actin, gelsolin resulting in DNA damage and apoptosis (Broughton *et al.,* 2009).

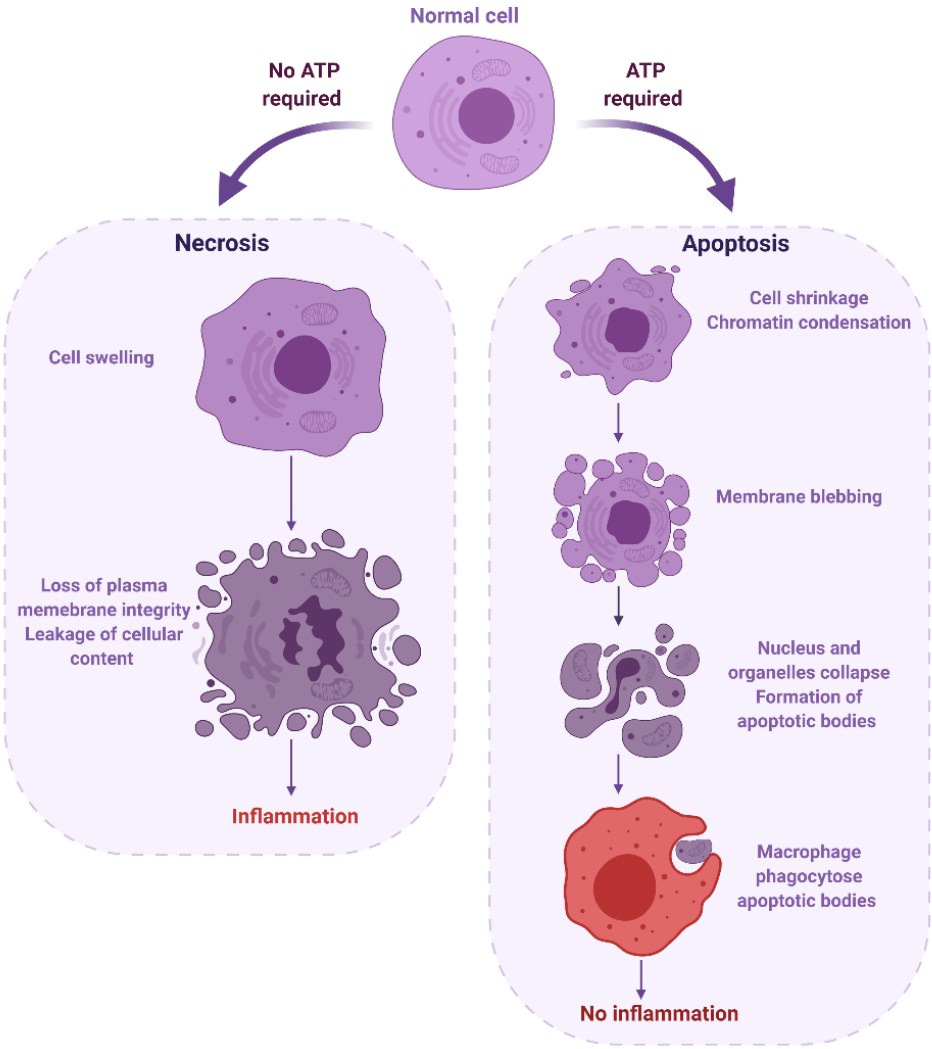

Figure 1.10. Figure illustrating apoptotic and necrotic cell death. Necrosis is irreversible cell damage that occurs due to a dramatic reduction in CBF. Necrotic cells become oedematous, cytoskeleton breaks down resulting in disruption of the plasma membrane, thus releasing the intracellular content. Apoptosis is an energy-consuming process that results in DNA fragmentation, degradation of cytoskeletal and nuclear proteins, cross-linking of proteins, the formation of apoptotic bodies, and expression of ligands for phagocytic cell receptors As a result, apoptotic cells are rapidly cleared by phagocytosis without eliciting an inflammatory reaction (Image produced using Biorender).

Autophagy is a highly regulated, catabolic process, through which macromolecules such as damaged organelles and proteins are degraded and recycled to maintain cellular homeostasis (Wang *et al.,* 2018). As shown in Figure 1.11, autophagic cell death is highly regulated which involves the formation of phagophores which elongate to autophagosomes. An autophagosome is a double-membrane vesicle that envelops unnecessary or dysfunctional proteins before fusing with a lysosome to form an autolysosome, allowing cellular components to be digested (Kim *et al.,* 2018). Various studies have demonstrated the activation of autophagy in the brain cells such as astrocytes, microglia, neurons, and endothelial cells upon an ischaemic insult (Li *et al.,* 2018). The underlying mechanisms and the role of autophagy in ischaemic stroke are yet to be fully elucidated. Recent studies have suggested that insufficient or excessive autophagy results in cell death whereas mild / moderate autophagy has a neuroprotective effect (Kim *et al.,* 2018; Li *et al.,* 2018). Recently a link between apoptosis and autophagy has been identified. Both autophagy and apoptosis are regulated by the PI3K / Akt (phosphoinositide 3-kinase / Akt) pathway. Apoptosis is suppressed by the PI3K signalling of downstream proteins, including mTOR (mechanistic target of rapamycin) (Li *et al*., 2018). Bcl-2 is a protein found in mitochondria that is primarily anti-apoptotic and shown to inhibit cell death. Bcl-2 has also been identified as an anti-autophagic signalling molecule, through sustaining Beclin1. Some members of the Bcl-2 family are pro-death proteins believed to result in the disruption of the cell membrane that causes mitochondrial death. It is theorised that inhibition of pro-death Bcl-2 proteins and the promotion of prosurvival proteins may result in neuroprotection. However, studies have shown that the knockout (KO) of these proteins in mice was not capable of providing sufficient neuroprotection from MCAO (middle cerebral artery occlusion) (Vosler *et*

al., 2009). Beclin1 may also be cleaved by caspases in apoptosis, so the pro-autophagic activity of Beclin1 is destroyed. Additionally, this cleavage results in the amplification of pro-apoptotic signalling, inducing widespread cell death, indicating that there is a lot of crosstalk between apoptosis and autophagy signalling (Kang *et al*., 2011).

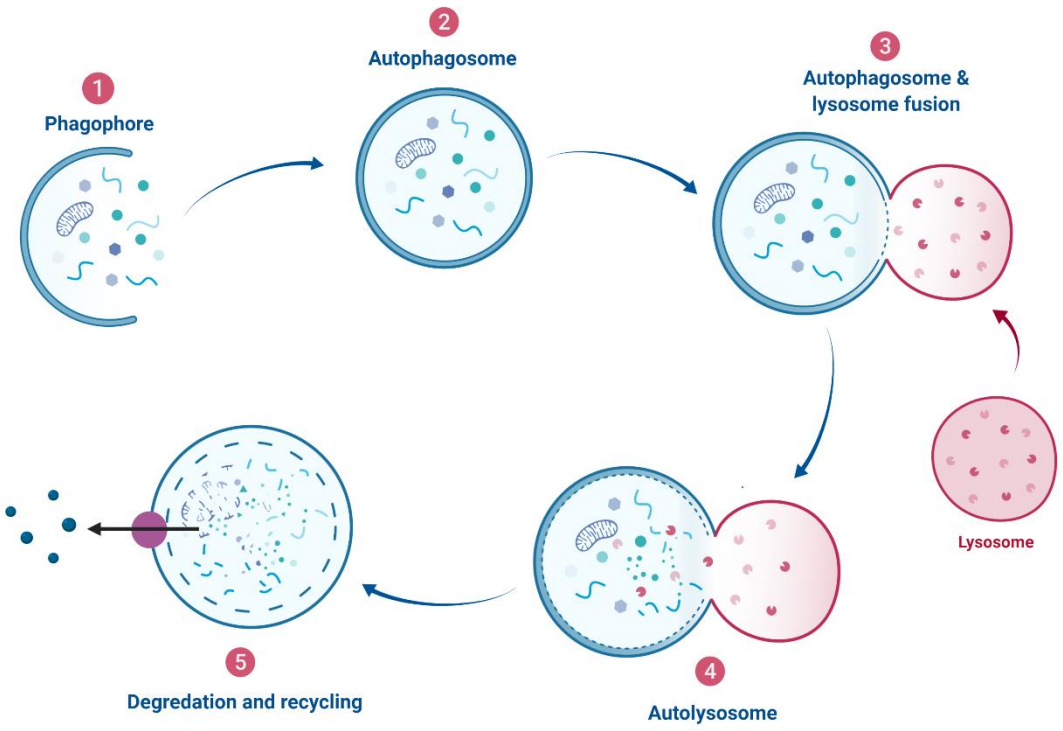

Figure 1.11. Represents the process in autophagic flux. This is a dynamic process involving the formation of phagophores initially, which elongate to form autophagosomes. An autophagosome is a double-membrane vesicle that envelops unnecessary macromolecules and fuses with lysosome to form autolysosome to allow digestion of the cellular material (Image produced using Biorender).

1.3 Current treatments and prophylaxis for ischaemic stroke

US FDA (Food and drug administration) approved the use of intravenous recombinant tissue plasminogen activator (rtPA) in 1996 following results of NINDS rtPA stroke trial which showed that use of rtPA has a positive impact and improved the outcomes of ischaemic stroke, however only if it was used within 3 h of onset of ischaemic stroke (Hacke *et al*., 2004). ECASS I, ECASS II, ATLANTIS A, and ATLANTIS B collectively analysed the benefits of rtPA in 3-4.5 h time-window and it showed improved outcome (Hacke *et al*., 2004). In 2008, results of ECASS III trial were consistent with the results of previous trials, and the time window for treatment with rtPA was increased to 4.5 h (Bluhmki *et al*., 2009). According to current guidelines, rtPA is recommended for the treatment of acute ischaemic stroke as early as possible within 4.5 h of stroke onset after excluding intracranial haemorrhage by imaging techniques (BNF 72, 2017). rtPA is a fibrinolytic, which activates plasminogen to form plasmin that degrades fibrin making the clot soluble and subject to proteolysis by other enzymes (Hacke *et al.,* 2008). Degradation of the clot results in the restoration of blood flow in the occluded blood vessels, supplying oxygen and nutrients to the brain. The commonly reported side-effects of rtPA include bleeding, anaphylaxis, and orolingual angioedema (Hacke *et al.,* 2008; NICE GUIDANCE, 2008; Jauch *et al*., 2013; NICE CKS, 2017). Even after the approval of rtPA, only about 5% of patients get the benefit because of its limited time window and its contraindications (Table 1.3) (Hill, M.D., 2014). Treatment with rtPA can lead to haemorrhagic transformation, which is a major complication that needs to be taken into account. Therefore**,** monitoring of blood pressure and signs of haemorrhage is constantly required (Jaillard *et al*., 1999). Even after 20 years of approval of rtPA, no other pharmacological treatment has been approved by the FDA

for use in the management of ischaemic stroke. It is therefore important to research drugs that could be used for the management of ischaemic stroke with a longer time window as well as fewer complications associated.

Table 1.3. Contraindications for use of rTPA (recombinant tissue plasminogen activator) in patients with ischaemic stroke

- Clinical presentation suggesting subarachnoid haemorrhage
- Intracranial haemorrhage on CT scan
- Only minor or rapidly improving stroke symptoms
- Neurosurgery, head trauma or stroke in the past 3 months
- Uncontrolled hypertension (>185 mmHg systolic blood pressure or >110 mmHg diastolic blood pressure)
- History of intracranial haemorrhage
- Known intracranial arteriovenous malformation, neoplasm or aneurysm
- Seizure at the onset of stroke
- Active internal bleeding
- Suspected or confirmed endocarditis
- Known bleeding diathesis (platelet count < 100,000; received heparin within 48 h and has an elevated aPTT (activated partial thromboplastin time); current use of oral anticoagulants (warfarin) and INR >1.7; current use of direct thrombin inhibitors or direct factor Xa inhibitors)
- Abnormal blood glucose (<50 or >400 mg / Dl)
- Lumbar puncture or recent arterial puncture at a non-compressible site
- Pregnancy or delivery within 14 days
- History of gastrointestinal or urinary tract haemorrhage within 21 days

Reference: NICE, 2012

Mechanical thrombectomy is a surgical intervention indicated in patients with acute ischaemic stroke due to large artery occlusion in the anterior circulation, who can be treated within 6 h time window of the onset of ischaemic stroke regardless of whether they have received rtPA. Only 9% of patients presenting between 6 and 24 h may qualify for mechanical thrombectomy. Two main issues are limiting the use of thrombectomy. Firstly, only 10% of patients with acute ischaemic stroke have large artery occlusion in the anterior circulation and present early enough to qualify for thrombectomy. Secondly, only a few stroke-centers have the expertise and resources to deliver the therapy (Elgendy *et al*., 2015; Mokin *et al.,* 2019).

It is estimated that controlling modifiable risk factors of stroke can reduce more than 50% of cases of stroke (Lee *et al*., 2011). Hypertension is the most common risk factor for stroke (Lee *et al*., 2011). There are various antihypertensives such as calcium channel blockers, beta-blockers, angiotensin-converting enzyme inhibitors (ACEIs), angiotensin II Type 1 Receptor Blockers (ARBs) and diuretics that can be used to reduce blood pressure to optimal levels. The choice of drug depends on the patient's characteristics such as renal impairment, cardiac disease, liver function, diabetes, and patients' preferences. The commonly recommended choice of drug is the use of diuretics alone or in combination with ACEIs for primary prevention of ischaemic stroke (Legge *et al*., 2012; Hisham and Bayraktutan, 2013). Some clinical trials have also demonstrated that ACEIs and ARBs can be used to reduce the risk of primary stroke independent of reducing blood pressure. Heart outcomes prevention evaluation (HOPE) trial showed that ACEIs reduce the risk of stroke when compared to placebo with only a small reduction in blood pressure. Losartan intervention for endpoint reduction in hypertension (LIFE) trial showed that like

ACEIs, ARBs could also reduce the risk of stroke (Strauss *et al*; 2009). In high-risk patients such as those with low-density lipoprotein (LDL) >4.1, age >45 years, positive family hypertension, smoking, hypertension, diabetes mellitus, atherosclerosis and left ventricular hypertrophy, statins are used to lower LDL cholesterol levels to prevent stroke (NICE GUIDANCE, 2008; Legge *et al*., 2012). Diabetes is another risk factor that needs to be controlled especially because many diabetic patients commonly have hypertension and dyslipidaemia that need to be controlled. Although there are no conclusive results on glycaemic control affecting the risk of stroke, the use of oral antidiabetics is recommended to control blood glucose levels (Legge *et al*., 2012). Patients with non-valvular AF are at increased risk of stroke therefore after taking into consideration CHA2DS2-VASc score and risk of bleeding (Lee *et al*., 2011), anticoagulation with warfarin is recommended. Alternatively, apixaban, dabigatran, or rivaroxaban may be considered (NICE pathway, 2016). In patients with a lower risk of stroke, aspirin alone may be considered (Legge *et al*., 2012). Lifestyle modifications such as diet, exercise, reducing alcohol intake, and stopping smoking are highly recommended to reduce the risk of primary stroke (NICE GUIDANCE, 2008; NICE CKS, 2017).

Long-term management for stroke involves secondary prevention (understanding the most likely cause of stroke and taking appropriate medication for its treatment), psychosocial care, rehabilitation, lifestyle modification, and management of comorbidities and risk factors of stroke (NICE GUIDANCE, 2008). After 24 h of treatment with rtPA or patients who were not thrombolysed, antiplatelet therapy is initiated with either clopidogrel, modified-release dipyridamole, aspirin, or a combination of aspirin-dipyridamole. Treatment with a high-intensity statin is initiated

after the diagnosis of stroke or TIA aiming to reduce non-HDL (high-density lipoprotein) cholesterol to less than 40%. Antihypertensives are also initiated for secondary prophylaxis of hypertension with thiazide-like diuretics, long-acting calcium channel blockers, or ACEIs. In patients with ischaemic stroke or TIA, anticoagulation with adjusted-dose warfarin is considered after excluding intracranial bleeding and other contraindications. In patients with high blood glucose levels, glucose levels are maintained with oral antidiabetics (NICE guidelines, 2008; Legge *et al*., 2012; Jauch *et al*., 2013; NICE CKS, 2017).

1.4 Neuroprotection for ischaemic stroke

Neuroprotection is a concept that has received significant attention over the past 30 years. Neuroprotection seeks to restrict injury to the brain parenchyma following an ischaemic insult by preventing salvageable neurons in the penumbra from dying (Sutherland *et al*., 2012; Majid A, 2014). Over the past 30 years, neuroprotection has received significant attention and has shown promise in experimental studies, but has failed to succeed in clinical trials. Many reasons exist for this**,** such as variable time windows of drug administration in preclinical and clinical studies**.** Preclinical studies have focused on the effectiveness within a very short time window whereas clinical trials allow longer time windows. Preclinical studies have relied on measuring infarct size to judge efficacy**,** whereas clinical trials rely on behavioural outcomes and long-term recovery. Experiment stroke models are homogenous, whereas human stroke is heterogeneous. The choice of animals in preclinical studies is usually young, healthy animals whereas in clinical trials stroke patients have a multitude of associated variables that affect the prognosis. Additionally, the presence of comorbidities in the patients can have an effect on drug efficacy in the patients (Ginsberg, 2008). Additionally**,** a complicated factor in the development of novel

neuroprotective strategies is the dual nature of many processes that occur during strokes such as the activity of astrocytes microglia, apoptosis, and autophagy, which can either be damaging or protective**,** depending on the magnitude, location and timing of the effect (Ginsberg, 2008).

In the past, several neuroprotective strategies targeting single molecules in the ischaemic cascade have failed, shifting current attention to targeting the brain's own evolutionarily conserved endogenous neuroprotective mechanisms (Ginsberg, 2008). A summary of the neuroprotective agents that have been tested over the years**,** is provided in Table 1.4.

Table 1.4. Summary of neuroprotective agents, prototype drugs and results of studies

Proposed mechanism of neuroprotection	Prototype drugs	Results
Glutamate receptor antagonists		
NMDA Antagonists	Selfotel	Clinical trials completed / no benefit
	Aptinagel	Clinical trials completed / no benefit
	MK-801	Clinical trials halted- neurophysiological adverse effects
	Dextromethorphan	Clinical trials halted- neurophysiological adverse effects
	Eliprodil	No efficacy in clinical trials
AMPA antagonists		
	YM872	Beneficial effects found in pre-clinical studies. Clinical trials results pending
	ZK200755	Beneficial effects found in pre-clinical studies. Clinical trials results pending
Ion channel modulators		

Calcium channel blockers	Nimodipine	Clinical trials completed / no benefit
	Flunarizine	Clinical trials completed / no benefit
Sodium channel blocker	Fosphenytoin	Clinical trials completed / no benefit
Pottasium channel blocker	Maxipost	Clinical trials completed / no benefit
GABA (Gamma aminobutyric acid) agonist	Diazepam	Clinical trials completed / no benefit
	Clomethiazole	Clinical trials completed / no benefit
Free radical scavengers	Citicoline	Clinical trials halted / no benefit
	Ebselen, Edaravone	Clinical trials completed / no benefit
	Tirilazad	Clinical trials completed / no benefit
	NXY-059	Clinical trials completed / no benefit
		Clinical trials completed / no benefit
Anti-inflammatory agents	Enlimomab	Worsening outcomes in clinical trials
	UK279276	Clinical trials halted / no benefit
	LeukArrest	Clinical trials halted / no benefit
	rNIF	Clinical trials halted / no benefit
Growth factors	G-CSF (Granulocyte-colony stimulating factor)	Clinical trials completed / no benefit

	rhEPO (Recombinant human EPO)	Clinical trials completed / no benefit
Multiple mechanisms	Minocycline	Beneficial effects in pre-clinical studies. Clinical trials results pending Weak neuroprotectant
	Magnesium	Shown benefit in non-cortical stroke subgroup
	Albumin	Clinical trials halted / no benefit
	Hypothermia	Beneficial effects in pre-clinical studies. Clinical trials results pending
	Stem cell therapies	Beneficial effects in pre-clinical studies. Found safe in phase II clinical trials Phase III clinical trial results pending

References: Ginsberg, 2008; Sutherland *et al*., 2012; Hess *et al.,* 2017

As summarised in Table 1.4, several neuroprotectants targeting individual molecules (such as glutamate, ROS, ions) in the ischaemic cascade have been studied for ischaemic stroke. These agents were found to be protective in preclinical studies, but all of them failed in subsequent clinical trials (Ginsberg, 2008). Therapies targeting multiple mechanisms such as moderate therapeutic hypothermia and stem cell regeneration are the most solidly evidence-based neuroprotective strategies available. Hypothermia has shown to have various mechanisms such as decreasing excitatory amino acid release, reducing free radical formation, enhancing small ubiquitin-related modifier (SUMO)-related pathways, attenuating protein kinase C activity, and slowing cellular metabolism. Several trials have proven safety and

feasibility and several trials are ongoing to fully establish the utility in the clinical setting (Tahir and Pabaney, 2016). Neural stem cells can regenerate and restore brain function that is lost due to injuries such as stroke. In animal models, stem cells migrated to the site of injury and promoted revascularisation, enhanced plasticity, and regulated inflammatory responses. Stem-cell therapies for ischaemic stroke have shown promising neuroprotective effects in pre-clinical studies (Chu *et al.,* 2008; Fiorella *et al.,* 2011). Various small clinical studies have indicated that stem cell therapies are effective, feasible, and safe (Hung *et al.,* 2010; Stone *et al.,* 2013). In phase II clinical trials stem-cell therapies were found safe (Hess *et al.,* 2017) and effective (Bhasin *et al*., 2016; Levy *et al*., 2019). The study by Hess *et al.,* 2017 progressed in phase III clinical trials to determine the efficacy of stem cell therapies during acute ischaemic stroke (clinical trials called MASTER-2 by Athersys).

1.5 Hypoxia-inducible factor (HIF) and its modulation

The production of oxygen by photosynthesis had increased 1-2 billion years ago resulting in oxygen concentrations much greater than those required. Bigger organisms have**,** therefore**,** evolved sophisticated transport systems such as lungs, heart, and blood to transport oxygen to cells and tissues (Ratcliffe *et al.,* 1998). Organisms have developed abilities to sense oxygen availability as well as undergo adaptive gene expression changes (Table 1.5) to enhance oxygen delivery or promote survival during hypoxia. An evolutionary-conserved pathway mediated by oxygen-dependent post-translation hydroxylation factor called hypoxia-inducible factor (HIF)**,** plays an important role in the process (Kaelin and Ratcliffe, 2008).

Table 1.5. Oxygen regulated genes that are upregulated during hypoxia to adapt to the reduction in oxygen delivery

Process	**Oxygen-regulated genes upregulated during hypoxia**
Erythropoiesis	Erythropoietin
Glycolysis	Lactate dehydrogenase, Phosphoglycerate kinase-1, Aldolase, Phosphofructokinase L and C, Enolase
Glucose transport	Glucose transporter 1 and 3
Catecholamine synthesis	Tyrosine hydroxylase
Iron transport	Transferrin
Growth factors	Vascular endothelial growth factor, transforming growth factor β, platelet-derived growth factor B
Nitric oxide synthesis	Inducible nitric oxide synthase
Vasomotor regulator	Endothelin-1
High-energy phosphate metabolism	Adenylate kinase-3
Haem metabolism	Haem oxygenase 1

Reference: Ratcliffe *et al.,* 1998

1.5.1 The structure of HIF

HIF is a transcription factor that is activated during hypoxia and has upregulated hundreds of human genes that code for various cellular processes (Chan *et al*., 2016). HIF was discovered in 1990 by the Semenza laboratory and since then it has been a new therapeutic target for several diseases, e.g. anaemia, ischaemic diseases, inflammation, and cancer (Semenza, 2001). HIF transcription complex is heterodimeric consisting of α and β subunit. Oxygen-regulated α subunit has three known isoforms HIF1α, HIF2α, and HIF3α. The structures of HIF subunits are shown in Figure 1.12. HIF1β subunit also known as ARNT (aryl hydrocarbon receptor nuclear translocator) is constitutively expressed. HIF is a member of the bHLH (basic-helix-loop-helix)-PAS (PER-ARNT-SIM) domain family. The α subunit has an additional ODD (oxygen-dependent degradation) domain rendering the proteins to easy alteration in the presence of oxygen (Chan *et al*., 2016). HIF1α and HIF2α contain two-transactivation domain (TAD) known as N-terminal TAD (N-TAD) and C-terminal TAD (C-TAD) that mediate interactions with coactivators such as p300 and CBP (CREB-binding protein) (Karuppagounder and Ratan, 2012). HIF1α and HIF2α are structurally related**,** sharing 48% overall amino acid identity. HIF1α is ubiquitously expressed whereas HIF2α and HIF3α are more tissue-restricted. HIF2α is commonly expressed in the CNS, lung, carotid body, and endothelium (Chan *et al*., 2016). There is little information about HIF3α and further research is required (Karuppagounder and Ratan, 2012).

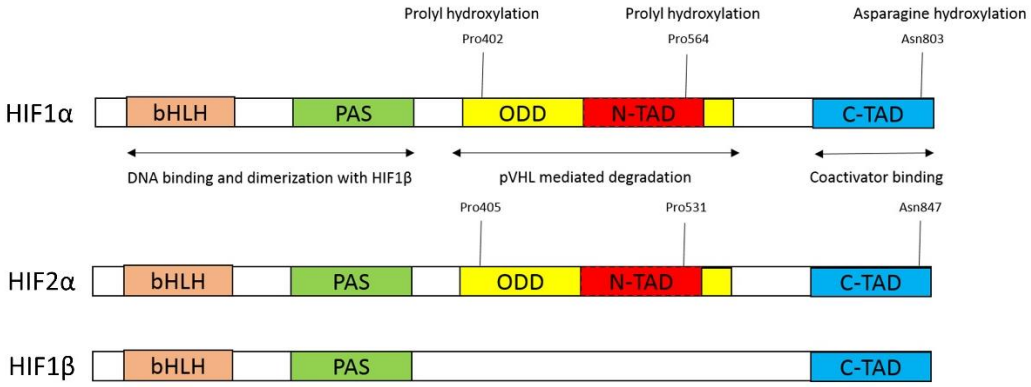

Figure 1.12. Different structures of HIF isoforms: HIF1α, HIF2α, and HIF1β. All the subunits share similar domain regions, characterised by the presence of bHLH (basic helix-loop-helix)-PAS (Per / ARNT / Sim) and C-TAD domains. The α subunits additionally possess an ODD and N-TAD domains. The Proline and Asparagine residues differ on HIF1α and HIF2α domains (Image produced using Biorender).

1.5.2 Propyl-4-hydroxylase (PHDs) and factor inhibiting HIF (FIH)

HIF1α is regulated by oxygen-dependent enzymatic hydroxylation followed by proteasomal degradation. Studies have shown that HIF1α hydroxylation is mediated by propyl-4-hydroxylase domain proteins (PHDs). So far**,** four isoforms of PHDs have been identified- PHD1, PHD2, PHD3, and PHD4. PHD 1-3 have shown abilities to hydroxylate HIF, while studies on PHD4 are inconsistent (Lieb *et al.,* 2002; Epstein *et al.,* 2001). PHD1 is localized in the nucleus and is mainly expressed in the testis and liver. PHD2 is localized in the cytoplasm and is commonly expressed in the heart, testis, brain, kidney, and liver. PHD3 is localized in both cytoplasm and nucleus. It is expressed in the heart, liver, kidney, and brain (Lieb *et al.,* 2002). All the PHDs can hydroxylate HIFα subunits, however**,** their relative activities vary with PHD2 being the primary regulator followed by PHD3 that has comparatively lesser activity and PHD1 having the least activity (Epstein *et al.,* 2001). Studies have shown

that inhibition of PHD2 is sufficient for the upregulation of HIF1α and HIF2α in various cell types. PHD1 and PHD3 have a higher affinity to HIF2α (Appelhoff *et al.,* 2004)

PHDs share a common motif, a double-stranded β-helix core fold consisting of eight β-strands. PHDs require oxygen, 2-oxoglutarate (2-OG), iron, and ascorbate as co-substrates for hydroxylation of HIF1α subunits (Bruick and McKnight, 2001). PHDs require iron for catalytic activity that binds to His1-X-Asp / Glu-Xn-His2 motif. PHDs require a reducing agent such as ascorbate to retain iron in the active site (Epstein *et al.,* 2001). Within PHDs, 2-OG undergoes decarboxylation resulting in the hydroxylation of the two specific proline residues 402 and 564 within the ODD domain of human HIF1α from proline to trans-4-hydroxyproline, with succinate and carbon dioxide formed as by-products (Chan *et al*., 2016). Hydroxylation of the proline residues of HIF1α allows it to bind to VHL (Von Hippel Lindau) tumour suppressor protein forming VCB-Cul2 E3 ligase complex. Both proline residues 402 and 564 contain a LXXLAP motif**,** and hydroxylation occurs at the fourth position of the motif. Hydroxylated HIF1α is polyubiquitinated and directed to 26S proteasome for degradation. In normoxic (ambient air) conditions, the half-life of HIF1α is <5 minutes (Huang *et al.,* 1998). As shown in Figure 1.13, under hypoxic conditions, the PHD activity is inhibited**,** resulting in stabilization and accumulation of HIF1α in the cytoplasm, which then translocates into the nucleus. HIF1α dimerizes with HIF1β in the nucleus forming HIF1 transcription factor that binds to hypoxia-response element (HRE), targeting genes that code for various cellular processes such glucose transporter-1 (GLUT1), phosphofructokinase, aldolase, pyruvate kinase, lactate dehydrogenase (LDH) and erythropoietin (EPO) (Semenza, 1996). HIF1α and HIF2α

are regulated similarly, binding to similar sites on DNA but recruit different co-activators resulting in distinct functions. HIF1α recruits co-activator complexes such as p300 / CBP and steroid-receptor co-activator (SRC), while HIF2α recruits nuclear factor-κb essential modulator (NEMO).

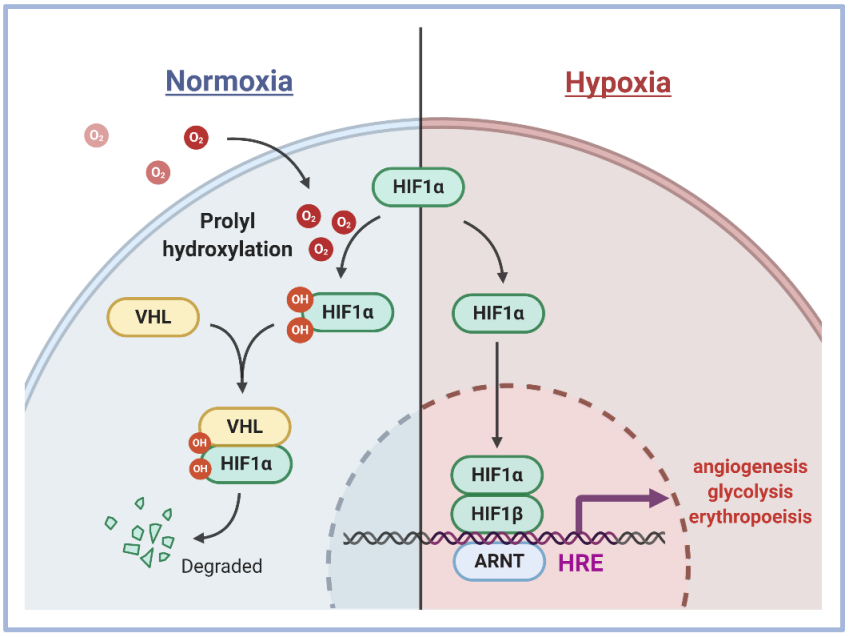

Figure 1.13. Schematic representation of the activity of PHDs on HIF1α under hypoxia versus normoxia. Under normoxia, PHDs use oxygen to hydroxylate key residues within HIF1α subunit. Hydroxylation of the ODD signals for VHL binding and ubiquitination occurs, leading to proteasomal degradation. In hypoxia, PHDs are inhibited and HIF1α is stabilized. HIF1α translocates to the nucleus and dimerizes with HIF1β, resulting in the expression of various target genes (Adapted from Karuppagounder and Ratan, 2012) (Image produced using Biorender).

As discussed above PHDs require 2-OG as a cosubstrate. As shown in Figure 1.14, 2-OG is one of the products formed of the tricarboxylic acid (TCA) cycle in the mitochondria that are transported outside the mitochondria via the malate / aspartate

shuttle. Studies have also reported that other TCA cycle intermediates such as citrate, isocitrate, succinate, fumarate, malate, oxaloacetate, and pyruvate inhibit PHDs (Isaacs *et al.,* 2005; Selak *et al.,* 2005; Dalgard *et al.,* 2004). Most consistent studies have reported fumarate and succinate to inhibit all three PHDs competitively (O' Flaherty *et al.,* 2010). This, therefore, indicates that changes in metabolic intermediates can modulate HIF1α regulation and they play a crucial role in the activity of PHDs.

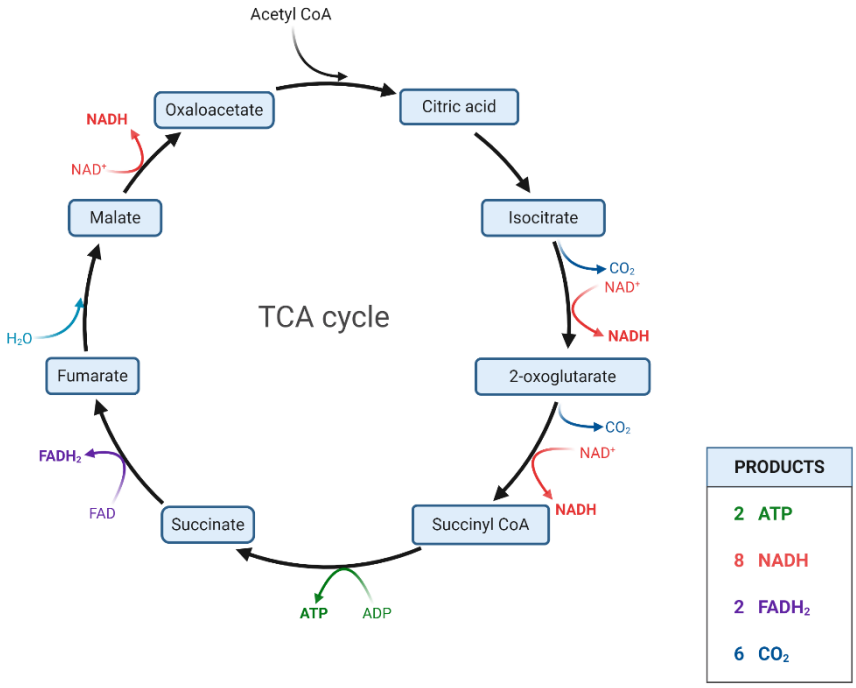

Figure 1.14. Tricarboxylic acid (TCA) cycle. The TCA cycle takes place in the mitochondria. TCA cycle is a series of chemical reactions that occur to release energy in the form of ATP through oxidation of acetyl-CoA. Glycolysis of glucose / fatty acids results in the formation of pyruvate. Pyruvate is then decarboxylated to form acetyl-CoA that enters the TCA cycle. Most importantly, 2-OG is a product formed in the TCA cycle, which is required by various dioxygenases such as PHDs in this case. 2-OG is shuttled outside the mitochondria via the malate / aspartate shuttle (Adapted from Sweetlove *et al.,* 2010) (Image produced using Biorender).

In addition to PHDs activity, another oxygen-dependent modification occurs in the C-TAD region of HIF1α by factor inhibiting HIF (FIH). FIH is localized in both cytoplasm and nucleus. FIH is highly expressed in breast, testis, ovary, and kidney (Elkins *et al.,* 2003). Some studies on rats show that it is highly distributed in the CNS (Fukuba *et al.,* 2008). Similar to PHDs, the structure consists of a jellyroll like β-barrel formed from eight β-strands and the iron-binding site contains two histidine and one carboxylate group. FIH is an asparaginyl hydroxylase, which in presence of iron, 2-OG, and oxygen**,** catalyzes the hydroxylation of asparagine residue Asn803 in the C-TAD region of HIF1α, restricting the interaction between HIF1α and co-activators. This prevents the formation of HIF1α / HIF1β heterodimer. In hypoxic conditions, FIH activity is inhibited resulting in successful interaction of HIF1α with co-activators promoting gene transcription (Elkins *et al.,* 2003).

1.5.3 Neuroprotective role of HIF during cerebral ischaemia

Studies have shown that hypoxia induces HIF1α expression and HIF DNA binding in mammalian cell lines and mice (Bergeron *et al.,* 1999). Exposure of the brain of neonatal rats to hypoxia (8% O_2) 24 h before transient MCAO reduced brain damage and increased survival rate. HIF1α was upregulated, resulting in the expression of genes such as GLUT1, enolase, VEGF (vascular endothelial growth factor), and EPO in peri-infarct penumbra within 7.5 h after focal cerebral ischaemia. This was further increased by 19 h and 24 h (Bergeron *et al.,* 1999). Exposure to hypoxia for 1, 3, or 6 h duration before focal permanent ischaemia in adult mice induced tolerance and reduced infarct size by 30%. EPO and VEGF levels were increased by 24 h after exposure to hypoxia (Bernaudin *et al.,* 2002). Zhang *et al*., (2010) demonstrated that HIF1α levels in the brain of rats with transient MCAO were

induced within 1 h with maximal expression at 12 h and decreased within 48 h showing that the window for rescuing neural cells was from 12 to 48 h. Baranova *et al.,* (2007) showed that after MCAO, there was an increase in expression of HIF1α for up to 6 h**,** followed by a decrease after 24 h. Later on, HIF1α increased after 48 h and remained for up to 8 days (Baranova *et al.,* 2007). These studies indicate that the HIF1α accumulation in the penumbra is associated with the promotion of survival of neurons in the penumbra.

Most of the pharmacological HIF1α modulators act via PHD inhibition. Currently, the PHD inhibitors that stabilise HIF1α and mimic hypoxia work by reducing Fe^{2+} availability (iron chelators), introducing metal ions that compete with Fe^{2+}, or 2-OG analogs. Iron chelators are small molecules that bind to iron and reduce the amount of Fe^{2+} available for PHD mediated HIF1α hydroxylation. Desferrioxamine (DFO) is an iron chelator and Cobalt chloride ($CoCl_2$) competes with Fe^{2+}, resulting in reduced Fe^{2+} available for PHD mediated HIFα hydroxylation. Dimethyloxalylglycine (DMOG) and 3,4-dihydroxybenzoic acid (DHB) are 2-OG analogs, which compete with 2-OG and inhibit PHD activity (Davis *et al*., 2019). Table 1.6 summarizes the *in vivo* and *in vitro* studies that have explored the neuroprotective effects of DFO, $CoCl_2$, DMOG, and DHB against cerebral ischaemia.

All the studies indicate that HIF1α is useful for prophylaxis and treatment of ischaemic stroke, however, these PHD inhibitors are not safe for clinical use. Iron chelators (DFO, $CoCl_2$) reduce Fe^{2+} levels and can deplete iron stores leading to anaemia (Ferriero *et al.,* 2005). The 2-OG analogs (DMOG, DHB) can interfere with

other 2-OG dependent dioxygenases such as collagen prolyl-hydroxylase and citric acid cycle-derived α-ketoglutarate dehydrogenase (Ogle *et al.,* 2012). In addition, these PHD inhibitors also have additional mechanisms of action such as anti-oxidant effect, and it is difficult to conclude whether their effectiveness solely depends on HIF1α activation. Hence it is important for further research on specific inhibitors PHD inhibitors that primarily upregulate HIF1α and have an effect in the brain without interfering with other enzymatic reactions in the body.

Table 1.6. **Table summarizing the *in vivo* and *in vitro* studies that have explored the neuroprotective effects of DFO, $CoCl_2$, DMOG, and DHB against cerebral ischaemia.**

Study	Time of administration	Stroke model	Outcome
		DFO	
Zaman *et al*., 1999	Immediately or for up to 10 h after HCA (Homocysteic acid)	Glutathione depletion (Primary cortical rat neurons)	DFO (100μM) protected neurons from glutathione depletion and oxidative stress-induced cell death. Enhance DNA binding of HIF-1 and transcription of EPO

Bergeron *et al*., 2000	24 h before ligation	Unilateral carotid artery ligation (Sprague-Dawley rats)	Significant reduction in infarct size (~40%) in DFO (200mg / kg) pre-treated group. DFO increased the level of HIF1α protein.
Prass *et al*., 2002	Preconditioning with DFO 72 h before 90 mins MCAO or OGD	MCAO (Wistar rats) OGD (primary cortical rat neurons)	Significant reduction in infarct size (~40%) in DFO (150μM / L) pre-treated group. DFO protected neurons from OGD induced cell death.
Mu *et al*., 2005	Immediately after MCAO	MCAO (Sprague-Dawley rats)	Significant reduction in infarct size (~40%) in DFO treated group. Increased expression of HIF1α and EPO.
Siddiq *et al*., 2005	6 h before glutamate treatment	Glutamate mediated excitotoxicity (primary cortical rat neurons)	100μM DFO protected cells from glutamate toxicity. 100μM DFO stabilised HIF1α.
Hamrick *et al*., 2005	1 h before and during OGD	OGD model (primary rat hippocampal neurons)	Pre-treatment with 10 mM / L DFO decreased OGD induced cell death by 45% compared to the control. The protection conferred by

			DFO diminished upon anti-HIF1α transfection.
Freret *et al*., 2006	24 h after 60 minutes MCAO	MCAO (Sprague-Dawley rats)	Improved behavioural outcomes post MCAO.
Jones *et al*., 2008	24 h before MCAO	MCAO (Sprague-Dawley rats)	Preconditioning with DFO (200 mg / kg) before MCAO, resulted in reduced infarct size compared to control.
Li *et al*., 2008	Preconditioning with DFO 36 h before 60 mins MCAO	MCAO (Sprague-Dawley rats)	Significant reduction in infarct size (~28%) in DFO treated group. Neurological function improved on the second day after administration of DFO for up to 7 days.
Hanson *et al*., 2009	Pre-treatment with intranasal DFO 48 h before MCAO	MCAO (Sprague-Dawley rats)	Significant reduction in infarct volume (~55%) in DFO treated group.
Zhao and Rempe, 2011	Every day up to 4 weeks before MCAO	MCAO (mice)	Significant reduction in infarct volume in DFO treated group. DFO remained protective in HIF1α KO mice.

		$CoCl_2$	
Zaman *et al*., 1999	Immediately or for up to 10 h after HCA	Glutathione depletion (Primary cortical rat neurons)	$CoCl_2$ (>200µM) protected neurons from glutathione depletion and oxidative stress-induced cell death. Elevated HIF1α protein expression
Bergeron *et al*., 2000	24 h before ligation	Unilateral carotid artery ligation (Sprague-Dawley rats)	Significant reduction in infarct size (~75%) in $CoCl_2$ pre-treated group. $CoCl_2$ increased the level of HIF1α protein.
Jones and Bergeron, 2001	24 h before MCAO	MCAO (Sprague-Dawley rats)	Preconditioning with $CoCl_2$ (60 mg / kg) before MCAO, resulted in 76% brain protection, compared to control. $CoCl_2$ did not alter expression of HIF-1 target genes.
Jones *et al*., 2008	24 h before MCAO	MCAO (Sprague-Dawley rats)	Preconditioning with $CoCl_2$ (60 mg / kg) before MCAO, resulted in reduced infarct size compared to control.

		DMOG	
Ogle *et al*., 2012	24 h before OGD 24 h before 30-60 mins MCAO	OGD (primary rat cortical neurons) MCAO (adult mice)	In primary neurons, DMOG reduced OGD induced cell death and upregulated HIF1α. In adult mice, the infarct volume significantly decreased 12 h after MCAO.
Nagel *et al*., 2011	Multiple times before MCAO and one time after MCAO	Permanent and transient MCAO (wistar rats)	DMOG pre- and post-treatment reduced the infarct size and improved behaviour. Associated with increased mRNA and protein levels of VEGF and eNOS (endothelial nitric oxide synthase).
		DHB	
Siddiq *et al*., 2005	6 h before MCAO	MCAO (Sprague-Dawley rats)	DHB pre-treatment reduced infarct volume compared to control. Associated with HIF1α upregulation.

Several studies have evaluated the effects of some novel PHD inhibitors, which are small molecule, highly potent and selective in *in vivo* and *in vitro* models of

ischaemia. *In vitro* treatment of primary murine astrocytes and murine cerebrovascular endothelial cell line bEnd.3 with FG4497 was seen to stabilize HIF1α. FG4497 exceeded the capacity of DMOG to protect HIF1α against proteolytic degradation. FG4497 treated endothelial cell line bEnd.3 sustained the membrane localization of ZO-1 and occludin that is otherwise disrupted in ischaemia. Following FG4497 treatment, mRNA expression of VEGF and EPO significantly increased. Pre-treatment of mice with FG4497, 6 h before MCAO significantly reduced the infarct size and decreased formation of oedema 24 h after reperfusion. Post-treatment with FG4497 was also seen to improve recovery from ischaemic stroke. Pre-treatment of mouse hippocampal neuronal HT-22 cells with FG4497 followed by OGD (1% O_2) showed an improved survival rate of neurons (Reischl *et al.,* 2014). Similarly preconditioning of male rats with oral GSK360A**,** 18 h before transient MCAO showed improved long-term outcomes such as sensory, motor, and cognitive outcomes as well as reduced brain injury. Similarly, GSK360A was associated with increased EPO and VEGF mRNA and plasma levels (Zhou *et al.,* 2017). Studies have also shown that preconditioning with selective PHD inhibitor IOX3, 24 h before ischaemic insult**,** protects the brain from ischaemic damage at lower doses. Higher doses (60 mg / kg) however did not exhibit protective effects. EPO was seen as the main mediator that resulted in the exhibition of protective effect. Pre-treatment with IOX3 on RBE4 cells was seen to prevent barrier disruption from subsequent OGD (1% O_2) (Chen *et al.,* 2014). Another novel PHD inhibitor, TM6008 decreased hypoxia-induced cell death and upregulated HIF1α in SHSY-5Y cells (Kontani *et al*., 2013). These studies indicate that pharmacological preconditioning with selective PHD inhibitors is a promising strategy for the treatment of ischaemic stroke and further research is highly beneficial.

Studies have shown that in mice with neuron-specific KO of HIF1α subjected to transient focal cerebral ischaemia, there was increased tissue damage and mortality (Baranova *et al.,* 2007). Preconditioning mice with PHD inhibitors that increased HIF1α in the brain had a neuroprotective effect, however, a similar effect was seen in neuron-specific HIF1α KO mice indicating there might be other mechanisms rather than HIF1α activation (Baranova *et al.,* 2007). In neuron-specific HIF1α KO mice brain, there was an increased expression of HIF2α and EPO, which may have played an important role in neuroprotection (Baranova *et al.,* 2007). This indicates that PHD inhibition is not equal to HIF activation and HIF is just one of the many growing substrates known to be modulated via PHD inhibition (Baranova *et al.,* 2007). Another study showed that neuron-specific KO mice deficient for HIF1α and HIF2α subjected to 60 minutes or 30 minutes of MCAO followed by 24-72 h of reperfusion, showed no significant alteration in infarct and oedema size in comparison to control, suggesting both HIFα subunit might compensate for each other (Barteczek *et al*., 2017). In HIF1α / HIF2α double KO mice subjected to 30 minutes MCAO, global cell death, and oedema was reduced upon 24 h reperfusion but not 72 h reperfusion. There was also reduced expression of anti-survival genes such as BCL2 / adenovirus E1B 19 kDa protein-interacting protein 3 (Bnip3), Bnip3-like (Bnip3L), and Phorbol-12-Myristate-13-Acetate-Induced Protein 1 (Pmaip1). This shows that in HIF1α / HIF2α- deficient mice, there might be protection from early acute neuronal cell death and neurological impairment indicating the benefit of HIF pathway inhibition in neurons in very acute phase after ischaemic stroke (Barteczek *et al*., 2017). Similar results were observed when methyoxyestradiol (2-ME2), a HIF1α inhibitor was tested in rat models of global cerebral ischaemia, where lower

cell survival rate was observed in rats treated with 2-ME2 (Zhou *et al.,* 2008). YC-1 (3-(5′-Hydroxymethyl-2′-furyl)-1-benzyl indazole) another inhibitor of HIF1α resulted in suppression of expression of VEGF, EPO, and GLUT3 (glucose transporter 3) in the MCAO mice. The study indicated that suppression of HIF1α prevented BBB damage during cerebral ischaemia**,** however**,** there was an increase in brain infarct volume and mortality (Yan *et al.,* 2011). These results contradict other studies by suggesting that HIF1α resulted in BBB damage, however**,** there could be other mechanisms resulting in the damage as YC-1 is not a specific inhibitor of HIF1α.

HIFα accumulation in the ischaemic brain triggers the expression of several genes that exhibit a neuroprotective effect during ischaemia. Below are discussed the most commonly activated genes by HIF and their mechanisms for neuroprotection in ischaemic stroke.

EPO is synthesized primarily in the kidney and liver with the main role of erythropoiesis. EPO has a neuroprotective effect and it is stipulated that EPO exerts its effects by direct and indirect mechanisms. The direct mechanism involves inhibition of apoptosis by maintaining expression of Bcl-2 and Bcl-xL or by inactivation of caspases (Li *et al.,* 2007). EPO is also seen to decrease glutamate toxicity, reduce inflammation by decreasing the production of pro-inflammatory cytokines such as TNFα, IL6, and mitogen-activated protein (MAP-1), decrease NO mediated injury and reduce oxidative stress (Villa *et al.,* 2003). EPO may also stimulate angiogenesis in the brain increasing blood and oxygen flow to the brain (Marti *et al.,* 2000; Li *et al.,* 2007).

Vascular endothelium growth factor (VEGF) and VEGF receptors (VEGF-R) are upregulated by increased transcription of HIF1. VEGF and VEGF-R mediate angiogenesis in the ischaemic boundary resulting in increased blood flow and metabolism. VEGF also causes neurogenesis in the SVZ (subventricular zone) region. VEGF is seen to be involved in both angiogenesis and neurogenesis in ischaemic brain (Wang *et al.,* 2004). HIF1 also upregulates stromal-derived factor-1 (SDF-1) and chemokine-receptor type-4 (CXCR4). SDF-1 interacts with CXCR4 receptors in neuroblasts and attracts them to the ischaemic boundary. HIF1 transcription factor also targets for increased expression of BDNF and glial-derived neurotrophic factor (GDNF) (Wang *et al.,* 2004). BDNF is seen to exhibit anti-apoptotic and anti-inflammatory effects during ischaemia. BNDF also promotes neurogenesis (Wang *et al.,* 2004). GDNF is also seen to have neuroprotective and neurogenerative effects during ischaemia. GDNF may also exhibit anti-apoptotic properties by inactivation of caspases-3 (Harvey *et al.,* 2005).

HIF1 upregulation is also seen to have resulted in the upregulation of **glucose transporters such as GLUT1, GLUT3** as well as enzymes such **as aldolase, enolase, LDH, pyruvate Dehydrogenase Kinase 1 (PDK-1), and glucophosphate isomerase.** Hypoxia results in glucose deprivation in the brain during which astrocytes enhance glycolysis and release lactate (Semenza *et al.,* 1996). Lactate is used as a primary source of energy. HIF1 activation also upregulates genes involved in the anaerobic glycolytic pathway, for example, LDH that catalyzes the conversion of pyruvate to lactate (Semenza *et al.,* 1996). Therefore**,** during hypoxia, HIF1

increases glucose transport via GLUT receptors and anaerobic glycolysis by upregulation of glycolytic enzymes to provide active neurons with lactate and maintaining energy homeostasis.

1.5.4 Detrimental role of HIF during cerebral ischaemia

In contrast to the neuroprotective role of HIF1, some studies have also suggested that HIF1 may mediate apoptosis during hypoxia. HIF1 accumulation resulted in the induction of p53 and p21 that stimulates apoptosis in embryonic stem cells in hypoxia (<0.5% O_2) (Greijer, 2004). *In vitro* studies on primary cortical neurons showed HIF1α signalling during ischaemia stimulated apoptosis (Halterman *et al.,* 1999). HIF1α upregulation induces apoptosis by stabilising tumour suppressor gene p53 and also by the increased expression of pro-apoptotic family members such as BNIP3, Nip-like protein X (NIX), and NOXA (Chen *et al.,* 2009). Stabilising tumour suppressor p53 can induce Bax and Bak proteins that regulate the release of cytochrome C into the cytoplasm that binds to the apoptotic protease activating factors (Apaf-1). Apaf-1 activates caspase 9, which in turn cleaves caspases 3 and 7 leading to apoptosis (Figure 1.14) (Greijer, 2004). Studies have shown that inhibition of HIF1α by 2-ME2 and D609 (tricyclodecan-9-yl-xanthogenate) decreased expression of VEGF and BNIP3 resulting in neuroprotection. Studies have shown that HIF1α upregulates BNIP3 resulting in mitochondrial dysfunction, membrane depolarization, and MPTP opening (Chen *et al.,* 2007; Yeh *et al.,* 2007; Yeh *et al.,* 2011). A study by Baranova *et al., (*2007), showed that neuron-specific ablation of HIF1α in rats reduced survival rate and increased tissue damage when subjected to focal MCAO for 30 minutes. In contrast studies by Helton *et al.,*2005 showed that there was reduced ischaemic damage and increased survival rate in neuron-specific HIF1α KO rats that were subjected to bilateral common carotid artery occlusion

(BCCAO) for 75 minutes. This correlated with the notion that in mild hypoxia HIF1α induced cell survival by upregulation of genes such as EPO, GLUT1, and VEGF whereas in severe hypoxia, HIF1α induced apoptosis by activation of genes such as BNIP3, BNIP3L, and p53 stabilization. This shows that the effects of HIF1α depend on various factors such as the severity of ischaemia, time subjected to ischaemic insult, and the type of cell (Chen *et al.,* 2009).

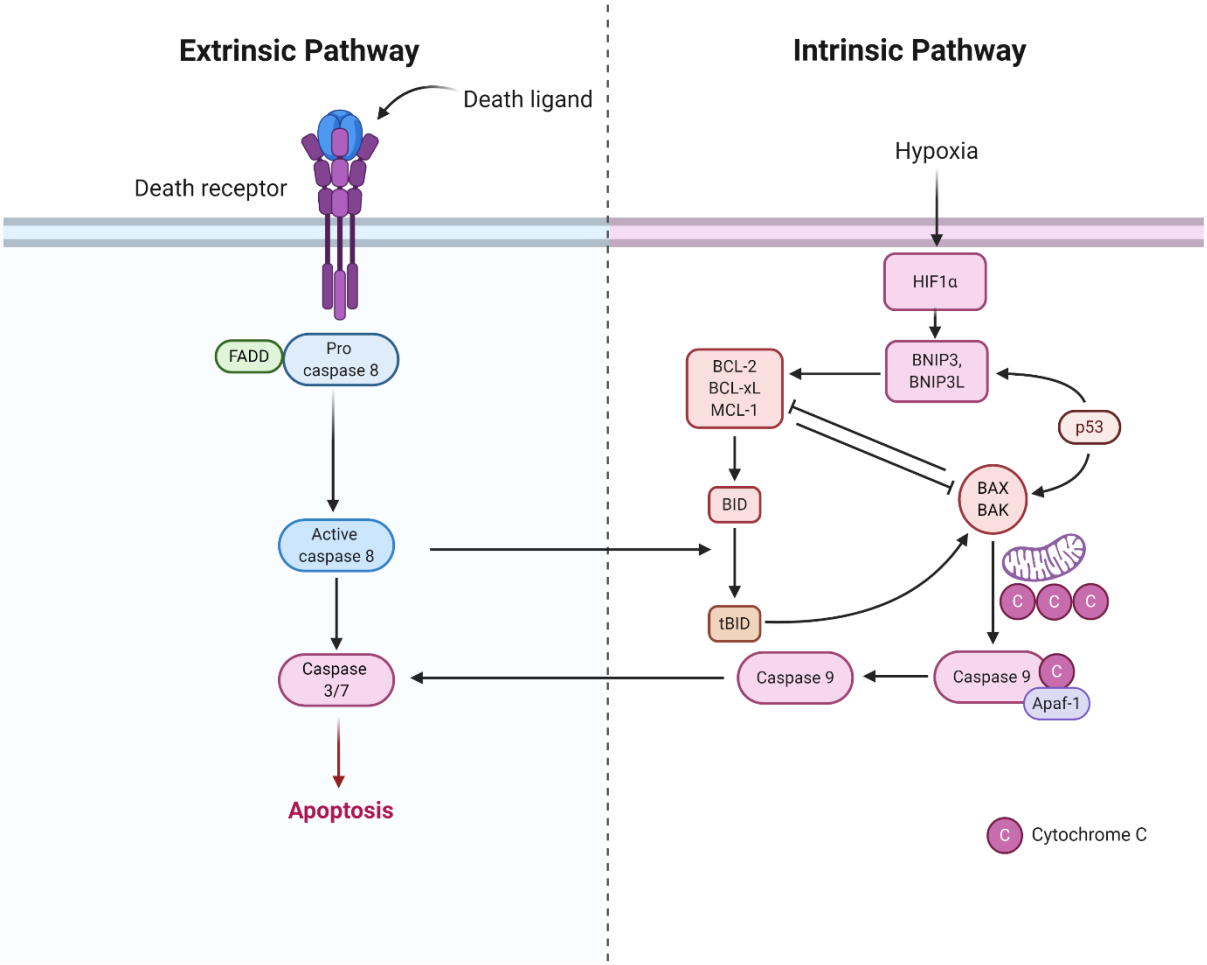

Figure 1.15. Schematic representation of the apoptosis pathway in hypoxia.

Hypoxia leads to stabilisation of HIF1α that results in stabilisation of p53 leading to the expression of proteins such as Bnip3, Bnip3L, Bax, and Bak that regulate the release of cytochrome C into the cytoplasm. Cytochrome C binds to Apaf-1. Apaf-1 activates caspase 9, which in turn cleaves caspases 3 and 7 leading to apoptosis. FADD (Fas Associated Via Death Domain), Bak (Bcl-2 antagonist / killer 1), MCL-1 (myeloid cell leukemia 1) (Image produced using Biorender).

Studies have shown that HIF1 results in increased vascular permeability due to increased expression of VEGF and MMPs. MMPs disrupt the BBB by disturbing the tight junction and cytoplasmic accessory proteins resulting in gap formation, leucocyte infiltration, and brain oedema (Balabh *et al.,* 2004; Lakhan *et al.,* 2013). Hypoxia resulted in increased BBB permeability and a study by Yang *et al.,* 2015, has shown that minocycline reduced BBB permeability *in vivo* and *in vitro*. Minocycline inhibits HIF1α by mechanisms involving the upregulation of p53, suppressing the AKT / mTOR / p70S6K / 4E-BP1 signalling pathway (Kachoie *et al.,* 2015) and increased expression of PHD2 resulting in proteasomal degradation of HIF1α (Li *et al.,* 2014). Studies have shown that increased levels of HIF1α in the brain of dystrophic mdx mice resulted in VEGF upregulation and ZO-1 phosphorylation leading to re-arrangement of the BBB and increasing BBB permeability (Nico *et al.,* 2007). A study by Higashida *et al.,* 2011 also supported the notion that HIF1α played an important role in BBB disruption and oedema formation in the brain via pathways involving expression of aquaporin-4 (AQP-4) and MMP-9. Studies have also shown that inhibition of HIF1α by YC-1 or 2ME-2 (2-methoxyestradiol) prevented BBB damage and oedema formation whereas the upregulation of HIF1α by DMOG ameliorated BBB permeability (Yeh *et al.,* 2007; Engelhardt *et al.,* 2014). In contrast, recent studies have shown that FG4497, a PHD2 inhibitor upregulated HIF1α but the preconditioned endothelial cells sustained the membrane localization of ZO-1 and occludin that are otherwise disrupted in ischaemia (Reischl *et al.,* 2014). Pre-treatment with PHD-inhibitor, IOX3 on RBE4 cells was seen to prevent barrier disruption from subsequent OGD (Chen *et al.,* 2014). This, therefore, indicates that HIF1 may have different effects in different types of cells resulting in different outcomes during ischaemia and BBB permeability.

Different types of genes are activated in different cells and it is important to study the effect HIF1 upregulation would have on ischaemia. There are beneficial and detrimental effects of PHD inhibitors, however**,** further research is required to determine the place PHD inhibitors have for the treatment of ischaemic stroke.

1.6 Aims and objectives

Modulating endogenous protective pathways such as HIF1 offers the hope in ischaemic stroke therapies, in contrast to majority of the neuroprotective targeting single molecules. The main research question this thesis aimed to address is whether modulation of HIF1 pathways would provide protective in *in vitro* models ischaemia. In addition, this research aimed to understand the downstream mechanisms and develop a suitable treatment protocol that can translate into clinical success. It is hypothesized that modulating the HIF1 pathway would provide neuroprotection via endogenous protective pathways during ischaemia.

The main aims of this thesis were as follows:

1. To develop suitable *in vitro* model of ischaemia for subsequent studies
2. To study the safety and efficacy of novel, small molecule, orally active PHD inhibitors on the *in vitro* models of ischaemia
3. To study the roles of astrocytes in cerebral ischaemia *in vitro*

The objectives of each chapter in this thesis were:

Chapter 3: *In vitro* PC12 cells and primary rat neuronal models of ischaemia

In this chapter, the effects of oxygen and / or glucose deprivation were evaluated on neuronal viability, HIF1α and HIF2α expression and downstream pathways. These studies were performed to characterise the validate *in vitro* ischaemia models for further studies.

Chapter 4: Characterizing ischaemic tolerance in PC12 cells and primary rat neurons

In this chapter, the effectiveness of preconditioning with oxygen and / or glucose deprivation was investigated against severe OGD insults in PC12 cells and primary rat neurons in this chapter. The underlying mechanism and the role of glucose were evaluated on ischaemic tolerance.

Chapter 5: Characterizing the effects of novel prolyl hydroxylase (PHD) inhibitors in PC12 cells and primary neurons

In this chapter, the safety and effectiveness of novel PHD inhibitors were investigated against OGD insults in PC12 cells and primary rat neurons. The effects of these PHD inhibitors on expression of HIF1α, HIF2α proteins, and their downstream genes and autophagic proteins were evaluated to understand their molecular mechanisms.

Chapter 6: **Astrocytes modulated protection against ischaemic injury in primary rat neurons**

In this chapter, the effects of oxygen and / or glucose deprivation were evaluated on astrocyte viability, HIF1α and HIF2α expression and downstream pathways. These studies were performed to validate suitable *in vitro* ischaemia models for further studies. Astrocytes are known to secrete several neuroprotective or neurotoxic molecules, therefore the effectiveness of astrocyte conditioned media (ACM) was investigated on the primary neuronal model of ischaemia.

Chapter 2.

Materials and methods

2.1 Materials and equipment

Table 2.1. Table of material and company / country they were obtained from

Company name	Materials
Sigma Aldrich, UK	Rat adrenal pheochromocytoma (PC12) cells (cat#88022401), Dulbecco's Modified Eagle's Media (DMEM) containing high glucose (4.5 g / L) (cat#D5671), Dulbecco's Phosphate buffered saline (D-PBS) (cat#D8537), Fetal bovine serum (FBS) (cat#F7524), inactivated horse serum (HS) (cat#H1270), poly-D-lysine (PDL, 50x) (cat#A-003-M), trypsin (50x) (cat#T1426), Deoxyribonuclease from Bovine pancreas (100x) (cat#DN25), sterile dimethyl sulfoxide (cat#D2650), dimethyl sulfoxide (cat#246855), trypan blue, 3-(4, 5-dimethylthiazol-2-yl)-2, 5-diphenyltetrazolium bromide (MTT), dimethyl sulfoxide (DMSO), Trypan Blue (cat#93595), Dithiothreitol (DTT) (cat#43819), Protease inhibitor cocktail (cat#P8340), 10x RIPA buffer (radio-immunoprecipitation assay) (cat#20188), phenylmethylsulfonyl fluoride (PMSF) (cat#10837091001), Tween-20 (cat#P1379), Sodium chloride (cat#S9625), Tris-base (cat#TRIS-RO), Glycine (cat#G8898), Sodium-dodecyl sulphate (SDS) (cat#L3771), Rabbit polyclonal anti-Lc3b (cat#L8918), Bovine serum albumin (BSA) (cat#A7030), Triton X-100

	(cat#T9284), paraformaldehyde (cat#158127), goat anti-rabbit FITC conjugated (cat#F7367), goat anti-mouse FITC conjugated (cat#F5387), DMOG (cat#D3695), Rapamycin (cat#37094)
Gibco (Invitrogen) by Thermofisher Scientific, UK	Glucose-free Dulbecco's modified eagle media (cat#A1443001), penicillin - streptomycin (10000 units / mL & 10000 µg / mL) (cat#10378016), Neurobasal-A media (no L-glutamine) (cat#12349015), Neurobasal-A media (no D-glucose, no sodium pyruvate) (cat#A2477501), B-27 supplement serum-free (50x) (cat#12587001), Hank's balanced salt solution with Ca^{2+}, Mg^{2+} and no phenol red (HBSS) (cat#88284), L-glutamine 200Mm (cat#25030081), TrypLE express (no phenol red) (cat#12604013), 0.22 µm syringe filter (cat#SLGSV255F)
Lonza Biotech, USA	Sodium pyruvate 100Mm (cat#BE-13115E)
Cayman Chemicals, UK	FG4592 (Roxadustat) (cat#CAY15294)
Schofield Group, Oxford University	FG4592, FG2216, Bayer85-3934, GSK1278863
Merck Millipore, USA	Guava cell dispersal reagent (cat#4500-0050), Guava nexin kit (cat#4500-0455), Guava instrument cleaning fluid (part#4200-0140), Guava Easy check kit (part#4500-0025)
Promega, UK	CytoTox 96 Nonradioactive cytotoxicity assay kit (cat#G1780)

Bioline Reagents Ltd, UK	Tetro cDNA synthesis kit (cat#BIO6043), SensiFAST™ SYBR Hi-ROX kit (cat#BIO73005)
Qiagen, UK	RNeasy Plus Mini kit (cat#74034), Nuclease-free water (cat#1291)
Eurofin genomics, UK	All primers (forward and backward) for qRT-PCR
Bio-Rad Laboratories Inc, UK	4 x Laemmli sample buffer (cat#1610747), 4-15% Mini-PROTEAN TGX Precast polyacrylamide gel (cat#4561086EU), fat-free skimmed milk powder (cat#1706404XTU), Precision plus Protein Dual Colour Standard (cat#1610374), Extra-thick blot filter paper (cat#1703965), 10x Tris / Glycine / SDS running buffer (cat#1610732), 10x Tris / Glycine transfer buffer (cat#1610771)
Thermofisher, UK	Pierce bicinchoninic acid (BCA) kit (cat#23225), Pierce ECL western blotting substrate (cat#32132)
VWR, UK	Amersham™ Protran® Premium nitrocellulose blotting membranes (cat#10600045), phosphate-buffered saline (PBS) (cat#444057Y)
Novus Biologics, UK	Rabbit polyclonal anti-p62 (SQSTM1), Mouse monoclonal anti- Hif1α (cat#NB100-105)
R&D Systems, UK	Mouse monoclonal anti-Hif2α (cat#MAB2886)
Cell signalling technology, UK	Rabbit polyclonal anti-Beclin-1 (cat#3738S)
Abcam, UK	Rabbit polyclonal anti- β-actin (cat#ab8227), Rabbit polyclonal anti-Map2 (cat#ab5392)

Agilent (DAKO), UK	Goat anti-rabbit HRP- conjugated (cat#P044801), Goat anti-mouse HRP- conjugated (act#P044802), Rabbit polyclonal anti-Gfap (cat#Z0334)
Vector labs, UK	Vectashield with DAPI (cat#H-1200)
Biolegend, USA	Mouse monoclonal anti-Tubulin β 3 (clone Tuj1) (cat#801201)
Falcon, Corning Brand, USA	Sterile cell scraper (cat#353086), 70 µm cell strainer (cat#352350), 15 mL centrifuge tube (cat#352196), 50 mL centrifuge tube (cat#352070)
Greiner Bio-One, UK	1.5 mL eppendorf tubes (cat#717201), sterile 96- (cat#650101), 24- (cat#657824) and 6- (cat#657160) well plates, 35- (cat#627979), 100- mm (cat#624970) cell culture dishes, 5 mL sterile pipettes (cat#606107), 10 mL sterile pipettes (cat#607107), 25 mL sterile pipettes (cat#760107)
Starlab, USA	TipOne 10 (cat#S1111-3000), 200 (cat#S1111-1006) and 1000 µL (cat#S111-6000) tips
Sarstedt AG, Germany	T25 (cat#83310002), T75 (cat#833911002), and T175 (cat#833912502) cell culture vessel
Hitachi, Tokyo, Japan	Hitachi Koki 20 mL ultracentrifuge tubes (part#90592000)
Malvern Panalytical, UK	Folded capillary zeta cell (part#DTS1070)

Table 2.2. Table of equipment and company / country they were obtained from

Company	Equipment
VELP Scientific, Inc, USA	ARE Heating magnetic Stirrer Classic vortex mixer (part#F202A0173)
Star Lab, UK	Dry bath system Dual Block (part#N2400-4002)
Bio-Rad Laboratories Inc, UK	Transblot SD Semi-Dry transfer cell (part#1703940), Mini- PROTEAN Tetra system (part#1658001), PowerPac Basic Powersupply (part#1645050), ChemiDoc MP imaging system (part#1701402)
Fisher Scientific, Thermofisher, UK	Electrophoresis power supply 150W (cat#EC1000XL2), Fisherbrand Seastar Digital Orbital Shaker (cat#12846016), NanoDrop 1000 spectrophotometer (cat#1318796), GeneAmp PCR system 2700 (cat#15860383), Techne Prime Pro 48 Real-Time qPCR machine (cat#PRIMEPRO48) (data acquired by Prime Pro 48 software and analysed using Prime Pro 48 study software), MAX Q 4450 Benchtop Orbital shaker (cat#SHKE4450)
Ohaus Corporation, USA	Ohaus Adventurer analytical balance (part#AX224)
Sciquip, UK	Sigma 1-14K microcentrifuge (part#10020)
Ruskinn Technologies, UK	Purpose-built INVIVO$_2$ 400 humidified hypoxia workstation (part#UM037)

Wolflabs, UK	Panasonic Incusafe cell culture CO_2 incubator (part#MCO-170AIC), Faster Bio48 biological safety cabinet (part#BIO-48), Clifton NE1-14 unstirred water bath (part#10031816)
Olympus Lifesciences, USA	Olympus CKX31 inverted microscope (part#48692)
MSE, East Sussex, UK	Harrier 18 / 80R centrifuge (part#MSB080)
Tecan, Switzerland	Tecan Infinite M200 PRO microplate reader using i-control 1.9 software (part#I200PRO)
Merck Millipore, USA	Guava easyCyte flow cytometer (part#0500-4020) using Guava data acquisition and analysis software
Nikon, Tokyo, Japan	Nikon Eclipse 80i fluorescence microscope connected with Hamamatsu (C4742-95) digital camera, Nikon High-pressure mercury lamp power supply, Hamamatsu camera controller using NIS-Element BR 3.22.14 software
Hitachi, Tokyo, Japan	Hitachi Micro Ultracentrifuge CS 150NX (part#91109201)
Malvern Panalytical, UK	Malvern Zetasizer Nano ZS

2.2 Cell cultures

2.2.1 Ethical permissions

All animals used in these experiments were humanely killed under Schedule 1 according to the Animals Scientific Procedures Act (1986) (ASPA). The work is exempt from the need for Animal Welfare and Ethical Review Board (AWERB) approval under the ASPA and all subsequent amendments under both the UK and

European Law. All animals used in this study have been treated in accordance with ASPA guidelines.

2.2.2 PC12 cell culture

Thawing and freezing PC12 cells

PC12 cells were obtained from Sigma-Aldrich, UK in a frozen state in cryopreservation media containing 10% DMSO and stored at -80^{o}C. As shown in Figure 2.1, the cryovials was quickly thawed in a 37^{o}C water bath. The cells were transferred into a 15 mL falcon containing 10 mL of 'complete' PC12 cell media [high-glucose DMEM (Dulbecco's Modified Eagle's Media with 4,500 mg / ml glucose, L-glutamine and sodium bicarbonate, without pyruvate) supplemented with 5% fetal bovine serum (FBS), 5% horse serum (HS) and 1% penicillin-streptomycin (PS)] and mixed well by pipetting (trituration). The cells were then centrifuged at 100 rcf (relative centrifugal force) for 5 minutes. The supernatant was discarded, the cells were re-suspended in fresh complete media and the cell suspension was transferred into a T25 flask (passage 1: P1). The PC12 cells were incubated at 37^{o}C in a humidified atmosphere of 5% CO_2 in air and examined every day. The culture media (approximately two-thirds) was renewed every 2-3 days. Upon ~80% coverage, the cells were passaged. The cell suspension was transferred into a 15 mL falcon tube and centrifuged at 100 rcf for 5 minutes. Two-thirds of the media was discarded and fresh media (approximately 10 mL) was added. The cell suspension was transferred into 4 x T25 flasks (P2). Upon ~80% coverage, following the same procedure, the cells were passaged further. Cultures at P3 were frozen (procedure detailed below)

or used for experiments. The PC12 cells were used for experiments up to a maximum of P8.

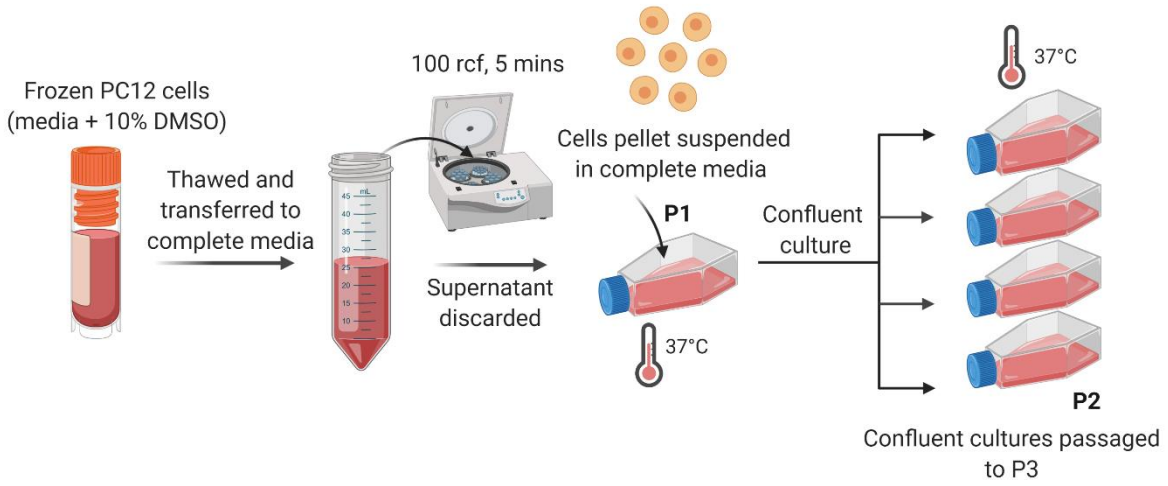

Figure 2.1. Diagrammatic representation of thawing and culturing PC12 cells. (Image produced using Biorender).

Cryopreservation the PC12 cells for future use: cell suspension was centrifuged at 100 rcf for 5 minutes. Cryopreservation media containing 10 % sterile DMSO in complete media was prepared. DMSO is a cytoprotectant added to prevent the formation of intracellular and extracellular crystals during freezing. The cell pellet was suspended in the cryopreservation media (approximately 1 x10^6 cells in 1.5 mL). The suspension was triturated in cryovials and placed in a freezing container. The container was frozen at -20^{o}C for 2 h followed by -80^o C overnight and then transferred into a liquid nitrogen cylinder for long term storage.

Seeding / plating for experiments: PC12 cells were seeded (1.2 x 10^6 cells in 5 mL complete medium) in uncoated T25 flasks for protein / RNA extraction, flow cytometry, and trypan blue exclusion assays. For MTT and LDH assays, poly-D-lysine (PDL) coated 96 well plates received 1.2 x 10^4 cells per well (100 µL).

2.2.3 Poly-D-lysine (PDL) coating

PDL (0.1 mg / mL) was used to coat cell culture plates / flasks. Enough solution to cover the cell culture plates / flasks was added (1 mL per 25 cm^2 area) and left for 2 h or overnight (maximum). The solution was aspirated and the plates / flasks were washed 3 times with D-PBS. The plates / flasks were left to dry for a minimum of 2 h before introducing cells.

2.2.4 Counting cells

For all experiments, cells were counted using a Neubauer chamber. Cells were suspended in fresh cell culture media and triturated. 10 µL of the cell suspension was mixed with 10 µL 0.4 % trypan blue stain for 5 minutes. 10 µL of trypan-blue treated cell suspension was applied to each side of the Neubauer chamber and viewed under an inverted microscope. The viable (cells exhibiting bright halo under phase microscopy) were counted in each large red square (Figure 2.2). The viable cell count per mL was determined using the equation below.

$$\text{Viable cell count per mL} = \frac{\text{Number of live cells}}{\text{Number of large squares counted}} \times \text{dilution factor} \times 10{,}000$$

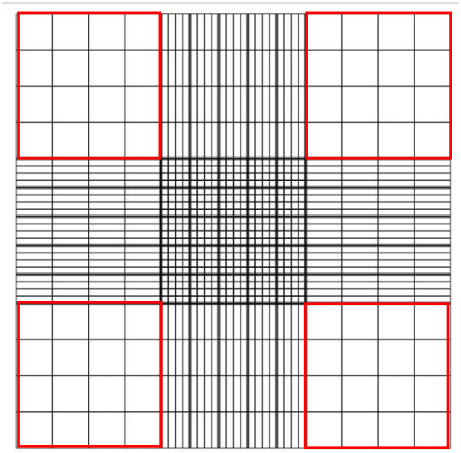

Figure 2.2. Neubauer chamber. The viable were counted in each large red square under phase microscopy.

2.2.5 Primary rat cortical neuronal cultures

Rat embryos E17-18 were removed from time-mated Sprague-Dawley pregnant rat. The rat embryos were removed and placed in ice-cold Hank's balanced salt solution (HBSS) in a petri dish. The embryos were removed from their placental sac and each embryo was decapitated at the head / neck junction. The head was placed in ice-cold HBSS in a new petri dish. The embryonic brains were removed from the head cavity. Brainstem, cerebellar tissue, meninges then hippocampus (darker, C-shaped region) were discarded. The cortices were collected in a fresh Petri dish containing ice-cold HBSS, then dissociated in another fresh Petri (1 mL cold Neurobasal media) using a scalpel. 1 mL of Neurobasal media containing 0.05% trypsin and 100 µg / mL deoxyribonuclease (DNAse) was prepared in a 15 mL falcon tube and warmed for 15 minutes at 37^{o}C. The minced cortices were transferred into the falcon tube, triturated using a pipette (20-30 times), and incubated for 15 minutes at 37^{o}C. Thereafter, 6 mL pre-heated (37^{o}C) Neurobasal media containing 10 % FBS was added to inactivate the trypsin. The cortices were further triturated (20-30 times). The suspension was centrifuged at 200 rcf for 5 minutes, the supernatant

was discarded and, 10 mL of 'complete' Neurobasal media (Neurobasal media supplemented with 2% B27 serum-free supplement, 2mM L-glutamine and 1% PS) was added. The suspension was sieved through a 70µm cell strainer. The cells were counted using a Neubauer chamber. The cells were plated onto PDL coated plates at densities of 1.5 x 10^6 cells in 5 mL (T25 flasks for protein / RNA extraction), 3 x 10^4 cells / 100 µL (96 well plates for MTT / LDH assay) and 1.5 x 10^5 cells / 300 µL (24 well plates for immunofluorescence (IF) staining) and placed in an incubator with a humidified atmosphere containing 5% CO_2 at 37ºC (Figure 2.3). The cultures were examined and 50% media change with fresh media was performed on DIV (days *in vitro*) 1, thereafter the 50% media change was performed every 2-3 days until confluency. Typically, experiments were performed at DIV 9-14.

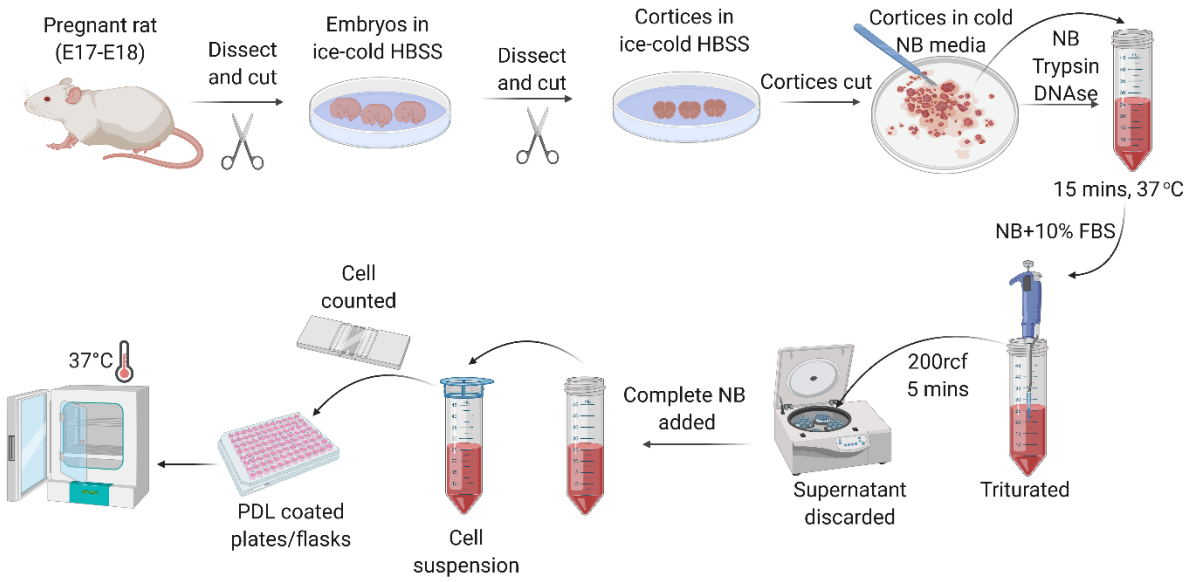

Figure 2.3. Primary rat cortical neuronal culture. (Image produced using Biorender).

2.2.6 High purity primary rat cortical astrocytes

Dissection media (48.25 mL HBSS, 1.25 mL 4-(2-hydroxyethyl)-1-piperazineethanesulfonic acid (HEPES), and 0.5 mL 1% PS) was prepared and placed on ice before dissection. Sprague-Dawley rats (postnatal days 1-3) were sacrificed by decapitation. The skull was exposed by cutting skin from the back of the skull to the nose. The brains were harvested and placed in ice-cold dissection media in a petri-dish. The olfactory bulb and cerebellum were removed. The cortices were then retrieved and the meninges were removed. The cerebral cortices were placed in ice-cold dissection media. The cortices were dissociated using a scalpel and transferred to a 50 mL falcon tube. The tissue was triturated using a pipette (20-30 times), then using a 21G needle on a syringe and a 23G needle on a syringe. The dissection media containing tissue was sieved through a 70 µm cell strainer and then a 40 µm cell strainer. The 50 mL falcon tube was centrifuged at 300 rcf for 5 minutes. The supernatant was discarded and the pellet was suspended in 10 mL of D10 media (High glucose DMEM containing 4500mg / ml glucose, L-glutamine and sodium bicarbonate, without pyruvate supplemented with 1mM sodium pyruvate, 10% FBS, and 1% PS) and dissociated into a single cell suspension by pipetting using 1 mL and then 200 µL tips. The cells were counted (Section 2.2.3), plated in PDL (Section 2.2.2) coated T75 flasks ($1x10^6$ cells / 20 mL), and incubated in an incubator with a humidified atmosphere containing 5% CO_2 at 37^oC. The cells were examined and 50% media was changed with fresh D10 media every 2-3 days. After 7-8 days, when the astrocytes are confluent, the media was discarded and 20 mL fresh media was added. The flasks were shaken at 180 rpm for 30 minutes on an orbital shaker to remove microglia (confirmed by microscopy). The media was discarded, the cell layer washed with D-PBS and 20 mL of fresh D10 media was

added to each flask. The flasks were placed in the incubator for 3-6 h for gas exchange. Thereafter, the flasks were shaken at 220 rpm overnight (~18 h) to remove oligodendrocyte precursor cells (OPCs). The media was discarded, the cell layer was washed with D-PBS and fresh D10 (20 mL) was added. The flasks were placed in a standard incubator for gas exchange and shaken at 220 rpm overnight (~18 h) again. The sequential shaking was performed for 3-4 days. Afterward, the remaining astrocyte layer was washed with D-PBS. 5 mL of TrypLE was added to each flask, shaken on an orbital shaker for 5 minutes, and hit sharply 2-3 times to detach cells. The cell suspension was collected in a 15 mL falcon tube and centrifuged at 300 rcf for 5 minutes. The supernatant was aspirated and the cell pellet was suspended in 10 mL of fresh D10 media. The cells were counted (Section 2.2.3). The astrocytes were plated onto PDL (Section 2.2.2) coated T75 flasks (1.5 x 10^6 per 20 mL). Upon confluency, the astrocytes were re-trypsinized (TrypLE), counted and plated onto PDL coated plates at densities of 1.5 x 10^6 cells in 5 mL (T25 flasks for protein / RNA extraction), 3 x 10^4 cells / 100 µL (96 well plates for MTT / LDH assay) and 1.5 x 10^5 cells / 300 µL (24 well plates for IF staining). The cultures were placed in a standard incubator with a humidified atmosphere containing 5% CO_2 at 37^{o}C. The media (50%) was replaced with fresh D10 media every 2-3 days until confluency. Confluent cultures were used for experiments (Figure 2.4). The procedure was modified from the experimental protocol published by Pickard *et al.,* 2010 to obtain the primary rat astrocyte cultures.

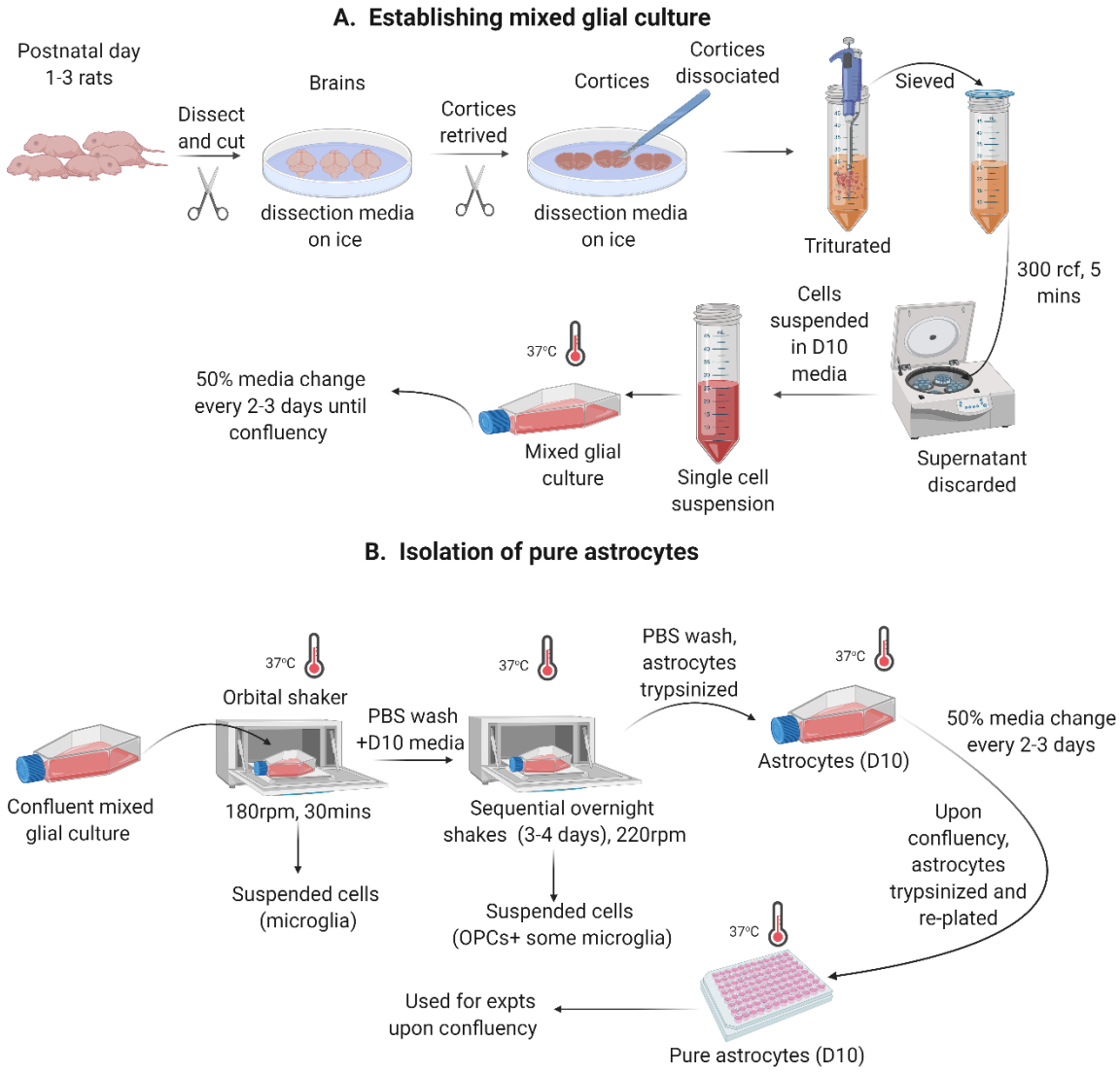

Figure 2.4. Primary rat cortical astrocytes culture. (Image produced using Biorender).

2.3 Glucose and / or Oxygen deprivation

Four treatment conditions, Normoxia (Nx), glucose deprivation (GD), oxygen deprivation (OD), and oxygen-glucose deprivation (OGD) were commonly used in the study (Table 2.3).

Table 2.3. Summary of commonly used treatment conditions.

	20.9% oxygen	**0.3% oxygen**
Glucose (4.5 g / L)	Nx	OD
No glucose (0)	GD	OGD

For Nx and OD, PC12 cells, primary neurons, and primary astrocytes were treated with ‘complete’ PC12 cell media, ‘complete’ Neurobasal media, and D10 media respectively (all indicated under cell culture for each cell). For GD and OGD, all the other constituents for the media were identical, with the sole exception of the absence of glucose (summarised in Table 2.4).

Table 2.4. Table summarising media and supplements used in different cultures

Media name	DMEM (high glucose) containing L-glutamine, sodium pyruvate	DMEM (glucose-free) containing L-glutamine, sodium pyruvate	Neurobasal (high glucose)	Neurobasal (glucose-free)	DMEM (high glucose) containing L-glutamine, sodium pyruvate	DMEM (glucose-free) containing L-glutamine, sodium pyruvate
Culture use	PC12 Nx, OD	PC12 GD, OGD	Primary neurons Nx, OD	Primary neurons GD, OGD	Primary astrocytes Nx, OD	Primary astrocytes GD, OGD
Glucose	4.5 g / L	0	4.5 g / L	0	4.5 g / L	0
Supplements	5 % FBS 5 % HS 1 % PS	5 % FBS 5 % HS 1 % PS	2 % B27 2 mM L-glutamine 1 % PS	2 % B27 2 mM L-glutamine 1 % PS	1 mM sodium pyruvate 10 % FBS 1 % PS	1 mM sodium pyruvate 10 % FBS 1 % PS

For Nx and GD: the cells were placed in a standard incubator with a humidified atmosphere containing 5% CO_2 at 37ºC. The conditions for reperfusion are identical to Nx. For Nx, GD and reperfusion, cells were treated in ambient air conditions. For OD and OGD: the cells were placed in a purpose-built INVIVO$_2$ 400 humidified hypoxia workstation (0.3% O_2, 5% CO_2, 94% N_2 at 37ºC). The media in filter-capped flasks was placed within the hypoxia workstation for 24 h before use, to deplete oxygen (Figure 2.5).

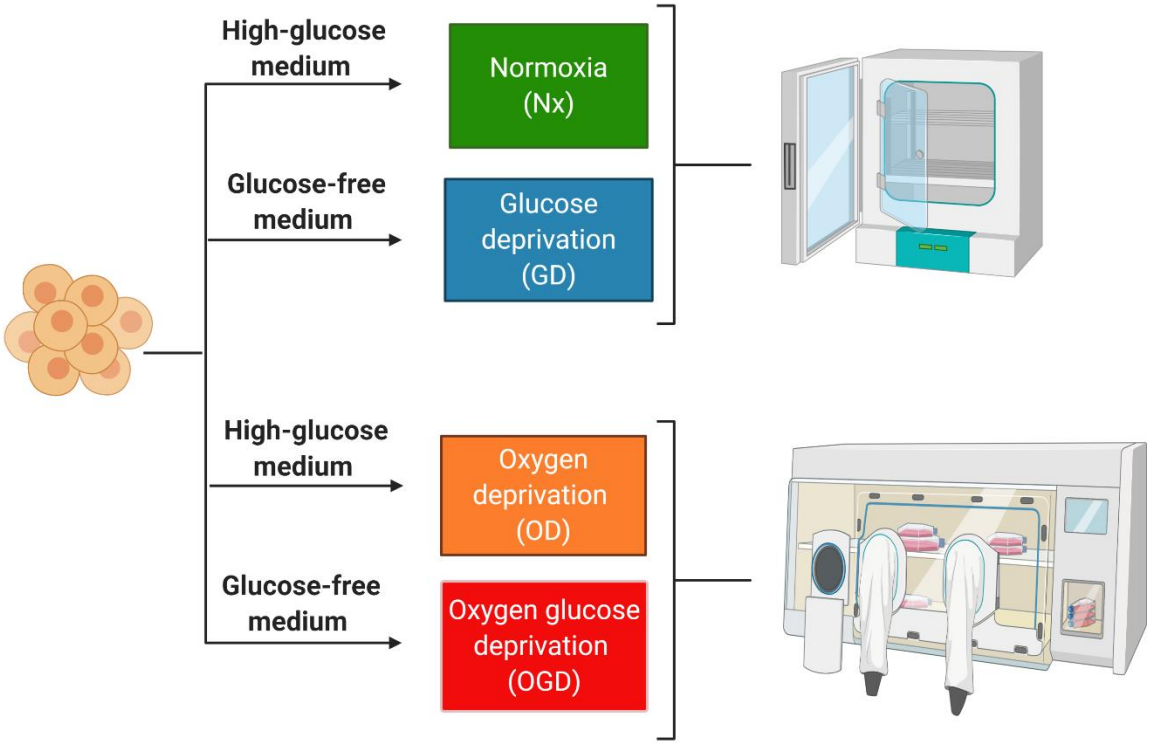

Figure 2.5. Figure illustrating the different treatment conditions. The procedure for applying (i) Normoxia (Nx) (ii) glucose deprivation (GD) (iii) oxygen deprivation (OD), and (iv) oxygen-glucose deprivation (OGD) to the cells. (Image produced using Biorender).

2.4 Drug administration

PHD inhibitors (FG2216, FG4592, GSK1278863, and Bayer85-3934) were used alongside a non-specific PHD inhibitor, DMOG (Figure 2.6). All the novel PHD inhibitors except FG4592 were obtained from Schofield Lab, Oxford University. Additionally, an autophagy inducer Rapamycin was used as a positive control for autophagy. All the PHD inhibitors and Rapamycin were initially dissolved in DMSO to a concentration of 10mM and subsequently diluted in the treatment appropriate culture media to the required concentrations.

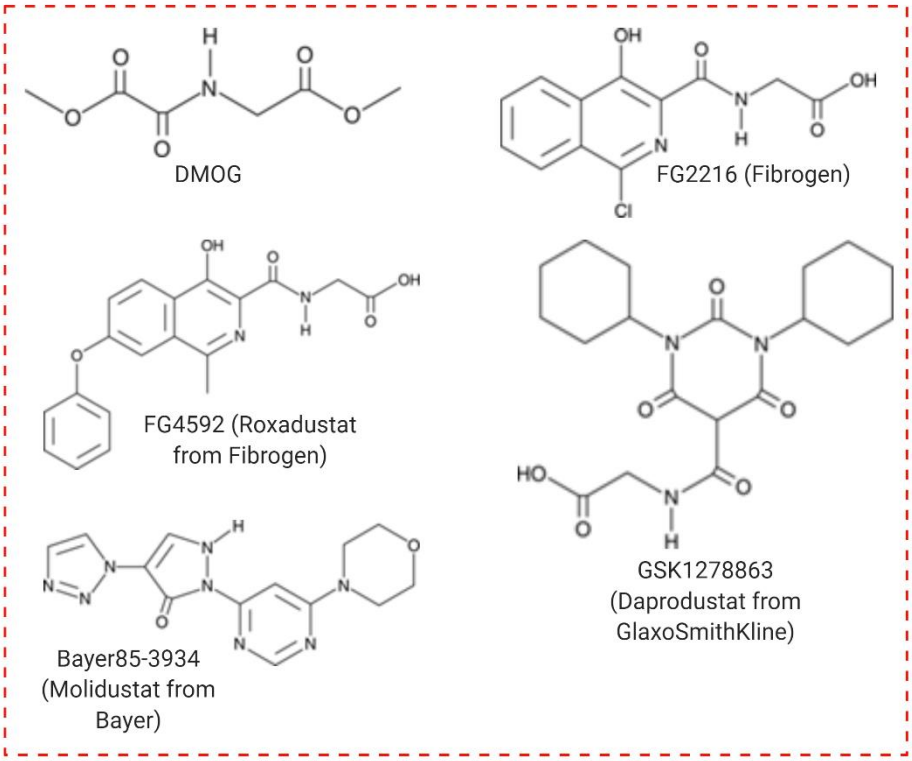

Figure 2.6. Chemical structures of PHD inhibitors. (Image produced using Biorender).

2.5 Assessment of cell viability

2.5.1 MTT assay

Mitochondrial activity was evaluated by a standard colorimetric assay for mitochondrial succinate dehydrogenase catalysed reduction of yellow MTT (3-(4,5-dimethylthiazol-2-yl)-2,5-diphenyltetrazolium bromide, a tetrazole) to a purple formazan product. The amount of colour formed is proportional to the number of metabolically active cells. Initially, MTT solution was prepared by dissolving 5 mg of MTT powder in 1 mL of D-PBS in the dark. Four hours before the completion of the treatment period, 10 µL MTT solution was added to the culture media (final concentration, 0.5mg / mL), and all samples were incubated at 37^{o}C under treatment conditions. After 4 h, the culture supernatant was aspirated, the formazan crystals formed by surviving cells were solubilised in 50 µL DMSO, and incubated at 37^{o}C for further 10 minutes. The optical density (OD) value of each well was determined by reading absorbance at 540 nm using a microplate reader. The DMSO background was subtracted from absorbance readings and MTT activity of cells for each treatment group was calculated based on the following formula:

$$\text{Mitochondrial activity (\% of control)} = \frac{\text{OD value (Experimental group)}}{\text{OD value (control group)}} \times 100\%$$

MTT activity was normalised as the percentage of the control. Results were expressed as the percent of absorbance measure in untreated controls.

2.5.2 LDH release assay

Lactate dehydrogenase (LDH) assay quantified LDH release in the culture media. LDH is a stable cytoplasmic enzyme present in all cells which catalyse the interconversion of lactate and pyruvate. When the cell plasma membrane is damaged, intracellular LDH is rapidly released into the culture supernatant.

Released LDH is measured with an enzymatic assay, which results in the conversion of tetrazolium salt, iodonitrotetrazolium (INT) into a red formazan product in the presence of diaphorase. The amount of colour formed is proportional to the number of lysed cells. In this study, a non-radioactive cytotoxicity assay kit was used. The reagent containing tetrazolium salts was prepared by mixing 12 mL of assay buffer with substrate mix in the dark. After treatment, 50 µL of each sample media was transferred to an unused 96-well flat bottom plate, after which, 50 µL of the prepared reagent was added. The mixture was incubated at room temperature for 30 minutes, protected from light. After 30 minutes, 50 µL of stop solution was added to each well and mixed. Maximum LDH release control was generated by adding 10 µL 10x lysis solution to wells containing control cells, 45 minutes before adding the reagent mixture. Thereafter, the amounts of formazan dye formed were assessed by measuring the absorbance with a microplate reader at 490 nm. % LDH release was quantified using the equation below

$$\text{LDH release (\%)} = \frac{\text{Experimental LDH release}}{\text{Maximum LDH release}} \times 100\%$$

The data are expressed as the mean percent of LDH release from the maximum control.

2.5.3 Trypan blue exclusion assay

Trypan blue exclusion was used to determine viable cells present in a cell suspension. After treatment, the viable cells were counted in each culture following procedures described in Section 2.2.4 (counting cells). Five samples were analysed from each treatment condition. The % of live cells was obtained using the following equation:

$$\text{Cell viability (\%)} = \frac{\text{Viable cells}}{\text{Total number of cells (Viable+dead)}} \times 100\%$$

Cell viability was normalized to percentage control. Cell viability was expressed as a percentage of viable cells from the total number of cells.

2.6 Flow cytometry to detect apoptosis

Guava Nexin Kit containing Annexin V and 7-amino-actinomycin D (7-AAD) double stain was used to assess early apoptosis in cells. Annexin V is a calcium-dependent phospholipid-binding protein with affinity for phosphatidylserine (PS), a membrane component normally localized to the internal face of the cell membrane. Early apoptosis results in translocation of PS molecules to the outer surface of the cell membrane where Annexin V can bind them. 7-AAD is a membrane impermeant dye that is generally excluded from viable cells. 7-AAD penetrates dead or damaged cells and binds to double-stranded DNA by intercalating between base pairs in G-C-rich regions. After cell treatment, 100 µL of cell suspension was transferred into a 1.5 mL microcentrifuge tube. To break cell clusters, 50 µL 0.8x Guava cell dispersal reagent was added to the tube and incubated for 20 minutes at 37^{o}C. The cell suspension was microcentrifuged for 5 minutes (14500g) and the culture media was aspirated. 100 µL of DMEM and 100 µL of Guava Nexin reagent was added. The sample was stained for 20 minutes at room temperature and acquired on Guava easyCyte flow cytometer. The data was analysed using Guava analysis software. A total of 10000 events in the gate were acquired for each sample and three samples were acquired per condition. The data were expressed as % of cells in each quadrant. Cells in the lower left quadrant represented viable cells (Annexin V and 7-AAD negative cells), the cells in the lower right quadrant represent early apoptotic cells (Annexin V positive and 7-AAD negative cells), and the cells in the upper right column represent necrotic / late apoptotic cells (Annexin V and 7-AAD positive cells).

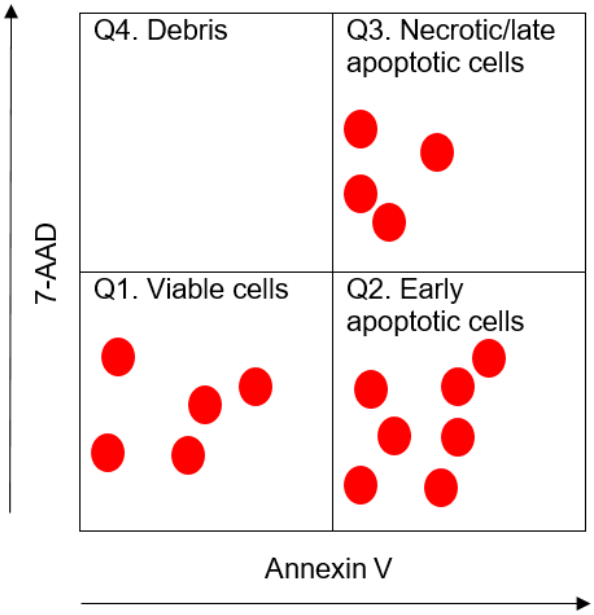

Figure 2.7. Schematic of data acquired by flow cytometry using Annexin V / 7-AAD double staining. (Image produced using Biorender).

2.7 Quantitative Real-time Polymerase Chain Reaction (qRT-PCR)

The complete procedure for RNA (ribonucleic acid) extraction, conversion to cDNA (complementary deoxyribonucleic acid), and qRT-PCR (quantitative real-time polymerase chain reaction) are presented in Figure 2.8. RNA was extracted from cells using the RNeasy Plus Mini Kit. The cell pellet was harvested by transferring cell suspension to a 15 mL falcon and centrifuging (5 minutes, 100 rcf). Fixed cells were trypsinized (TrypLE) before centrifugation. After which the supernatant was discarded and 600 µL RLT plus containing 40 µM dithiothreitol (DTT) was added to lyse the cell pellet and mixed thoroughly by pipetting. DTT is a reducing agent used to deactivate ribonuclease (RNase). The homogenised lysate was then transferred to the supplied generic DNA (gDNA) Eliminator spin column and centrifuged at 8000g for 30 seconds. The column was discarded and the flow-through was mixed with an equal volume of 70% ethanol (aids RNA precipitation). The sample was transferred

to the RNeasy spin column (700 µL at a time) and centrifuged (8000g for 15 seconds). The RNA pellets were washed with RW1 buffer (700 µL, 8000g for 15 seconds) and twice with RPE buffer (500 µL, 8000g for 15 seconds then 8000g for 1 minute). The culminating RNA pellets were eluted in 50 µL nuclease-free water and the concentration measured on the NanoDrop 1000 Spectrophotometer. The quality of the RNA samples was assessed using the 260 / 280 and 260 / 230 absorbance measurements. After extraction, a total RNA concentration of 2 µg was transferred to an RNase-free PCR reaction tube on ice, ready for cDNA synthesis using the Tetro cDNA synthesis kit. 1 µL each of Oligo$(dT)_{18}$ primers, 10mM deoxynucleoside triphosphates (dNTP) mix, Ribosafe RNase inhibitor, Tetro reverse transcriptase, and 4 µL of 5 x reverse transcriptase (RT) buffer was added to the reaction tube. The mixture was made up to 20 µL with diethylpyrocarbonate (DEPC) -treated water and mixed gently by pipetting. The samples were incubated at 45^{o}C for 30 minutes followed by 85^{o}C for 5 minutes to terminate the reaction using the GeneAmp PCR system 2700. The cDNA samples were stored at -20^{o}C.

For cDNA amplification and quantification, 100 ng cDNA template, 2.5 µL SensiFAST SYBR Hi-ROX, 0.2 µL of forward and reverse primer mix (10 µM) made up to 5 µL with DEPC treated water, was placed in a well (48 well qPCR plate). SYBR Hi-ROX binds to the double-stranded DNA (dsDNA) molecule by intercalating between DNA base and the fluorescence intensity is proportional to the dsDNA concentration. cDNA was amplified using the Techne PROPLATE48. An initial activation step was performed for 2 minutes at 95^{o}C before 40 cycles of a 3-step cycling program consisting of 95^{o}C for 5 seconds, 60^{o}C for 10 seconds, and 72^{o}C for 15 seconds. The primer sequences are described in Table 2.5. *Usp14*, *Actin, and*

Rpl32 were used as internal controls. The relative levels of mRNA were normalised to *Actin*. Quantification of mRNA expression was performed using the comparative delta Ct method.

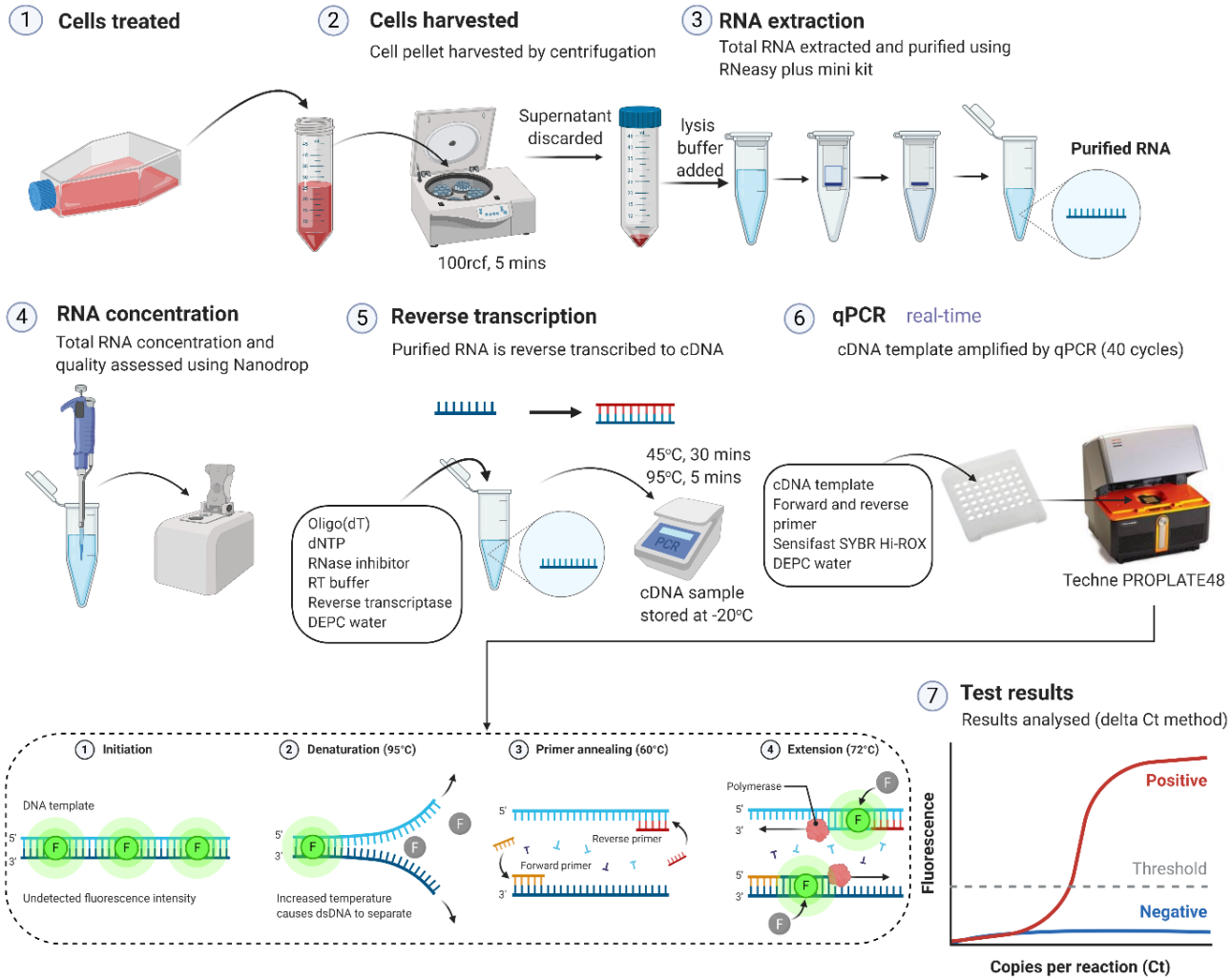

Figure 2.8. Procedure for determining gene expression through qRT-PCR.

(Image produced using Biorender).

Table 2.5. List of primers used for qRT-PCR studies and their forward (FW) / reverse (RV) sequences

Hypoxia inducible factor 1 alpha (Hif1α)	FW TCAAGTCAGCAACGTGGAAG RV TATCGAGGCTGTGTCGACTG
Hypoxia inducible factor 2 alpha (Hif2α),	FW ACC TGG AAG GTC TTG CAC TGC RV TCA CAC ATG ATG ATG AGG CAG G
Bcl2 interacting protein 3 (Bnip3)	FW TTTAAACACCCGAAGCGCACAG RV GTTGTCAGACGCCTTCCAATGTAGA
Prolyl hydroxylase domain-containing protein 2 (Phd2), also known as *egl-9 family hypoxia inducible factor 1* (*Egln1*)	FW TGCATACGCCACAAGGTACG RV GTAGGTGACGCGGGTACTGC
Erythropoietin (Epo)	FW CCA GCC ACC AGA GAG TCT TC RV TGC AGA AAG TAT CCG GTG TG
Glucose transporter type 1 (Glut1), also known as *solute carrier family 2 member 1* (*Slc2a1*)	FW GGTGTGCAGCAGCCTGTGTA RV GACGAACAGCGACACCACAGT
Vascular endothelial growth factor (Vegf)	FW TTACTGCTGTACCTCCAC RV ACAGGACGGCTTGAAGATA
6-phosphofructo-2-kinase / fructose-2,6-bisphosphatase 1 (Pfkfb1)	FW AACCGCAACATGACCTTCCT RV CAACACAGAGGCCCAGCTTA
6-phosphofructo-2-kinase / fructose-2,6,bisphosphatase 3 (Pfkfb3)	FW CTGTCCAGCAGAGGCAAGAA RV CGCGGTCTGGATGGTACTTT
Lactate dehydrogenase A (Ldha)	FW AAGGTTATGGCTCCCTTGGC RV TAGTGACGTGTGACAGTGCC

2.8 Western Immunoblotting

2.8.1 Preparation of lysates from cell culture

Before protein extraction from cells, a cell extraction buffer was made on ice (5 mL 1 x radioimmunoprecipitation assay (RIPA) buffer, 50 µL 1mM phenylmethylsulfonyl fluoride (PMSF) and 50 µL protease inhibitor cocktail). RIPA buffer is a cell lysis solution that effectively extracts nuclear, cytoplasmic, and membrane proteins. Both PMSF and protease inhibitor cocktail used to inhibit various proteases and prevent protein degradation after cell lysis. Cell cultured plates were placed on ice and washed with ice-cold PBS. Ice cold lysis buffer (0.5 mL per 75 cm^2) was added to the plates and mixed on an orbital shaker for 15 minutes. The adherent cells were scraped using a cell scraper and transferred to an ice-cold 1.5 mL microcentrifuge tube. This sample was vortexed and then microcentrifuged for 10 minutes (14500g). The resulting supernatant was transferred to a new microcentrifuge tube and stored at -20^oC.

2.8.2 Protein concentration assay

Protein concentration was determined using bicinchoninic acid (BCA) protein assay kit (96 well plate protocol). Blank standard (distilled water) and bovine serum albumin (BSA) protein standards: 25, 125, 250, 500, 750, 1000, and 1500 (µg / mL) were prepared by series of serial dilutions of 2 mg / mL BSA solution. 1:1 dilution of protein samples was performed with 1 x RIPA buffer. 25 µL of prepared standards and samples were loaded in a 96 well plate in triplicates. 200 µL of working reagent (a mixture of reagent A&B from BCA kit in a 50:1 ratio) was added to each well, the plate was covered, and incubated at 37^oC for 30 minutes. The absorbance of the plate was obtained at 562 nm using a plate reader. The protein concentration of the samples was determined using a standard graph of the absorbance measurements

for each albumin standard concentration (µg / mL) and correcting for the amount of sample loaded. The average absorbance measurement of the blank standard was subtracted from all standard and sample replicates (Figure 2.9).

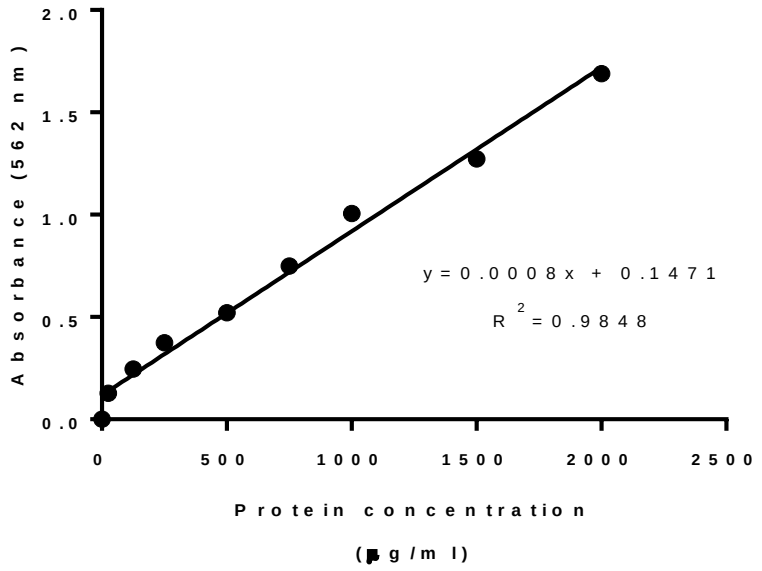

Figure 2.9. Sample standard BSA standard concentration. Bovine serum albumin (BSA) protein standards: 25, 125, 250, 500, 750, 1000, and 1500 (µg / mL) were prepared by series of serial dilutions of 2 mg / mL BSA solution.

2.8.3 Gel electrophoresis, Western blotting, and detection

20-40 µg protein was denatured for 5 minutes in 4 x Laemmelli buffer at 95^{o}C. The commercially obtained Laemmelli buffer consists of 2-mercaptoethanol to reduce disulphide bonds, sodium dodecyl sulphate (SDS) to denature the proteins by disrupting covalent linkages and giving them an overall negative charge, glycerol to increase the density of the sample, bromophenol blue dye, and Tris buffer to maintain the pH of the sample

The proteins were resolved using gel electrophoresis. The denatured protein samples were loaded onto pre-cast 4-20% polyacrylamide miniPROTEAN TGX gels (10 well). 10 µL of Precision plus ProteinTM standards (10-250kD) was loaded in each gel. The gels were run in 1 x Tris / Glycine / SDS running buffer in a BioRad Mini-PROTEAN tetra Cell at 100 volts until blue dye reached the bottom (black line) of the gel. The running buffer provides essential ions that carry a current, allowing separation of the proteins whilst maintaining pH levels. Tris maintains the pH level between 6.7-6.8. At this pH, ionised chloride ions (from Tris-HCl) migrate rapidly raising the pH behind them and creating a voltage gradient. This causes glycine to ionise and migrate behind the chloride front. Most peptides in the sample are negatively charged due to bound SDS and migrate between the chloride and glycine.

Upon completion of electrophoresis, the gels were removed from their cassettes, and placed into 1 x transfer buffer (1x Tris / Glycine buffer with 20% methanol). Methanol aids in stripping the SDS from proteins, increasing their ability to bind to the membrane. Trans-Blot SD Semi-Dry Electrophoretic transfer cell was used for the transfer. Gels were placed onto the nitrocellulose membrane and assembled with extra-thick filter paper. Protein molecules bind to nitrocellulose membranes through hydrophobic interactions. The pore size of 0.45 µm was used as it was suitable for most protein sizes. The transfer was performed at 20 volts for 1 h.

The membranes were blocked with 5% milk powder in 1 x 0.1% PBS-Tween for 1 h to reduce non-specific binding. Following this, membranes were incubated in a primary antibody overnight at 4°C. The primary antibodies are summarised in Table 2.6. Primary antibodies were prepared in 1% milk powder in 1 x TBS-T (recipe in

Appendix, Table 1). After the overnight incubation membranes were washed in 1 x TBS-T three times for 5 minutes each to remove unbound antibodies. The membranes were then incubated for 1 h in horseradish peroxidase (HRP) conjugated secondary antibody (dilution factor 1:1000), made in 1% milk powder in 1 x TBS-T. The blots were washed again three times with 1 x TBS-T to remove unbound antibodies and minimise background. The primary antibodies were specific and bound to the protein of interest. The secondary antibodies were specific to the host species of the primary antibodies. The HRP conjugated secondary antibody binds to the primary antibody attached to the target protein.

Table 2.6. The primary antibodies and dilution factor used for Western blotting for each protein

Primary antibodies	Dilution factor
Rabbit polyclonal anti-Lc3b (microtubule-associated protein 1 light chain beta)	1:500
Rabbit polyclonal anti-p62 (also known as sequestosome 1, SQSTM1)	1:500
Mouse monoclonal anti- Hif1α (hypoxia inducible factor 1 alpha)	1:500
Mouse monoclonal anti-Hif2α (hypoxia inducible factor 2 alpha)	1:500
Rabbit polyclonal anti-Beclin1	1:500
Rabbit polyclonal anti-β-actin	1:5000

The blots were developed by Pierce enhanced chemiluminescence (ECL) western blotting substrates. Each membrane was incubated with 2 mL (1:1 Reagent A / Reagent B) for 1 minute. Reagent A was a stable peroxide solution and reagent B was an enhanced luminol solution. The HRP present on the secondary antibody catalyses the oxidation of luminol by peroxide results in the formation of 3-aminophthalate and light (at 425 nm). The membranes were placed in clear cling film and imaged using the ChemiDoc MP imaging system. The imaging device captured the chemiluminescent signal. The complete procedure for protein extraction, gel electrophoresis, blocking, antibody incubation, and detection is illustrated in Figure 2.10.

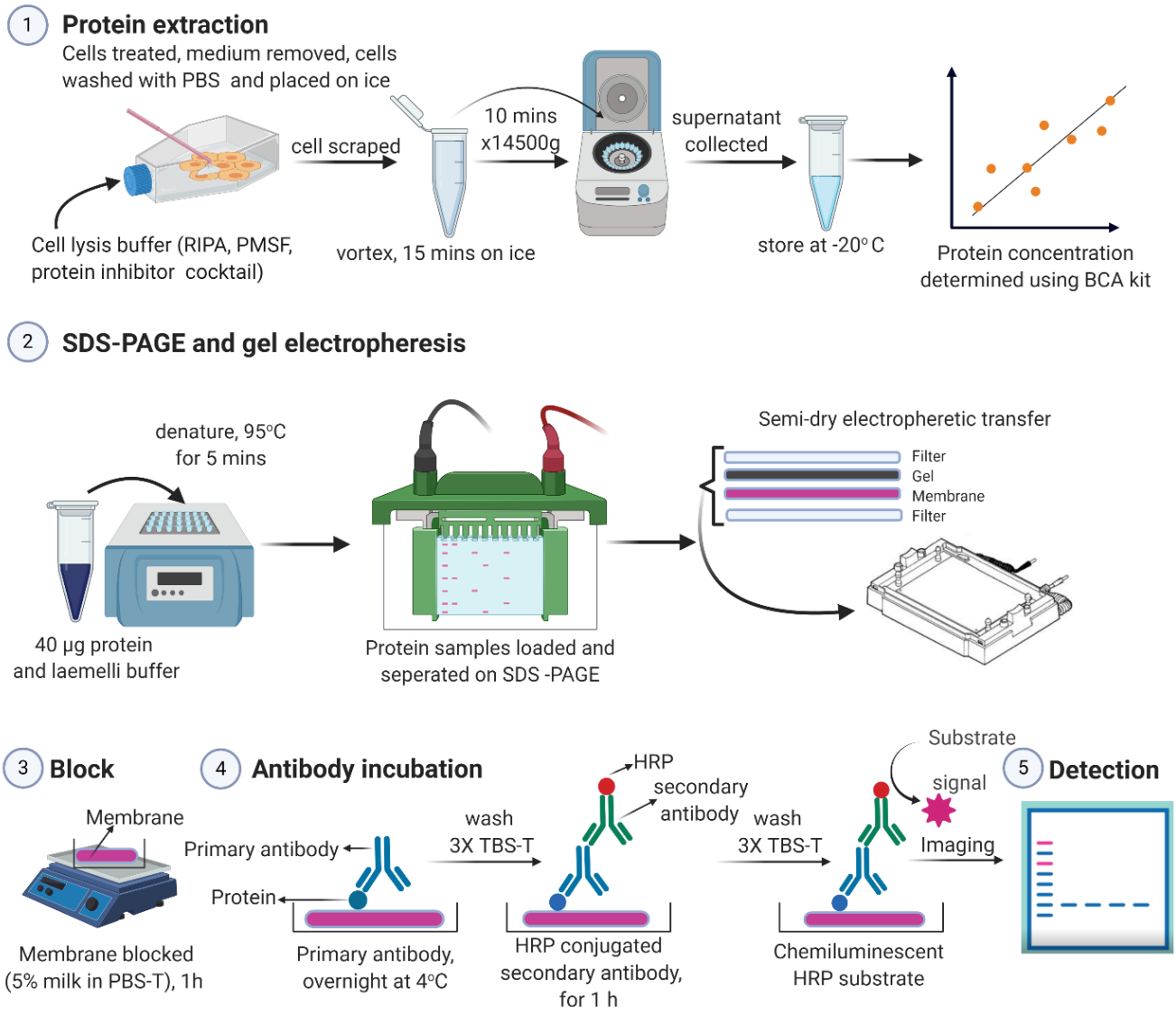

Figure 2.10. Procedure for determining protein expression through Western blotting. (Image produced using Biorender).

The blots were washed twice with each of the following: mild stripper buffer (recipe in Appendix, Table 2) for 15 minutes, 1 x TBS-T for 5 minutes, and 1 x PBS for 10 minutes. The membranes were incubated with 5% milk in 1 x TBS-T for 1 h. The membranes were blocked with 5% milk powder in anti-β-actin (1:5000 in 1% milk powder in 1 x TBS-T) overnight at 4°C. After the overnight incubation, membranes were washed in 1 x TBS-T three times for 5 minutes each to remove unbound antibodies. The membranes were then incubated for 1 h in HRP conjugated secondary antibody, made in 1% milk powder in 1 x TBS-T. The blots were washed again three times with 1 x TBS-T.

The protein levels were quantified by densitometric analysis using Image J (NIH, USA). The rectangular selection tools were used to select bands of interest and plot relative density of each band. The area of each peak was quantified. Values were normalized to β-actin and corresponding control.

2.9 Immunocytofluorescence

Primary neurons or astrocytes were grown on coverslips (1.5 x 10^5 cells). Following treatment, the coverslips were washed with PBS. 300 µL of 4% paraformaldehyde (PFA) was added onto the coverslips and incubated for 20 minutes at room temperature (on the orbital shaker). PFA is a fixative agent that reacts with the primary amines on proteins to form cross-links known as methylene bridges. PFA was aspirated and the coverslips were washed three times with PBS.

The cell membranes were permeated with 0.5% Triton X-100 in PBS for 15 minutes at room temperature and washed three times with PBS. Non-specific binding sites were blocked with 3% BSA in 0.1% PBS-Tween for 1 h. The blocking solution was

aspirated. Primary antibody (Table 2.5) prepared in 1% BSA in 0.1% PBS-Tween was added including a negative control well without primary antibody and incubated overnight at 4^{o}C. The cells were washed three times with PBS and incubated with the corresponding fluorescein isothiocyanate (FITC)-conjugated secondary antibody prepared in 1% BSA in 0.1% PBS-Tween for 3 h at room temperature (dilution factor 1:200). The cells were washed three times with PBS and the coverslips were mounted onto microscopic slides using Vectashield with DAPI (4′, 6-diamidino-2-phenylindole). Images were obtained by the Nikon Eclipse 80i fluorescence microscope (Hamamatsu digital camera, obtained with NIS-Element BR 3.22.14 software).

Table 2.7. The primary antibodies and their dilution factor for IF staining

Primary antibodies	**Dilution factor**
Mouse monoclonal anti-Tubulin β 3 (clone Tuj1)	1:1000
Rabbit polyclonal anti-GFAP (glial fibrillary acidic protein)	1:500
Rabbit polyclonal anti-Map2 (microtubule-associated protein 2)	1:1000

2.10 Isolation of extracellular vesicles (EVs)

Extracellular vesicles (EVs) were isolated from ACM (chapter 6) by sequential centrifugation using a Hitachi Micro Ultracentrifuge CS 150NX. ACM (15 mL / tube) was transferred to Hitachi Koki centrifuge tubes and weighed to ensure consistency (±0.001g). ACM was centrifuged at (i) 10 minutes at x 300g (ii) 10 minutes at x

2000g (iii) the media was filtered through a 0.22µm syringe filter into a new Hitachi Koki tube (iv) centrifuged for 30 minutes at x 10,000g. The pellet was discarded, the supernatant was transferred into another Hitachi Koki tube and centrifuged for 60 minutes at x 100,000g. After this, the supernatant was collected in a 50 mL falcon tube. The pellet was re-suspended in 15 mL of D-PBS and centrifuged for 60 minutes at x 100,000g to obtain exosomes. D-PBS was discarded and the exosome pellet was suspended in 1 mL of complete Neurobasal medium. The exosomes were sized (procedure below) and stored at -80^{o}C (Figure 2.11).

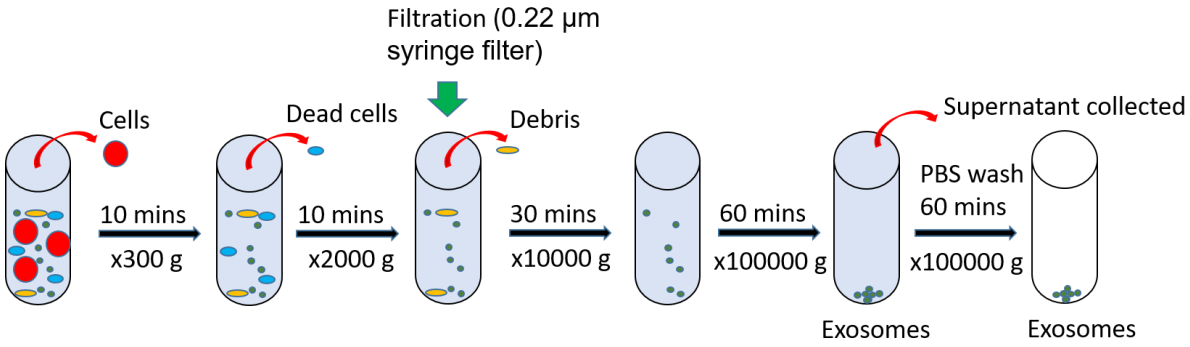

Figure 2.11. Sequential ultracentrifugation scheme to separate ACM into soluble proteins (supernatant) and exosomes. (Image produced using Biorender).

The size of the exosomes obtained by sequential ultracentrifugation was measured using the Malvern Zetasizer Nano ZS that measures particle size from 0.3 nm to 10 microns range. 200 µL of media (containing exosomes) was transferred to folded capillary zeta cell and placed in Zetasizer Nano ZS. The size was obtained using Zetasizer Size software version 7.02.

2.11 Data analysis

For studies in PC12 cells, n represents studies performed on cells being derived from separate flasks (different streams of cultured cells). In studies performed with primary neuronal cultures, n represents studies performed on cells derived from different rats. In studies performed with primary astrocyte cultures, n represents studies performed on cells from different rat litters. For each biological replicate, at least three technical replicates were performed. In experiments employing 96 well plates, at least 8 well replicates were performed on each plate. The dataset obtained for each treatment condition was independent of other conditions (i.e. independent sampling; one rat, one number). The data obtained from each of the biological replicates were averaged. The data were represented as mean ± standard deviation (S.D.). The data were tested for normality using the Anderson-Darling normality test. For normally distributed data, one-way or two-way ANOVA with Tukey's post hoc analysis was performed. For data that were not normally distributed, the non-parametric Kruskal-Wallis test was used. For all data analysis, PRISM version 8 (Graph Software Inc, CA, USA) for Windows version 10 was used. Values of $p < 0.05$ were considered statistically significant

Chapter 3.

Establishment of *in vitro* models of cerebral ischaemia with PC12 cells and primary rat neurons

3.1 Introduction

Cerebral ischaemia is caused by the disruption of blood and oxygen supply to the brain, particularly the cerebrum. Oxygen concentration in the normal brain are around 3-5 % (Chen *et al*., 2018), however, during cerebral ischaemia the oxygen levels fall between 1-3 % (Holloway and Gavins, 2017). Re-introduction of oxygen and glucose following cerebral ischaemia is known as reperfusion, which is the fundamental treatment for ischaemic stroke (Ryou and Mallet, 2018). Currently, there are only two acute stroke management options. One is intravenous rTPA and the other one is surgical clot removal through thrombectomy. Both of these interventions aim to restore oxygen and blood supply (i.e. reperfusion). Often paradoxically, reperfusion triggers ischaemia-reperfusion (I / R) injury cascade culminating in cell death (Hill, 2014; Ryou and Mallet, 2018). The current treatment acute stroke therapies have several restrictions and only benefit ~10% of all patients, therefore there is a serious requirement to develop novel medical interventions to reduce and delay the impact of ischaemia (Hill, 2014). In order to study novel stroke therapies, it is essential to develop suitable i*n vitro* models of cerebral ischaemia.

Ischaemic stroke therapies are initially tested using *in vitro* cell culture models followed by *in vivo* model of cerebral ischaemia and successful therapies progress into clinical trials. *In vitro* models have a high throughput, are cost effective and technically easier to process compared to *in vivo* studies. Due to limited availability and ethical considerations, it is not viable to study every single therapy *in vivo*. It is therefore suitable to test several treatment strategies *in vitro* and understand their mechanism of action.

The complexity of ischaemic stroke makes it difficult to be modelled in an *in vitro* system. Nevertheless, *in vitro* models are indispensable for the investigation of basic biochemical and molecular mechanisms. Oxygen-glucose deprivation (OGD) is commonly used to mimic ischaemia and involves switching culture from normal O_2 / CO_2 atmosphere to N_2 / CO_2 atmosphere. When glucose is maintained in the anoxic buffer, it results in hypoxia (oxygen deprivation, OD) and simultaneous omission of glucose results in OGD (Holloway and Gavins, 2016). Cultured cells subjected to OGD followed by re-introduction of glucose and oxygen imitates I / R injury (Ryou and Mallet, 2018).

Primary cells are commonly used for studying neurobiological, molecular properties, and cell differentiation (Westerink and Ewing, 2007). Primary neuronal cultures are widely used to model cerebral ischaemia *in vitro*. Primary neurons are laborious and time-consuming to grow, making it difficult to screen various treatment options and understanding their underlying mechanisms (Hillion *et al.,* 2006). At the early stages of research, using a cell line is more suitable for *in vitro* studies. PC12 cells are a widely used and accepted model for neurochemical and neurobiological studies. PC12 cells can synthesize and store dopamine upon calcium-dependent depolarisation (Westerink and Ewing, 2007). PC12 cells can be adapted for cell-based assays and screened to determine molecular mechanisms that can later be validated in primary neuronal cultures (Hillion *et al.,* 2005; Hillion *et al.,* 2006). In this chapter, the responses of PC12 cells and primary neuronal cultures to glucose and / or oxygen deprivation were evaluated on cell viability, apoptosis, HIF activation and hypoxic gene expression at varying time intervals with / without reperfusion. These

studies were performed in order to establish a suitable *in vitro* model of cerebral ischaemia to screen novel treatment strategies.

3.2 Materials and methods

PC12 cells and primary rat cortical neurons were cultured according to procedures described in Section 2.2.

3.2.1 Treatment protocol

Adherent PC12 cells and primary neuronal cultures were used for experiments. The complete media (100 %) was aspirated and the cells were washed twice with glucose-free media prior to experiments. For all experiments, complete media changes were performed on a staggered basis, such that all treatment durations either end or are switched to reperfusion simultaneously and end together.

PC12 cells were treated with Nx, GD, OD, and OGD for various durations (2 h, 4 h, 6 h, 12 h, and 24 h). Additionally, the effect of reperfusion was evaluated following GD, OD, and OGD (Figure 3.1). For these experiments, PC12 cells were subjected to Nx, GD, OD, and OGD for various duration, followed by 24 h reperfusion. The OGD media was aspirated completely and replaced with complete media. The cells were returned in a standard incubator for 24 h.

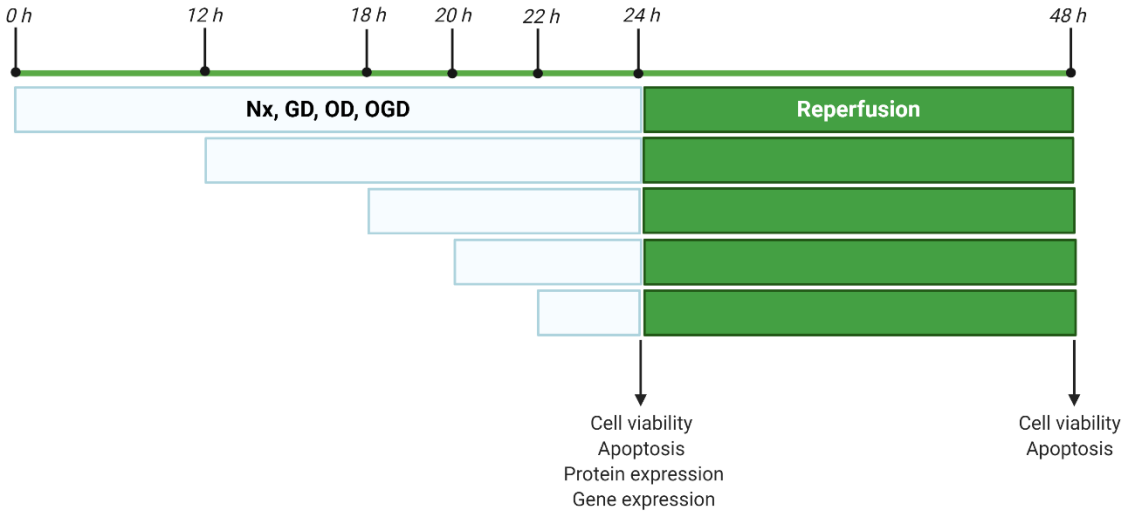

Figure 3.1. Timeline of PC12 cell treatment. PC12 cells were subjected to normoxia (Nx; ambient air), glucose deprivation (GD), oxygen deprivation (OD), and oxygen-glucose deprivation (OGD) for 2 h, 4 h, 6 h, 12 h, and 24 h followed by 24 h reperfusion. All the conditions were initiated on a staggered basis, such that all experiments terminated together. (Image produced using Biorender).

Primary rat cortical neuronal cultures were exposed to Nx, OD, and OGD for various durations (2 h, 4 h, and 6 h). Additionally, the effect of 24 h reperfusion was evaluated following Nx, OD, and OGD (Figure 3.2). The complete experimental conditions for Nx, GD, OD, OGD, and reperfusion were described in Section 2.3.

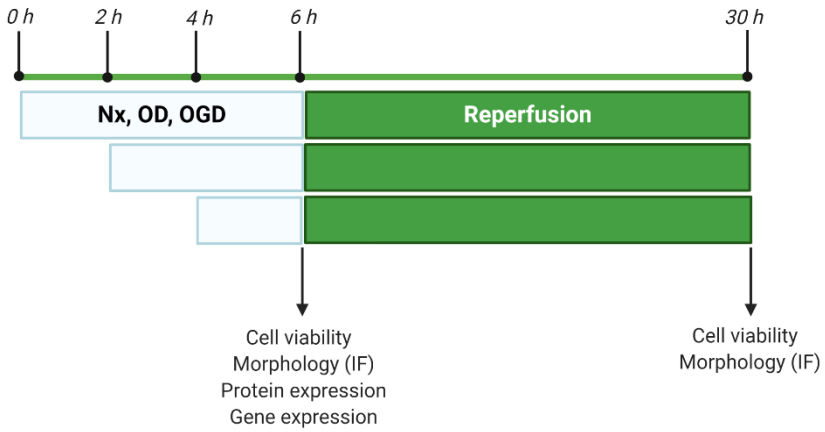

Figure 3.2. Timeline of treatment of primary rat cortical neurons. Primary neurons were subjected to Nx, OD, and OGD for 2 h, 4 h, and 6 h followed by 24 h reperfusion. All the conditions were initiated on a staggered basis, such that all experiments terminated together. (Image produced using Biorender).

Cell viability (MTT, LDH, and trypan blue exclusion assay; Section 2.5), apoptosis (PC12 cells only; Section 2.5), morphological changes (IF staining; section 2.8), gene expression (Section 2.6), and protein expression (Section 2.7) were evaluated in PC12 cells and primary neurons.

3.3 Results

3.3.1 Effects of GD, OD, and OGD on PC12 cells viabilities

Ideally *in vitro* ischaemia is simulated by exposing cells to OGD, whereas OD mimics hypoxia (Holloway and Gavins, 2016). Various studies have reported O_2 levels ranging from 1-3% in the penumbra during ischaemia, whereas the ischaemic core has potentially very little oxygen supply (Holloway and Gavins, 2016). Therefore, the lowest achievable O_2 levels in the lab (0.3%) were used for the experiments. PC12 cells were subjected to Nx, GD, OD (0.3% O_2), and OGD (0.3% O_2) for 2 h, 4 h, 6 h, 12 h, and 24 h followed by 24 h reperfusion. Cell viability was assessed (i) at the end of GD, OD, or OGD for the specified time, and (ii) at the end of reperfusion (Figure 3.1). Firstly, PC12 cell viabilities were assessed at various duration following Nx, GD, OD, and OGD (Figure 3.3).

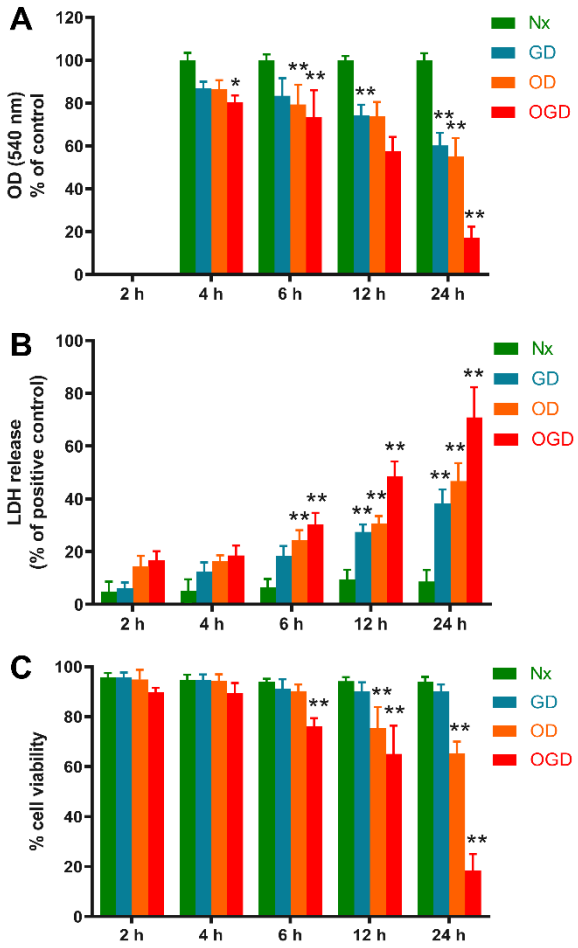

Figure 3.3. PC12 cell viabilities in response to GD, OD, and OGD. Bar graphs representing PC12 cell viabilities in response to Nx, GD, OD, and OGD at various durations. (A) MTT assay revealed a significant reduction in mitochondrial activity by GD (12 h, 24 h), OD (6 h, 12 h, 24 h), and OGD (6 h, 12 h, 24 h) compared to Nx (same time point). (B) LDH assay revealed a significant increase in LDH release by GD (12 h, 24 h), OD (6 h, 12 h, 24 h), and OGD (6 h, 12 h, 24 h) compared to Nx (same time point). (C) Trypan blue exclusion assay revealed a significant reduction in cell viability by OD (12 h, 24 h) and OGD (6 h, 12 h, 24 h) compared to Nx (same time point). *(For all graphs, * represents $p < 0.05$ and ** represents $p < 0.01$ versus Nx (same time point); two-way ANOVA followed by Tukey's post-hoc analysis; n=5)*

Results revealed significant reduction in mitochondrial activity and increase in LDH release by GD (12 h, 24 h) versus Nx (same time point). There were no significant (*p>0.05*) changes in mitochondrial activity and LDH release at 24 h compared to 12 h GD. Trypan blue assay revealed no significant changes in cell viability by GD (up to 24 h) compared to Nx.

Results revealed significant reduction in mitochondrial activity and increase in LDH release by OD (6 h, 12 h, 24 h) versus Nx (same time point). Compared to 6 h and 12 h OD, mitochondrial activity was significantly (*p<0.05*) lower at 24 h OD. Similarly, LDH release was significantly (*p<0.05*) greater at 24 h OD, compared to 6 h and 12 h OD. There were no significant (*p>0.05*) differences in mitochondrial activity and LDH release at 12 h compared to 6 h OD. Trypan blue assay results revealed significant reductions in cell viability at 12 h and 24 h OD compared to Nx (same time point), with no significant (*p>0.05*) difference between 12 h and 24 h OD.

Results revealed significant reductions in mitochondrial activity by OGD (4 h, 6 h, 12 h, and 24 h) versus Nx (same time point). Compared to 4 h, 6 h, and 12 h OGD, mitochondrial activity was significantly (*p<0.01*) lower at 24 h OGD. Mitochondrial activity was significantly (*p<0.01*) lower at 12 h OGD compared to 4 h OGD. Compared to Nx (same time point), OGD (6 h, 12 h, 24 h) resulted in a significant increase in LDH release. The increase in LDH release by OGD was time-dependent (*p<0.01* for 6 h vs 12 h OGD and 12 h vs 24 h of OGD). Trypan blue assay results revealed significant reductions in cell viability at 6 h, 12 h, and 24 h OGD compared to Nx (same time point). Compared to 6 h and 12 h OGD, cell viability was

significantly ($p<0.05$) lower at 24 h OGD (there is no significant ($p>0.05$) difference between 6 h and 12 h OGD).

Reperfusion provides energy and supports the recovery of salvageable neurons, but also potentiates I / R injury cascade potentiating cell death (Ryou and Mallet, 2018). The effects of I / R were evaluated in PC12 cells. Following initial exposure of PC12 cells to Nx, GD, OD, and OGD (2, 4, 6, 12, 24 h); the cells were subjected to 24 h reperfusion. Figure 3.4 lists quantitative comparisons between PC12 cell responses before and after 24 h reperfusion.

Reperfusion following 12 h and 24 h GD or OD resulted in a further reduction in mitochondrial activity (compared to without reperfusion) but no significant changes in LDH release (Figure 3.4A). Reperfusion following 6 h GD or OD, exhibited no significant changes in mitochondrial activity, cell viability, and LDH release (Figure 3.4B). Reperfusion following 6 h and 12 h OGD resulted in a further reduction in mitochondrial activity, cell viability, and an increase in LDH release (compared to without reperfusion). 24 h OGD alone was too harsh for the cells, leading to 70.8 ± 11.4 %, and 82.7 ± 9.1 % LDH release w / o reperfusion respectively (Figure 3.4C).

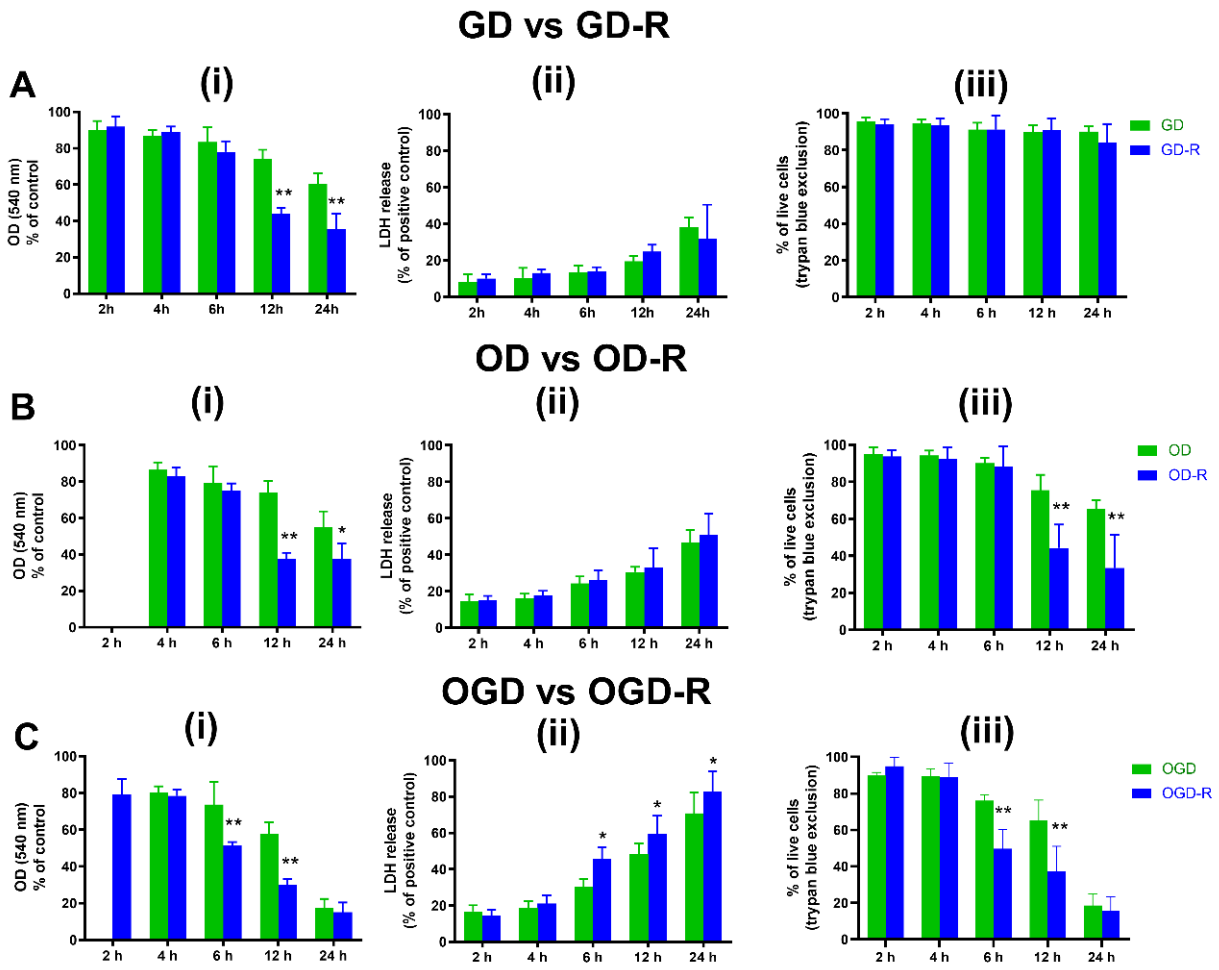

Figure 3.4. Comparison of PC12 cells response to GD, OD, and OGD before and after 24 h reperfusion. Bar graphs representing PC12 cell viabilities in response to GD, OD, and OGD following 24 h reperfusion (R). (A) GD vs GD-R (B) OD vs OD-R (C) OGD vs OGD-R. (i) MTT assay. Compared to without reperfusion, results revealed a further reduction in mitochondrial activity following reperfusion in cells pre-exposed to 12 h, 24 h GD or OD and 6 h, 12 h OGD. (ii) LDH assay. Compared to without reperfusion, results revealed a further reduction in LDH release following reperfusion in cells pre-exposed to 6 h, 12 h, and 24 h OGD. (iii) Trypan blue exclusion assay. Compared to without reperfusion, results revealed a further reduction in cell viability following reperfusion in cells pre-exposed to OD (12 h, 24 h) and OGD (6 h, 12 h). *(For all graphs, * represents $p < 0.05$ and ** represents $p < 0.01$*

versus response to the identical condition before reperfusion (same time point); two-way ANOVA followed by Tukey's post-hoc analysis; n=5)

3.3.2 Effects of GD, OGD, and OGD on apoptosis in PC12 cells

The effects of Nx, GD, OD, and OGD (2, 4, 6, 24 h) alone and following 24 h reperfusion were evaluated on PC12 cells apoptosis using flow cytometry (Annexin-V and 7-AAD). The % of viable (AV^- / $7\text{-}AAD^-$), early apoptotic (AV^+ / $7\text{-}AAD^-$), and necrotic cells (AV^+ / $7\text{-}AAD^+$) were quantified out of the total number of cells. Compared to Nx (same time points), at a number of early time points, GD (2 h, 4 h, 6 h), OD (2 h, 4 h), and OGD (2 h), without and with reperfusion did not result in apoptosis or necrosis; the majority of cells (~90%) were viable.

Compared to Nx (same time point), significant increases in early apoptotic cells and reduction in viable cells were seen following OD (6 h), and OGD (4 h, 6 h); there was no significant necrosis. The outcomes of these conditions varied following reperfusion. Reperfusion following 4 h OGD was protective (significant reduction in early apoptotic cells and an increase in viable cells), however, reperfusion following 6 h OD and OGD worsened the injury (significant reduction in early apoptotic cells and increase in necrotic cells). Compared to Nx (24 h), significant reduction in viable cells, and an increase in early apoptotic and necrotic cells were seen following 24 h GD, OD, and OGD. There was further increase in necrotic cells in these conditions with reperfusion (Figure 3.5).

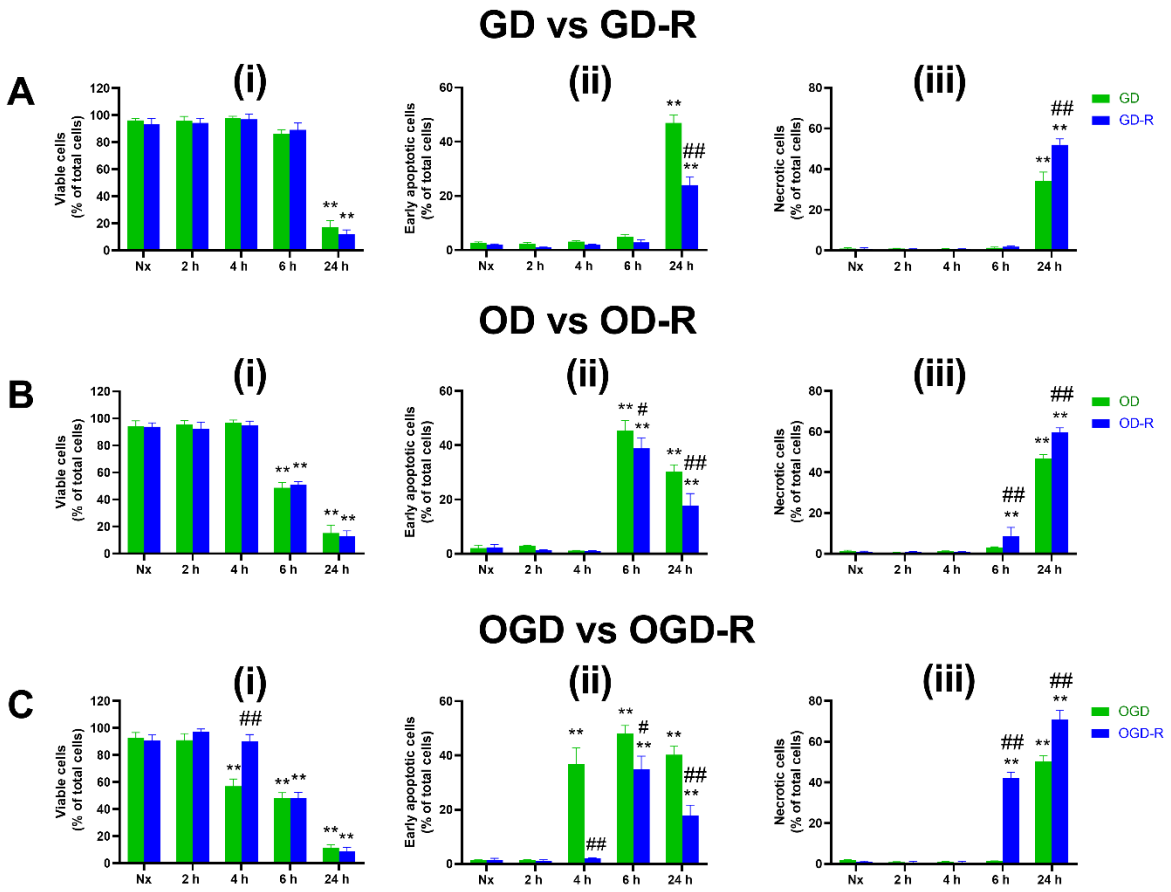

Figure 3.5. PC12 cell apoptosis in response to Nx, GD, OD, and OGD before and after 24 h reperfusion. Bar graphs representing PC12 cell apoptosis using FACS (Fluorescence-activated cell sorting) analysis (Annexin-V and 7-AAD) in response to Nx, GD, OD, and OGD at 2, 4, 6, 24 h, before and after 24 h reperfusion (R) (A) GD vs GD-R (B) OD vs OD-R (C) OGD vs OGD-R. (i) Bar graphs representing viable cells (AV^- / $7\text{-}AAD^-$), % of total cells. Compared to Nx, there was a significant reduction in viable cells by GD (24 h), OD (6 h, 24 h), and OGD (4 h, 6 h, 24 h). (ii) Bar graphs representing early apoptotic cells (AV^+ / $7\text{-}AAD^-$), % of total cells. Compared to Nx, there was a significant increase in early apoptotic cells by GD (24 h), OD (6 h, 24 h), and OGD (4 h, 6 h, 24 h). There is a significant reduction in early apoptotic cells and greater number of viable cells following reperfusion in cells pre-exposed to 4 h OGD. Reperfusion following 6 h OD and OGD resulted in a

reduction in early apoptotic cells and increase in necrotic cells. (iii) Bar graphs representing necrotic cells (AV^+ / $7\text{-}AAD^+$), % of total cells. There was a significant increase in necrotic cells by GD (24 h), OD (24 h), and OGD (24 h); there is a further increase in necrotic cells following reperfusion. *(For all graphs, ** represents $p < 0.01$ against Nx (same time point); $^{\#}$ represents $p < 0.05$ and $^{\#\#}$ represents $p < 0.01$ against response to the identical condition before reperfusion (same time point); two-way ANOVA followed by Tukey's post-hoc analysis; n=3).*

3.3.3 Effects of GD, OGD, and OGD on HIF1α and HIF2α protein in PC12 cells

The HIF1α and HIF2α protein expression at various durations (2 h, 4 h, 6 h, and 24 h) of GD, OD and OGD in PC12 cells were studies with Western immunoblotting. Compared to Nx (at the same time point), there were no significant changes in HIF1α and HIF2α expression following 2 h GD, OD, and OGD, while, both HIF1α and HIF2α were significantly upregulated at 4 h OGD (~4.5 and 3 folds) and 6 h OGD (~3 and 6folds) respectively. HIF2α expression was significantly greater at 6 h versus 4 h OGD. Compared Nx (same time point), there were no significant changes in HIF1α and HIF2α expression following 4 h and 6 h of GD and OD. On the other hand, compared to Nx (24 h), both HIF1α and HIF2α were significantly upregulated at 24 h GD and OD, but not 24 h OGD. More than ~80% of cells were dead by 24 h OGD insult (Figure 3.6).

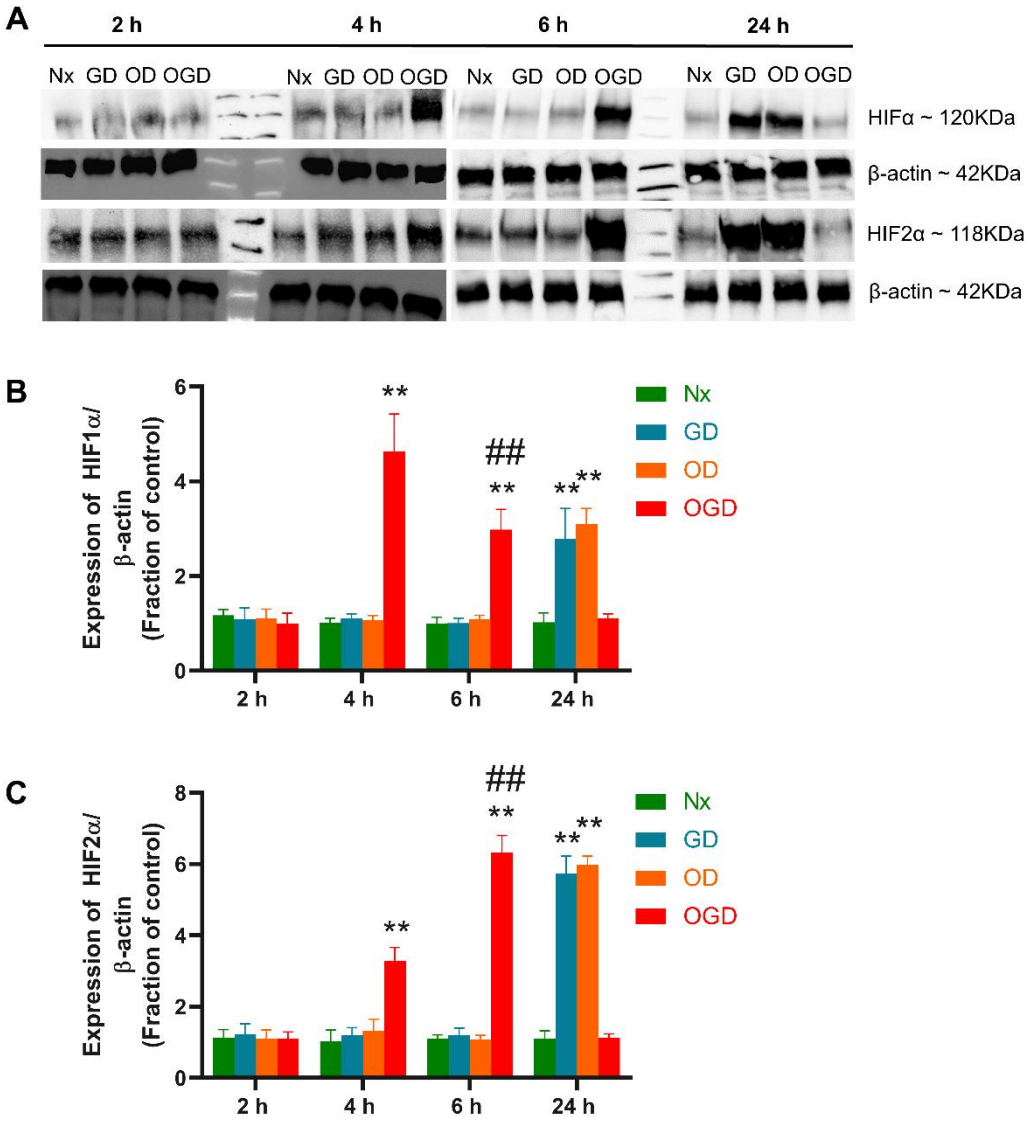

Figure 3.6. HIF1α and HIF2α expression in response to GD, OD, and OGD in PC12 cells. (A) Representative HIF1α, HIF2α, and corresponding β-actin western blots of PC12 cells exposed to Nx, GD, OD, and OGD (2 h, 4 h, 6 h, and 24 h). The protein levels were quantified by densitometric analysis using Image J. Values were normalized to β-actin and corresponding control (B) Bar graph representing normalised HIF1α expression. HIF1α was significantly upregulated by 4 h, 6 h OGD, and 24 h GD / OGD compared to Nx (same time point) (C) Bar graph representing normalised HIF2α expression. HIF2α was significantly upregulated by 4 h, 6 h OGD, and 24 h GD / OGD compared to Nx (same time point). *(For all graphs, ** represents*

$p < 0.01$ against Nx (same time point) and $^{\#\#}$ represents $p < 0.01$ against 4 h OGD; two-way ANOVA followed by Tukey's post-hoc analysis; n=4).

3.3.4 Effects of GD, OD, and OGD on gene expression in PC12 cells

The expression of a panel of hypoxic genes were evaluated on PC12 cells at multiple time points in response to GD, OD, and OGD (normalised to Nx) using qPCR. No significant changes in the expression of *Hif1α* (Figure 3.7A) and *Pfkfb1* (Figure 3.7F) were seen in response to GD, OD, and OGD (all time points) compared to Nx (same time point). *Phd2* was significantly upregulated at 6 h OGD compared to 6 h Nx. (Figure 3.7B). *Bnip3* was significantly upregulated in response to 24 h OD and OGD compared to 24 h Nx (Figure 3.7E). *Vegf* (Figure 3.7C), *Glut1* (Figure 3.7D), *Pfkfb3* (Figure 3.7G), and *Ldha* (Figure 3.7H) were significantly upregulated by GD (24 h) and OD (12 h, 24 h) compared to Nx (same time point). *Ldha* and *Pfkfb3* expression levels were significantly ($p<0.01$) higher at 24 h OD compared to 12 h OD. There were no significant ($p>0.05$) differences in *Vegf* and *Glut1* expression at 24 h OD compared to 12 h OD. Compared to Nx (same time point), *Vegf* was significantly upregulated by 4 h and 6 h OGD. There was no significant difference in *Vegf* expression at 4 h OGD versus 6 h OGD. *Glut1*, *Ldha,* and *Pfkfb3* were significantly upregulated at 4 h, 6 h, and 12 h of OGD. The expression of *Ldha* and *Glut1* was significantly ($p<0.05$) higher at 12 h OGD compared to 6 h OGD and at 6 h OGD compared to 4 h OGD. The expression of *Pfkfb3* was significantly ($p<0.05$) higher at 12 h OGD compared to 4 h OGD. There was no significant ($p>0.05$) difference in *Ldha* expression at 6 h OGD versus 4 h OGD.

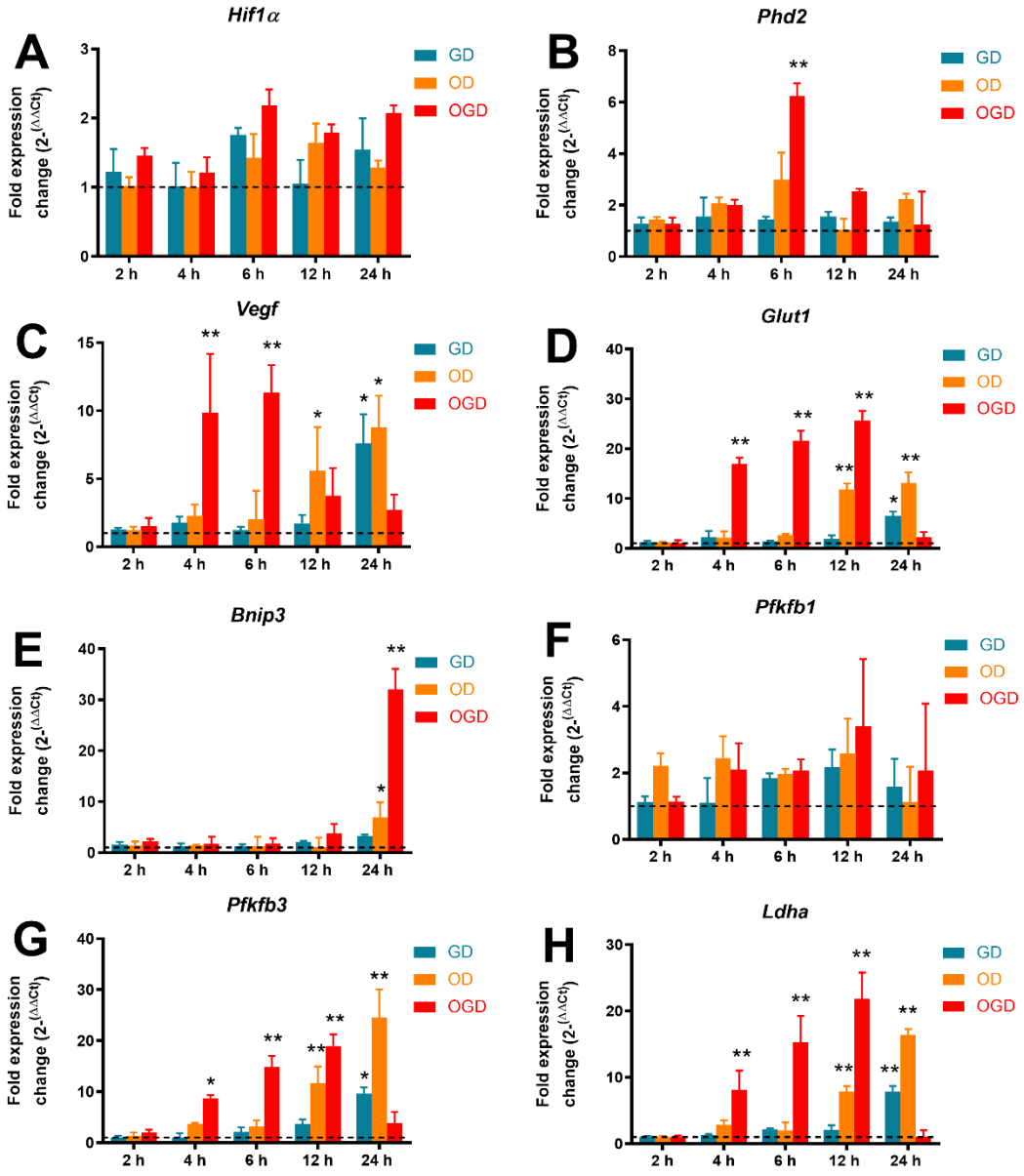

Figure 3.7. Hypoxic gene expression in response to Nx, GD, OD, and OGD in PC12 cells. Bar graphs representing normalised gene expression in PC12 cells in response to GD, OD, and OGD at various time points (2 h, 4 h, 6 h, 12 h, and 24 h). There were no significant changes in (A) *Hif1α* and (F) *Pfkfb1* expression by GD, OD, and OGD compared to Nx (at the time points studied). Compared to Nx, (B) *Phd2* was significantly upregulated by 6 h OGD. Compared to Nx, (C) *Vegf* was significantly upregulated by GD (24 h), OD (12 h, 24 h) and OGD (4 h, 6 h). Compared to Nx, (D) *Glut1* was significantly upregulated by GD (24 h), OD (12 h, 24

h) and OGD (4 h, 6 h, 12 h). Compared to Nx, (E) *Bnip3* was significantly upregulated by 24 h OD and OGD. Compared to Nx, (G) *Pfkfb3* and (H) *Ldha* were upregulated by GD (24 h), OD (12 h, 24 h) and OGD (4 h, 6 h, 12 h). The gene expression was measured against the housekeeping gene *β-actin* and normalised to Nx. Dotted line represents basal gene expression. *(For all graphs, * represents $p < 0.05$ and ** represents $p < 0.01$ against Nx (same time point); two-way ANOVA followed by Tukey's post-hoc analysis; n=3).*

3.3.5 Effects OD and OGD on primary neuronal viabilities

The primary rat neuron culture was characterized by IF staining with Tuj1 and Map2. Tuj1 is a neuron-specific stain found in the cell bodies, dendrites, axons, and axonal terminals (Holloway and Gavins, 2016), whereas Map2 is found in the cell bodies and dendrites of neurons (Holloway and Gavins, 2016). A typical healthy culture consisted of 65.84%±7.23% $Tuj1^+$ nuclei (Figure 3.8A) and 76.31%±11.48% $Map2^+$ nuclei. Healthy neurons consisted of numerous, long axons (Tuj1 staining) and dendrites (Map2 staining).

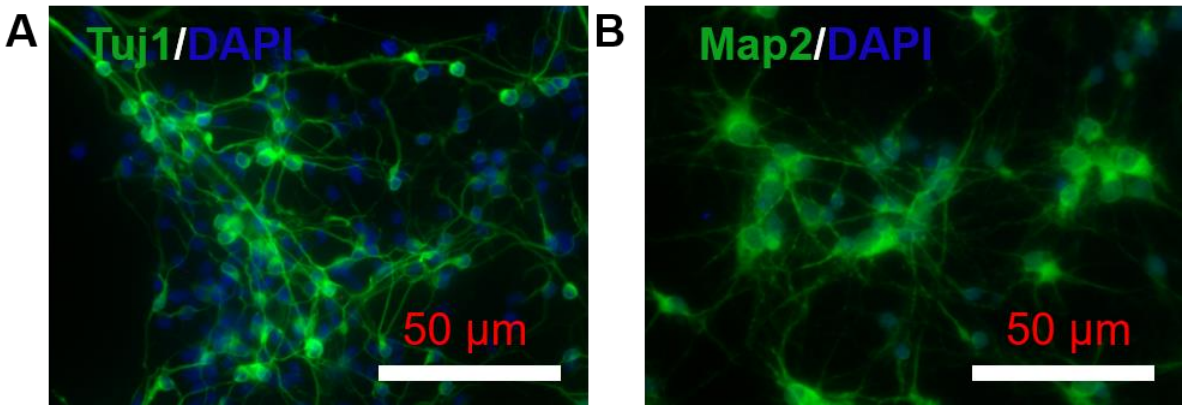

Figure 3.8. Fluorescence micrographs of typical primary rat cortical neuronal culture. (A) Representative double merged micrograph of Tuj1 (FITC) and DAPI stained neuronal culture. A healthy culture consisted of neurons ($Tuj1^+$) with numerous axons. A typical healthy culture consisted of 65.84%±7.23% $Tuj1^+$ nuclei. (B) Representative double merged micrograph of Map2 (FITC) and DAPI stained neuronal culture. A healthy culture consisted of neurons ($Map2^+$) with numerous dendrites. A typical healthy culture consisted of 76.31%±11.48% $Map2^+$ nuclei.

Following studies in PC12 cells, responses of primary neuronal cultures to OD and OGD were studied. GD was not evaluated on primary neurons, as it least mimics the conditions of cerebral ischaemia *in vitro*. Primary rat neurons were treated with Nx, OD, and OGD for 2 h, 4 h, and 6 h. Cell viability and morphological changes were assessed at the end of each treatment (OD, OGD) duration and following 24 h reperfusion (Figure 3.2).

In primary neurons, OD (6 h) and OGD (4 h, 6 h) significantly reduced mitochondrial activity compared to Nx (same time point) (Figure 3.9A). Compared to 4 h OGD, mitochondrial activity was significantly ($p<0.05$) lower at 6 h OGD. OD (4 h) had no significant effect on mitochondrial activity compared to Nx (4 h). There were no significant changes in mitochondrial activity after reperfusion in cells exposed to prior 6 h OD and 4 h OGD. Reperfusion after 6 h OGD resulted in a further reduction in mitochondrial activity. Compared to Nx (6 h), LDH release significantly increased at 6 h OGD (Figure 3.9B). All other conditions (2, 4, 6 h of OD and 2, 4 h OGD; with / without reperfusion) were not cytotoxic (no LDH release) compared to Nx (same time point). Reperfusion after 6 h OGD resulted in a further increase in LDH release.

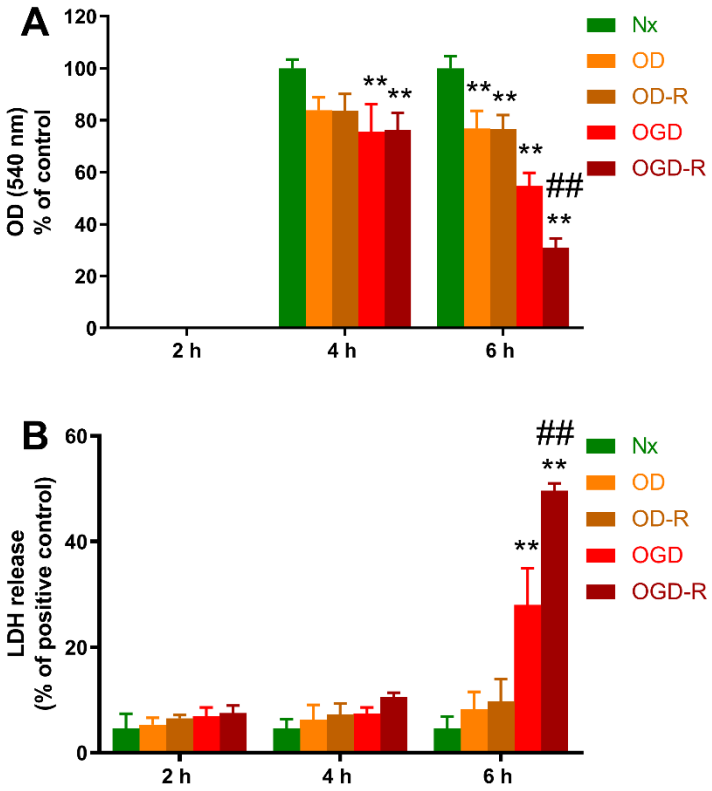

Figure 3.9. Responses of primary rat neurons to Nx, OD, and OGD. Bar graphs representing responses of primary neuronal cultures to Nx, OD, and OGD at varying time points. The responses were compared before and after 24 h reperfusion. (A) MTT assay revealed a significant reduction in MTT activity by OD (6 h) and OGD (4 h, 6 h). A significant further reduction in MTT activity was seen following 24 h reperfusion in cells pre-exposed to 6 h but not 4 h OGD. (B) LDH assay revealed a significant increase in LDH release by 6 h OGD and a further increase was seen following reperfusion. *(For all graphs, ** represents $p < 0.01$ against Nx and $^{\#\#}$ represents $p < 0.01$ against response to the identical condition before reperfusion; two-way ANOVA followed by Tukey's post-hoc analysis; n=3).*

Morphological changes (Map2 staining) were evaluated in primary neurons subjected to Nx, OD, and OGD for 2 h, 4 h, and 6 h, both before and after reperfusion. Healthy cultures (Nx) consisted of neurons surrounded by numerous $Map2^{+}$ dendrites (7.6±4.2 dendrites per neuron, with each dendrite measuring 31.4±12.69 µm). OD (2 h, 4 h, and 6 h ± reperfusion) and OGD (2 h, 4 h ± reperfusion) did not alter neuron morphology, dendrite length, or dendrite numbers. Compared to Nx (same time point), 6 h OGD resulted in significant changes in neuron morphology (degradation of dendrites: 1.8±0.6 dendrites per neuron, with each dendrite measuring 5.2±2.4µm; *$p<0.05$ versus 6 h Nx*). Following reperfusion, there was a complete loss of neuronal dendrites. In 6 h OGD alone and after reperfusion, the dendrites were degrading and there was a loss of Map2 indicating degeneration of neurons (Figure 3.10).

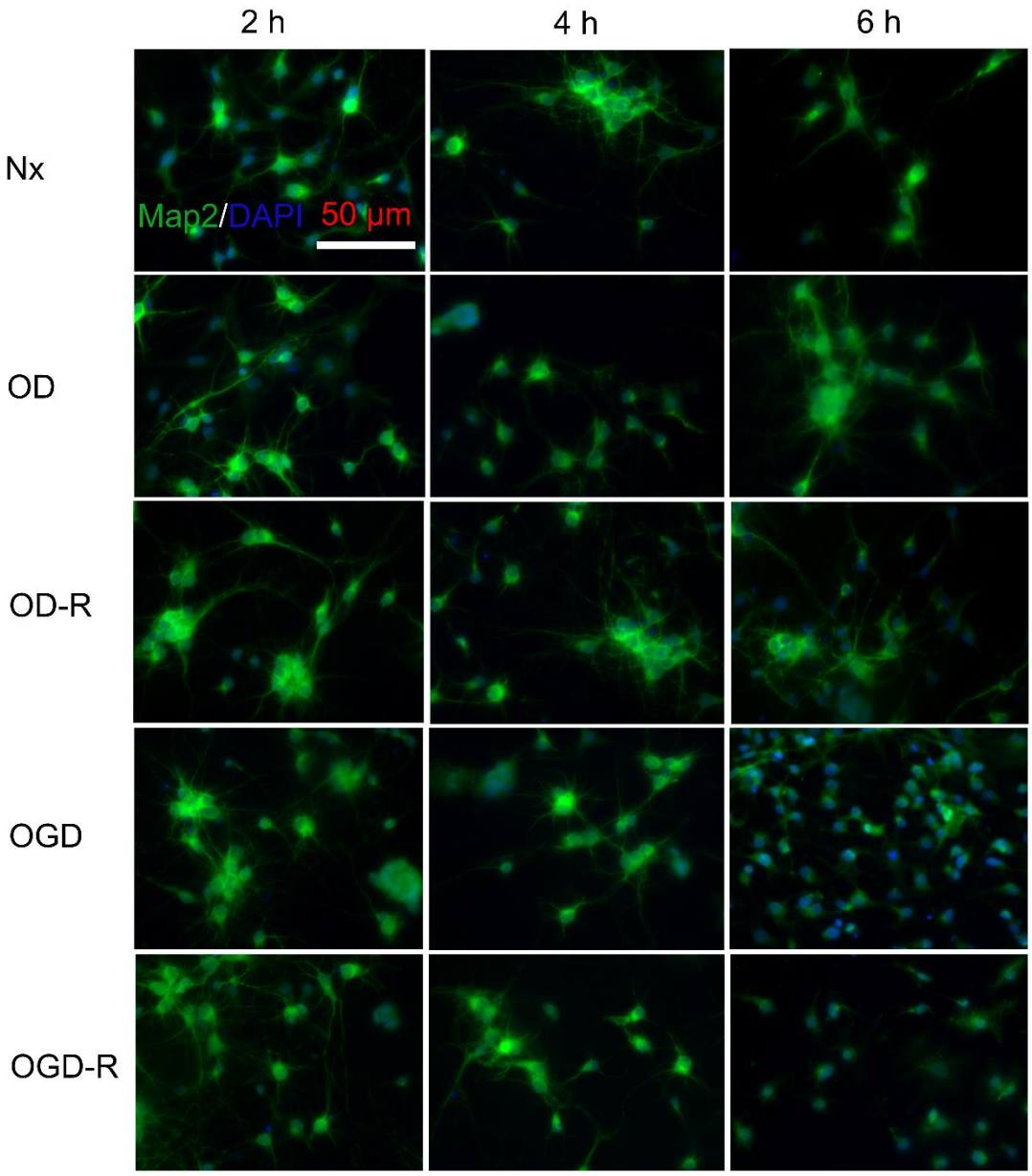

Figure 3.10. Fluorescence micrographs of neuronal cultures subjected to Nx, OD, and OGD. Representative double merged micrographs of Map2 (FITC) and DAPI stained neuronal cultures following exposure to Nx, OD, and OGD for 2, 4, and 6 h alone and after reperfusion. Healthy culture (Nx) consisted of neuronal nuclei ($Map2^{+}$) surrounded by numerous dendrites. Compared to Nx (same time point), there were no changes in neuronal morphology following OD (2 h,4 h, 6 h) and OGD (2, 4 h), both before and after reperfusion. Cultures subjected to 6 h OGD alone and after reperfusion displayed neurons with reduced / no dendrites compared to 6 h Nx.

3.3.6 HIF1α and HIFα expression in primary neurons in OD and OGD

The expression of HIF1α and HIF2α were evaluated in primary neurons exposed to OD and OGD (2 h, 4 h, 6 h) in comparison to Nx (Figure 3.11). There was no significant HIF1α and HIF2α expression at 2 h and 4 h OD but significantly increase in HIF1α (~4.8 folds) and HIF2α (~2.8 folds) at 6 h OD compared to Nx (same time point). HIF1α was significantly upregulated following 2 h (~3.7 folds), 4 h (~3.6 folds) and 6 h (~4.6 folds) OGD. Compared to Nx (same time point), HIF2α was significantly upregulated following 4 h (~3.4 folds) and 6 h (~4.8 folds) OGD. There is no significant ($p>0.05$) difference in HIF2α expression at 6 h versus 4 h OGD.

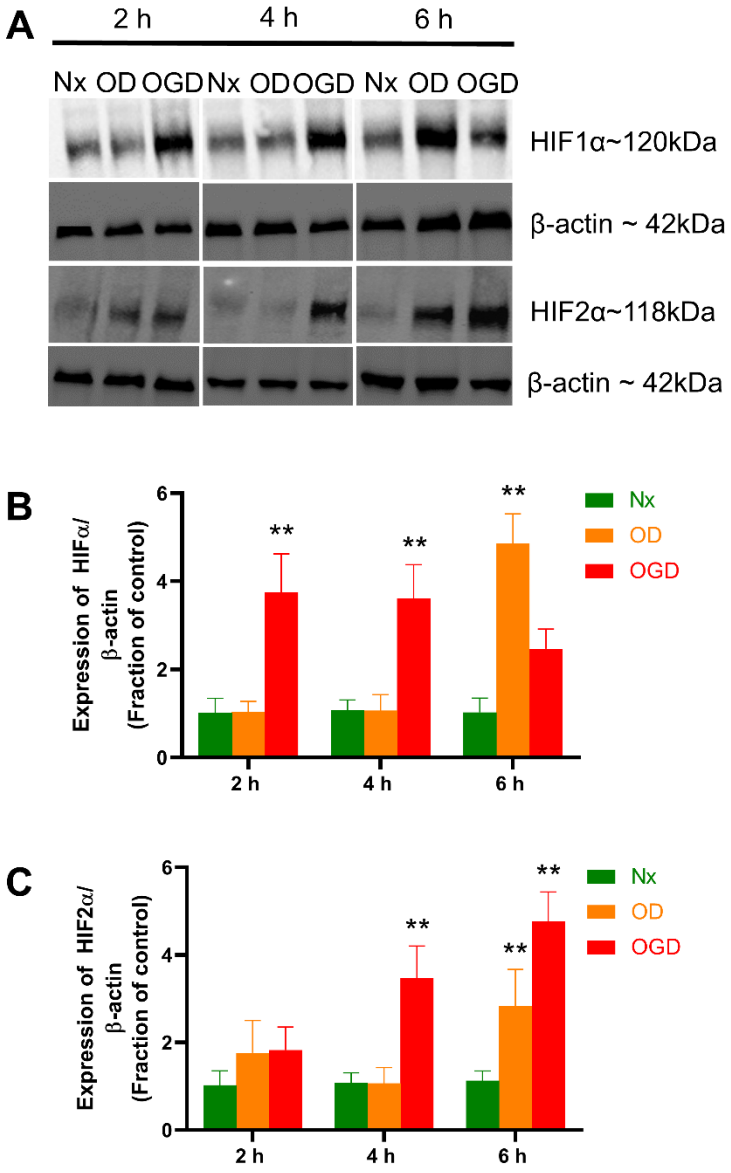

Figure 3.11. Effects on OD and OGD on HIF1α and HIF2α expression in primary neurons. (A) Representative HIF1α, HIF2α, and corresponding β-actin western blots of primary neurons exposed to Nx, OD, and OGD for 2 h, 4 h, and 6 h. The protein levels were quantified by densitometric analysis using Image J. Values were normalized to β-actin and corresponding control. (B) Bar graph representing normalised HIF1α expression. HIF1α was upregulated by OD (6 h) and OGD (2 h, 4 h). (C) Bar graph representing normalised HIF2α expression. HIF2α was upregulated

by OD (6 h) and OGD (4 h, 6 h). *(For all graphs,** represents $p < 0.01$ against Nx (same time point); two-way ANOVA followed by Tukey's post-hoc analysis; n=3).*

3.3.7 Gene expression in primary rat neurons in OD and OGD

The expressions of a panel of hypoxic genes were evaluated on primary neurons in response to 2 h, 4 h, and 6 h of OD and OGD (normalised to Nx) using qRT-PCR. Compared to Nx (same time point), there were no significant changes in *Hif1α* (Figure 3.12A)*, Hif2α* (Figure 3.12B)*, Glut1* (Figure 3.12G)*, Pfkfb1* (Figure 3.12I), and *Pfkfb3* (Figure 3.12J) expression following OD and OGD (all time points). *Phd2* was significantly upregulated by 6 h OD and OGD compared to 6 h Nx. Compared to Nx (same time point), OD and OGD (2 h, 4 h) had no significant effect on *Phd2* expression (Figure 3.12B). *Epo* (Figure 3.12D), *Vegf* (Figure 3.12E), and *Ldha* (Figure 3.12H) were significantly upregulated following 6 h OD compared to Nx (same time points). OD for 2 h and 4 h did not alter *Epo*, *Vegf*, and *Ldha* expression. OD (2, 4, and 6 h) did not alter *Bnip3* expression compared to Nx (same time point) (Figure 3.12F)*. Epo*, *Vegf,* and *Bnip3* were significantly upregulated following 2 h, 4 h, and 6 h OGD compared to Nx (same time point). There were no significant differences between *Epo*, *Vegf,* and *Bnip3* expression at 6 h OGD compared to 2 h or 4 h OGD. Compared to Nx (same time point), *Ldha* was significantly upregulated following 4 h and 6 h, but not 2 h OGD. *Ldha* expression was significantly ($p<0.05$) higher at 6 h OGD compared to 4 h OGD.

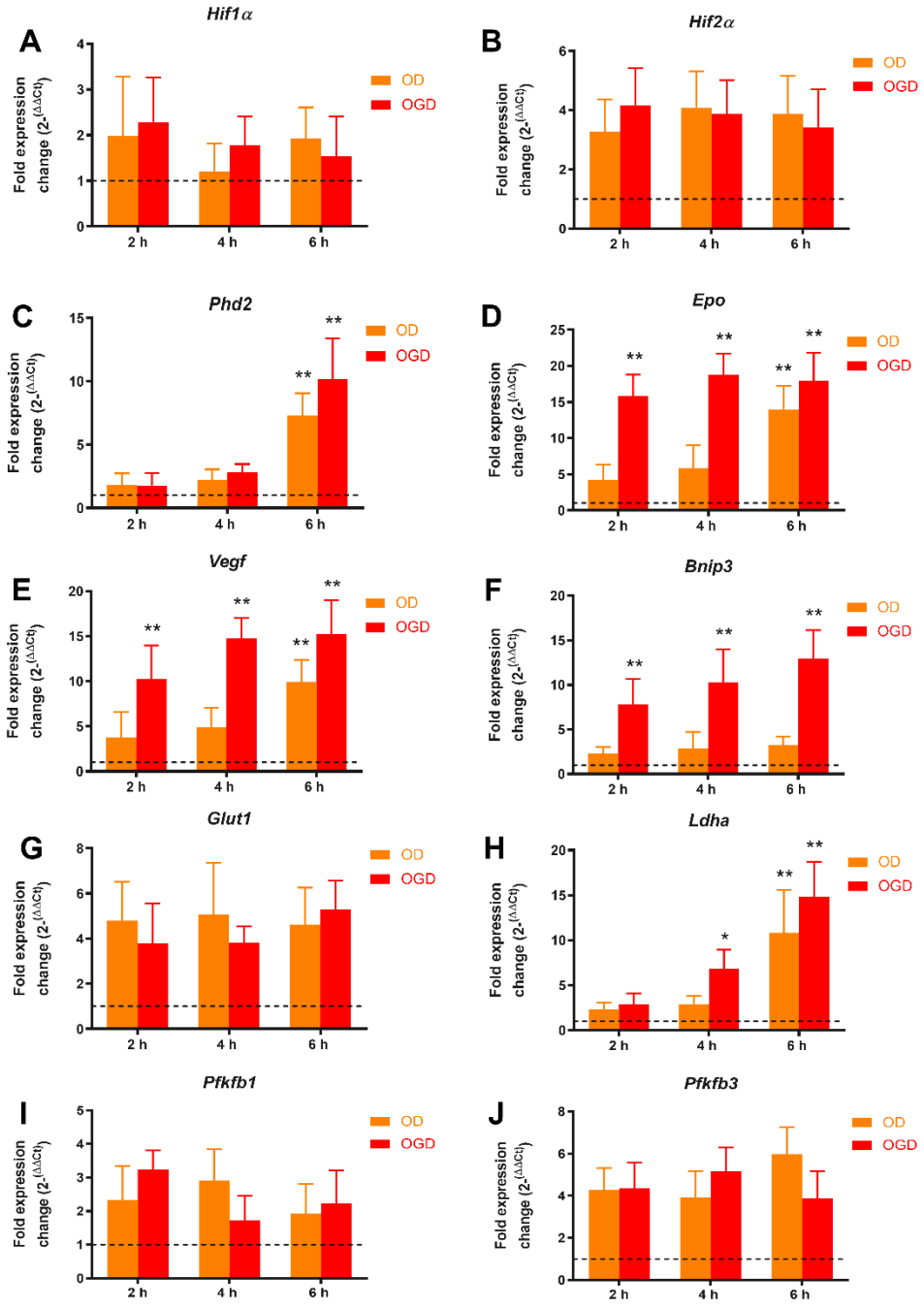

Figure 3.12. Hypoxic gene expression in response to OD and OGD in primary neurons. Bar graphs representing normalised gene expression in primary neuronal cultures in response to OD and OGD at various time points (2 h, 4 h, and 6 h). Compared to Nx, there were no significant changes in (A) *Hif1α,* (B) *Hif2α,* (G) *Glut1,*

(I) *Pfkfb1*, and (J) *Pfkfb3* expression by OD and OGD (at the time points studied). Compared to Nx, (C) *Phd2* was significantly upregulated by 6 h OD and OGD. Compared to Nx, (D) *Epo* and (E) *Vegf* were significantly upregulated by OD (6 h) and OGD (2 h, 4 h, and 6 h). Compared to Nx, (F) *Bnip3* was significantly upregulated by OGD (2 h, 4 h, and 6 h). Compared to Nx, (H) *Ldha* was significantly upregulated by OD (6 h) and OGD (4 h, 6 h). The gene expression was measured against the housekeeping gene *β-actin* and normalised to Nx. Dotted line represents basal gene expression. *(For all graphs, * represents $p < 0.05$ and ** represents $p < 0.01$ against Nx (same time point); two-way ANOVA followed by Tukey's post-hoc analysis; n=3).*

3.4 Discussion

The experiments in this chapter were performed to determine the time points at which OGD induced toxicity in PC12 cells and primary neurons, to inform choices for ischaemic insult (cell death evident) and sublethal ischaemia (cell death minimal or absent) for future experiments. In summary, results revealed that 2 h OGD did not result in cell death or alter mitochondrial activity of PC12 cells and primary neurons. There was a significant reduction in mitochondrial activity by 4 h OGD in both PC12 cells and primary neurons; however, there was no significant cell death. Both 2 h and 4 h OGD were sublethal. OGD (6 h) resulted in significant cell death in PC12 cells and primary neurons. Reperfusion following 6 h OGD, further propagated cell death. OGD treatment from 2 h (primary neurons) and 4 h (PC12 cells) onwards, significantly upregulated HIF1α. In both PC12 cells and primary neurons, HIF2α expression significantly increased from 4 h OGD onwards.

Glucose and oxygen are essential factors to maintain cell activity. Due to the lack of blood vessels for constant oxygen and glucose supply, the *in vitro* environments can differ from *in vivo*. However, preliminary *in vitro* studies are suitable to understand the underlying molecular mechanisms and perform several experiments. Three factors influence the oxygen present in the cells: the gaseous oxygen in the atmosphere surrounding the culture, dissolved oxygen in culture media, and oxygen consumed by the cells in the culture dish. Although 21% O_2 represents the fraction of oxygen in dry air, cell culture incubators also introduce volumes of water vapour and carbon dioxide, thereby the concentration of oxygen in the culture media is much less than 21%. Studies have reported that in the atmosphere surrounding the cell culture plate in the incubator, there is around 18.6% O_2 (considering the following

are constant: 5% CO_2, 100% humidity, 37^oC, atmospheric pressure at sea level) (Place *et al*., 2017; Newby *et al*., 2005).

Although there are several types of cell culture media, all the commercially available media behave similarly in regards to oxygen solubility. Factors that affect solubility of oxygen in cell culture media are temperature, altitude and salinity. The solubility of oxygen in a liquid is inversely proportional to the temperature and salinity of the liquid. As salinity increases, oxygen competes for space between molecules to dissolve, thereby decreasing oxygen binding (Neutsch *et al.,* 2018). As seen physiologically, oxygen does not dissolve in blood (i.e. hot saline liquid) and binds to haemoglobin. Similarly, increase in temperature and salinity of culture media, results in reduced oxygen dissolution (Newby *et al.,* 2005). Factors such as protein concentration (0.3 – 0.45 mg / dL) and ionic strength (150-200 mM; similar to blood plasma) are very similar in all culture media. Dissolved oxygen levels in culture media are typically between 10-12% O_2 (at 37^OC, fresh media) (Place *et al*., 2017). *In vivo,* circulating arterial blood contains 10.5-13% O_2, venous blood return contains ~7% O_2 and the brain function at 3-5% O_2. During ischaemic stroke, the O_2 levels in the penumbra range from 1-3% and in the core are less than 1%. (Holloway and Gavins, 2017). For OD and OGD conditions in all experiments in this thesis, O_2 levels were maintained at 0.3% in a hypoxia chamber to mimic the core region. Newby *et al.* (2005) and Mohammad *et al*. (2015) reported that media can take up to 24 h to equilibrate with oxygen levels in the hypoxia chamber. Because of these factors, the media was always degassed in the hypoxia chamber for 24 h prior to experiments in this study.

The *in vitro* oxygen levels during normoxia and reperfusion are higher than those found *in vivo*. Returning cells to high oxygen levels during reperfusion can potentiate free radical formation. Additionally, cells can also be resistant to oxidative stress if they are grown in hyperoxic environments prior to ischaemic challenge (Holloway and Gavins, 2017). The rate of oxygen and glucose diffusion into cells depends on several factors such as depth of media, cell density, and cell type (Place *et al*., 2017). Although the oxygen and glucose uptake were not monitored in these experiments, volume of media and cell densities were kept consistent in all the replicates to ensure accuracy and reliability.

In addition to the oxygen levels, even the glucose levels in the culture media far exceed physiological levels. The complete media used for experiments in PC12 cells, primary neurons, and primary astrocytes (Chapter 6) consisted of approximately 22.5, 24, and 22.7 mM of glucose respectively (Table 3.1). Plasma glucose range from 5.5 to 7.8 mM, while brain glucose levels range from 0.82 to 2.4 mM (Holloway and Gavins, 2017). Glucose found in the media is at least 10 times more than *in vivo* glucose levels in the brain. These media are widely used for studies *in vitro* studies as they influence cell growth and can maintain cells for 2-3 days without media changes. However, these can negatively affect cell viability and alter their metabolic profile. They can also influence pathways such as AMPK and alter the cellular responses to stress conditions (Holloway and Gavins, 2017).

Table 3.1. Glucose concentration in media used in different cultures.

Media	Glucose (mM)	Approximate glucose concentration
PC12 cell media	High glucose DMEM contains 25 mM glucose 5% of HS contains 0.1 mM glucose 5% of FBS contains 0.15 mM glucose	The media was supplemented with 10% serum and 1% PS so 89% of total glucose (25.25 mM) is equivalent to around 22.5 mM
Primary neuronal culture media	High glucose Neurobasal media contains 25 mM glucose There was no serum supplementation and B27 did not contain glucose.	The media was supplemented with 2% B-27, 1% PS, and 1% Glutamine so 96% of total glucose (25 mM) is equivalent to around 24 mM
Primary astrocyte culture media	High glucose DMEM contains 25 mM glucose 10% of FBS contains 0.3 mM glucose	The media was supplemented with 10% serum, 1% PS, and 1% Glutamine so 88% of total glucose (25.3 mM) is equivalent to around 22.7 mM

Initial experiments were performed using PC12 cells. PC12 cells originated from the adrenal medulla of rat and have been extensively used in neurobiological studies such as investigation of signal transduction mechanisms, apoptosis, calcium signalling, Alzheimer's disease, Parkinson's disease, cerebral ischaemia, and Huntington's disease (Hillion *et al.*, 2005; Chen *et al.,* 2012). PC12 cells closely resemble neurons with smaller vesicles and quantal size. Undifferentiated PC12 cells have some characteristics of neurons such as abilities to synthesize, store and release dopamine and norepinephrine in response to extracellular potassium ion concentration, rise of nicotinic acetylcholinesterase receptor and existence of GABA, acetylcholinesterase and tyrosine hydroxylase (Chen *et al.,* 2012). PC12 cells have abilities to differentiate into neurons in response to NGF (Greenberg, 1985). Upon differentiation with NGF, the morphology, physiology, and biochemistry of PC12 cells change into parasympathetic neuron type. They display neurites, more potassium channels, and possess electrical excitability (Greenberg, 1985). Studies have implicated that NGF exerts a neuroprotective role against ischaemia in PC12 cells (Sun *et al.*, 2017; Lahiani *et al.*, 2015; Tabakman, 2005). Many studies have demonstrated that non-differentiated PC12 cells respond to ischaemia in similar ways to differentiated cells (Mei *et al.,* 2011; Hillion *et al.*, 2006; Hillion *et al.*, 2005; Vaghefi, 2004), due to which non-differentiated PC12 cells were used for experiments.

In PC12 cells, GD for up to 6 h did not significantly alter mitochondrial activity and LDH release. GD (12 h, 24 h) resulted in a significant reduction in mitochondrial activity and an increase in LDH release compared to Nx (same time point). There

was no significant difference in response at 12 h compared to 24 h GD. GD (up to 24 h) did not alter cell viability (trypan blue assay). A study by Liu *et al.,* 2003 reported a significant reduction in MTT activity to ~50% by 24 h GD.

In experiments involving deprivation of oxygen (OD, OGD), oxygen levels were reduced to 0.3%. These oxygen levels are similar to levels during ischaemia in the core region (Miyamoto and Auer, 2000). Compared to Nx (same time points), 6 h OD resulted in a significant reduction in mitochondrial activity and an increase in LDH release. Compared to 6 h OD, mitochondrial activity and LDH release did not change at 12 h OD but significantly changed (further increase in mitochondrial activity and reduction in LDH release) at 24 h OD. Cell viability (trypan blue assay) was not altered at 6 h OD compared to Nx but significantly reduced at 12 h and 24 h OD. A study by Ma *et al*. (2017), revealed a reduction of cell viability to around ~50 % (versus 100% control) and 3 fold increase (compared to untreated control) in LDH release by 24 h OD (0% O_2) in PC12 cells. Results revealed no significant changes in mitochondrial activity, cell viability, and LDH release at 4 h OD compared to Nx. However, a study by Luo *et al.,* 2011 showed a significant increase in LDH release and reduction in cell viability by 3 h OD (2% O_2).

PC12 cells were most sensitive to the simultaneous omission of oxygen and glucose (OGD) compared to OD and GD. OGD (4 h) reduced mitochondrial activity but did not result in cell death. OGD for 4 h significantly reduced mitochondrial activity but did not alter LDH release or cell viability (trypan blue assay). From 6 h onwards, OGD resulted in a time-dependent reduction in both mitochondrial activity LDH release and cell viability (trypan blue assay). A study by Mang *et al*., 2013 revealed a

significant reduction in MTT activity by 6 h (~80%), 12 h (~60%), and 24 h (~20%) of OGD (0.5% O_2). Xian *et al*., 2016 also revealed a significant increase in LDH release to ~60% following 8 h OGD (1% O_2) insult. Sun *et al*., 2017 revealed that 12 h OGD resulted in significant reduction in PC12 cell viability (CCK8: 28% vs 100% in control).

MTT and LDH assay results varied from each other because the end-points of both these assays are different. MTT is a reliable indicator of cellular metabolic activity, whereas LDH assay is representative of membrane depolarisation and measures cell membrane integrity (Bopp and Lettieri, 2008). Ischaemia results in alteration of cellular metabolic activity to cope up with the reduction in glucose and / or oxygen supply, without altering cell membrane integrity. Both trypan blue exclusion and LDH assay rely on cell membrane integrity. However, compared to LDH assay, trypan blue assay may result in underestimation of cell death. Trypan blue assay is a dye exclusion assay that relies on the principle that living cells possess an intact cell membrane that excludes the die, whereas dead cells do not. However it is important to consider that lethally damaged cells may require several days to lose membrane integrity, the surviving cells continue to proliferate and some lethally damaged cells may not appear stained with dye as they may undergo early disintegration.

Reperfusion following lethal GD, OD and OGD insults, resulted in further worsened outcomes (further reduction in mitochondrial activity, cell viability, and an increase in LDH release). The results are in line with several studies that have revealed that reperfusion following OGD (6 h) resulted in a significant reduction in PC12 cell viability (Yuan *et al*., 2018; Li *et al*., 2018, Singh *et al.,* 2009). A study by Yuan *et al.,*

(2018) found that 24 h reperfusion following 6 h OGD (0.5% O_2) resulted in a significant reduction in cell viability (CCK8: 50% vs 100% in control), and increase in LDH release (3.4 folds greater than control) in PC12 cells. Li *et al.,* (2018) reported that 24 h reperfusion following 6 h OGD (1% O_2) resulted in a significant reduction in cell viability (CCK8: 68% vs 100% in control). Singh *et al.,* (2009) found that 24 h reperfusion following 6 h OGD (0.5 % O_2) resulted in significant cell death (Trypan blue: 45% vs 6% in control). Guo *et al.,* (2014) found that 12 h OGD (1% O_2) followed by reperfusion resulted in significant reduction in PC12 cell viability (MTT activity: 60% vs 100% control; LDH release: 40% vs 15% control). It is widely accepted that the extent of I / R injury is influenced by the magnitude and duration of ischaemia. Reperfusion provides oxygen and glucose that are essential to salvage ischaemic tissue, however, reperfusion itself paradoxically potentiates damage (Lin *et al.,* 2016; Nour *et al.,* 2013). There are several complex and multifactorial mechanisms underlying I / R injury, which involve ROS generation (and lipid peroxidation), calcium overload, the opening of MPTP, endothelial dysfunction, and prominent inflammatory responses such as leucocyte infiltration, platelet activation, and complement activation (Kalogeris *et al.,* 2012; Dorweiler *et al*., 2007; Pan *et al.,* 2007).

Apoptosis is a programmed cell death mechanism, the features of which include: DNA fragmentation, nuclear condensation, cell shrinkage, the formation of apoptotic bodies, and expression of ligands for phagocytic receptors (Section 1.2.4). Apoptotic cells are rapidly cleared by phagocytosis, without eliciting an inflammatory response (Broughton *et al.*, 2009). Necrosis is an irreversible form of cell death that involves disruption of the plasma membrane (Dirnagl *et al.,* 1999; Durukan and Tatlisumak,

2007). Early apoptosis and necrosis were studied using flow cytometry (Annexin-V and 7-AAD double staining). Annexin-V is a widely used marker of early apoptosis based on the expression of phosphatidylserine groups of extracellular surfaces. On the other hand, 7-AAD is a membrane impermeant dye that is excluded in viable cells.

The following conditions: GD (2 h, 4 h, 6 h); OD (2 h, 4 h); OGD (2 h) did not result in any significant apoptosis or necrosis and majority of the cells remained viable. In line with MTT assay results, there was a significant reduction in viable cells and an increase in early apoptotic cells following 4 h OGD (compared to Nx), however, after reperfusion, the early apoptotic cells recovered. A study by Li *et al.,* 2018 revealed that 4 h OGD (0.5% O_2) resulted in significant apoptosis (flow cytometry was used to measure % apoptosis (AV^+ / 7-AAD^- out of total cells): 24% vs 6% in control) in PC12 cells. Studies have reported that apoptosis (early stages) is reversible and can be often recovered upon timely reperfusion (Prabal *et al.,* 2010; Dirnagl *et al.,* 1999). Significant reductions in viable cells and increase in early apoptotic cells were seen following 6 h OD and OGD (versus Nx). Before reperfusion, no significant necrosis was found; however, after 24 h reperfusion, the early apoptotic cells reduced and necrotic cells increased. A study by Yuan *et al.,* (2018) found that 24 h reperfusion following 6 h OGD (0.5% O_2) resulted in significant apoptosis (flow cytometry was used to measure % apoptosis (AV^+ / 7-AAD^- out of total cells): 31% vs 7% control) in PC12 cells. Reperfusion increases apoptosis by providing the energy required for the completion of apoptosis (Broughton *et al.*, 2009). Compared to Nx, there was a significant reduction in viable cells and subsequent increase in early apoptotic and necrotic cells by 24 h GD, OD, and OGD; after reperfusion, there was a reduction in

early apoptotic cells and an increase in necrotic cells. A study by Li *et al.,* (2003) showed that both necrosis and apoptosis were significant at 24 h GD in PC12 cells. Sun *et al.,* (2017) found that 12 h OGD (1% O_2) resulted in significant apoptosis (TUNEL positive cells: 50% vs 10% control) and necrosis (propidium iodide (PI) positive cells: 38% vs 5% in control), which further increased following 1 h reperfusion (PI^+ cells: 51% and TUNEL positive cells: 60%). Guo *et al.,* 2014 also (found) that 12 h OGD (1% O_2) followed by reperfusion resulted in significant apoptosis (flow cytometry was used to measure % apoptosis (AV^+ / PI^- out of total cells): 45% vs 6% control) in PC12 cells.

Microtubule-associated proteins (MAPS) are a family of proteins that bind to and stabilise microtubules. Map2 is a neuron-specific isoform that is involved in the assembly of tubulin into microtubules. Map2 is primarily expressed in the dendrites of mature neurons, influencing the density of microtubules and length of dendrites (Soltani *et al.,* 2005; Hubber and Matus, 1984). In response to neuronal stress (such as OGD), Map2 staining reveals the degradation of dendrites progressing to complete loss of Map2 staining (Bonde *et al.,* 2002). Tuj1 is part of the tubulin family that are major building blocks for microtubules and structural component of the cytoskeleton. Tuj1 is also neuron-specific; found in cell bodies, dendrites, axons, and axonal terminals of immature and differentiated neurons. Tuj1 reveals alteration of the cytoskeleton and progressive loss of neurites upon injury (Geisert and Frankfurter, 1989). Morphology of primary neurons was initially assessed using Map2 and Tuj1 staining; however, the Map2 staining was pursued further for understanding stress-related changes in neuron structure as it specifically stained the soma of mature neurons and was less complex.

Following studies in PC12 cells, the effects of OD and OGD were evaluated in primary rat cortical neuron cultures. Results revealed that OD (up to 6 h) did not result in significant changes. Similar to PC12 cells, OD (up to 6 h) did not alter mitochondrial activity or result in cell death in primary neuronal cultures. Lu *et al.,* (2014) also showed significant cell death in primary cortical neurons initiated from 12 h of OD (0.5% O_2) onwards. 24 h OD resulted in ~50% cell death (Lu *et al.,* 2014). There was a significant reduction in mitochondrial activity but no effect on LDH release or neuron morphology (Map2; dendrites length and number) following 4 h OGD (versus Nx). The changes in mitochondrial activity found following 4 h OGD, were not significantly altered after reperfusion. OGD for 6 h (versus Nx) resulted in a significant increase in mitochondrial activity, reduction in LDH release, and morphological changes (Map2; reduction / absence of dendrites and a significant reduction in dendrites length). Following reperfusion, there was a further reduction in mitochondrial activity and an increase in LDH release. Similarly, a study by Zhang *et al*., (2017) revealed that 6 h OGD (0% O_2) resulted in significant neuronal death (LDH release: 56.7% vs 19.5% in untreated control) and apoptosis (TUNEL positive cells: 16.5% vs 2% in untreated control). Tian *et al*., (2018) also showed a significant increase in LDH leakage (~3 folds greater than untreated control) and reduction in cell viability (MTT activity: ~50% vs 100% in untreated control) by 6 h OGD (1% O_2) in primary rat cortical neurons. In contrast, Bhuiyan *et al.,* (2011) showed that 4 h OGD (0% O_2), followed by 24 h reperfusion resulted in significant cytotoxicity (LDH release: 60% vs 10% in untreated control). Another study also showed that 1 h of OGD (1% O_2) followed by 24 h of reperfusion resulted in a 20% decrease in cell viability indicating a moderate degree of cellular stress compared with 3 h OGD

where the viability was decreased by more than 50% (Wappler *et al.,* 2013). Both Bhuiyan *et al.,* (2011) and Wappler *et al.,* (2013) used EBSS (Earl's balanced salt solution) for OGD conditions. In contrast, for experiments in this chapter and other studies (Zhang *et al*., 2017; Tian *et al*., 2018) glucose-free Neurobasal medium supplemented with B27 was used. A recent study by Sunwoldt *et al.,* (2017) found that B27 protected neurons from cell death during OGD in comparison to neurons incubated in EBSS. Bhuiyan *et al.,* (2011) also found DIV10 rat cortical neurons were more resistant to OGD-reperfusion injury than DIV7 neurons. For this study, mature (DIV10-14) neurons were used, due to which the impact of OGD insult varied from other studies. Factors such as OGD medium and its components, maturity of neurons during experiments, the origin of neurons (hippocampal, cortical, or mixed), and the magnitude of OGD account for the variations in results in different studies.

The responses of primary neurons and PC12 cells to OGD were similar. Six hours OGD was cytotoxic in both primary neurons and PC12 cells. MTT assay results indicated slightly lower mitochondrial activities in primary neurons compared to PC12 cells by 6 h OGD.

Results revealed that the effects of reperfusion depended on the initial duration of OGD. Reperfusion following 4 h OGD was protective in PC12 cells. However, reperfusion following prolonged OGD (6 h and 24 h) further worsened the injury. Similarly, in primary neurons, reperfusion following 6 h OGD further worsened the outcomes. In contrast, reperfusion following 2 h and 4 h OGD did not have any significant effect on primary neurons. Overall, results revealed that the effect of

reperfusion depended on the initial duration of OGD. Reperfusion following prolonged OGD insults was detrimental; however, reperfusion following acute OGD insults was cytoprotective. These results are in line with the current treatment option of acute ischaemic stroke i.e. reperfusion. Immediate reperfusion (within 4 h) following ischaemia is an acute stroke therapy that helps in restoration of oxygen and blood supply to the cells and aiding their recovery. However, reperfusion can also potentiate cell apoptosis (energy-consuming process) by restoring cellular energy and increasing ROS production (Durukan and Tatlisumak, 2007; Prabal et al., 2010).

HIF is an oxygen-sensing molecule and a key regulator of genetic response following anoxia (discussed in section 1.5). Absence of oxygen results in PHD inhibition and accumulation of the oxygen-regulated HIF1α, which then dimerizes with HIF1β and binds to HRE inducing transcription of various genes (Bergeron *et al.*, 1999; Dirnagl *et al.*, 2009). In PC12 cells, HIF1α was upregulated by OGD (4 h, 6 h) but not 2 h, whereas in primary neurons HIF1α upregulation commenced earlier, from 2 h OGD onwards. In PC12 cells, the expression of HIF1α was greater at 4 h compared to 6 h OGD; however, in primary neurons there were no significant differences in HIF1α at 2 h and 4 h OGD. In both PC12 cells and primary neurons, HIF2α was upregulated by 4 h and 6 h OGD. In PC12 cells, HIF2α expression was significantly higher at 6 h compared to 4 h OGD, however, in primary neurons, there were no significant differences. HIF1α and HIF2α are structurally related, sharing 48% overall amino acid identity (Kenneth and Rocha, 2008; Karuppagounder and Ratan, 2012). It has been reported that HIF1α is involved in adaptation to acute hypoxia whilst HIF2α mediates adaptation to chronic hypoxic and oxidative stress (Mengelbier *et al.,*

2006). HIF1α and HIF2α were upregulated after a much longer period of OD in PC12 cells (~24 h) and primary neurons (~6 h). Results also showed that 24 h GD stabilised HIF1α and HIF2α in PC12 cells. Some studies have also shown that HIF1 also mediates adaptation to hypoglycemia (Soucek *et al.,* 2003) and GD (Nishimoto *et al.,* 2014). Both HIF1α and HIF2α were upregulated following a much shorter duration of OGD than OD. It is evident that the absence of glucose plays an essential role in the degree of HIF activation. Novak *et al.,* (2019) also revealed that in addition to oxygen, glucose also plays an essential role in the magnitude of HIF activation following OGD.

HIF activation is linked with the transcription of several downstream genes that play essential roles in adapting to low oxygen levels. HIF1α and HIF2α share some similar transcriptional targets such as *Glut1*, *Vegf*. HIF1α and HIF2α also regulate distinct subsets of genes. HIF1α regulates *Pdk*, *Ldha*, and *Bnip3,* whilst HIF2α regulates *Epo* and *CyclinD*1 (Martín-Aragón Baudel *et al.,* 2017).

In both PC12 cells and primary neurons, no significant changes in *Hif1α* and *Hif2α* were found following GD, OD, and OGD (versus Nx). Various studies have indicated that HIF is mainly regulated at the post-transcriptional level during ischaemia and hypoxia (Wenger *et al.,* 1997). In PC12 cells, *Phd2* was upregulated by 6 h OGD (versus Nx). In primary neurons, *Phd2* was upregulated by 6 h OD and OGD (compared to Nx). In response to HIF1α protein expression, *Phd2* is upregulated as a negative feedback response (Berra *et al*., 2003).

HIF has two well-known targets, *Vegf* and *Epo*. Three *Vegf* gene isoforms exist but only *Vegfa* is known to be regulated by hypoxia (Martín-Aragón Baudel *et al.,* 2017). There was no significant change in *Vegf* expression at 2 h OGD (compared to Nx) in PC12 cells. However, in primary neurons, *Vegf* was significantly upregulated from 2 h OGD onwards, with peak and sustained (~15 folds) expression at 4 h and 6 h OGD. In PC12 cells, *Vegf* was upregulated at 4 h (~9 folds) and 6 h (~11 fold) OGD, but the fold change was slightly lower compared to primary neurons. In line with HIF1α and HIF2α expression, *Vegf* was upregulated following longer periods of OD in PC12 cells (12 h, 24 h) and primary neurons (6 h) and 24 h GD in PC12 cells. The *Epo* primer did not work in PC12 cells, but significant changes were seen in primary neurons. Similar to *Vegf*, *Epo* was upregulated by 4 h OGD (~18 folds), which sustained at 6 h OGD (~18 folds). *Epo* was also upregulated following 6 h OD in primary neurons. Semenza et al., (2000) reported significant *Vegf* and *Epo* mRNA upregulation in hypoxic neurons. *Vegf* was upregulated by 4 h OGD in neurons (Zhang *et al.,* 2009). *Epo* was upregulated by hypoxia and ischaemia in neurons *in vivo* and *in vitro* (Marti, 2004; Bernaudin *et al.,* 2000). VEGF plays an important role in neuroprotection as it mediates angiogenesis and neurogenesis during ischaemia resulting in increased blood flow and metabolism (Bernaudin *et al*, 2002; Zhang and Chopp, 2009). EPO is also known to stimulate erythropoiesis, neurogenesis, and neuroprotection in the brain. Both Vegf and Epo are known to promote cell survival through inhibition of apoptosis (Marti, 2004).

In PC12 cells, *Bnip3* was upregulated by 24 h OD and OGD. *Bnip3* upregulation was reported starting at 12 h, with a peak at 72 h in PC12 cells subjected to hypoxia / ischaemia (Liu *et al.,* 2017). In contrast, *Bnip3* was upregulated from 2 h OGD

onwards in primary neurons. *Bnip3* upregulation was triggered by 1 h OGD in primary hippocampal neurons (Zhao *et al*., 2009). OD (2 h, 4 h, and 6 h) did not alter *Bnip3* expression in primary neurons. Zhang *et al.,* 2007 showed that *Bnip3* upregulated at 36 h by OD in primary neurons. Studies have shown that HIF1α upregulates BNIP3 resulting in mitochondrial dysfunction, membrane depolarization, MPTP opening and apoptosis (Chen *et al*., 2007; Yeh *et al.*, 2007), however more recent studies have reported that BNIP3 exhibits a protective effect during hypoxia by promoting mitophagy (Ma *et al.*, 2017).

In PC12 cells, *Glut1* was upregulated by GD (24 h), OD (12, 24 h), and OGD (4, 6, 12 h). In primary neurons, OD and OGD did not alter *Glut1* expression. GLUT1 is a glucose transporter that facilitates glucose transport across the plasma membrane and is upregulated in response to reduced glucose supply in the brain (Jurcovicova, 2014). Studies have reported that GLUT1 is predominantly expressed in astrocytes and endothelial cells in the brain (Winkler *et al.,* 2015). In the absence of oxygen, cells shift to anaerobic glycolysis for energy. A key regulator of glycolytic flux is glucose-2, 6-bisphosphate, which is an allosteric regulator of phosphofructokinases (Minchenko *et al.*, 2003). In PC12 cells, OD (12, 24 h) and OGD (4, 6, 12 h) significantly upregulated *Pfkfb3*. In primary neurons, OD and OGD did not alter *Pfkfb3* expression. *Pfkfb3* was upregulated in PC12 cells because they are proliferating cancer cells (Minchenko *et al.*, 2003); whereas in the brain, PFKFB3 is abundantly expressed in astrocytes but not typically found in neurons (Olga *et al.,* 2019). *Pfkfb1* expression was not altered following GD, OD, or OGD in PC12 cells and primary neurons. PFKFB1 is restricted to muscle and liver cells (Minchenko *et al.,* 2003). *Ldha* was significantly upregulated by 6 h OD in primary neurons. In PC12

cells, *Ldha* was significantly upregulated by 12 h and 24 h OD. In primary neurons, *Ldha* was upregulated by 4 h and 6 h OGD. Similarly, in PC12 cells, *Ldha* was upregulated by 4 h, 6 h, and 12 h OGD. Ldha is another glycolytic enzyme that facilitates the conversion of pyruvate to lactate (Minchenko *et al.,* 2003).

Key findings:

- OGD (6 h) onwards was cytotoxic in PC12 cells and primary neurons and therefore a suitable model for ischaemic insult.
- OGD (2 h, 4 h) altered mitochondrial activity but did not result in cell death and therefore considered sub-lethal.
- Reperfusion following OGD insults further increased cell death.
- Oxygen sensing proteins (HIF1α and HIF2α) were stabilised by varying time point of OD and OGD in both PC12 cells and primary neurons.

In conclusion, both PC12 cells and primary neurons had similar sensitivities towards OD and OGD. Both PC12 cells and primary neurons are suitable to model ischaemia *in vitro* for preliminary studies. Simultaneous omission of glucose and oxygen (OGD) most closely mimics ischaemia *in vitro* and is a suitable model of ischaemic insult

Chapter 4.

Characterizing ischaemic tolerance in PC12 cells and primary rat neurons

4.1 Introduction

Ischaemic tolerance is a phenomenon whereby exposure to a brief period of sub-lethal noxious stimuli (in a process known as 'preconditioning') confers transient tolerance to subsequent ischaemic insult in the brain (Figure 4.1). Tolerance to an ischaemic insult can result from various stimuli such as cortical depression spreading, hypothermia, hyperthermia, sleep deprivation, hypoxia, ischaemia and many more (Liu *et al.,* 2009). This study focused on determining the effectiveness and mechanism behind ischaemic tolerance conferred by three stimuli: glucose-deprivation preconditioning (GD-PC), hypoxic preconditioning (HPC) and ischaemic preconditioning (IPC). HPC and IPC were initially identified in the heart and several clinical trials have revealed effectiveness and great prospect (Anttila *et al.,* 2016). Identifying the underlying protective mechanisms of HPC and IPC is attractive for therapeutic modulation. These strategies could be beneficial in high-risk patients such as patients with risk of ischaemic stroke, subarachnoid haemorrhage, or TIA (Dirnagl *et al.,* 2009). Both HPC and IPC have shown promise in various *in vivo* and *in vitro* models of ischaemic stroke (Bergeron *et al.,* 1999; Bernaudin *et al.,* 2002; Baranova *et al.,* 2007; Zhang*,* 2009). However, the underlying molecular mechanism remains unclear. Some common features include the promotion of angiogenesis, vascular remodelling, erythropoiesis, depression of metabolic rate, modulation of glycolytic enzymes, and reduction of ion channel fluxes (Ginsberg, 2008).

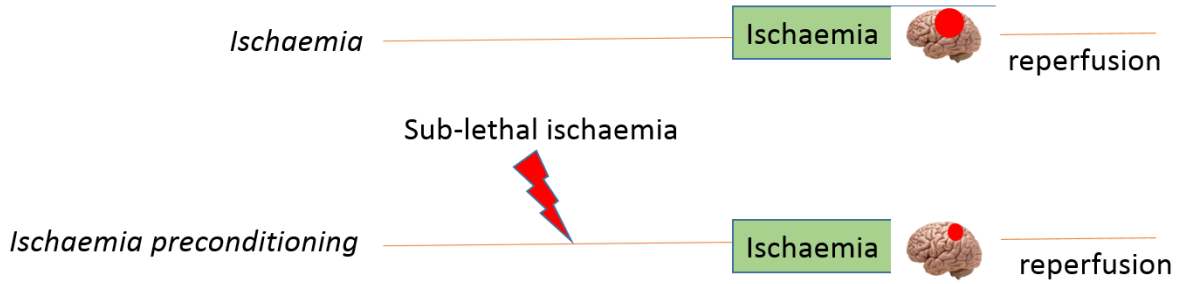

Figure 4.1. Schematic representation of the concept of IPC induced ischaemic tolerance. Exposure of brain tissue to a brief period of sub-lethal IPC insult prior to ischaemia (known as 'preconditioning') results in development of tolerance to subsequent ischaemic insult in the brain. Sublethal IPC results in smaller infarct size compared to untreated brain after an ischaemic insult. (Image produced using Biorender).

Application of local IPC is not clinically applicable in most patients, therefore another phenomenon known as remote ischaemic preconditioning (RIPC) has shown great potential for translation into clinical practice (Hepponstall *et al.,* 2012). RIPC involves the application of brief episodes of ischaemia to a tissue such as a limb (using blood pressure cuffs) resulting in protection against ischaemic injury in an organ at a remote location such as the heart. In clinical trials, RIPC has shown benefit in patients undergoing cardiac surgery or in patients with acute myocardial infarction by inducing genomic responses (Hummitzsch *et al.,* 2019; Hepponstall *et al.,* 2012).

This chapter aimed to study the effectiveness of *in vitro* HPC, IPC, and GD-PC in PC12 cells and primary rat neurons. An additional study was performed in PC12 cells involving preconditioning with various glucose concentrations to determine the role of glucose in preconditioned induced neuroprotection.

4.2 Materials and methods

PC12 cells and primary rat cortical neurons were cultured according to procedures described in Section 2.2.

4.2.1 Experimental protocol

Confluent PC12 cells and primary neuronal cultures were used for experiments. The complete media was aspirated and the cells were washed twice with glucose-free media before experiments. The PC12 cells and primary neurons were preconditioned with sham (Nx), GD, OD, and OGD for varying time points (i.e. 2, 4, 6 h) (Figure 4.2.). This was followed by 24 h reperfusion. The media (preconditioning treatment) was aspirated (100%), replaced with complete media, and place in the standard incubator for 24 h. This was followed by a 6 h OGD insult. For OGD, complete media was aspirated, cells rinsed twice with glucose-free medium, and incubated with glucose-free media in the hypoxia chamber where O_2 level was set at 0.3%.

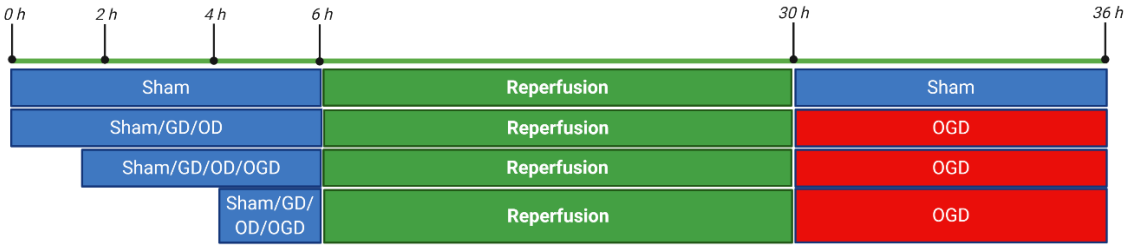

Figure 4.2. Timeline for GD, OD, and OGD preconditioning treatment against 6 h OGD insult. PC12 cells and primary neurons were subjected to sham (Nx), GD, OD, OGD (2, 4, and 6 h) followed by 24 h reperfusion (normoxia, complete media) and 6 h OGD (0.3% O_2, hypoxia chamber). Positive control cultures were treated identically but maintained in normoxia throughout (untreated control, C). All experiments were initiated on a staggered basis, such that all treatment duration end together. (Image produced using Biorender).

In PC12 cells, an additional study was performed studying the effect of preconditioning in normoxia versus hypoxia (0.3% O_2) with varying glucose concentrations for 4 h (0, 0.565, 1.125, 2.25, 4.5 g / L). The media was aspirated from confluent PC12 cell culture, cells were washed twice with glucose-free media and treated with DMEM with the desired glucose concentration. The high glucose DMEM was diluted with glucose-free DMEM to achieve the desired glucose concentrations (Table 4.1). High glucose DMEM contains 25 mM glucose was supplemented with 5% of HS containing 0.1 mM glucose, 5% of FBS containing 0.15 mM glucose, and 1% PS so 89% of total glucose (25.25 mM) is equivalent to around 22.5 mM. All other glucose concentrations are also adjusted to serum in Table 4.1. Preconditioning treatments were followed by 24 h reperfusion and 6 h OGD insult as stated above (Figure 4.3).

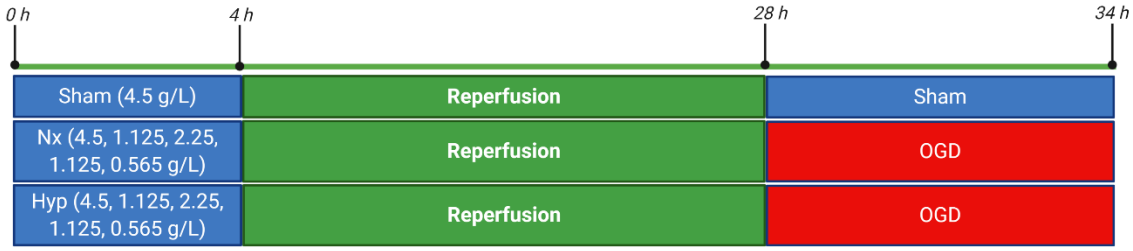

Figure 4.3. Timeline for preconditioning treatment with varying glucose concentrations against 6 h OGD insult. PC12 cells were subjected to normoxia versus hypoxia with media containing varying glucose concentrations for 4 h followed by 24 h reperfusion (normoxia, complete media) and 6 h OGD (0.3% O_2, hypoxia chamber). Positive control cultures were treated identically but maintained in normoxia throughout (untreated control, C). (Image produced using Biorender).

For all experiments, positive controls (untreated control, C) were treated identically but maintained in normoxia (complete medium) throughout the treatment. All experiments were initiated on a staggered basis, such that all treatment duration ends at the same time point.

Table 4.1. Dilution table for experiments involving preconditioning with varying glucose concentrations

Glucose concentration	Glucose concentration adjusted to serum	Dilution percentage of DMEM
0 g / L	0 mM (0 g / L)	Glucose-free DMEM (100%)
0.565 g / L	2.81 mM (0.5 g / L)	High-glucose DMEM (12.5%) and glucose-free DMEM (87.5%)
1.125 g / L	5.6 mM (1 g / L)	High-glucose DMEM (25%) and glucose-free DMEM (75%)
2.25 g / L	11.25 mM (2 g / L)	High-glucose DMEM (50%) and glucose-free DMEM (50%)
4.5 g / L	22.5 mM (4 g / L)	High-glucose DMEM (100%)

Cell viability (MTT, LDH, and trypan blue exclusion assay; Section 2.5), apoptosis (PC12 cells only; Section 2.5), morphological changes (IF staining; section 2.8), gene expression (Section 2.6), and protein expression (Section 2.7) were evaluated in PC12 cells and primary neurons.

4.3 Results

4.3.1 IPC induced tolerance in PC12 cells

Initial experiments were performed to determine the time points at which GD, OD, and OGD induced toxicity, to inform choices for ischaemic insult (evident cell death), and preconditioning treatment (sublethal; cell death should be minimal or absent). In both primary neurons and PC12 cells, OGD for 6 h was found cytotoxic and was determined to be a suitable representative of ischaemic insult. GD and OD (2 h, 4 h, and 6 h) and OGD (2 h and 4 h) were not found cytotoxic and thus deemed sub-lethal. Sub-lethal GD, OD, and OGD preconditioning followed by reperfusion were studied against 6 h OGD insult in primary neurons and PC12 cells. The effectiveness of these preconditioning treatments was compared to sham-PC cells (Figure 4.1). In PC12 cells, for all preconditioning treatments (including sham-PC), 6 h OGD insult resulted in significantly ($p<0.01$) reduced mitochondrial activity, increase LDH release, and reduced cell viability, compared to untreated controls. Some protection against OGD insult was conferred by OGD-PC (4 h) and GD-PC (4 h and 6 h), compared to sham-PC (same time point), for all three assays. All three assays revealed that OGD-PC (4 h) conferred significantly greater protection than GD-PC (4 h) (Figure 4.4).

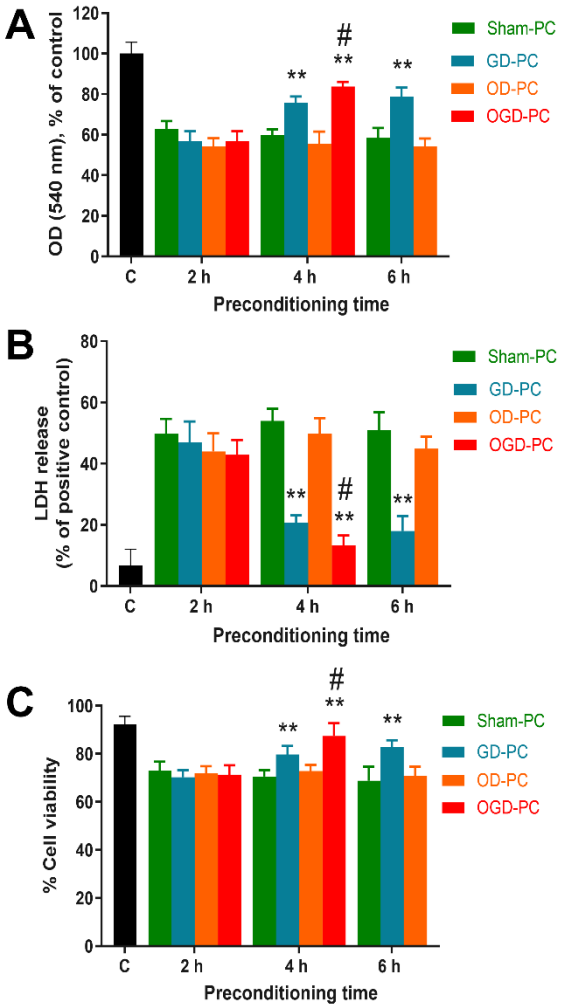

Figure 4.4. PC12 cells response to GD, OD, or OGD preconditioning (PC). Cells were exposed to sham-PC, GD-PC, OD-PC, or OGD-PC (2, 4, or 6 h) followed by 24 h reperfusion and 6 h OGD insult. Untreated control (C) was treated identically but maintained in normoxia throughout (positive control). (A) Bar chart representing MTT assay results. (B) Bar chart representing LDH assay results. (C) Bar chart representing trypan blue assay results. All three assays revealed that GD-PC (4, 6 h) and OGD-PC (4 h) prior to 6 h OGD protected the cells compared to sham-PC (same time point). *(For all graphs, ** represents $p < 0.01$ versus sham-PC (same time point) and $^{\#}$ represents $p < 0.05$ against GD-PC (same time point); two-way ANOVA followed by Tukey's post-hoc analysis; n=4)*

4.3.2 The effect of glucose concentration on IPC- induced tolerance in PC12 cells

As 4 h GD-PC was cytoprotective in PC12 cells, studies were performed to determine the role of glucose by preconditioning PC12 cells with varying glucose concentrations (4 h, with normoxia or hypoxia) (Figure 4.3). For all preconditioning treatments, subsequent insults resulted in reduced mitochondrial activity, increased LDH release, and reduced cell viability, versus untreated controls, with the sole exception of 0 g / L hypoxia in the trypan blue assay (Figure 4.5). For mitochondrial activity, some protection against these insults was conferred by glucose reduction (0.565 g / L) or complete deprivation (0 g / L), in both normoxic and hypoxic conditions, compared to sham (complete media (4.5 g / L) in normoxia) (Figure 4.5A). Complete glucose deprivation (0 g / L) offered greater protection against mitochondrial toxicity in hypoxia (versus normoxia, 0 g / L). Reduced glucose concentrations exhibited a dose-dependent protective effect in the LDH assay. In both normoxic and hypoxic conditions, all concentrations showed lower LDH release versus sham, with 0.565 and 0 g / L showing significant reductions in LDH release versus 2.25 g / L (for same oxygen conditions; Figure 4.5B). No differences in LDH release were noted between normoxic and hypoxic conditions. In terms of viability assessed by trypan blue assay, some protection was evident in the absence of glucose (0 g / L), for both normoxia (83.7 ± 4.4%) and hypoxia (89.2 ± 5.1%), versus sham (70.1 ± 4.2%; Figure 4.5C). All other glucose concentrations were indistinguishable from full glucose (4.5 g / L), with no differences evident between normoxia and hypoxia.

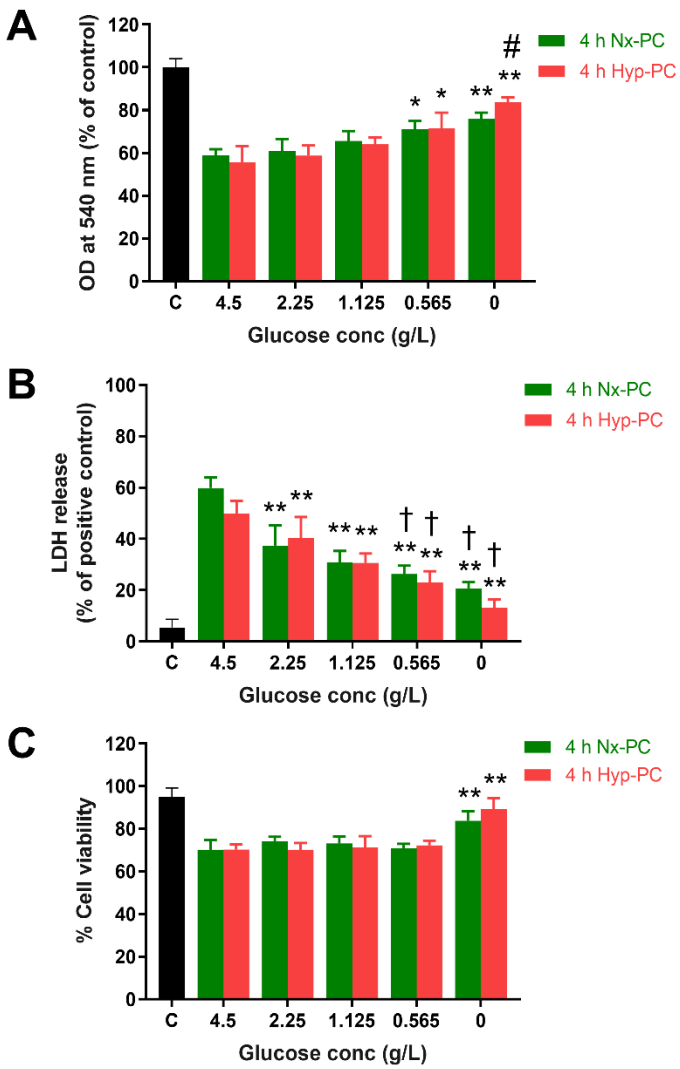

Figure 4.5. The effect of varying glucose concentration on ischaemic preconditioning induced tolerance. PC12 cells were preconditioned in normoxia (Nx-PC; 21% O_2) or hypoxia (Hyp-PC; 0.3% O_2) for 4 h with varying glucose concentrations (0, 0.565, 1.125, 2.25, 4.5 g / L), followed by 24 h reperfusion and 6 h OGD insult, except untreated control, C (full glucose and normoxia throughout). (A) Bar chart representing MTT assay results. Compared to untreated controls, all conditions showed reduced mitochondrial activity ($p<0.05$). All similar to sham (4.5 g / L, normoxia), except for a significantly lower reduction in mitochondrial activity for the lowest glucose concentrations (0 and 0.565 g / L), with or without hypoxia

(versus 4.5 g / L Nx-PC). Complete glucose deprivation (0 g / L) with hypoxia showed greater mitochondrial activity than normoxia (0 g / L). (B) Bar graph representing LDH assay results. Compared to untreated controls, all conditions showed greater LDH release ($p<0.05$). In comparison to sham (4.5 g / L Nx-PC), all reductions of glucose concentration (0 – 2.25 g / L), with or without hypoxia, were associated with significantly lower LDH release (less cell death). Both 0.565 g / L and 0 g / L also showed significant reductions in LDH release versus 2.25 g / L (for the same oxygen conditions; $p<0.05$). No differences were noted between normoxic and hypoxic conditions. (C) Bar chart representing trypan blue assay results. Compared to untreated controls, all conditions showed reduced cell viability ($p<0.01$) except 0 g / L Hyp-PC ($p>0.05$). For all reduced-glucose concentrations, cell viability was similar to sham (4.5 g / L Nx-PC; ~60-70%). Viability was greater without glucose in both normoxic and hypoxic conditions (versus 4.5 g / L Nx-PC). *(For all graphs, * represents $p<0.05$ and ** represents $p < 0.01$ versus sham-PC (4.5 g / L in normoxia), $^{\#}$ represents $p < 0.05$ against Nx-PC (same glucose concentration), $^{\dagger}p < 0.05$* represents versus 2.25 g / L (for the same oxygen conditions;)*; two-way ANOVA followed by Tukey's post-hoc analysis; n=3)*

In addition to the cell viability assays, apoptosis was assessed (flow cytometry; Annexin-V / 7-AAD) for these conditions. For all preconditioning treatments, subsequent insults resulted in reduced cell viability (AV^- / $7\text{-}AAD^-$) and increased apoptosis (AV^+ / $7\text{-}AAD^-$), versus untreated control, with the sole exception of 0 g / L hypoxia. Some protection against these insults was conferred by complete glucose deprivation, in both normoxic (GD-PC) and hypoxic (OGD-PC) conditions. Complete glucose deprivation (0 g / L) offered greater protection against apoptosis in hypoxia (OGD-PC; versus normoxia, 0 g / L: GD-PC). All other glucose concentrations were indistinguishable from full glucose (4.5 g / L), with no differences between normoxia and hypoxia (Figure 4.6).

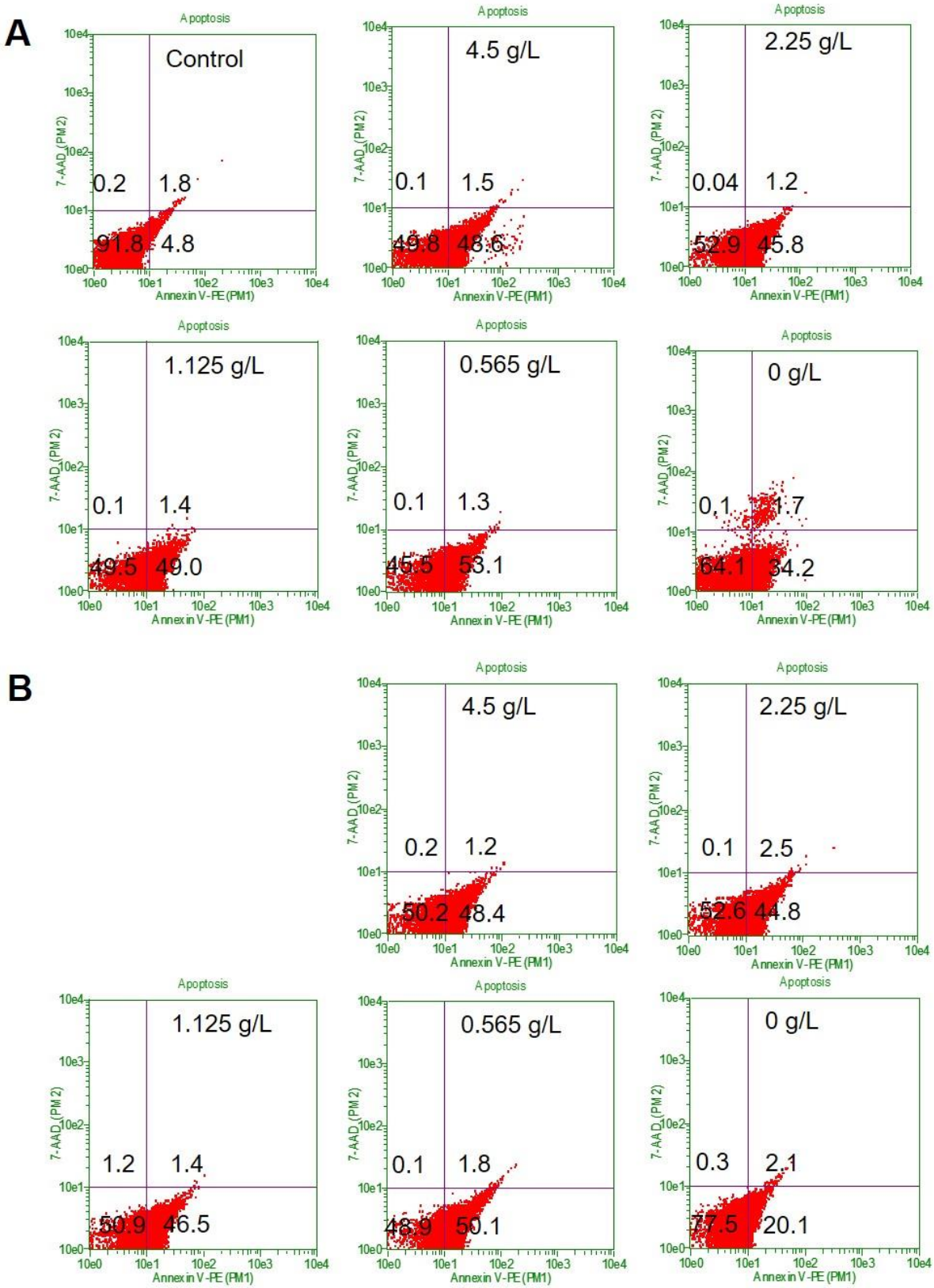
A
Apoptosis
Control
0.2
1.8
91.8
4.8
4.5 g/L
0.1
1.5
49.8
48.6
2.25 g/L
0.04
1.2
52.9
45.8
1.125 g/L
0.1
1.4
49.5
49.0
0.565 g/L
0.1
1.3
45.5
53.1
0 g/L
0.1
1.7
64.1
34.2
B
4.5 g/L
0.2
1.2
50.2
48.4
2.25 g/L
0.1
2.5
52.6
44.8
1.125 g/L
1.2
1.4
50.9
46.5
0.565 g/L
0.1
1.8
48.9
50.1
0 g/L
0.3
2.1
77.5
20.1
7-AAD (PM2)
Annexin V-PE (PM1)
10e0
10e1
10e2
10e3
10e4

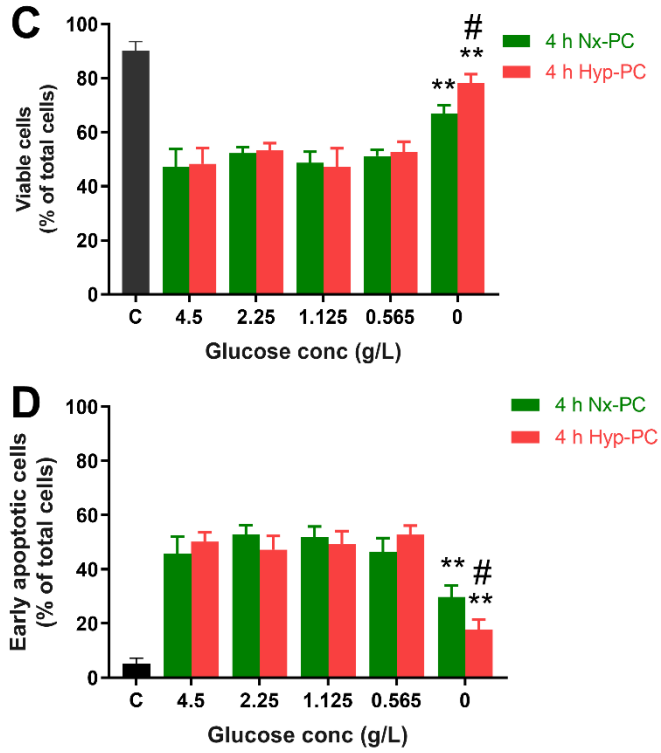

Figure 4.6. Flow cytometric analysis of the effect of varying glucose concentration on preconditioning-induced tolerance to ischaemic insult. PC12 cells were preconditioned in normoxia (Nx-PC; 21% O_2) or hypoxia (Hyp-PC; 0.3% O_2) for 4 h with varying glucose concentrations followed by 24 h reperfusion and 6 h OGD insult, except untreated control, C (full glucose and normoxia throughout). (A) Representative dot plot of PC12 cells preconditioned in normoxia (21% O_2) for 4 h with varying glucose concentration. C represents untreated control. (B) Representative dot plot of PC12 cells preconditioned in hypoxia (0.3% O_2) for 4 h with varying glucose concentration. (C) Bar chart representing viable (7-AAD$^-$) cells as a percentage of all cells. Compared to untreated control, all conditions showed reduced cell viability ($p<0.01$), except 0 g / L Hyp-PC ($p>0.05$). For all reduced (non-zero) glucose concentrations, cell viability was similar to sham (4.5 g / L Nx-PC; ~45-55%). Complete glucose deprivation (0 g / L) with hypoxia showed greater viability

than normoxia. (D) Bar chart representing early apoptotic (Annexin-V^+ / 7-AAD^-) cells as a percentage of all viable (7-AAD^-) cells. Compared to untreated controls, all conditions showed a greater expression of marker for early apoptosis (*$p<0.05$).* For all reduced (non-zero) glucose concentrations, the percentage of early apoptotic cells were similar to sham (4.5 g / L Nx-PC; ~45-55%). A lower percentage of early apoptotic cells was seen in both normoxic and hypoxic conditions without glucose. Complete glucose deprivation (0 g / L) with hypoxia showed a lower percentage of early apoptotic cells than normoxia. *(For all graphs, ** represents $p < 0.01$ versus sham-PC (4.5 g / L in normoxia), $^{\#}$ represents $p < 0.05$ against Nx-PC (same glucose concentration; two-way ANOVA followed by Tukey's post-hoc analysis; n=3)*

The expression of HIF1α was studied in PC12 cells treated with varying glucose concentrations (0, 0.565, 1.125, 2.25, 4.5 g / L) in normoxia or hypoxia for 4 h. Compared to normoxia (4.5 g / L; Nx), HIF1α was significantly upregulated in PC12 cells exposed to complete glucose deprivation (0 g / L) in hypoxia compared to 4.5 g / L normoxia (untreated control). There were no significant changes in HIF1α expression in cells exposed to all the other glucose concentrations in both normoxia and hypoxia (Figure 4.7).

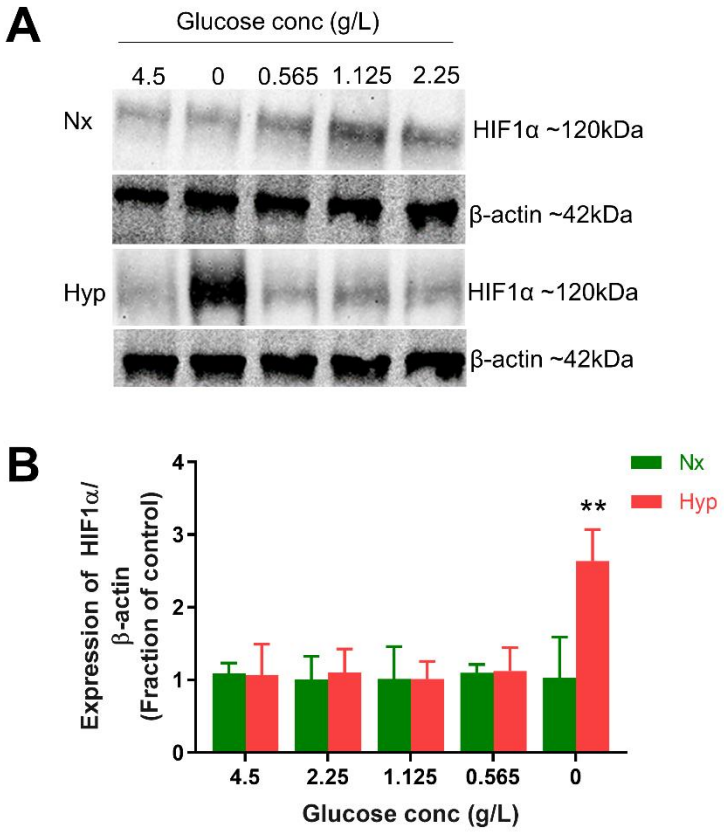

Figure 4.7. Effects of varying glucose concentration in normoxia and hypoxia on HIF1α levels in PC12 cells. (A) Representative HIF1α immunoblots were shown with those for β-actin of PC12 cells treated with normoxia (21% O_2) and hypoxia (0.3% O_2) with varying glucose concentrations of 0, 0.565, 1.125, 2.25, 4.5 g / L for 4 h. (B) Bar graph representing normalised HIF1α expression. Compared to sham (4.5 g / L, Nx), only complete glucose deprivation (0 g / L) in hypoxia significantly increased Hif1α. *(For graph, ** represents $p < 0.01$ against 4.5 g / L in normoxia (untreated control); two-way ANOVA followed by Tukey's post-hoc analysis; n=4).*

The expression of a panel of hypoxic genes was studied in PC12 cells treated with varying glucose concentrations (0, 0.565, 1.125, 2.25, 4.5 g / L) in normoxia or hypoxia for 4 h. *Vegf* (~ 11 fold), *Glut1* (~ 15 fold), *Pfkfb3* (~ 7.5 fold), and *Ldha* (~ 6 fold), were significantly upregulated in cells exposed to complete glucose deprivation (0 g / L) in hypoxia (OGD) compared to 4.5 g / L normoxia (untreated control). All other treatment conditions had no significant effect on *Vegf*, *Glut1, Pfkfb3,* and *Ldha* expression (versus untreated control). All treatment conditions had no significant effect on *Hif1α*, *Bnip3, and Pfkfb1* expression (Figure 4.8).

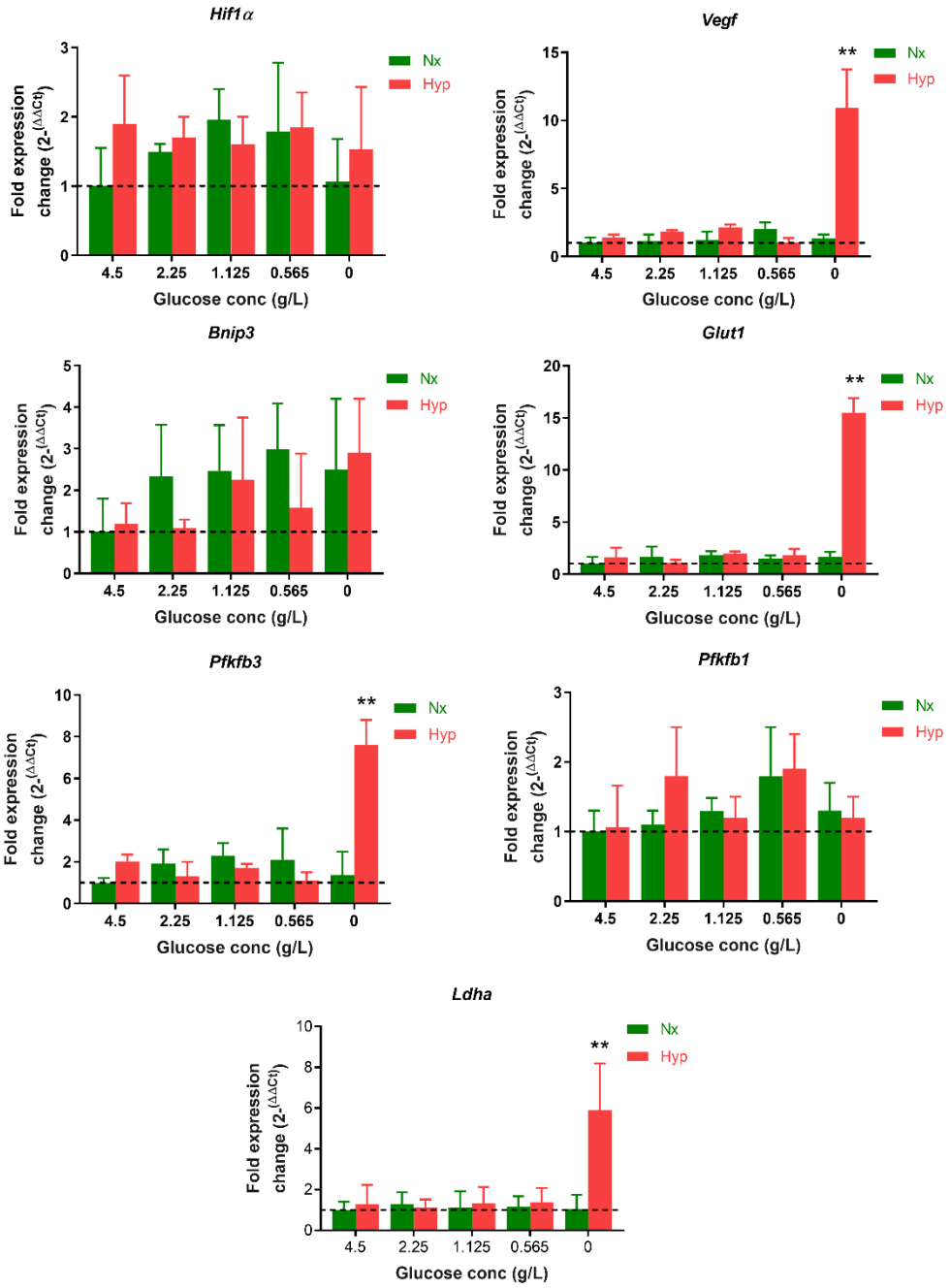

Figure 4.8. Gene expression in PC12 cells cultured in normoxia and hypoxia with varying glucose concentration. PC12 cells exposed to varying glucose concentrations (0, 0.565, 1.125, 2.25, 4.5 g / L) of normoxia or hypoxia for 4 h. Compared to 4.5 g / L normoxia (untreated control), there were no significant changes in (A) *Hif1α,* (B) *Bnip3*, and (E) *Pfkfb1* expression in all treatment groups. Compared to 4.5 g / L normoxia (ambient air), complete glucose deprivation (0 g / L)

in hypoxia (i.e. OGD) significantly upregulated (B) *Vegf*, (D) *Glut1*, (F) *Pfkfb3*, and (G) *Ldha* expression. The gene expression was measured against the housekeeping gene *β-actin* and normalised to 4.5 g / L Nx (untreated control). The dotted line represents the basal gene expression. *(For all graphs, ** represents $p < 0.01$ against 4.5 g / L in normoxia (untreated control); two-way ANOVA followed by Tukey's post-hoc analysis; n=3).*

4.3.3 IPC induced tolerance in primary rat cortical neurons

Similar to PC12 cells, the effects of preconditioning followed by reperfusion were evaluated against 6 h OGD insult in primary neurons with the same protocol (Figure 4.2). Primary rat neuronal culture established in Chapter 3, Section 3.3.5 were used for these experiments. In primary neuronal cultures, for all preconditioning treatments (including sham-PC), OGD insults resulted in reduced mitochondrial activity and increased LDH release, versus untreated controls (Figure 4.9). Both LDH and MTT assay revealed that some protection against OGD insult was conferred by OGD-PC (2, 4 h) and OD-PC (6 h), compared to sham-PC (same time point). There was no significant ($p<0.05$) between 2 h and 4 h OGD-PC induced protection. Compared to sham-PC, GD-PC (all time points) had no significant effects on primary rat neurons followed by 6h OGD.

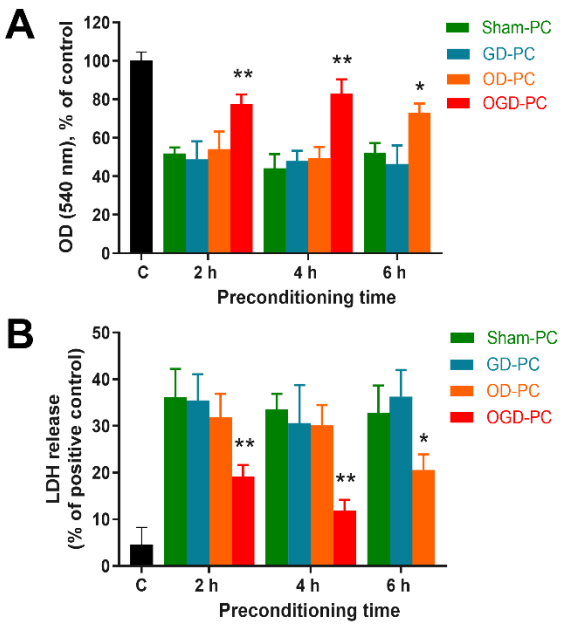

Figure 4.9. Primary rat cortical neurons response to GD, OD, or OGD preconditioning (PC) and 24 hours reperfusion before 6 hours OGD. Primary neurons were exposed to sham-PC, GD-PC, OD-PC, or OGD-PC followed by 24 h reperfusion and 6 h OGD insult, except untreated control, C (full glucose and normoxia throughout). (A) Bar chart representing MTT assay results. Compared to untreated controls, all conditions showed reduced mitochondrial activity (*p<0.01)*. All were similar to sham, except for significantly lower reduction (less toxicity) for OGD-PC (2, 4 h) and OD-PC (6 h), versus sham-PC (same time point). (B) Bar graph representing LDH assay results. Compared to untreated control, all conditions showed greater LDH release (*p<0.01).* All were similar to sham, except for significantly lower LDH release for OGD-PC (2, 4 h) and OD-PC (6 h), versus sham-PC (same time point). *(For all graphs,* represents p <0.05 and **represents p < 0.01 versus sham-PC (same time point); two-way ANOVA followed by Tukey's post-hoc analysis; n=3).*

Compared to untreated control (Map2: 10.2±3.1 dendrites per neuron, with each dendrite measuring 36.1±6.1µm), 6 h OGD insults resulted in changes in neuron morphology (Map2: sham-PC; consisted of 3.2±0.7 dendrites per neuron, with each dendrite measuring 3.2±1.6µm, $p<0.05$ versus untreated control; indicating neuron degradation). There was no significant improvement in neuron morphology in cultures subjected to GD-PC (2 h, 4 h, and 6 h) and OD-PC (2 h and 4 h). Compared to sham-PC, there was a significant ($p<0.05$) improvement in neuron morphology in 2 h OGD-PC (11.1±2.8 dendrites per neuron, with each dendrite measuring 38.1±4.1µm), 4 h OGD-PC (13.1±2.8 dendrites per neuron, with each dendrite measuring 36.6±6.9µm), and 6 h OD-PC (12.5±4.3 dendrites per neuron, with each dendrite measuring 37.4±5.1µm), indicating protective effect against OGD insult (Figure 4.10).

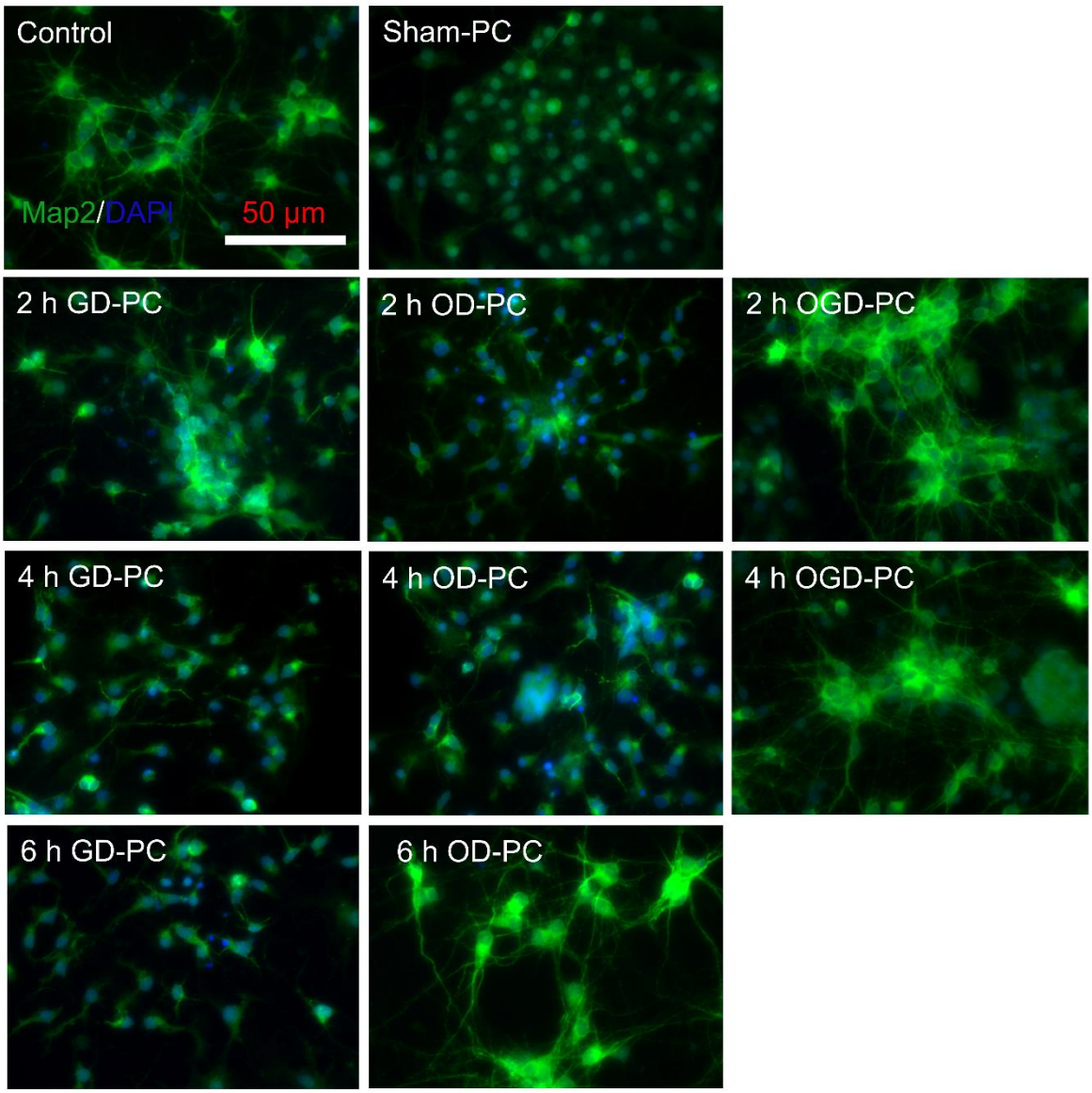

Figure 4.10. Fluorescence micrographs of primary rat cortical neurons subjected to GD, OD, or OGD preconditioning and 24 h reperfusion before 6 h OGD insult. Representative double merged micrographs of Map2 (FITC) and DAPI stained neuronal cultures following exposure to sham-PC, GD-PC, OD-PC, and OGD-PC followed by 24 h reperfusion and 6 h OGD insult, except control (normoxia throughout). Healthy culture (untreated control) consisted of neuronal nuclei ($Map2^{+}$) surrounded by numerous dendrites. Sham-PC cultures preconditioned cultures consisted of neurons with reduced or no dendrites (Map2 degradation; neuron degeneration). GD-PC (2 h, 4 h, and 6 h) and OD-PC (2 h and 4 h) did not improve

the neuron morphology and consisted of neurons similar to sham-PC. OGD-PC (2 h and 4 h) and OD-PC (6 h) consisted of healthier neurons (similar to untreated control; numerous dendrites) indicating cytoprotective effect against 6 h OGD insult.

4.4 Discussion

The experiments in this chapter were performed to determine the effectiveness of GD, OD, and OGD preconditioning in PC12 cells and primary neurons, assessed in terms of protective against OGD insult. Additionally, the expression of HIF1α and its downstream genes were evaluated, as they have been reported to play a crucial role in HPC- and IPC- induced tolerance.

One of the most promising avenues of stroke research is the concept HPC and IPC, in which brief periods of hypoxia or ischaemia to the brain have shown to induce tolerance against a more severe insult (Zhang *et al*., 2009). IPC and HPC have shown promise in various *in vivo* and *in vitro* studies (Liu *et al*., 2009; Baranova *et al*., 2007; Sharp *et al.,* 2004; Bernaudin *et al*., 2002; Dave *et al*., 2001; Miller *et al*., 2001; Bergeron *et al*., 1999) by targeting various endogenous pathways, however, the precise mechanism remains unclear. Studies have commonly pointed out that the reprogramming of the endogenous transcription response to ischaemia induces the neuroprotective response, limiting the impact of an actual ischaemic event (Durukan and Tatlismuk, 2010; Ginsberg, 2008).

As insufficient glucose and oxygen supply are representative of cerebral ischaemia (Fan *et al.,* 2017), the effectiveness of preconditioning induced tolerance was studied against OGD insult. Preliminary studies (chapter 3) in PC12 cells and primary neurons revealed that 6 h of OGD (0.3% O_2) resulted in significant cell death, therefore various time points of GD, OD, and OGD preconditioning treatments were studied against 6 h OGD. Following preconditioning, the cells were exposed to 24 h reperfusion. Both IPC and HPC induced tolerance require RNA translation and *de*

novo protein synthesis. Matsuyama *et al*., (2000) suggested that a period of reperfusion following IPC / HPC is essential to mediate *de novo* protein synthesis and neuroprotection

For PC12 cells, preconditioning with GD (4 h and 6 h) was found cytoprotective against 6 h OGD insult. A shorter period (2 h) of GD preconditioning was not found protective. However, this was not the case in primary neurons, in which GD-PC (all durations) was not found protective. There is limited literature on GD-PC modulated neuroprotection, but one study found that transient GD of the heart confers preconditioning-like protection against a subsequent ischaemia / reperfusion injury *in vivo* (Awan *et al.,* 2000).

In PC12 cells, OD-PC (2, 4, and 6 h) was not found cytoprotective. A long period (6 h) of OD-PC was found protective in primary neurons. As summarized in Table 4.2, HPC has shown promise against ischaemic insults in the heart and brain *in vivo* (Stevens *et al.,* 2014; Sharp *et al.,* 2004; Miller *et al.,* 2001; Gidday *et al.,* 1994) and *in vitro* (Bernaudin *et al*., 2002; Arthur *et al.,* 2004). HPC has not been widely studied in PC12 cells. A study by Li-Ying *et al.,* 2009 showed that HPC (48 hours, 10% O_2) protected against acute anoxia induced necrosis in PC12 cells. In line with this study, Wick *et al.,* 2002 found that exposure of cerebellar granule neurons to HPC for 9 hours (but not 1-3 hours) resulted in a reduction of cell death following glutamate toxicity. Arthur *et al.,* (2004) showed HPC for 25 minutes, 24 hours before OGD significantly reduced cortical neuronal death from 83% to 22% following 40 minutes OGD (0% O_2; EBSS). Studies by Zhang *et al.,* 2006; Sheng *et al.,* 2014 found that

HPC protected cortical neurons against glutamate toxicity. Bickler *et al.,* (2015) found HPC in hippocampus brain slices induced neuroprotective effects following OGD treatments. The duration (6 h) that was found cytoprotective in primary neurons correlated with HIF1α and HIF2α upregulation (chapter 3). As discussed previously, 6 h (but not 2 and 4 h) of OD upregulated HIF1α, HIF2α proteins (and their downstream genes) in primary neurons. However, in PC12 cells, a much longer duration (24 h) of OD was required to significantly upregulate HIF1α and HIF2α. Various studies reported that HPC induced tolerance involved HIF protein expression and transcription of its target genes such as *Epo* and *Vegf* (Sharp *et al.,* 2004; Wick *et al.,* 2002).

Table 4.2. Table summarizing the *in vivo* and *in vitro* studies that have explored the neuroprotective effects of HPC in cerebral ischaemia models.

Study	Model	Protocol of administration	Outcome
Gidday *et al.*, 1994	Unilateral carotid artery ligation (neonatal rat pups)	HPC (8% O_2, 3 h), 24 h before ligation	Significant reduction in infarct size (34%) in HPC treated group. No evidence of necrosis in the hemisphere.
Miller *et al.*, 2001	Transient focal MCAO (Swiss-Webster ND4 mice)	HPC (11% O_2, 2 h), 48 h before MCAO	Significant reduction in infarct size (64%) in HPC treated group compared to the untreated group.
Wick *et al*., 2002	Glutamate mediated excitotoxicity (Cerebellar granule neurons)	HPC (5% O_2, for 1, 3, and 9 h), 24 h before glutamate treatment	HPC (9 h) but not 1 h and 3 h protected from cell death following glutamate toxicity.
Bernaudin *et al*., 2002	Permanent focal MCAO (Male adult Swiss mice)	HPC (8% O_2 for 1 h, 3 h, or 6 h), 24 h before MCAO	Significant reduction in infarct size (30%) in HPC treated group compared to the untreated group.

Arthur *et al*., 2004	OGD model (Primary rat cortical neurons)	HPC (0% O_2, 25 minutes), 24 h before 40 minutes OGD (0% O_2, EBSS).	HPC prior to OGD significantly reduced cell death from 83% to 22% (necrosis) and 68% to 11% (apoptosis).
Zhang *et al.*, 2006	Glutamate mediated excitotoxicity (Primary rat cortical neurons)	HPC (1% O_2, 30 minutes), 30 minutes before glutamate treatment.	HPC reduced glutamate-induced neuronal injury.
Li-Ying *et al*., 2009	Acute anoxia (PC12 cells)	HPC (10% O_2, 48 h), 24 h before acute anoxia (0% O_2, 24 h).	HPC protected against acute anoxia induced necrosis in PC12 cells.
Sheng *et al.*, 2014	Glutamate mediated excitotoxicity (Primary rat cortical neurons)	HPC (4% O_2, 8 h), 12 h before glutamate treatment.	HPC reduced glutamate-induced neuronal injury.
Bickler *et al.*, 2015	OGD model (Hippocampal brain slices)	HPC (0% O_2, 15-30 minutes), 24 h before 1 h OGD (0% O_2).	HPC protected hippocampal neurons from OGD induced death.

In both PC12 cells and primary neurons, OGD-PC exhibited significant cytoprotection; however, the effect was time-dependent and varied between these two cell types. In PC12 cells, 4 h (but not 2 h) OGD-PC was cytoprotective; whereas in primary neurons, both 2 h and 4 h of OGD-PC protected against 6 h OGD insult. A previous study by Hillion *et al.,* (2005) reported that IPC protected PC12 cells against a subsequent lethal OGD insult. Several studies have evaluated the effect of IPC in primary neurons *in vitro* (summarized in Table 4.3). IPC was studied against shorter periods of OGD insults in hippocampal neurons. Various studies have found that hippocampal CA1 neurons are more vulnerable to OGD induced cell death than cortical neurons (Koszegi *et al.,* 2017; Bianco-Suarez and Hanley 2014). Some *in vivo* studies have explored IPC induced tolerance against MCAO (summarized in Table 4.3), however, RIPC is more clinically relevant. Studies have found that remote limb preconditioning was found protective against focal cerebral ischaemia (Hu *et al*., 2012; Hahn *et al*., 2011; Malhotra *et al*., 2011). Various *in vivo* and *in vitro* have shown that HIF1α mediated gene expression plays a pivotal role in IPC induced tolerance (Ruscher *et al.,* 1998; Sharp *et al.,* 2004; Tang *et al.,* 2006; Jones *et al.,* 2006; Dirnagl *et al.,* 2009; Liu *et al.,* 2009). As discussed in Chapter 3, HIF1α and HIF2α proteins and their downstream genes were significantly upregulated from 4 h OGD onwards in PC12 cells; the time at which OGD-PC was found protective in this study. In primary neurons, 2 h of OGD was sufficient to upregulate HIF1α. The protective effect of OGD-PC correlated with HIF1α upregulation in primary neurons and PC12 cells.

Table 4.3. Table summarizing the *in vivo* and *in vitro* studies that have explored the neuroprotective effects of IPC in cerebral ischaemia models.

Study	Model	Protocol of administration	Outcome
Kitagawa *et al*., 1990	Global ischaemia (Gerbils)	Two 2 minutes global ischaemia, at a 1 day interval 2 days before 5 minutes ischaemic insult	Animals pre-treated with 2 minutes of global brain ischemia showed marked protection against CA1 neuronal loss after 5 minutes global ischemia.
Ruscher *et al.,* 1998	OGD model (Primary rat cortical neurons)	OGD (0% O_2, 60 minutes), 24 h before 90 minutes OGD insult	OGD preconditioning protected primary neurons from OGD insult induced cell death.
Stagliano *et al*., 1999	MCAO model (mice)	One, or three 5 minute episodes of global ischaemia, 30 minutes before 1 h (transient) or 24 h (permanent) MCAO	Brief MCAO induced protection (reduced volume) against transient and permanent MCAO.
Tauskela *et al*., 2003	OGD model (Primary rat cortical neurons)	OGD (0% O_2, 60-70 minutes), 24 h before 75-90 minutes OGD insult	OGD preconditioning protected primary neurons from OGD insult induced cell death.

Hillion *et al*., 2005	OGD model (PC12 cells)	OGD (2% O_2, 6 h), 24 h before 15 h OGD insult	OGD preconditioning protected PC12 cells from OGD insult induced cell death.
Gaspar *et al.*, 2006	OGD model (Primary rat cortical neurons)	9 h energy deprivation (glucose and amino acids), 24 h before 3 h OGD (0% O_2)	Cell viability was greater in energy deprivation group (80.1 ± 1.27%) compared to the untreated group (33.1 ± 0.52%).
Gao *et al.*, 2015	OGD model (Primary mouse hippocampal neurons)	OGD (0% O_2, 15 minutes), 24 h before 55 minutes OGD insult	Cell viability was greater in OGD preconditioned group (77.3%) compared to the untreated group (51.5%).
Keasey *et al.*, 2016	OGD model (Primary rat hippocampal neurons)	OGD (0% O_2, 30 minutes), 24 h before 90 minutes OGD insult	Cell viability was greater in OGD preconditioned group (75%) compared to the untreated group (51%).

In addition to the HIF pathway, various pathways have been reported to play an important role in IPC induced tolerance in primary neurons. Zhang *et al.,* (2006) found that IPC induced protection in primary rat neurons via δ-opioid receptor activation. In primary neurons, it was also found that phosphatidylinositol-3 kinase / protein kinase B (PI3K / Akt) plays an important in IPC induced tolerance (Constantino *et al.,* 2018). A study by Lin *et al.,* 2011 reported that IPC mediated tolerance in mixed neuron / astrocyte culture via signal transducers and activators of transcription (STAT3) activation following ε protein kinase C (εPKC) and extracellular signal-regulated kinase (ERK1 / 2) activation. Although IPC induced tolerance is very promising, the underlying mechanism seems to be an interplay between various cell signalling pathways, and therefore concluding to one particular mechanism would be unrealistic. The studies performed in this Chapter were mainly to characterise ischaemic tolerance in PC12 cells and primary neurons for further studies involving pharmacologically induced ischaemic tolerance via HIF inducers (Chapter 5).

Cytoprotection by GD-PC but not OD-PC in PC12 cells was intriguing, therefore further studies were performed by preconditioning cells with varying glucose concentrations (0, 0.565, 1.125, 2.25, 4.5 g / L) in both normoxia and hypoxia to determine whether glucose concentrations play a vital role in IPC induced tolerance. As discussed in Chapter 3, brain glucose levels range from 0.82 to 2.4 mM, therefore the media containing 0.5 g / L (2.8 mM) most closely mimics *in vivo* glucose levels in the brain, whilst all other dilutions contain relatively higher glucose levels than *in vivo*. Greater MTT activity was found, in both normoxia and hypoxia preconditioned cells with 0-0.565 g / L of glucose. LDH assay results were slightly different, where both normoxic and hypoxic preconditioned cells with 0-2.25 g / L of glucose

significantly reduced LDH release. Similar to MTT assay results, preconditioning in the absence of both glucose and oxygen (OGD-PC) (hypoxia, 0 g / L glucose) was found to be the most cytoprotective. Similarly, significantly greater cell viabilities were found in GD-PC (normoxia, 0 g / L) and OGD-PC (hypoxia, 0 g / L). To confirm these findings, apoptotic and necrotic cell death was studied using flow cytometric analysis. There was a significant reduction in % of apoptotic cells and greater % of viable cells in GD-PC (~35%) and OGD-PC (~20%) in comparison to sham-PC (~50%). Interestingly, all three assays and flow cytometry showed a protective effect against 6 h OGD insults in PC12 cells by GD-PC and OGD-PC. Thus, indicating the absence of glucose plays a vital role in IPC induced tolerance in PC12 cells. HIF1α was only upregulated by 4 h OGD (0.3 % O_2, 0 g / L glucose) in PC12 cells. Also, HIF1α downstream genes such as *Vegf*, *Glut1*, *Pfkfb3*, and *Ldha* were significantly upregulated by 4 h OGD only; therefore the protective effect of GD-PC may not attribute to HIF activity.

It is worth noting that the PC12 cell line used in this study is a rat adrenal medulla cancer cell line. It has been observed that in various cancer cells, glucose-dependent glycolysis is enhanced and oxidative phosphorylation capacity is reduced. As proposed by Otto Warburg (“Warburg effect”), cancerous cells rely on glycolysis due to the permanent impairment of mitochondrial oxidative phosphorylation for the product of lactate for energy (Potter, 2016). Some cancer genes, such as *Ras, cMys,* and *P53* were involved in the regulation of Warburg effect (Dang and Semenza 1999). Therefore, PC12 cells could be more sensitive to GD, and less sensitive to OD compared to other cells, e.g. neurons (Teng *et al.,* 2006). The Warburg effect

therefore could play an important role in the GD preconditioning induced tolerance we observed in PC12 cells and warrants further investigation.

Key findings:

- Preconditioning with sub-lethal OGD induced ischaemic tolerance in PC12 cells and primary rat neurons.
- Preconditioning with sub-lethal GD was protective in PC12 cells but not primary rat neurons.
- Glucose concentration in preconditioning is inversely related to the level of protection conferred in PC12 cells.
- HIF1α and downstream gene upregulation are associated with OGD – (but not GD-) induced ischaemic tolerance

In conclusion, preconditioning PC12 cells and primary rat neurons with OGD followed by reperfusion protected the cells against a subsequent OGD insult. Longer periods of OD preconditioning were cytoprotective in primary neurons but not PC12 cells. Both OD and OGD induced tolerance involved HIF1α upregulation. GD induced ischaemic tolerance in PC12 cells but not primary neurons; PC12 cells being cancer cells have different metabolism such as Warburg effect. GD induced tolerance was HIF-independent and understanding the underlying mechanism would be beneficial.

Chapter 5.

Characterizing a panel of novel prolyl hydroxylase (PHD) inhibitors in ischaemic tolerance in PC12 cells and primary neurons

5.1 Introduction

As discussed in Section 1.5.3, HIFs are regulators of acute cellular responses to hypoxia in mammals. HIF mediated responses involve increases in the expression of multiple genes in a context-dependent manner, including those associated with glycolysis, erythropoiesis, and angiogenesis (Wilkins *et al.,* 2016). Under normoxic conditions, efficient catalysis by the ferrous iron and 2-oxoglutarate (2OG) dependent PHDs (1-3 in humans) promotes binding of HIF1α to the VHL tumour suppressor protein, resulting in proteasomal degradation of HIF1α (Schofield and Ratcliffe, 2004). During hypoxia, PHD activity is reduced resulting in the stabilization and accumulation of HIF1α in the cytoplasm, which then translocates to the nucleus forming the HIF1 transcription factors that upregulate expression of multiple genes (Kaelin and Ratcliffe, 2008). The array of genes targeted by the HIF system makes it an appealing pharmacological target.

Despite being discovered 20 years ago, the role of HIF in stroke pathophysiology remains debatable. Neuron-specific HIF1α knock out (KO) in mice resulted in a worse neurological outcome and larger infarct volume following 30 minutes middle cerebral artery occlusion (MCAO) (Baranova *et al.,* 2007), however, neuron-specific HIF1α KO mice had better neurological outcomes after 75 minutes global ischaemia (Helton *et al.,* 2005). Single HIF1α or HIF2α KO mice had a similar infarct volume following MCAO compared to the respective wild type mice, possibly due to mutual compensation (Barteczek *et al.,* 2017). Double HIF1α and HIF2α KO resulted in significant impairment 72 h after MCAO, suggesting that HIF is involved in functional recovery after cerebral ischaemia (Barteczek *et al.,* 2017). Indirect induction of HIF, via genetic ablation of PHD1 or PHD2, reduced infarct volume, and improved

sensorimotor function following transient ischaemia (Quaegebeur *et al.,* 2016). It is postulated that pharmacological inhibition of PHD2, and / or PHD1 could stimulate adaptations that protect against damage from ischaemic stroke (Davis *et al.,* 2018). A pharmacological approach for ischaemic tolerance is clinically appealing due to its non-invasive application. Currently, no available drug specifically inhibits a single PHD isoform. Researchers are currently focusing on generating inhibitors targeting PHD2, as it is proposed to be the most important PHD isoform in regulating HIF1α levels in normoxia (Yeh *et al.,* 2017).

Pharmacological PHD inhibition mediated HIF upregulation is currently being studied for the treatment of several diseases including anaemia, ischaemic stroke, and wound healing (Davis *et al.,* 2018). Currently, four PHD inhibitors: FG4592 (Roxadustat) from FibroGen, GSK1278863 (Daprodustat) from GlaxoSmithKline, Bayer85-3934 (Molidustat) from Bayer, and AKB-6548 (Vadadustat) from Akebia are in clinical use or trials for anaemia treatment in patients with CKD (Ariazi *et al*., 2017; Yeh *et al.,* 2017; Chan *et al.,* 2016).

As summarised in Section 1.5.3, several PHD inhibitors (DMOG, DFO, DHB, $CoCl_2$) have been studied in stroke models either *in vivo* or *in vitro*, where these compounds showed neuroprotective effects following an ischaemic insult (Ogle *et al.,* 2012; Nagel *et al.,* 2011; Davis *et al.,* 2018). However, these compounds are not suitable for clinical use due to their multiple targets. Novel PHD inhibitors such as (FG4497, GSK360A, IOX3) also showed neuroprotective effects (Chen *et al.,* 2014; Reischl *et al.,* 2014; Zhao and Rempe., 2011).

In this chapter, the effectiveness of three novel clinical PHD inhibitors (FG4592, GSK1278863, Bayer85-3934) alongside FG2216 and DMOG a non-specific 2OG analogue, were studied on the previously established (chapter 3) OGD model in PC12 cells. Upon establishing protective effects on PC12 cells, the effects of FG4592 and DMOG were also evaluated in primary rat cortical neurons. In addition to their effectiveness, the effects of PHD inhibitors were evaluated on HIF1α, HIF2α, and autophagic (Lc3b, p62) proteins. Additionally, the effects of the PHD inhibitors were also studied on hypoxia downstream genes. Only FG4592 was pursued in primary neurons, as it was the most clinically advanced PHD inhibitor during this study (Table 2.1). So far the PHD inhibitors (such as DMOG, DFO, $CoCl_2$) evaluated *in vitro* and *in vivo* have several off-target effects, however, the novel PHD inhibitors (FG4592, GSK1278863, Bayer85-3934) were found safe in phase 2 clinical trials, therefore have a great potential for clinical use in ischaemic stroke if found effective. The novel class of PHD inhibitors that are currently in clinical trials for anaemia (Table 2.1) have not yet been explored in ischaemic stroke models. A study by Chen *et al*. (2014), found preconditioning with IOX3 (FG2216), 24 h before ischaemic insult protective against ischaemic damage. Table 2.1 summarizes the status of the clinical trials of the novel PHD inhibitors (FG4592, GSK1278863, and Bayer85-3934) pursued in this chapter.

Table 5.1. Clinical trial status of novel PHD inhibitors

PHD inhibitors	Most recently completed trials	Results	Ongoing trials and status
Daprodustat (GSK1278863)	Japan, phase 3, 52 weeks, randomized, double-blind, parallel-group (Darbepoetin Alfa), to evaluate efficacy and safety of daprodustat versus Darbepoetin Alfa in patients with anaemia in HDD-CKD (n=271) (NCT02969655)	Oral daprodustat met its primary endpoint of non-inferiority to darbepoetin alfa. Mean change in Hb to evaluation period: Daprodustat groups + 10.89 g / dL, Darbepoetin Alfa +10.83 g / dL	Phase III trials: Ascend-D (NCT02879305) and ASCEND-ND (NCT02876835) Filed in Japan for clinical use
Roxadustat (FG4592)	26 countries, OLYMPUS, phase 3, 52 weeks, randomized, double-blind, placebo-controlled trial to evaluate the efficacy and safety of roxadustat versus placebo for the treatment of NDD patients with	OLYMPUS: Oral roxadustat met its efficacy endpoint. Mean change in Hb to evaluation period: Roxadustat groups + 1.85 g / dL, placebo +0.13 g / dL (*p<0.001*)	Roxadustat is currently approved in China for the treatment of anaemia in patients with CKD, regardless of whether they require dialysis, and in Japan for the treatment of dialysis

	anaemia in CKD (n=2,781). 18 countries, ROCKIES, phase 3, 52 weeks, randomized, open-label, active-controlled trial to evaluate efficacy and safety of roxadustat versus epoetin alfa for the treatment of patients with anaemia in DD-CKD (n=2,133).	ROCKIES: Oral roxadustat met its primary endpoint of non-inferiority to epoetin alfa. Mean change in Hb to evaluation period: Roxadustat groups + 1.22 g / dL, epoetin alfa +0.99 g / dL (*p<0.001*)	patients with anaemia from CKD
Molidustat (Bayer85-3934)	15 countries, phase 2b, 16 weeks, randomized, double-blind placebo-controlled (n=121) (NCT02021370) 13 countries, phase 2b, 16 weeks, randomized, open-label, active comparator (Darbepoetin Alfa) (n=124) (NCT02021409)	Oral molidustat increased Hb in NDD CKD patients in a dose-dependent fashion of at least 1.14 g / dL, compared to 0.09 g / dL increase in placebo (*p<0.001*) Mean change in Hb to evaluation period: Molidustat groups +	Ongoing phase 3 trials: Miyabi ND-C (NTC03350321) and Miyabi HD-M (NTC035443657)

	0.46 g / dL, Darbepoetin Alfa +0.18 g / dL (*p<0.001*)

5.2 Materials and methods

PC12 cells and primary rat cortical neurons were cultured according to procedures described in Section 2.2.

5.2.1 Drug administration

The PHD inhibitors (DMOG, FG2216, FG4592, GSK1278863, Bay 85–3934) and an autophagy inducer (rapamycin) were initially dissolved in DMSO (final concentration of 1%) and subsequently diluted in the treatment appropriate culture medium to the indicated concentrations. To analyse the cytoprotective effects of the PHD inhibitors, final concentrations of 1, 10, 50 or 100 μM were applied in PC12 cells. Additionally, DMOG was studied at the final concentrations of 1, 10, 50, 100, 250, 500, 1000, and 2000μM. The effect of rapamycin was studied at a final concentration of 1 and 10 μM. In primary rat cortical neurons, the PHD inhibitors DMOG (100, 250, 500, 1000, and 2000μM) and FG4592 (1, 10, 30, 50, 100, and 200μM) were studied at varying concentrations as indicated. For the vehicle control group, a final concentration of 1% (v / v) aqueous DMSO was used throughout. To study the cytotoxicity of PHD inhibitors initial experiments involved exposure for 24 h to varying concentrations during normoxia in ‘complete’ medium.

5.2.2 Treatment protocol

Initially, the effects of 24 h treatments (complete media, normoxia) with the PHD inhibitors were evaluated on cell viability, apoptosis, proteins (HIF1α, HIF2α, Lc3b, Beclin1, p62) and hypoxic genes in PC12 cells and primary neurons (Figure 5.1).

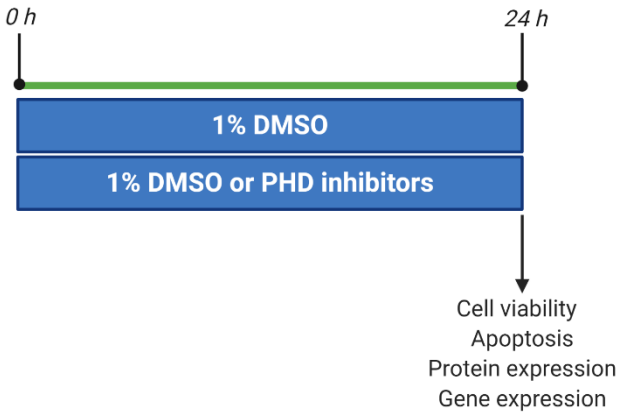

Figure 5.1. Timeline for studying the safety of PHD inhibitors. In PC12 cells and primary neurons, 24 h treatment with PHD inhibitors versus 1% DMSO (normoxia, complete media) were evaluated on cell viability, apoptosis, protein, and hypoxic gene expression. (Image produced using Biorender).

Three different treatment protocols were implemented in PC12 cells. The cytoprotective effects of PHD inhibitors were tested against 6 h OGD (0.3% O_2) insults in the following protocols. At the end of each treatment condition, cell viability (MTT, LDH, and trypan blue assay) was measured. For all experiments, positive controls (untreated control, C) were treated with 1% DMSO identically but maintained in normoxia (complete medium) throughout the treatment.

(1) PHD inhibitors in conjunction with OGD insult (acute effect): The complete media was aspirated from the cell cultures. The cells were washed twice with glucose-free media. PHD inhibitors or 1% DMSO were added directly to the OGD media at the start of 6 h OGD insult (Figure 5.2).

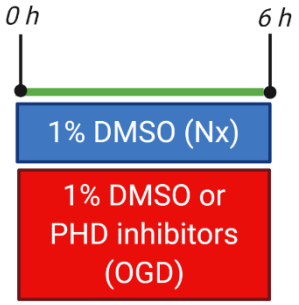

Figure 5.2. Timeline for PHD inhibitors effects during OGD. DMSO or PHD inhibitors were added directly to the OGD media and treated for 6 h (0.3% O_2, hypoxia chamber). The cells were maintained in 1% DMSO (normoxia) as a positive control. (Image produced using Biorender).

(2) Preconditioning: The complete media was aspirated from the cell cultures and replaced with fresh complete media. PHD inhibitors or 1% DMSO were added to the complete media and incubated for 24 h (normoxia). This was followed by a 6 h OGD insult. For OGD, complete media was aspirated, cells rinsed twice with glucose-free medium, and incubated with glucose-free media (Figure 5.3).

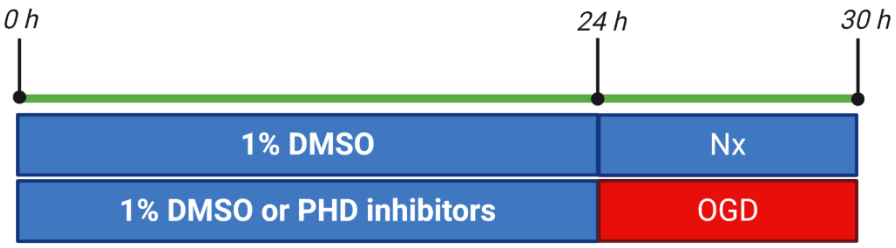

Figure 5.3. Timeline for effects of preconditioning with PHD inhibitors followed by OGD insult. PC12 cells were incubated with 1% DMSO or PHD inhibitors for 24 h (normoxia, complete media), followed by 6 h OGD insult (0.3% O_2, hypoxia chamber). The cells were incubated with 1% DMSO (normoxia) for 24 h followed by 6 h normoxia (complete media) as a positive control. (Image produced using Biorender).

(3) Preconditioning with reversion: The complete media was aspirated from the cell cultures and replaced with fresh complete media. PHD inhibitors or 1% DMSO were added to the complete media and incubated for 24 h (normoxia). After 24 h the PHD inhibitors / DMSO was aspirated and cells were reverted to normoxia (complete media in normoxia) for 24 h. followed by a period of reperfusion (24 h in normoxia). This was followed by a 6 h OGD insult. For OGD, complete media was aspirated, cells rinsed twice with glucose-free medium, and incubated with glucose-free media (Figure 5.4).

Figure 5.4. Timeline for effects of preconditioning with PHD inhibitors followed by reversion and OGD insult. PC12 cells were incubated with 1% DMSO or PHD inhibitors for 24 h (normoxia, complete media), followed by 24 h reversion (normoxia, complete media) and 6 h OGD insult (0.3% O_2, hypoxia chamber). The cells were incubated with 1% DMSO (normoxia) for 24 h followed by normoxia as a positive control. (Image produced using Biorender).

In primary neurons, only treatment protocol 3 (preconditioning with reperfusion, Figure 5.4) was pursued. Primary neurons were preconditioned with the PHD inhibitors for 24 h (complete media; normoxia), followed by a period of 24 h reversion (complete media; normoxia). For reversion, the media containing PHD inhibitors were replaced with complete medium (100%). This was followed by a 6 h OGD (0.3% O_2) insult. For OGD, complete media was aspirated, cells rinsed twice with glucose-free medium, and incubated with glucose-free media.

Cell viability (MTT, LDH, and trypan blue exclusion assay; Section 2.5), apoptosis (PC12 cells only; Section 2.5), morphological changes (IF staining; section 2.8), gene expression (Section 2.6), and protein expression (Section 2.7) were evaluated in PC12 cells and primary neurons.

5.3 Results

5.3.1 Effects of DMSO on PC12 cell viabilities in normoxia

Initial studies were performed to determine the non-cytotoxic concentration of DMSO. DMSO is a redox-active small molecule that could contribute to cell death (Hill, 2014). The effects of a range of DMSO concentrations (0.5%-10%) were evaluated in PC12 cells. Compared to control (0%), 5% and 10% DMSO resulted in a significant reduction in mitochondrial activity and an increase in LDH release. Compared to 5% DMSO, the mitochondrial activity was significantly ($p<0.01$) lower and LDH release was significantly higher ($p<0.01$) in 10% DMSO treated cells. All the other concentrations (0.5%, 1%, and 2%) had no significant effects on mitochondrial activity and LDH release compared to control (0% DMSO) (Figure 5.5). A final concentration of 1% DMSO was used in all experiments to dissolve the PHD inhibitors.

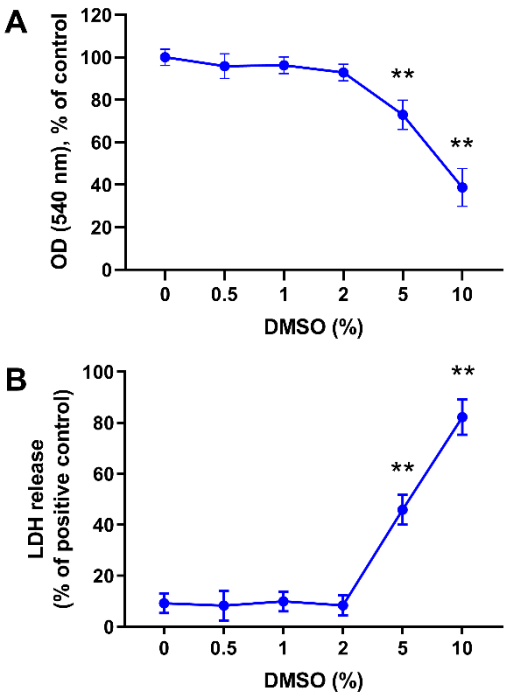

Figure 5.5. Effects of DMSO on PC12 cell viability. Bar graphs representing PC12 cells viabilities following 24 h treatment with indicated DMSO concentrations. (A) MTT assay revealed a significant reduction in mitochondrial activity by 5 and 10% DMSO compared to no DMSO (0%). (B) LDH assay revealed a significant increase in LDH release by 5 and 10% DMSO compared to no DMSO (0%). *(For all graphs, ** represents $p < 0.01$ versus 0% DMSO; One-way ANOVA followed by Tukey's post-hoc analysis; n=3)*

5.3.2 Effects of PHD inhibitors on PC12 cell viabilities and apoptosis

The effects of varying concentrations of the PHD inhibitors: FG2216, FG4592, GSK1278863, Bayer85-3934, and DMOG for 24 h (normoxia) were assessed on PC12 cell viabilities (Figure 5.1).

Compared to 1% DMSO, there was a significant reduction in mitochondrial activity by DMOG (250, 500, 1000, and 2000 µM). DMOG (100µM) did not alter mitochondrial activity compared to 1% DMSO (Figure 5.6A). Compared to 1% DMSO, there was a significant increase in LDH release (Figure 5.6B) and reduction in cell viability (trypan blue assay; Figure 5.6C) by DMOG (500, 1000, and 2000 µM). DMOG (100 and 250 µM) did not alter LDH release or cell viability compared to 1% DMSO.

Compared to 1% DMSO, there was a significant reduction in mitochondrial activity by FG4592 (100µM) and Bayer85-3934 (50 and 100µM). There were no significant differences in mitochondrial activity in 50µM versus 100µM Bayer85-3934 treated cells. Compared to 1% DMSO, there were no significant changes in mitochondrial activity by FG2216, GSK1278863, and all other concentrations (1 and 10µM) of FG4592, Bayer85-3934 (Figure 5.7A). Compared to 1% DMSO, there were no significant changes in LDH release (Figure 5.7B) and cell viability (trypan blue assay; Figure 5.7C) by FG2216, FG4592, GSK1278863, and Bayer85-3934 (at all the concentrations studied).

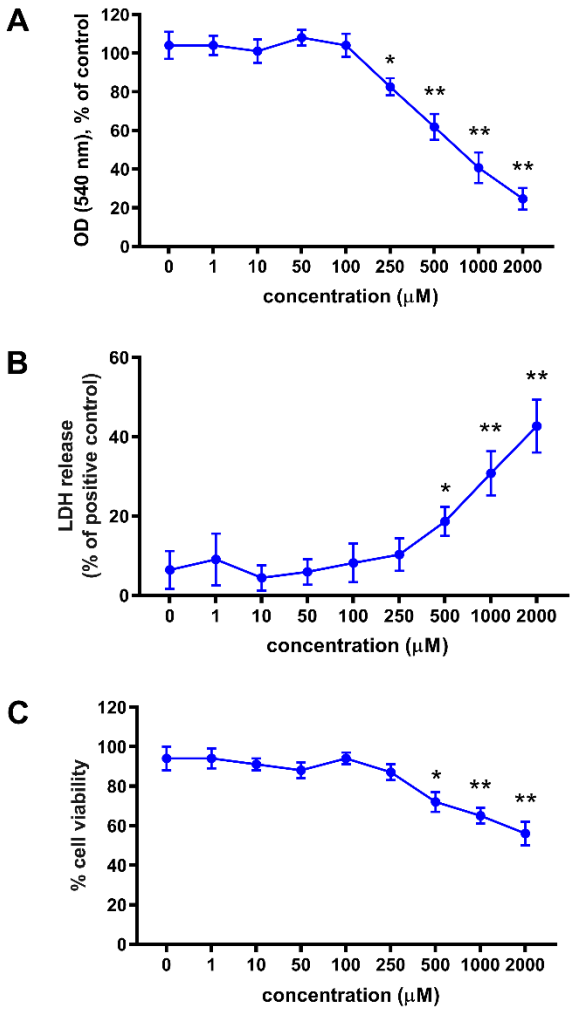

Figure 5.6. Effect of DMOG on PC12 cells during normoxia. Bar graphs representing PC12 cells viabilities following 24 h treatment with 1% DMSO (0) and DMOG (1, 50, 100, 250, 500, 1000, and 2000 µM) (A) MTT assays revealed a significant reduction in mitochondrial activity by 250, 500, 1000, and 2000 µM of DMOG compared to 1% DMSO. (B) LDH assays revealed a significant increase in LDH release by 500, 1000, and 2000 µM of DMOG compared to 1% DMSO. (C) Trypan blue exclusion assay revealed a significant reduction in cell viability by 500, 1000, and 2000 µM of DMOG compared to 1% DMSO. *(For all graphs,* represents $p < 0.05$ and ** represents $p < 0.01$ versus 1% DMSO; One-way ANOVA followed by Tukey's post-hoc analysis; n=3*

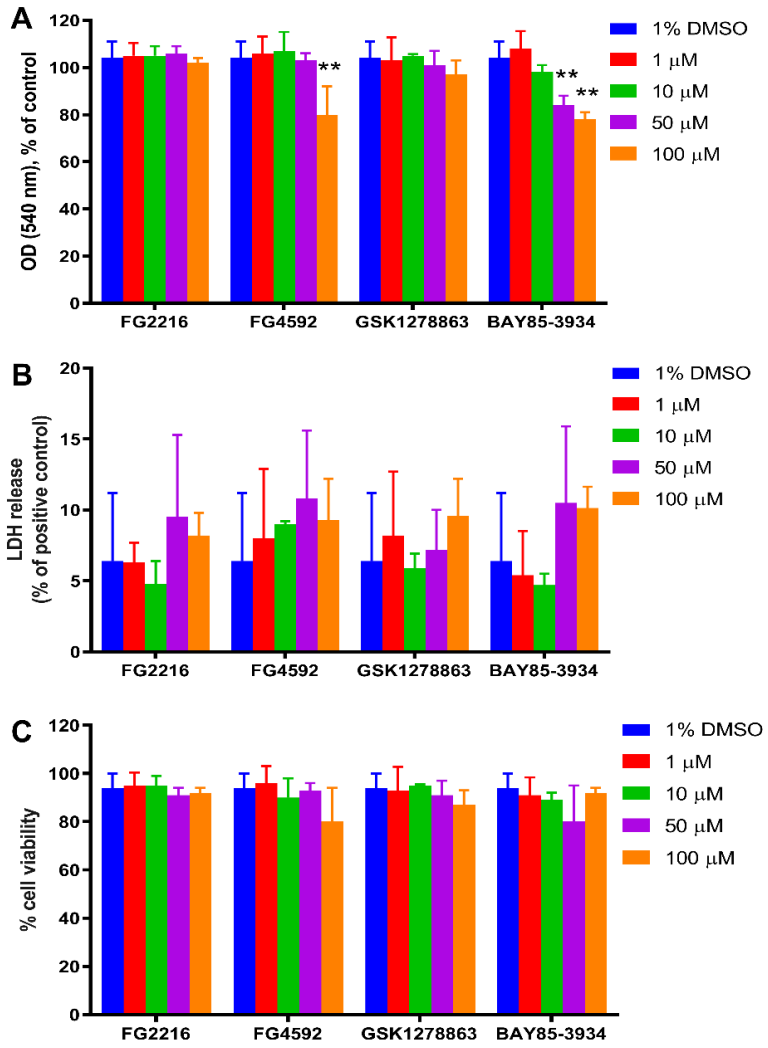

Figure 5.7. Effect of PHD inhibitors on PC12 cells during normoxia. Bar graphs representing PC12 cell viabilities following 24 h treatment with 1% DMSO and the PHD inhibitors (FG4592, FG2216, GSK1278863, Bayer85-3934). (A) MTT assays revealed a significant reduction in mitochondrial activity by 100μM FG4592 and 50μM / 100μM of Bayer85-3934 compared to 1% DMSO. (B) LDH assays revealed no significant changes in LDH release with all concentrations of PHD inhibitors studied. (C) Trypan blue exclusion assay revealed no significant changes in cell viability by all concentrations of PHD inhibitors. *(For all graphs, ** represents $p < 0.01$ versus 1% DMSO; Two-way ANOVA followed by Tukey's post-hoc analysis; n=3)*

The effects of 24 h treatment with PHD inhibitors (100µM) were evaluated on PC12 cells apoptosis using flow cytometry (Annexin-V and 7-AAD). Compared to 1% DMSO, 100µM treatment with all the PHD inhibitors did not alter the % of viable (AV^- / $7\text{-}AAD^-$), early apoptotic (AV^+ / $7\text{-}AAD^-$), and necrotic cells (AV^+ / $7\text{-}AAD^+$), the majority of cells (~90%) were viable (Figure 5.8).

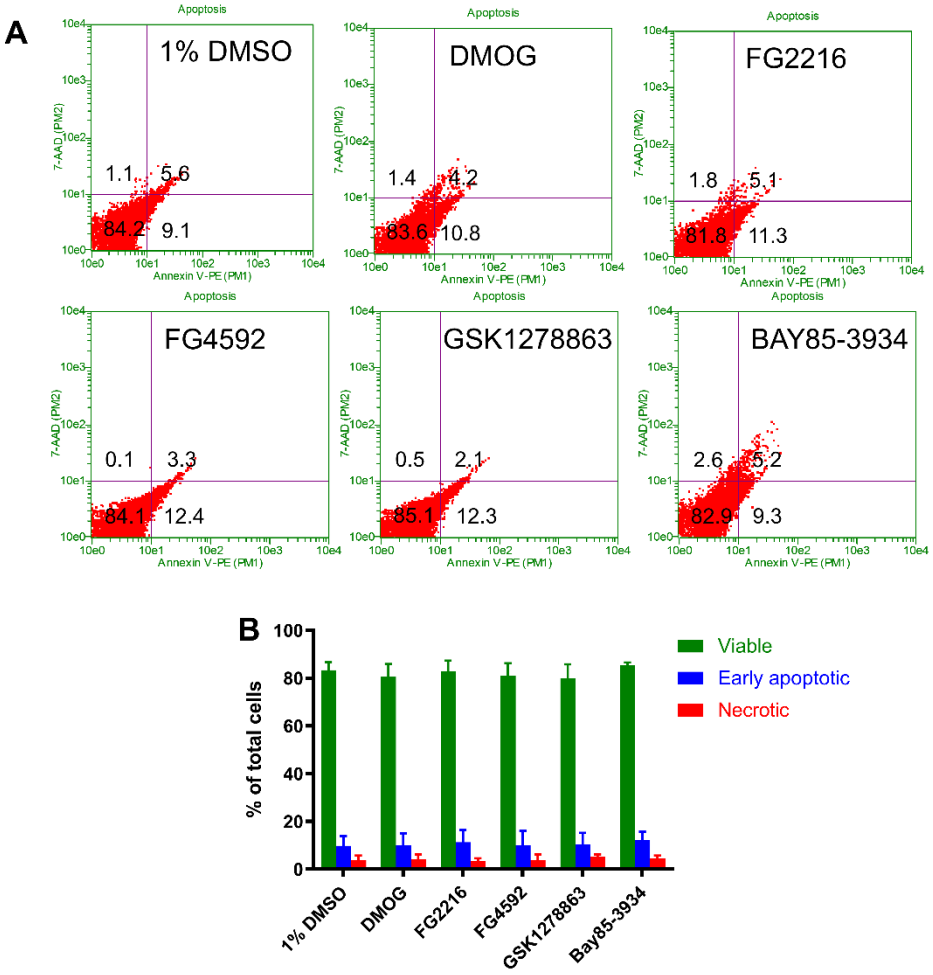

Figure 5.8. PC12 cells apoptosis in response to PHD inhibitors in normoxia for 24 h. PC12 cells were cultured and incubated in normoxia for 24 h with the PHD inhibitors (100µM) (A) Representative dot plots of Annexin-V / 7-AAD FACS analysis of cells treated with the 1% DMSO and the PHD inhibitors. Cells in the lower left quadrant represent viable cells, cells in the lower right quadrant represent early apoptosis, and cells in the upper right quadrant represented necrosis. (B) Bar graph representing % of viable (AV^- / $7\text{-}AAD^-$) cells, % of early apoptotic cells (AV^+ / $7\text{-}AAD^-$), and % necrotic cells (AV^+ / $7\text{-}AAD^+$); out of % of total cells. *($p > 0.05$, Two-way ANOVA followed by Tukey's post-hoc analysis; n=3)*

5.3.3 Effects of PHD inhibitors on autophagy in PC12 cells

The effects of 24 h treatment with the PHD inhibitors (100µM) were studied on autophagic markers (Lc3b, p62, and Beclin1) (Figure 5.9). Rapamycin, an established, autophagy inducer, was used in addition to the PHD inhibitors. Compared to 1% DMSO, there was a significant increase in Lc3b-II / Lc3b-I ratio and reduction in p62 in cells exposed to Rapamycin (1 and 10µM). There was a significant increase in the Lc3b-II / Lc3b-I in cells exposed to DMOG, FG2216, FG4592, GSK1278863, and Bayer85-3934 compared to 1% DMSO. Compared to 1% DMSO, p62 was significantly downregulated in cells exposed to DMOG, FG2216, FG4592, GSK1278863, and Bayer85-3934. Compared to 1% DMSO, there was a significant increase in Beclin1 expression in cells exposed to FG4592, GSK1278863, and Bayer85-3934 but not Rapamycin, DMOG, and FG2216.

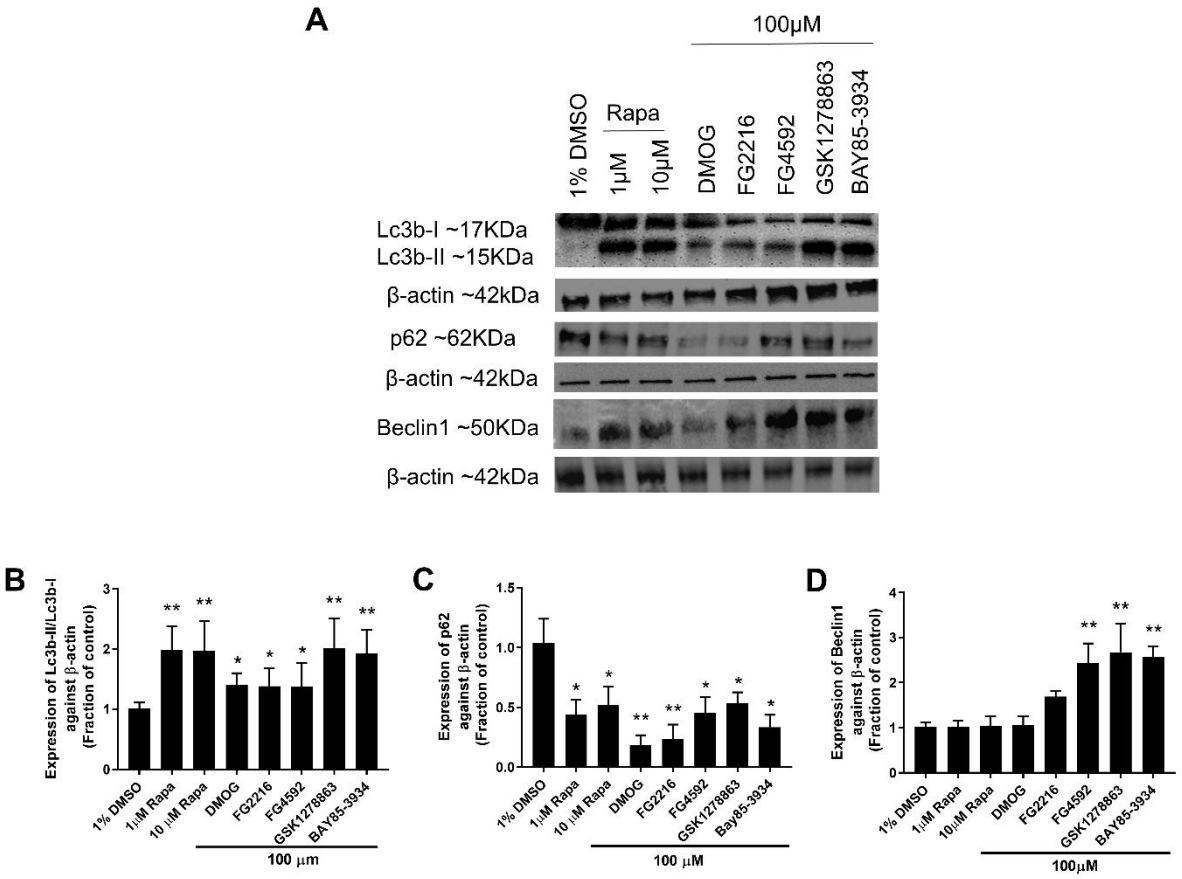

Figure 5.9. Effect of PHD inhibitors on autophagic markers. (A) Representative Lc3b-II / Lc3b-I ratio, p62, and Beclin1 immunoblots alongside β-actin of cells treated with 1% DMSO, PHD inhibitors (100μM), and Rapamycin (1μM and 10μM) for 24 h in normoxia. (B) Bar graphs representing normalised Lc3b-II / Lc3b-I ratio. Compared to 1% DMSO, Lc3b-II / Lc3b-I ratio was significantly upregulated by Rapamycin (1μM and 10μM) and all the PHD inhibitors (100μM). (C) Bar graphs representing normalised p62 expression. Compared to 1% DMSO, p62 was significantly degraded by Rapamycin (1μM and 10μM) and all the PHD inhibitors (100μM). (C) Bar graphs representing normalised Beclin1 expression. Compared to 1% DMSO, Beclin1 was upregulated by DMOG, FG4592, GSK1278863, and Bayer85-3934. *(For all graphs,* represents $p < 0.05$ and ** represents $p < 0.01$ versus 1% DMSO; One-way ANOVA followed by Tukey's post-hoc analysis; n=3)*

5.3.4 Effects of PHD inhibitors on HIF1α and HIF2α expression in PC12 cells

The effects of 24 h treatment with the PHD inhibitors (100μM) were studied on HIF1α and HIF2α expression. Compared to 1% DMSO, HIF1α was significantly upregulated by 100μM of all the PHD inhibitors (FG2216, FG4592, GSK1278863, and Bayer85-3934) except DMOG (Figure 5.10B). There were no significant changes in HIF2α expression by 100μM of all the PHD inhibitors compared to 1% DMSO (Figure 5.10C). As 100μM of DMOG did not upregulate HIF1α and HIF2α, further studies were performed with higher concentrations of DMOG (500, 1000, and 2000μM). Compared to 1% DMSO, HIF1α was significantly upregulated in cells exposed to 1000 and 2000μM of DMOG (Figure. 5.11B). HIF2α was significantly upregulated in cells exposed to 2000μM of DMOG (versus 1% DMSO) (Figure. 5.11C).

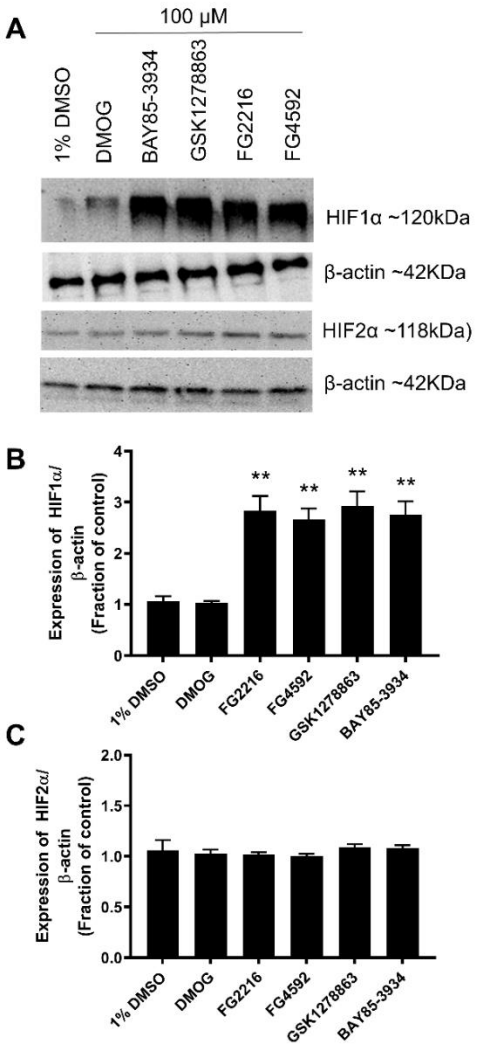

Figure 5.10. Effects of PHD inhibitors on HIF1α and HIF2α expression in PC12 cells. (A) Representative HIF1α and HIF2α immunoblots were shown with those for β-actin of cells treated with 1% DMSO or 100μM of the indicated PHD inhibitors for 24 h in normoxia. (B) Bar graphs representing normalised HIF1α expression. Compared to 1% DMSO, HIF1α expression was significantly higher in cells exposed to 100μM of all PHD inhibitors except DMOG. (C) Bar graphs representing normalised HIF2α expression. There were no significant changes in HIF2α expression by all the PHD inhibitors. *(For all graphs, ** represents $p < 0.01$ versus 1% DMSO; One-way ANOVA followed by Tukey's post-hoc analysis; n=3)*

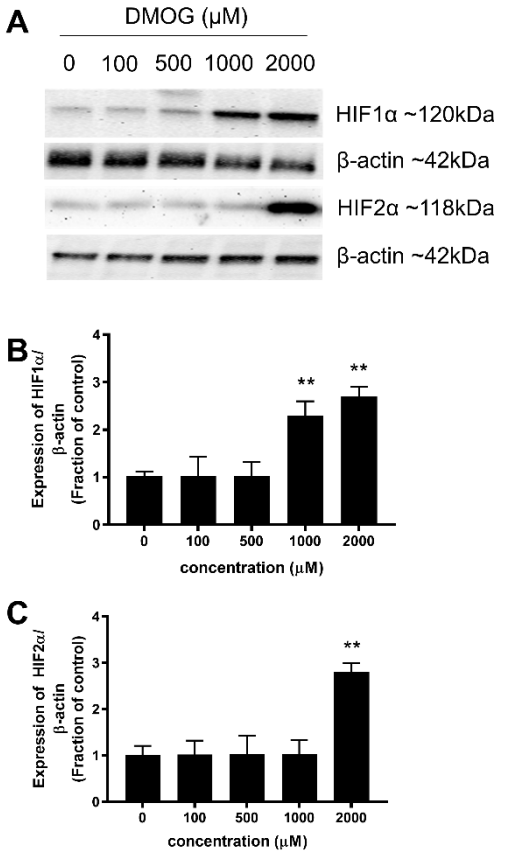

Figure 5.11. Effects of DMOG on HIF1α and HIF2α expression in PC12 cells. (A) Representative Hif1α and Hif2α immunoblots were shown with those for β-actin of cells treated with 1% DMSO and DMOG (100, 500, 1000, and 2000μM) for 24 h in normoxia. (B) Bar graph representing normalised HIF1α expression. Compared to 1% DMSO, HIF1α expression was significantly higher in cells exposed to 1000 and 2000μM of DMOG. (C) Bar graph representing normalised HIF2α expression. Compared to 1% DMSO, HIF2α expression was significantly higher in cells exposed to 2000μM of DMOG. *(For all graphs, ** represents $p < 0.01$ versus 1% DMSO; One-way ANOVA followed by Tukey's post-hoc analysis; n=3)*

5.3.5 Effects of PHD inhibitors on gene expression in PC12 cells

Using qRT-PCR, the effects of PHD inhibitors (100µM) were studied on hypoxic genes in PC12 cells (Figure 5.12). Compared to 1% DMSO, *Hif1α* expression was not significantly altered by all the PHD inhibitors. *Bnip3* was significantly upregulated by FG4592 and Bayer85-3934 with fold changes of ~8 and ~9, respectively compared to 1% DMSO. *Vegf* was upregulated in PC12 cells subjected to FG4592 (~28 folds) and Bayer85-3934 (~21 folds) compared to 1% DMSO. Compared to 1% DMSO, *Phd2* was mildly upregulated by the PHD inhibitors, but a significant fold change was only seen by FG4592 (~5 folds). Compared to 1% DMSO, *Pfkfb3* was significantly upregulated by DMOG (~8.5 folds), FG2216 (~7 folds), FG4592 (~9 folds), GSK1278863 (~6 folds), and Bayer85-3934 (~7.5 folds), while *Pfkfb1* expression was not significantly altered. Significant *Ldha* upregulation was observed with FG2216 (~5 folds), GSK1278863 (~5 folds), and Bayer85-3934 (~2 folds) compared to 1% DMSO.

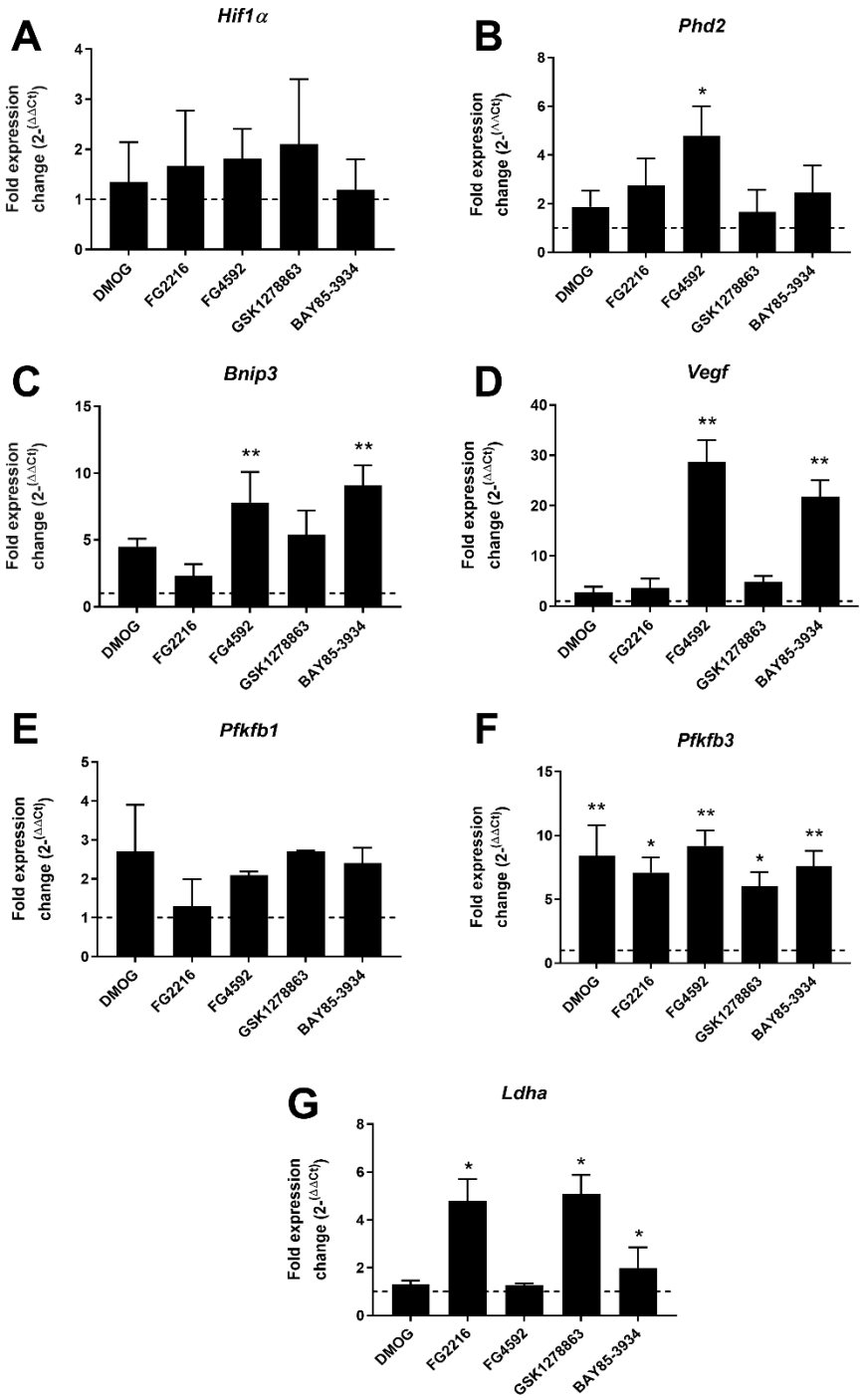

Figure 5.12. Effects of PHD inhibitors on hypoxic genes in PC12 cells. Bar graphs representing normalised PC12 cells gene expression in response to 100µM PHD inhibitors in normoxia for 24 h. Compared to 1% DMSO, there were no significant changes in *Hif1α* (A) expression by all the PHD inhibitors. Compared to 1% DMSO, *Phd2* (B) was only significantly upregulated by FG4592. Compared to

1% DMSO, *Bnip3* (C) and *Vegf* (D) were significantly upregulated by FG4592 and Bayer85-3934. Compared to 1% DMSO, there were no significant changes in *Pfkfb1* (E) expression by all the PHD inhibitors. Compared to 1% DMSO, all the PHD inhibitors studied significantly upregulated *Pfkfb3* (F). Compared to 1% DMSO, FG2216, GSK1278863, and Bayer85-3934 significantly upregulated *Ldha* (G). The gene expression was measured against the housekeeping gene *β-actin* and normalised to 1% DMSO. Dotted line represents basal gene expression. *(For all graphs, * represents $p < 0.05$ and ** represents $p < 0.01$ against 1% DMSO; One-way ANOVA followed by Tukey's post-hoc analysis; n=3).*

5.3.6 Effect of PHD inhibitors in PC12 cells against acute OGD insult

The PHD inhibitors (100µM: DMOG, FG2216, FG4592, GSK1278863, and Bayer 85-3934) were administered into PC12 cells immediately before 6 h OGD insult (Figure 5.2). Compared to untreated control, none of the PHD inhibitors (100µM) improved mitochondrial activity, reduced LDH release, or improved cell viability compared to 1% DMSO treated cells. Treatment with PHD inhibitors in conjunction with OGD was not effective in PC12 cells (Figure 5.13).

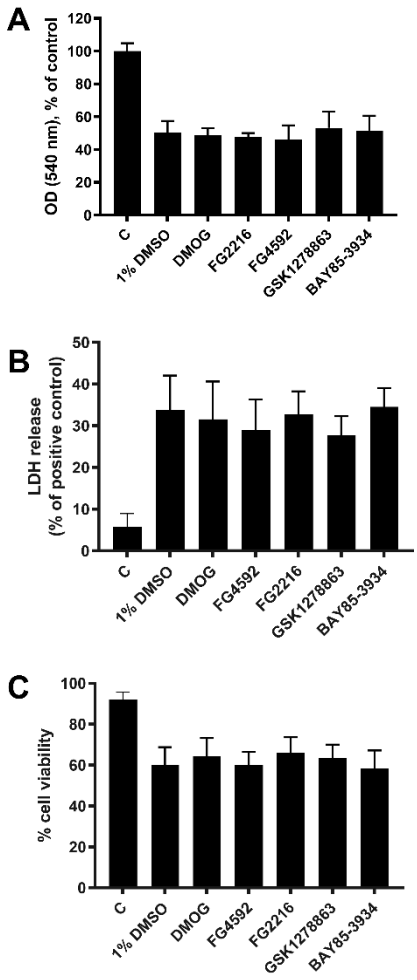

Figure 5.13. The effect of PHD inhibitors on PC12 cells during 6 h OGD insult.

Bar graphs representing cell viabilities of PC12 cells exposed to PHD inhibitors (100µM) in conjunction with 6 h OGD insult. Untreated control (C) were maintained in normoxia throughout (positive control). (A) MTT assay (B) LDH assay and (C) Trypan blue assay. Results revealed that treatment of PC12 cells with PHD inhibitors in conjunction with 6 h OGD insult did not protect the cells compared to untreated control. *(For all graphs, $p > 0.05$ against 1% DMSO treated cells; One-way ANOVA followed by Tukey's post-hoc analysis; n=3).*

5.3.7 Effects of preconditioning with PHD inhibitors against OGD insult in PC12 cells

The effects of preconditioning (24 h) with 100µM PHD inhibitors (DMOG, FG2216, FG4592, GSK1278863, and Bayer 85-3934) were evaluated against 6 h OGD insult (Figure 5.3) in PC12 cells. Compared to 1% DMSO preconditioned cells, there was no improvement in mitochondrial activity, cell viability or reduction in LDH release in cells preconditioned with the PHD inhibitors prior to 6 h OGD insult (Figure 5.14).

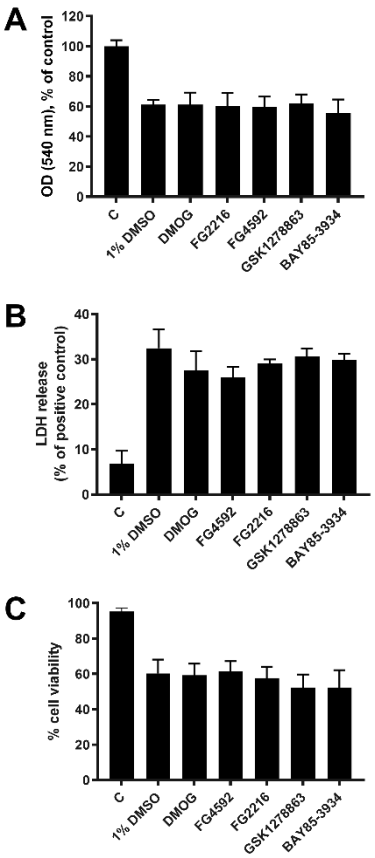

Figure 5.14. The effect of preconditioning with PHD inhibitors on PC12 cells. Bar graphs representing cell viabilities of PC12 cells exposed to 24 h of PHD inhibitors (100μM) followed by subsequent 6 h OGD insult. Untreated control (C) were maintained in normoxia throughout (positive control). (A) MTT assay (B) LDH assay and (C) Trypan blue assay. Results revealed that compared to 1% DMSO preconditioned cells, there were no significant changes in mitochondrial activity, LDH release and cell viability in cells preconditioned with the PHD inhibitors prior to 6 h OGD insult. *(For all graphs, $p > 0.05$ against 1% DMSO preconditioned cells; One-way ANOVA followed by Tukey's post-hoc analysis; n=3).*

5.3.8 Effects of preconditioning with PHD inhibitors followed by reversion and OGD insult in PC12 cells

The effects of preconditioning (24 h) with PHD inhibitors (DMOG, FG2216, FG4592, GSK1278863, and Bayer 85-3934) followed by reversion (24 h) were studied in PC12 cells against subsequent 6 h OGD insult (Figure 5.4). Initial studies revealed that this treatment protocol was protective, therefore the effects of various concentrations of PHD inhibitors (1, 10, 50, and 100 µM) were evaluated. Preconditioning with 100µM of DMOG, FG2216, FG4592, GSK1278863, and Bayer85-3934 followed by 24 h reversion resulted in significantly improved mitochondrial activity, greater cell viability and reduced LDH release against 6 h OGD compared to 1% DMSO preconditioned cells. Additionally, preconditioning with 50µM of FG4592 and Bayer85-3934 also resulted in significantly improved mitochondrial activity, but did not reduce LDH release or improve cell viability compared to 1% DMSO preconditioned cells. The improvement in mitochondrial activity observed in 100µM FG4592 and Bayer85-3934 preconditioned cells is not significantly different from those treated with 50µM. All other concentrations of PHD inhibitors (1 and 10µM) did not improve mitochondrial activity, cell viability, or reduce LDH release (Figure 5.15).

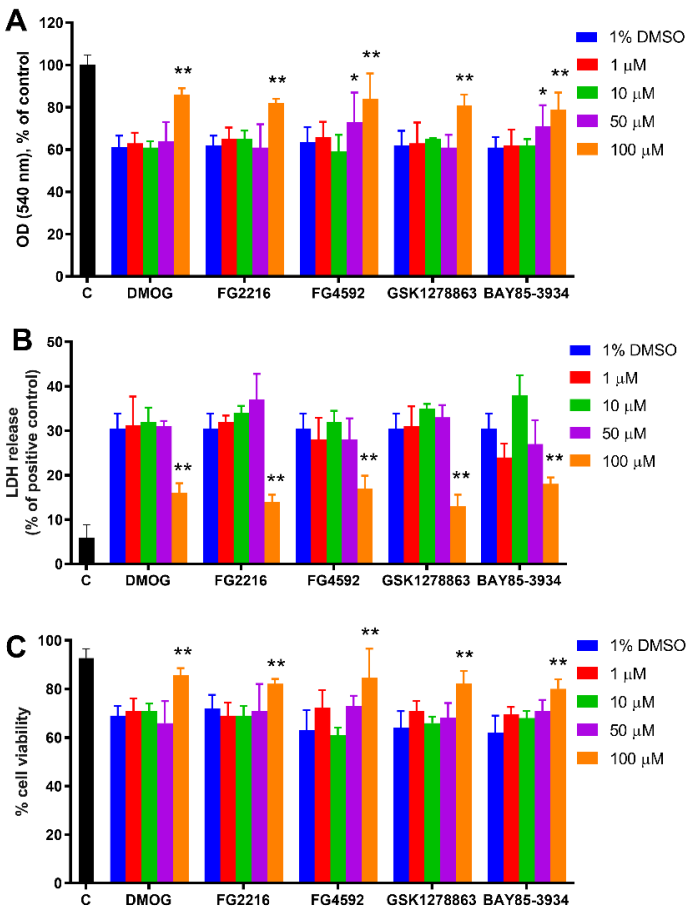

Figure 5.15. The effect of preconditioning with PHD inhibitors followed by 24 h reversion and 6 h OGD on PC12 cells. Bar graphs representing cell viabilities of PC12 cells exposed to 1% DMSO or PHD inhibitors for 24 h followed by 24 h reversion and 6 h OGD insult. Untreated control (C) were maintained in normoxia throughout (positive control). (A) MTT assay revealed significant improvement in mitochondrial activity in cells preconditioned with 100μM of DMOG, FG2216, and GSK1278863; and 50 / 100 μM of FG4592 and Bayer85-3934 (versus 1% DMSO treated cells). (B) LDH assay and (C) Trypan blue exclusion assay revealed significant reduction in LDH release and greater cell viability in cells preconditioned with 100μM of all the PHD inhibitors (versus 1% DMSO treated cells). *(For all graphs, * represents $p < 0.05$ and ** represents $p < 0.01$ against 1% DMSO preconditioned cells; Two-way ANOVA followed by Tukey's post-hoc analysis; n=3).*

In addition to cell viabilities, the effects of preconditioning with the PHD inhibitors (100μM) (24 h) followed by reversion (24 h) were studied in PC12 cells against subsequent OGD (6 h) insult using FACS analysis (Figure 5.16). Preconditioning with 1% DMSO followed by reversion and 6 h OGD resulted in a significant reduction in viable cells (54.4 ± 6.8%) and an increase in early apoptotic cells (32.5 ± 4.5%); there was no significant necrosis. Compared to cells preconditioned with 1% DMSO, there was a significant reduction in early apoptotic cells (AV^+ / $7\text{-}AAD^-$) when preconditioned with 100μM of DMOG (15.7 ± 4.9%), FG2216 (11.8 ± 5.1%), FG4592 (16.9 ± 7.1%), GSK1278863 (10.7 ± 4.8%), and Bayer85-3934 (12.3 ± 3.8%) before 6 h OGD. The majority of the cells (~75-85%) were viable, indicating a cytoprotective effect.

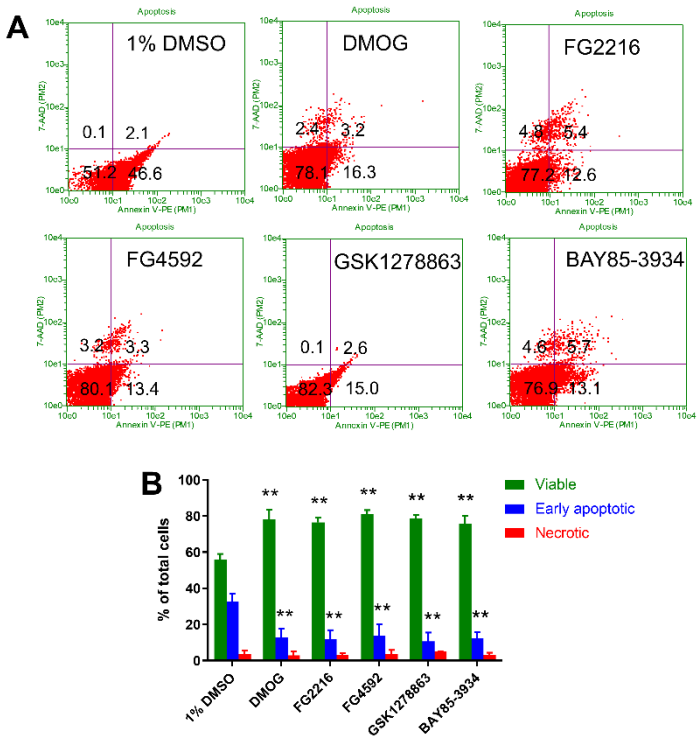

Figure 5.16. Annexin-V / 7-AAD FACS analysis of PC12 cells preconditioned with PHD inhibitors (24 h) followed by 24 h reversion and 6 h OGD. PC12 cells were treated with 1% DMSO or PHD inhibitors (100µM) for 24 h in normoxia followed by 24 h reversion and 6 h OGD insult (A) Representative Annexin-V / 7-AAD dot plots. Cells in the lower left quadrant represent viable cells, cells in the lower right quadrant represent early apoptosis, and cells in the upper right quadrant represented necrosis. (B) Bar graph representing % of viable, % of early apoptotic and % of necrotic cells, out of total cells. *(For all graphs, ** represents $p < 0.01$ against 1% DMSO preconditioned cells (against same cell group); Two-way ANOVA followed by Tukey's post-hoc analysis; n=3).*

5.3.9 Effects of DMSO on primary rat cortical neurons

The effects of a range of DMSO concentrations (0.5%-10%) were evaluated on primary neurons. Compared to control (0%), 5% and 10% DMSO resulted in a significant reduction in mitochondrial activity and an increase in LDH release. Compared to 5% DMSO, the mitochondrial activity was significantly ($p<0.05$) lower and LDH release was significantly ($p<0.01$) higher at 10% DMSO treatment. All the other concentrations had no significant effects on mitochondrial activity and LDH release compared to control (0% DMSO) (Figure 5.17). Similar to PC12 cells, a final concentration of 1% DMSO was used in all experiments to dissolve the PHD inhibitors.

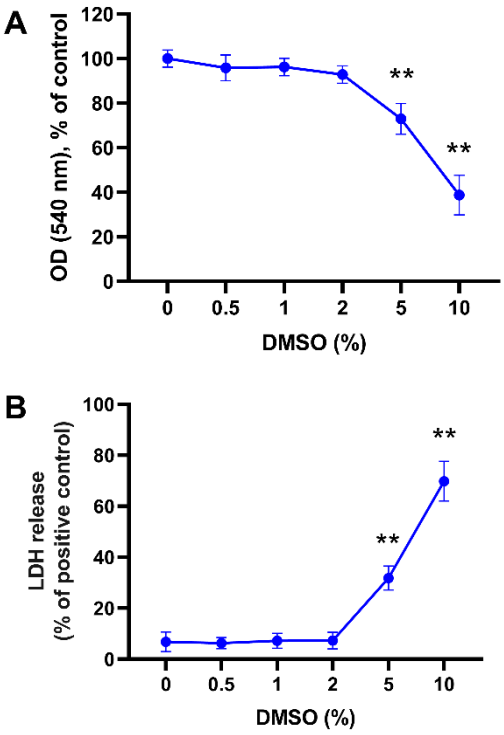

Figure 5.17. Effects of DMSO on primary neuronal viability. Bar graphs representing primary neuronal viabilities following 24 h treatment with indicated DMSO concentrations. (A) MTT assay (B) LDH assay. Results revealed that that 5% and 10% DMSO were cytotoxic compared to untreated (0% DMSO) cells. *(For all graphs, ** represents $p < 0.01$ versus 0% DMSO; One-way ANOVA followed by Tukey's post-hoc analysis; n=3)*

5.3.10 The effect of PHD inhibitors on primary neuronal viabilities

As the four clinical PHD inhibitors had similar efficacy and potency in the PC12 cells, we only studied FG4592 alongside a nonspecific PHD inhibitor DMOG in the primary rat neurons. The effects of 24 h treatment in normoxia with FG4592 (10, 30, 50, and 100μM) and DMOG (100, 250, 500, 1000, and 2000μM) were evaluated on primary neurons, using MTT, LDH assay, and neuron-specific Map2 IF staining for morphological changes. There were no significant changes in mitochondrial activity and LDH release by FG4592 (10, 30, 50, and 100μM) compared to 1% DMSO. DMOG (500, 1000, and 2000μM) resulted in a significant reduction in mitochondrial activity and an increase in LDH release compared to 1% DMSO (Figure 5.18).

Primary neuronal cultures subjected to 1% DMSO, consisted of $Map2^+$ neurons consisting of 9.4±3.8 dendrites per neuron, with each dendrite measuring 38.9±9.81μm. There were no significant changes in the number of dendrites per neuron, dendrites length, and neuron morphology by FG4592 (10, 30, 50, and 100μM) and DMOG (100 and 250μM). DMOG (500μM) resulted in a significant reduction in dendrites per neuron (2.8±1.2; *p<0.05 versus 1% DMSO*) and dendrite length (6.1±2.8μm; *p<0.05 versus 1% DMSO*). In cultures subjected to DMOG (1000 and 2000 μM), all the dendrites completely degraded, indicating the degeneration of neurons. DMSO (1%) treated cultures consisted of 42.6±10.3 $Map2^+$ nuclei per microscopic field. There were no significant changes in cell densities by FG4592 (10, 30, 50, and 100μM) and DMOG (100, 250, and 500μM). In line with LDH assay results, there was a significant reduction in cell densities by 1000μM (15.8±8.1 $Map2^+$ nuclei per microscopic field; *p<0.05 versus 1% DMSO*) and 2000μM (9.1±3.4

Map2^{+} nuclei per microscopic field; *p<0.01 versus 1% DMSO*) of DMOG (Figure 5.19).

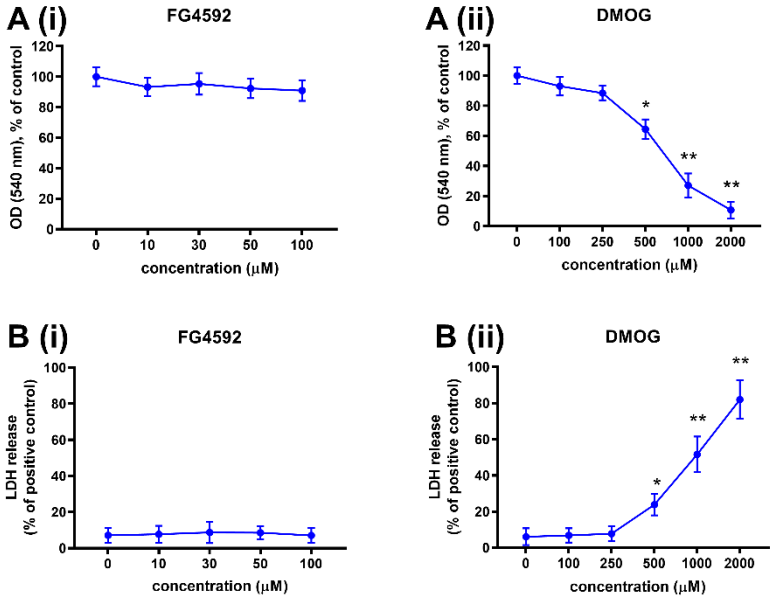

Figure 5.18. Effect of PHD inhibitors on primary neurons during normoxia. Bar graphs represent the viabilities of primary neurons subjected to 1% DMSO (0μM), FG4592 (concentration of 10, 30, 50, and 100μM) and DMOG (100, 250, 500, 1000, and 2000μM) for 24 h (normoxia). (A) (i) MTT assays revealed no significant changes in mitochondrial activity in primary neurons subjected to 10 to 100μM of FG4592 compared to 1% DMSO. (ii) Compared to 1% DMSO, DMOG (500, 1000, and 2000μM) significantly reduced mitochondrial activity. (B) (i) LDH assay revealed no significant changes in LDH release by 10 to 100μM of FG4592 compared to 1% DMSO. (ii) A significant increase in LDH release was seen by 500, 1000, and 2000μM of DMOG compared to 1% DMSO. *(For all graphs, * represents $p < 0.05$* and ** *represents $p < 0.01$ versus 1% DMSO only (represented as 0μM); One-way ANOVA followed by Tukey's post-hoc analysis; n=3)*

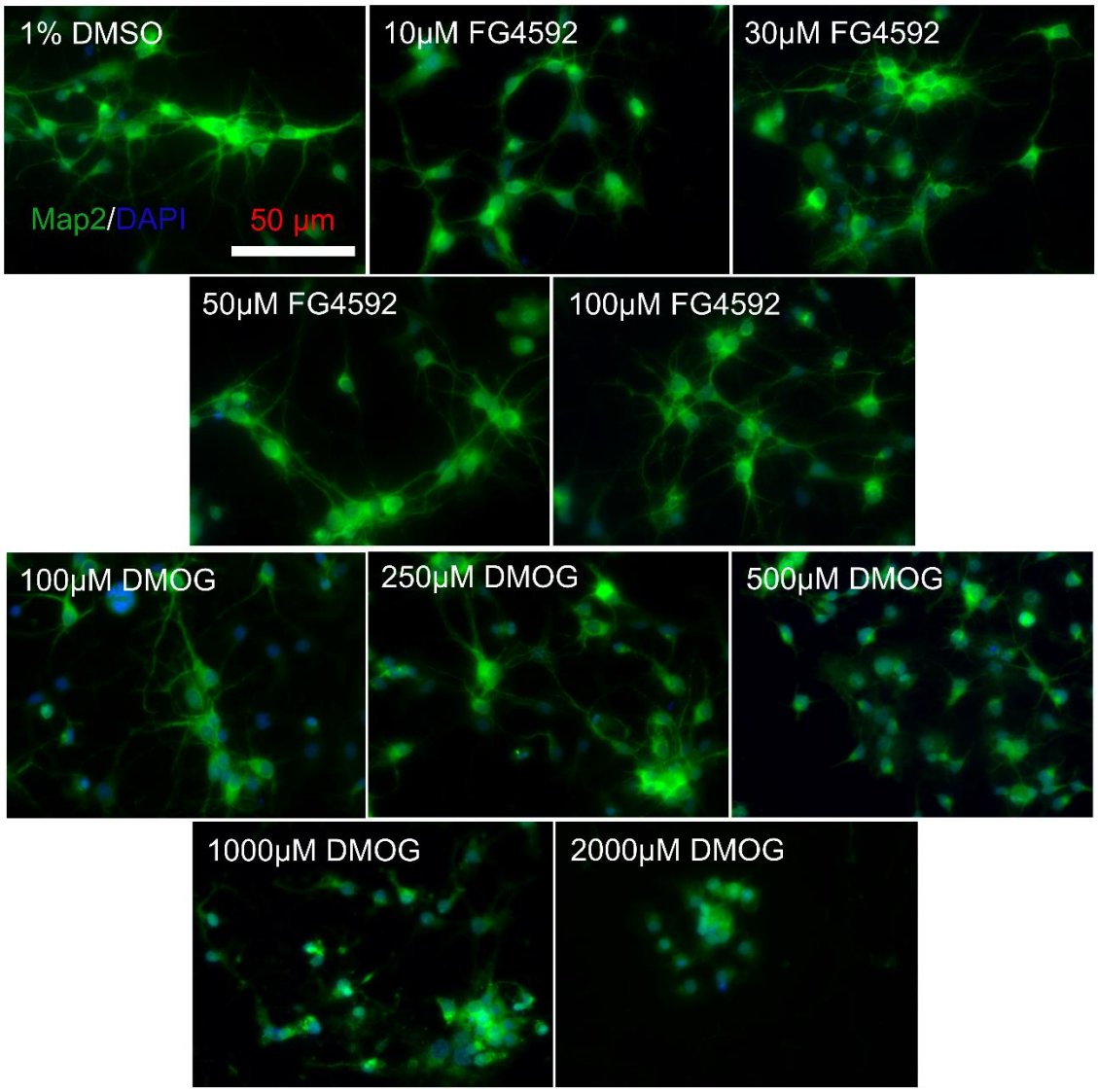

Figure 5.19. Fluorescence micrographs of neuronal cultures subjected to PHD inhibitors for 24 h in normoxia. Representative double merged micrographs of Map2 (FITC) and DAPI (blue) stained neuronal cultures following exposure to 1% DMSO, FG4592 (concentration of 10, 30, 50, and 100µM) and DMOG (100, 250, 500, 1000, and 2000µM) for 24 h in normoxia. DMSO (1%) treated cultures consisted of neuronal nuclei ($Map2^{+}$) surrounded by numerous dendrites. Compared to 1% DMSO, there were no changes in neuronal cultures by FG4592 (10, 30, 50, and 100µM) and DMOG (100 and 250µM). There was a reduction in the number of dendrites surrounding each neuron and dendrite length in cultures treated with

500μM DMOG. DMOG (1000 and 2000μM) resulted in complete loss of dendrites and a reduction in cell densities.

5.3.11 Effects of PHD inhibitors on autophagy in primary neurons

The effects of 24 h treatment with FG4592 (10, 30, 50, and 100µM) and DMOG (100, 250, and 500µM) were evaluated on LC3b and p62 expression in primary neurons (Figure 5.20). In primary neurons, FG4592 (30, 50, and 100µM) and DMOG (250 and 500µM) resulted in a significant increase in Lc3b-II / Lc3b-I ratio compared to 1% DMSO. Significant downregulation of p62 compared to 1% DMSO was seen by FG4592 (50 and 100µM) and DMOG (100, 250, and 500µM). A lower concentration of FG4592 (10µM) did not result in significant changes in LC3b-II and p62 expression compared to 1% DMSO.

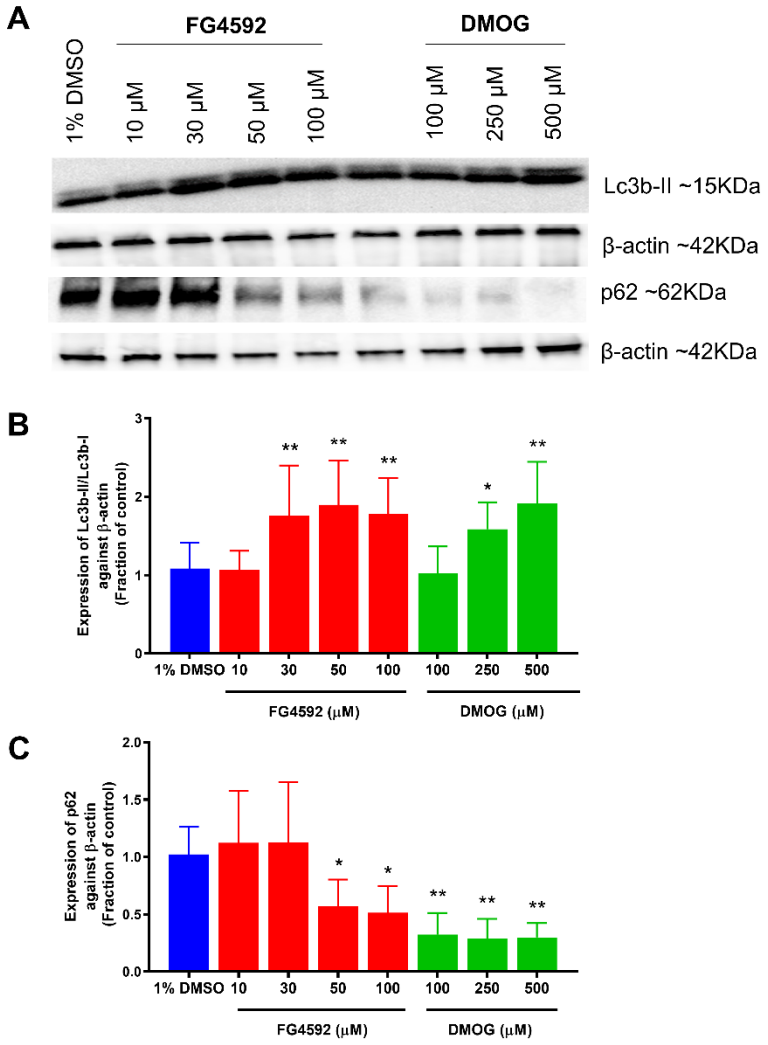

Figure 5.20. Effect of PHD inhibitors on the Lc3b-II / Lc3b-I and p62 expression in primary neurons. (A) Representative Lc3b-II / Lc3b-I ratio and p62 immunoblots alongside β-actin of primary neurons treated with 1% DMSO, FG4592 (10, 30 50, 100µM) and DMOG (100, 250, 500µM). (B) Bar chart representing normalised Lc3b-II / Lc3b-I ratio. FG4592 (30, 50 and 100µM) and DMOG (250 and 500µM) significantly upregulated Lc3b-II / Lc3b-I ratio compared to 1% DMSO. (C) Bar chart representing p62 expression. FG4592 (50 and 100µM) and DMOG (250 and 500µM) significantly degraded p62 compared to 1% DMSO. *(For all graphs, * represents $p < 0.05$* and ** *represents $p < 0.01$ versus 1% DMSO; Two-way ANOVA followed by Tukey's post-hoc analysis; n=3)*

5.3.12 Effects of PHD inhibitors on HIF1α and HIF2α in primary neurons

The effects of 24 h treatment with FG4592 (10, 30, 50, and 100μM) and DMOG (100, 250, and 500μM) was investigated on HIF1α and HIF2α expression in primary rat neurons (Figure 5.21). Compared to 1% DMSO, HIF1α was significantly upregulated by FG4592 (30, 50, and 100μM) but not FG4592 (10μM). HIF2α expression was not altered by FG4592 (10, 30, 50, and 100μM) compared to 1% DMSO. DMOG (100, 250, and 500μM) significantly upregulated HIF1α and HIF2α in primary neurons compared with 1% DMSO. HIF2α expression was significantly ($p<0.01$) lower in cells treated with 500μM DMOG compared to 100 and 250μM.

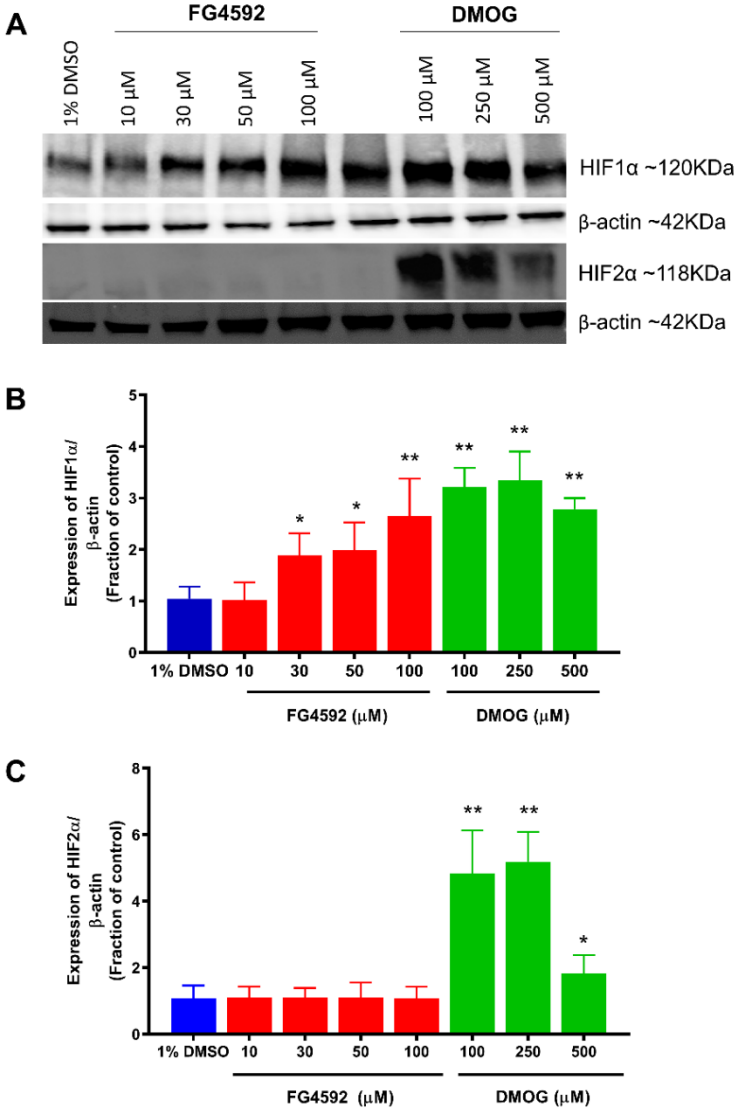

Figure 5.21. Effects of PHD inhibitors on HIF1α and HIF2α levels in primary rat cortical neurons. (A) Representative HIF1α and HIF2α immunoblots were shown with those for β-actin of primary neurons treated with 1% DMSO, FG4592 (10, 30 50, 100μM) and DMOG (100, 250, 500μM). (B) Bar graph representing normalised HIF1α level. (C) Bar graph representing normalised HIF2α level. FG4592 (30, 50, and 100μM) significantly increased HIF1α expression. DMOG (100, 250, and 500μM) significantly increased both HIF1α and HIF2α expression. *(For all graphs, * represents $p < 0.05$ and ** represents $p < 0.01$ versus 1% DMSO; Two-way ANOVA followed by T*

5.3.13 Effect of PHD inhibitors on gene expression in primary neurons

Using qRT-PCR, effects of 24 h treatment with FG4592 (10, 30, 50, and 100μM) and DMOG (100, 250, and 500μM) was investigated on hypoxia gene expressions (*Hif1α, Hif2α, Epo, Bnip3, Phd2, Vegf, Pfkfb1, Pfkfb3,* and *Ldha*) in primary neurons (Figure 5.22). *Hif1α, Hif2α, Bnip3, Pfkfb1,* and *Pfkfb3* expression was not significantly altered by FG4592 and DMOG (all concentrations studied compared to 1% DMSO). Compared to 1% DMSO, *Phd2* (~10 folds) and *Ldha* (~9 folds) were significantly upregulated by DMOG (500μM) only. *Vegf* was significantly upregulated by FG4592 (30μM, ~10 folds; 50μM, ~15 folds, 100μM, ~19 folds) and DMOG (100μM, ~12 folds; 250μM, ~18 folds, 500μM, ~15 folds). *Epo* was significantly upregulated by FG4592 (50μM, ~7 folds, 100μM, ~10 folds) and DMOG (100μM, ~8 folds; 250μM, ~12 folds, 500μM, ~10 folds).

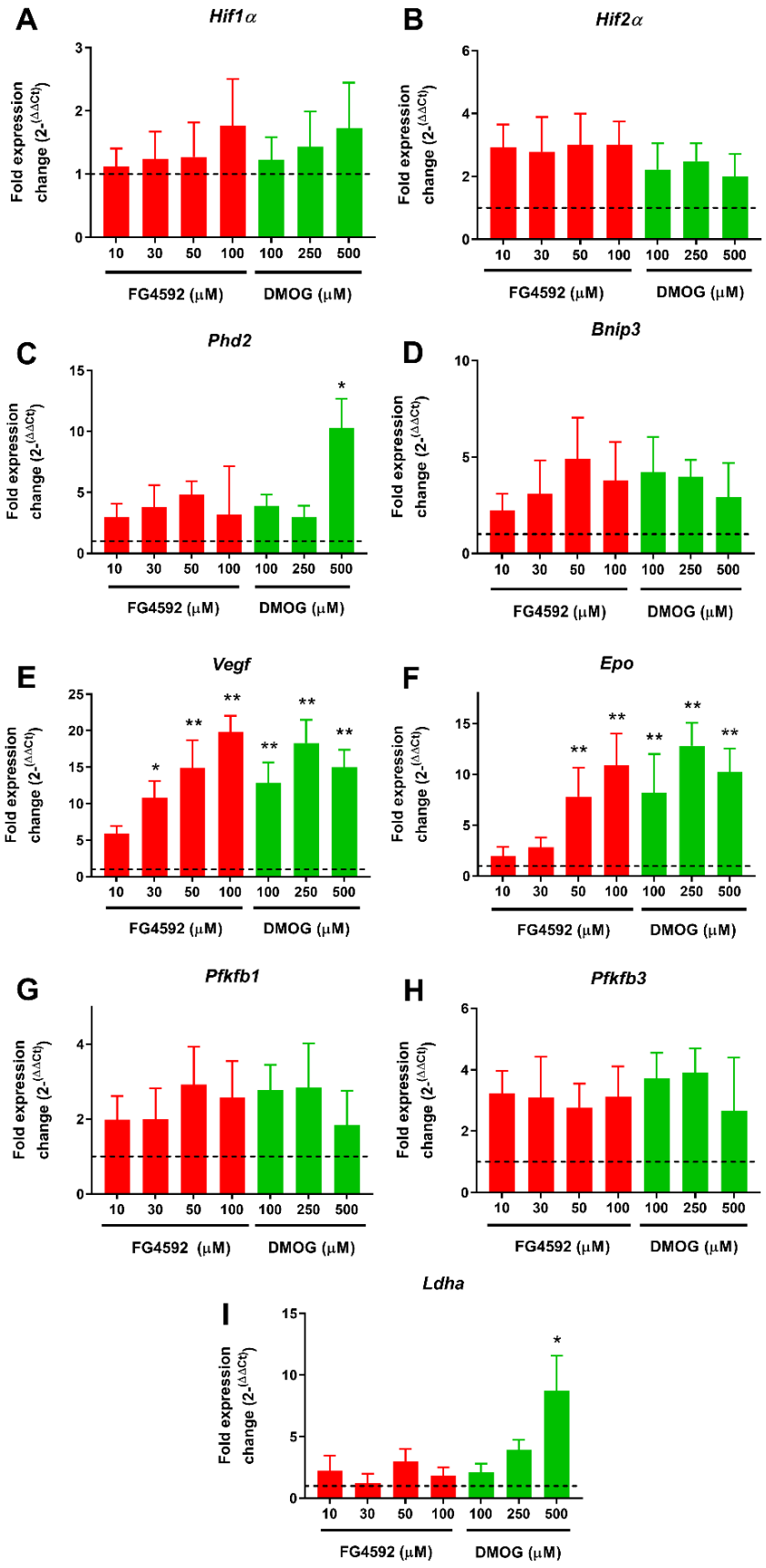
A
Hif1α
B
Hif2α
C
Phd2
D
Bnip3
E
Vegf
F
Epo
G
Pfkfb1
H
Pfkfb3
I
Ldha
Fold expression change (2-(ΔΔCt))
FG4592 (μM)
DMOG (μM)
10 30 50 100 100 250 500

Figure 5.22. Effects of PHD inhibitors on hypoxia gene expression in primary rat cortical neurons. Bar graphs representing normalised gene expression in primary neurons subjected to FG4592 (10, 30, 50, 100μM) and DMOG (100, 250, 500μM) for 24 h. There were no significant changes in (A) *Hif1α*, (B) *Hif2α,* (D) *Bnip3*, (G) *Pfkfb1*, and (H) *Pfkfb3* expression by DMOG and FG4592 at the concentrations studied versus 1% DMSO. Compared to 1% DMSO, (C) *Phd2* and (I) *Ldha* were significantly upregulated by DMOG (500μM). (E) *Vegf* was significantly upregulated by FG4592 (30μM, 50μM, and 100μM) and DMOG (100μM, 250μM, and 500μM). (F) *Epo* was significantly upregulated by FG4592 (50μM, 100μM) and DMOG (100μM, 250μM, and 500μM). The gene expression was measured against the housekeeping gene *β-actin* and normalised to 1% DMSO. Dotted line represents basal gene expression. *(For all graphs, * represents $p < 0.05$ and ** represents $p < 0.01$ against 1% DMSO; Two-way ANOVA followed by Tukey's post-hoc analysis; n=3).*

5.3.14 Effects of preconditioning with PHD inhibitors with reversion before OGD insult in primary neurons

The effect of preconditioning with FG4592 (10, 30, 50, and 100µM) and DMOG (100, 250µM) followed by reversion were studied against a 6 h OGD insult in primary neurons. Preconditioning with 1% DMSO and the PHD inhibitors (all concentrations) followed by reversion and 6 h OGD resulted in significantly ($p<0.05$) reduced mitochondrial activity and greater LDH release compared to untreated control. However, some protection against 6 h OGD insult was conferred in cells preconditioned with FG4592 (50 and 100µM) and DMOG (100 and 250µM) compared to 1% DMSO preconditioned cells, for both the assays. The reduction in LDH release was significantly ($p<0.05$) lower in 100µM FG4592 preconditioned cells compared to those treated with 50µM; there was no significant difference in mitochondrial activity. FG4592 (10 and 30µM) did not improve mitochondrial activity or reduce LDH release compared to 1% DMSO preconditioned cells (Figure 5.23).

In primary neuronal cultures preconditioned with DMSO (1%) followed by reversion and 6 h OGD insult, the neurons ($Map2^{+}$) consisted of 2.1±0.4 dendrites per neuron, with each dendrite measuring 6.1±1.2µm (indicating degradation of dendrites). Compared to 1% DMSO preconditioned cultures, there was no significant improvement in neuron morphology in FG4592 (10 and 30µM) preconditioned cultures. Compared to 1% DMSO preconditioned cultures, there was a significant ($p<0.05$) improvement in neuron morphology in FG4592 (50 and 100µM) and DMOG (100 and 250µM) preconditioned cultures. FG4592 (50µM: 10.2±3.2 dendrites per neuron, with each dendrite measuring 34.4±7.8µm and 100µM: 9.8±5.1 dendrites per neuron, with each dendrite measuring 31.8±9.1µm); DMOG (100µM: 11.3±3.1

dendrites per neuron, with each dendrite measuring 36.4±5.3μm and 250μM:10.7±5.1 dendrites per neuron, with each dendrite measuring 36.1±4.5μm). (Figure 5.24). LDH, MTT assay, and Map2 staining revealed that FG4592 (50 and 100μM) and DMOG (100 and 250μM) induced ischaemic tolerance and were cytoprotective against 6 h OGD insult.

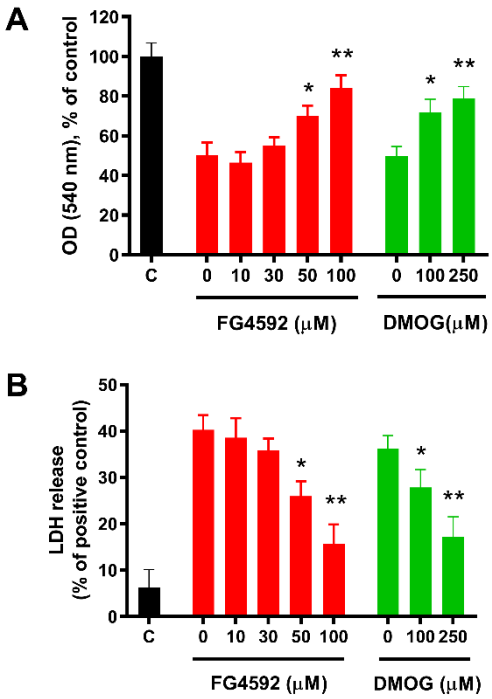

Figure 5.23. The effect of preconditioning with PHD inhibitors followed by 24 h reversion and 6 h OGD on primary cortical rat neurons. Bar graphs representing primary cortical rat neuronal viabilities following exposure to 1% DMSO (0μM), FG4592 (10, 30 50, 100, 200μM), and DMOG (100, 250μM) for 24 h in normoxia followed by 24 h reversion and subsequent 6 h OGD insult. Untreated control (C) were maintained in normoxia throughout (positive control). (A) MTT assay and (B) LDH assay revealed significant improvement in mitochondrial activities and reduction in LDH release in cells preconditioned with FG4592 (50μM and 100μM) and DMOG (100μM and 250μM) compared to 1% DMSO preconditioned cells. *(For all graphs, * represents $p < 0.05$ and ** represents $p < 0.01$ against 1% DMSO preconditioned cells; Two-way ANOVA followed by Tukey's post-hoc analysis; n=3).*

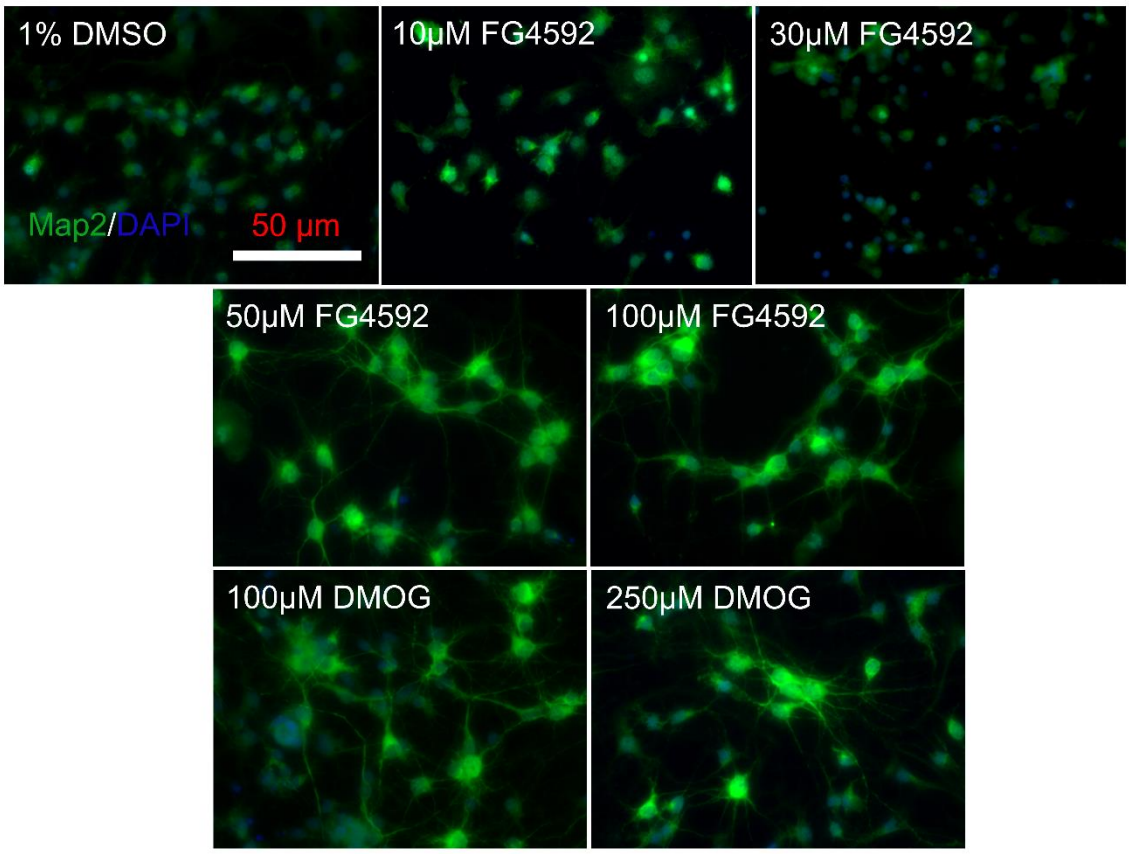

Figure 5.24. Fluorescence micrographs of neuronal cultures preconditioned with PHD inhibitors for 24 h followed by reversion and 6 h OGD insult. Representative double merged micrographs of Map2 (FITC) and DAPI (blue) stained neuronal cultures following exposure to 1% DMSO, FG4592 (10, 30, 50, and 100μM) and DMOG (100, 250μM) for 24 h in normoxia followed by 24 h reversion and 6 h OGD insult. DMSO (1%) preconditioned cultures consisted of neurons with reduced or no dendrites. There was no significant improvement in neuron morphology in FG4592 (10 and 30μM) preconditioned cultures. FG4592 (50 and 100μM) and DMOG (100 and 250μM) preconditioned cultures consisted of healthier neurons (numerous dendrites).

5.4 Discussion

The experiments in this chapter were performed to determine the effects of a novel class of PHD inhibitors as well as DMOG, a nonspecific PHD inhibitor on cell viabilities, expression of HIF1α, HIF2α proteins, their downstream genes, and autophagic proteins in PC12 cells and primary neurons. After this, the effectiveness of preconditioning PHD inhibition was evaluated against OGD insults in PC12 cells and in primary neurons.

Pharmacological PHD inhibition has shown promise in several *in vivo* and *in vitro* studies (Section 1.5.3, summarized in Table 1.5). DFO, $CoCl_2$, and DMOG are frequently studied PHD inhibitors that upregulate HIF1α (Jones *et al*., 2008). *In vivo* studies in neonatal rats have shown that preconditioning with DFO and $CoCl_2$ had a long-term protective effect against ischaemic injury (Jones *et al*., 2008). DFO preconditioning promoted tolerance against focal cerebral ischaemia in rats and rat cortical neurons subjected to OGD (Li *et al*., 2008). Similarly, DMOG preconditioning has shown to reduce OGD induced cell death (Ogle *et al*., 2012). *In vivo* studies showed reduced infarct size in DMOG preconditioned adult mice (Nagel *et al*., 2010). However, these molecules also have other mechanisms of action such as anti-oxidant effect, effect on citric acid cycle enzymes such as isocitrate dehydrogenase and 2-OG dehydrogenase (Ogle *et al*., 2012) indicating that their protective effect is not solely due to HIF activation. Although *in vitro* and *in vivo* studies using DFO, DMOG, and $CoCl_2$ have shown promise, they also have safety and toxicity concerns due to which they cannot be used in patients. Considering these requirements, studies in this chapter focused on evaluating the most clinically advanced small molecule PHD inhibitors at biologically safe concentrations. These PHD inhibitors

are in clinical trials for the treatment of anaemia, with aims to augment native EPO production (Gupta and Wish, 2017). In this chapter, three of the most recent and clinically advanced PHD inhibitors GSK1278863, FG4592, and Bayer85-3934 (Gupta and Wish, 2017) were studied, alongside widely studied DMOG and FG2216 for comparison.

A study by Yeh *et al*., (2017) revealed that PHD inhibitors in clinical trials FG4592, GSK1278863, and Bayer85-3934 work by active site iron-chelating mechanisms and compete with 2-OG. FG4592 and FG2216 coordinate with metal in PHD via glycinamide side chain, whereas Bayer85-3934 coordinates via the nitrogen of its pyrazolone and pyridine ring. GSK1278863 binds to the metal via amide oxygen and pyrimidinetrione oxygen. FG2216 has been replaced in clinical development by structurally related FG4592 following the appearance of adverse effects in phase II clinical trials (Gupta and Wish 2017). Any differences in results between FG4592 and FG22216 may be related to the difference in structure, with an additional phenoxy-group present on the phenyl isoquinolyl ring in FG4592 resulting in a more efficient binding than FG2216 (Yeh *et al*., 2017). Any differences in their potency and effectiveness depend on the extent to which the inhibitors project in the 2-OG binding site of PHD2 and influence substrate binding as well as differences in inhibition kinetics of these compounds (Yeh *et al*., 2017).

Before evaluating the effectiveness of PHD inhibitors against ischaemic insults, it is essential to determine the concentrations at which the PHD inhibitors are safe to use. In PC12 cells, there were no significant changes in cell viability, LDH release, and early apoptosis by all the novel PHD inhibitors (FG2216, FG4592, GSK1278863,

and Bayer85-3934 versus 1% DMSO) at the concentrations (1-100µM) studied. Mitochondrial activities were unchanged by these compounds except for FG4592 (100µM) and Bayer85-8934 (50 and 100µM), which significantly decreased mitochondrial activities compared to 1% DMSO. The extent to which they mimic hypoxia and reduce mitochondrial activity may vary and depends on the potency and mechanism of action of the drugs. However, it is important to comprehend that mitochondrial activity might decrease despite being viable cells. In primary neurons, only FG4592 was pursued alongside DMOG. When these experiments were performed, FG4592 was most advanced in clinical trials and was in clinical use in China (Gupta and Wish, 2017). FG4592 did not result in any significant LDH release, changes in mitochondrial activities and neuron morphology (Map2 staining) at the concentrations (10-100µM versus 1% DMSO) studied. Compared to 1% DMSO, DMOG (500µM, 1mM, and 2mM) resulted in significant LDH release and reduction in mitochondrial activities in PC12 cells and primary neurons. DMOG (250µM) also resulted in a reduction in mitochondrial activity in PC12 cells but not primary neurons. In primary neurons, Map2 staining revealed that high concentrations of DMOG (500µM, 1mM, and 2mM) resulted in the degradation of dendrites (loss of Map2, reduction in dendrites per neuron, and dendrite length). DMOG (1mM and 2mM) also resulted in a significant reduction in cell densities.

Next, the effects of the PHD inhibitors were studied on the autophagic marker (Lc3b, p62, and Beclin1). Rapamycin, an inducer of autophagy was used as a positive control in PC12 cells (Gunn *et al*., 2018). Upon induction of autophagy, cytosolic Lc3b-I is conjugated to phosphatidylethanolamine to form Lc3b-II, which is

incorporated into the autophagosomal membrane. The p62 protein binds to polyubiquitinated proteins through a ubiquitin-associated domain and combines with Lc3b-II through its Lc3b-interaction region domain for attachment to the autophagosome, which is finally degraded in autolysosome. In the process of autophagy, p62 is continuously degraded. Lc3b-II and p62 are used to monitor autophagic activity in various studies (Li *et al*., 2018). Results showed that 100µM of PHD inhibitors (DMOG, FG2216, FG4592, GSK1278863, and Bayer85-3934) and Rapamycin (1µM and 10µM) significantly increased Lc3b-II expression in PC12 cells compared to 1% DMSO. A subsequent downregulation of p62 was seen in PC12 cells treated with Rapamycin and the PHD inhibitors compared to 1% DMSO indicating degradation by autolysosomes was initiated. Similar results were observed in primary neurons, where FG4592 (50µM and 100µM) and DMOG (100µM, 250µM, and 500µM) significantly downregulated p62 compared to 1% DMSO. Additionally, Lc3b-II was significantly upregulated by FG4592 (30µM, 50µM, and 100µM) and DMOG (250µM and 500µM) compared to 1% DMSO. The effects of the novel PHD inhibitors have not been widely explored on autophagy. A study by Li *et al*., 2018 reported that FG4592 induced autophagy in SH-SY5Y cells characterised via Lc3b-II expression and p62 downregulation. A study by Bo *et al*., 2014 revealed that a PHD inhibitor, ethyl-3,4-dihydroxybenzoate (EDHB) promoted autophagy in oesophageal squamous cells.

The expression of Beclin1, which is commonly linked to HIF1α activation and autophagy was studied in PC12 cells (Cheng *et al*., 2017). Compared to 1% DMSO, results revealed that the novel PHD inhibitors (FG4592, GSK1278863, and Bayer85-3934) significantly upregulated Beclin1 in PC12 cells. These results are in line with

the study by Cheng *et al*., (2017) that showed that $CoCl_2$ induces autophagy via activation of the HIF1α / Beclin1 signalling pathway. Another study by Lu *et al*., (2018) showed that the HIF1α / Beclin1 signalling pathway modulates autophagy and contributes to HPC induced protection against OGD / R. It is postulated that HIF1α promotes the dissociation of Beclin1-Bcl2 complex resulting in Beclin1 release thereby initiating autophagy (Lu *et al*., 2018). On the other hand, although mTOR inhibitor Rapamycin promoted autophagy (shown by Lc3b-II upregulation and p62 downregulation), there were no significant changes in Beclin1. This was in line with studies by Li *et al*. (2013) and Grishchuk *et al*. (2011), which found that Rapamycin promoted autophagy via a Beclin-1 independent mechanism. They found that Rapamycin inhibited mTOR resulting in activation of Atg1 kinase complex to regulate autophagy. In PC12 cells, DMOG promoted autophagy through a different pathway from HIF1α / Beclin1 pathway as it has various mechanisms of action, one of which is the AMPK signalling pathway (Zhdanov *et al*, 2015). It is widely accepted that AMPK signalling is activated during energy crisis and oxidative stress. There are two mechanisms by which AMPK activation results in autophagy (1) inactivation of mTOR complex 1 (2) direct phosphorylation of protein kinase, ULK1, initiating autophagy. AMPK is known to contribute to autophagosome maturation and lysosomal fusion (Jang *et al*. 2018; Duran *et al*, 2013).

Autophagy is a self-catabolic process of damaged or dysfunctional cellular components that are recycled for providing energy and nutrients. The induction of autophagy is beneficial to degrade harmful materials produced during nutrient deprivation through lysosomal systems (Gunn *et al*., 2018). Various studies (Yan *et al*., 2011; Sheng *et al*., 2010; Park *et al*., 2009) have shown that IPC increased the

generation of autophagosomes and lysosomal activity. Inhibition of autophagy by 3-methyladenine or Bafilomycin A1 during IPC suppressed the neuroprotective effect of IPC, indicating that autophagy activation plays an important role in IPC induced tolerance. The induction of autophagy by the PHD inhibitors during pharmacological preconditioning is beneficial to degrade harmful materials through lysosomal systems. Additionally, the role of PHD inhibitors in promoting autophagy and having a protective role supports other studies that have found that preconditioning with autophagy inducer Rapamycin is protective in various *in vitro* (Kim *et al*., 2018) and *in vivo* (Li *et al*., 2014) models of ischaemic stroke.

Expression of HIF1α and HIF2α protein were studied in PC12 cells subjected to DMOG, FG2216, FG4592, GSK1278863, and Bayer85-3934. In PC12 cells, 100μM of all the PHD inhibitors studied except DMOG significantly upregulated HIF1α but not HIF2α compared to 1% DMSO. Compared to 1% DMSO, FG4592 significantly upregulated HIF1α from 30μM onwards up to 100μM in primary neurons. Similar to PC12 cells, no significant HIF2α expression was seen by FG4592 in primary neurons at the concentrations studied. A study by Li *et al*., 2018 showed that FG4592 (50μM) upregulated HIF1α expression in SH-SY5Y cells. FG4592 clinical trial concentration is 30μM (Chen *et al*., 2017), which was sufficient to upregulate HIF1α in primary neurons. Studies in human Hep3b and HeLa cell lines have shown that concentrations of 50μM and 100μM but not 10μM of FG4592, GSK1278863, and Bayer85-3934 upregulate HIF1α and HIF2α in the presence of oxygen (Susler *et al*., 2020; Yeh *et al*., 2017). Studies have demonstrated that Bayer85-3934 upregulates HIF1α (in normoxia) *in vitro* and *in vivo* (Böttcher *et al*., 2018; Beck *et al*., 2018).

Despite significant cytotoxicity, DMOG upregulated HIF1α (1mM and 2mM) and HIF2α (2mM) in PC12 cells. The results in PC12 cells are consistent with studies by Zhdanov *et al*., 2015 in PC12 cells and Chan *et al*., 2016 in MCF-7 cells, where 1mM DMOG significantly upregulated HIF1α. Unlike PC12 cells, in primary neurons, HIF1α and HIF2α were significantly upregulated by 100μM onward of DMOG. Badawi and Shi, 2017 treated primary rat neurons with 0.5, 1, and 2mM DMOG, and HIF1α protein levels were significantly increased by 57%, 83%, and 93% respectively. In line with the results in primary neurons, Ogle *et al*., 2012 reported that DMOG (500μM) treatment for 24 h in normoxia increased levels of HIF1α protein in primary rat neurons. Another study by Siddiq *et al*., 2009 showed that DMOG (500μM) for 24 h in normoxia upregulated HIF1α and HIF2α in primary rat cortical neurons.

The neuroprotective effects of the PHD inhibitors were evaluated in three different treatment protocols in PC12 cells. None of the PHD inhibitors provided any cytoprotection in PC12 cells when administered concurrently with OGD insult. Studies have demonstrated that downstream regulation of pro-survival genes of HIF1α occurs after 24 h, with sustained elevation of HIF1α. Additionally, during acute injury, HIF1α upregulates pro-apoptotic genes. The effects of PHD inhibitors are not protective during acute injury, as they required genetic reprogramming and *de novo* protein synthesis (Baranova et al., 2007). As summarized in Table 1.5 and Section 1.5.2, in most of the *in vivo* and *in vitro* studies, the PHD inhibitors are administered hours before ischaemia (preconditioning), or after ischaemia (postconditioning).

PC12 cells preconditioned with the PHD inhibitors followed by OGD insult immediately (without reversion) did not exhibit any significant cytoprotective effect. Preconditioning with 100µM of PHD inhibitors (DMOG, FG2216, FG4592, GSK1278863, Bayer85-3934) for 24 h followed by 24 h reversion significantly protected PC12 cells against 6 h OGD insult. Significantly greater mitochondrial activity, cell viability, and reduced LDH release were seen in cells preconditioned with PHD inhibitors compared to 1% DMSO preconditioned cells. The PHD inhibitor followed by a period of reversion resulted in genetic reprogramming and development of ischaemic tolerance. In primary neurons, preconditioning with FG4592 (50µM and100µM) and DMOG (100µM and 250µM) for 24 h followed by 24 h reversion was protective (greater mitochondrial activity and reduced LDH release) against 6 h OGD insult. In line with MTT and LDH assay results, Map2 staining also revealed that neuronal cultures preconditioned with FG4592 (50µM and100µM) and DMOG (100µM and 250µM) consisted of healthier neurons (surrounded with several dendrites, no degradation or loss of Map2 staining) compared to DMSO preconditioned cultures. This is consistent with the study by Ogle *et al*., (2012) in which preconditioning with DMOG (100µM) for 24 h before OGD significantly reduced OGD-induced cell cytotoxicity. Jones *et al*., 2013 reported that pre-treatment with DMOG > 30µM for 20 h before OGD significantly reduced OGD-induced neuronal death. DMOG induced protection has also been demonstrated *in vivo*, in which the systemic application of DMOG before the onset of cerebral ischaemia led to increased acute cerebral tissue preservation (Nagel *et al*., 2011). Pre-treatment with FG4497, 6 h before MCAO also reduced infarct size and decrease the formation of oedema 24 h after reperfusion. In an *in vitro* ischemia

model, pre-treatment of mouse hippocampal neuronal HT-22 cells with FG4497 followed by OGD showed an improved survival rate of neurons (Reischl *et al*., 2014). The effects of GSK1278863 have not been explored yet, however preconditioning for 18 h with another PHD inhibitor GSK360A from GlaxoSmithKline was shown to decrease infarct size and improve behaviour in rats subjected to transient MCAO (Zhou *et al*., 2017). Studies have not yet explored the effectiveness of novel PHD inhibitors in ischaemic stroke models.

DMOG showed a neuroprotective effect at 100μM, but HIF1α was not upregulated. DMOG (1mM and 2mM) upregulated HIF1α but also resulted in significant cytotoxicity. This is consistent with a study by Burr *et al*., (2016) using PC12 and HTC116 cell lines, which revealed that DMOG upregulated HIF1α at 1mM, but DMOG (0.1-1mM) decreased cellular respiration by inhibiting mitochondrial function. Inhibitions of 2-OG dehydrogenase and isocitrate dehydrogenase by DMOG can potentially change cell metabolism much faster than via HIF1 signalling (Burr *et al*., 2016). Zhdanov *et al*., (2015) suggested DMOG may inhibit cellular respiration via a HIF-independent pathway by directly trans-activating the gene encoding PDK1, thereby affecting mitochondrial activity. DMOG has also shown to have some other effects such as activation of the NF-κB (Nuclear factor Kappa B) pathway, suppression of TNFα, and activation of AMPK signalling which, coordinates metabolic adaptation to energy crisis and oxidative stress (Ogle *et al*., 2012).

Preliminary results revealed that 6 h OGD mainly resulted in early apoptosis, rather than necrosis in PC12 cells, consistent with the previous studies (Jones *et al*., 2013).

Preconditioning PC12 cells with PHD inhibitors (DMOG, FG2216, FG4592, GSK1278863, Bayer85-3934; 100μM) followed by reversion protected PC12 cells from apoptosis following 6 h OGD insult. These findings correlate with a finding of a study by Li *et al*., 2018, where FG4592 protected PC12 cells from undergoing apoptosis following TBHP (tert-butyl hydroperoxide) pre-treatment. FG4592 also reduced MPP+ (1-methyl-4-phenylpyridinium) induced apoptosis and improved mitochondrial function in SH-SY5Y cells (Li *et al*., 2018). Apoptosis is energy-dependent, programmed cell death that results in rapid clearance of cells by phagocytosis (Durukan and Tatlisumak, 2007). HIF1α upregulation induces apoptosis by stabilising p53, which induces Bax and Bak proteins regulating the release of cytochrome C (Schmid *et al*., 2004). HIF1α also results in the upregulation of pro-apoptotic family members such as Bnip3, Noxa, Nix, and downregulation of Bcl2 (Chen *et al*., 2009). In contrast, HIF1α can also protect cells from apoptosis by elevating Bcl2, BclxL, and Mcl1 levels, and decreasing pro-apoptotic Bid, Bax, and Bak levels (Matthew *et al*., 2002). The PHD inhibitors (100μM) treatment for 24 h significantly upregulated HIF1α and protected the cells from a subsequent OGD injury and apoptosis.

As PHD inhibition mediated upregulation of HIFα and HIF2α protein was established, qRT-PCR was performed to study the expression of their downstream genes. Although HIFα and HIF2α were upregulated at the protein level, all the PHD inhibitors (compared to 1% DMSO) did not alter *Hif1α* and *Hif2α* expression. Various studies have reported that Hif1α is mainly regulated at the post-transcriptional level (Obach *et al*., 2004). *Phd2* was upregulated by FG4592 (100μM) in PC12 cells and

DMOG (500 µM) in primary neurons. All other PHD inhibitors did not upregulate *Phd2* in PC12 cells and primary neurons.

Bnip3 was upregulated by 100µM of FG4592, Bayer85-3934 but not DMOG, FG2216, and GSK1278863 in PC12 cells. Compared to 1% DMSO, FG4592 (up to 100µM) and DMOG (up to 500µM) did not upregulate *Bnip3* in primary neurons. *Vegf* was upregulated by 100µM of FG4592, Bayer85-3934 but not DMOG, FG2216, and GSK1278863 in PC12 cells. In primary neurons, *Vegf* was upregulated by FG4592 (30µM, 50µM, and 100µM) and DMOG (100µM, 250µM, and 500µM). *Epo* was upregulated in primary neurons by FG4592 (50µM and 100µM) and DMOG (100µM, 250µM, and 500µM). Previously studies have demonstrated that DMOG increased the expression of *Vegf in vivo* (Nagel *et al*, 2011) and cortical neurons (Ogle *et al*., 2012). Similarly, GSK360A was associated with increased *Epo* and *Vegf* mRNA expression in rats (Zhou *et al*., 2017). Yeh *et al*., 2017 showed that FG4592, GSK1278863 and Bayer85-3934 upregulated *Vegf*, *Epo*, *Bnip3*, and *Glut1* expression in Hep3b and HeLa cell lines.

Compared to 1% DMSO, *Pfkfb3* was significantly upregulated by 100µM of DMOG, FG2216, FG4592, GSK1278863, and Bayer85-3934 in PC12 cells. There were no significant changes in *Pfkfb3* expression by FG4592 (up to 100µM) and DMOG (up to 500µM) in primary neurons. Minchenko *et al*., (2002) revealed that $CoCl_2$, DFO, and DMOG upregulated *Pfkfb3* expression in Hep3b cells. Compared to 1% DMSO, *Ldha* was significantly upregulated by 100µM of FG2216, GSK1278863, and Bayer85-3934 in PC12 cells, while FG4592 and DMOG did not. DMOG (500 µM)

upregulated *Ldha* in primary neurons but FG4592 (up to 100µM) did not. Zhdanov *et al*, 2015 showed that 1mM of DMOG upregulated *Ldha* in HCT116 cells during normoxia.

Any variations in the expression of HIF1α, HIF2α proteins and their target genes are likely due to differences in the metabolism of these inhibitors in different cells. The PHD inhibitors are structurally different and have different potencies, due to which they have a varying effect.

Key findings:

- Concentrations of up to 100µM of the novel class of PHD inhibitors were safe in PC12 cells and primary rat neurons.
- The novel PHD inhibitors upregulated HIF1α and promoted autophagy in PC12 cells and primary rat neurons.
- The novel PHD inhibitors are more potent than non-selective DMOG in terms of HIF1α and autophagy regulation.
- Preconditioning with novel PHD inhibitors followed by reversion induced ischaemic tolerance in PC12 cells and primary rat neurons.

In conclusion, the PHD inhibitors possess the capability to upregulate HIF1α protein and several hypoxia genes that promote ischaemic tolerance. The PHD inhibitors induced autophagy in both PC12 cells and primary neurons but did not promote apoptosis or cause cytotoxicity at 100µM. DMOG is less potent in upregulating HIF1α, promoting autophagy, and ischaemic tolerance compared to the novel PHD

inhibitors. Preconditioning with the PHD inhibitors followed by reversion was protective against ischaemic insult in both PC12 cells and primary neurons. The pharmacologically induced ischaemic tolerance requires the coordination of intricate pathways and mechanisms, such as HIF, mTOR, and autophagy.

Chapter 6.

Astrocytes conditioned medium (ACM) induced protection against ischaemic injury in primary rat neurons

6.1 Introduction

Previous studies on neuroprotection in ischaemic stroke focus on neurons, but none of them has been translated into the clinic (Sutherland et al., 2012; Majid A, 2014). Neurons, the functional cells in the brain are vulnerable to ischaemia and do not have the capabilities to protect themselves (Becerra-Calixto and Gomez, 2017). Astrocytes the major glial cells play an essential role in ischaemic stroke pathophysiology (Gonzalez-Perez *et al.,* 2015). Within the ischaemic core, astrocytes are better preserved (Liu and Chopp, 2016). Although astrocytes are generally more resistant to ischaemia than neurons, acute ischaemic insults result in reactive astrogliosis and production of cytokines such as TGFβ and various interleukins (such as IL-1β, IL-6) (Becerra-Calixto and Gomez, 2017; Patabendige *et al*., 2021).

Astrocytes react to neuronal stress by providing metabolic and trophic support to neurons. Astrocytes protect neurons via anti-excitotoxicity mechanisms such as (i) uptake of excess glutamate (ii) provision of EPO and glutathione (GSH) to neighbouring neurons to enhance neuron survival (iii) regulate anti-oxidant genes and activate nuclear erythroid factor 2 (Nrf2) (iv) receive damaged mitochondria from neurons and deliver healthy mitochondria (v) releasing glycogen stores to provide neurons with lactate for energy (vii) sequester free iron to protect against iron toxicity (viii) formation of glial scar around the ischaemic core to seclude viable tissue from harmful substances (Bylicky *et al*., 2007; Becerra-Calixto and Gomez, 2017). During acute ischaemia, astrocytes produce cytokines such as interleukins (IL-6, IL-10, and IL-1β), interferon γ (IFNγ), and TGFβ, which have multiple roles in neurodegeneration and neuroprotection. The expression of cytokines and

chemokines in astrocytes are regulated via the nuclear factor kappa B (NF-κB) signalling pathway (Becerra-Calixto and Gomez, 2017). Astrocytes also promote the secretion of various neurotrophic factors such as NGF, BDNF, neurotrophin 3 (NT-3), VEGF, epidermal growth factor (EGF), insulin growth factor (IGF), GDNF and basic fibroblast growth factor (bFGF). These trophic factors promote angiogenesis, neurogenesis, axonal remodelling, and growth / survival of neurons and oligodendrocytes during ischaemia (Buffo *et al.,* 2010; Barreto *et al.,* 2011).

The abilities of astrocytes to promote neuron survival during ischaemic stroke have been widely explored and shown great promise, but the mechanism is poorly understood. A study by Dhandapani *et al.,* (2003) reported that soluble factors in ACM protected murine neurons from serum-deprivation induced cell death by releasing TGFβ, which activates activator protein-1 (AP-1) protective pathway. A study has also reported that ACM constituents such as interleukins (IL-6, IL-10, and IL-1β) and TGFβ play a vital role in ACM induced ischaemic tolerance in neurons (Becerra-Calixto and Gomez, 2017). A study by Song *et al.,* (2019) demonstrated that ACM exerts neuroprotective effects in ischaemic stroke, through modulation of NT-3, GDNF, and TNFα secretion. Another study reported that ACM provides a neuroprotective effect by regulating apoptosis-related protein expression (Lu *et al.,* 2015). Narayan and Perez-Pinzon (2017) found that neurons incubated with ischaemic preconditioned astrocytes significantly protected neurons against ischaemic injury. Studies have previously pointed out that depending on the extent of ischaemic injury, the substances secreted by astrocytes may be neurodegenerative or neuroprotective (Buffo *et al.,* 2010).

In addition to soluble proteins, astrocytes also secrete EVs which are becoming increasingly popular in recent years. EVs can be widely divided into exosomes (less than 200 nm), microvesicles (200-1000 nm), and apoptotic bodies (larger than 1000nm). Exosomes are being widely pursued due to their abilities to cross the BBB and interact with target cells. Studies suggest that cells take up exosomes by endocytosis via receptor-mediated adhesion, direct fusion, or ligand-receptor interactions. Exosomes originate from plasma membranes as a result of astrogliosis due to nutrient deprivation such as ischaemia. Exosomes are homogenous in shape surrounded by membranes enriched with cholesterol, sphingomyelin, and ceramide. Exosomes may contain proteins, lipids, metabolites, miRNA / sRNA, DNA, enzymes, growth factors, and cytokines; depending on their origin and target (Hong *et al.,* 2018). Studies have previously studied the protective effect of ACM as a whole without isolating and considering the role of EVs in neuroprotection. It is therefore important to consider that in conjunction with the soluble proteins, ACM also contains EVs with various components that may have a protective role during ischaemic injury.

The studies in this chapter were performed in two parts. In the first part, the effects of an *in vitro* hypoxia (OD) and ischaemia (OGD) were studied on primary rat astrocytes. The effects of OD and OGD (6, 24, and 48 h) were evaluated on cell viability, GFAP expression / morphologies, HIF1α / HIF2α protein expression, and their downstream genes. In the second part of this study, ACM was collected from astrocytes subjected to 6 h and 24 h OGD insult and separated into soluble protein and EVs by sequential ultracentrifugation. Following this, the complete ACM, soluble proteins (supernatant), and EVs (pellet) were applied to primary rat cortical neurons.

The effectiveness of ACM and its separated components were evaluated in the previously established ischaemic injury model in primary neurons (Chapter 3). Additionally, the effects of ACM were evaluated on HIF1α / HIF2α proteins, autophagic markers (Lc3b, p62), and HIF downstream genes in primary neurons.

6.2 Materials and methods

6.2.1 Primary astrocytes responses to OD and OGD

Primary rat cortical astrocytes were cultured according to procedures described in Section 2.2.5. Confluent astrocyte cultures were used for experiments. The complete media (100%) was aspirated and the cells were washed twice with glucose-free media prior to experiments. Primary astrocytes were treated with Nx, OD, and OGD for various durations (6, 24, and 48 h). Additionally, the effect of reperfusion was evaluated following OD and OGD. For these experiments, primary astrocytes were treated with Nx, OD, and OGD for various duration followed by 24 h reperfusion (Figure 6.1). For all experiments, 100% media changes were performed on a staggered basis, such that all treatment durations either end or are switched to reperfusion simultaneously and end together. The complete treatment conditions for Nx, OD, OGD, and reperfusion are described in Section 2.3. Cell viability (MTT and LDH assay; Section 2.5), IF imaging (GFAP; Section 2.8), gene expression (Section 2.6), and protein expression (Section 2.7) were evaluated in primary astrocytes.

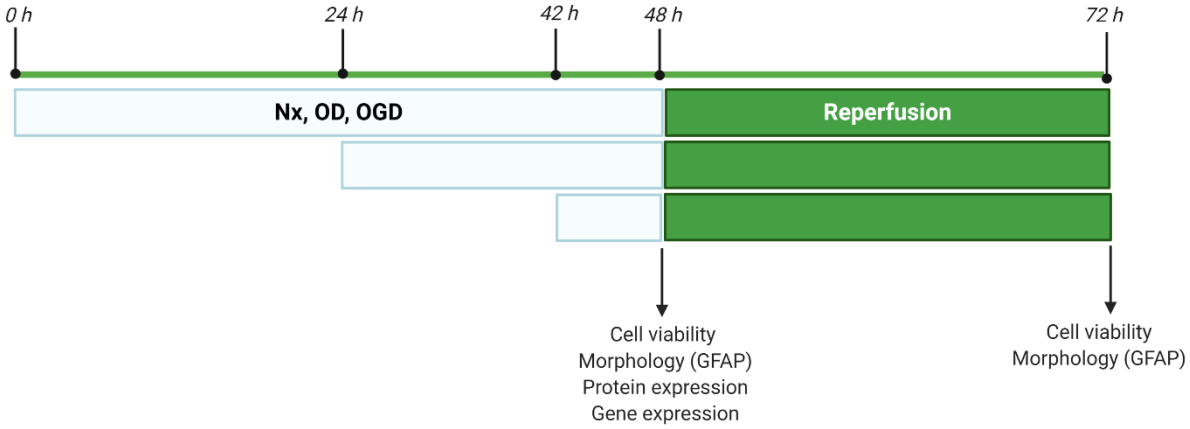

Figure 6.1. Timeline of primary astrocytes treatment. All primary astrocyte cultures were established in parallel, with 0 h indicating the onset of treatment [normoxia (Nx), oxygen deprivation (OD), and oxygen-glucose deprivation (OGD) for 6 h, 24 h, and 48 h followed by 24 h reperfusion. All the conditions were initiated on a staggered basis, such that all experiments terminated together. (Image produced using Biorender).

6.2.2 Application of ACM to primary neuronal cultures

Primary rat astrocytes were obtained as per procedure in Chapter 2. T175 flasks containing pure astrocytes ($4x10^6$ in 20 mL) were incubated in D10 medium in a standard incubator with a humidified atmosphere (5% CO_2 at 37^{o}C). Media change (50%) with D10 medium was performed every 2 days until ~70-80% confluence. The astrocytes cultures were washed twice with D-PBS and switched to complete Neurobasal media (100% media change). The cultures were maintained in the standard incubator for 2 days. After 2 days, 100% of the media was aspirated from the T175 flasks and treated with three different conditions (i) 24 h Nx; complete Neurobasal media in the standard incubator with a humidified atmosphere containing 5% CO_2 at 37^{o}C (ii) 6 h OGD; Glucose-free Neurobasal media in purpose-built

INVIVO$_2$ 400 humidified hypoxia workstation (0.3% O_2, 5% CO_2, 94% N_2 at 37^{o}C) (iii) 24 h OGD; identical conditions to 6 hours OGD; for 24 hours. The 100% media changes were performed on a staggered basis, such that all treatment durations end together. Upon completion of treatment, the ACM was collected. In addition, the cells in the T175 flasks (subjected to Nx) were trypsinized and counted (counting cells, Section 2.2.3) to determine cell densities. (Figure 6.2). On average, T175 flasks (~70-80% confluence) used for experiments consisted of an average of 16.3x10^6 cells (S.D. 1.1x10^6 cells, n=4).

As described in Section 2.9, sequential centrifugation of 15 mL ACM (Nx, 6 h OGD, and 24 h OGD) was performed to separate soluble protein (supernatant) and EVs (pellet). The supernatant was collected and the EVs pellet from each T175 flasks (15 mL media) was suspended in 1 mL of fresh Neurobasal media (Chapter 2, Section 2.9). Zetasizer was used to determine the size of the particles (complete Neurobasal media (control), whole ACM, EVs pellet, and supernatant). From each T175 flasks, 5 mL of the whole ACM was retained for experiments. The collected ACM, EVs, supernatant, and complete Neurobasal media were stored at -80^{o}C until required for experiments. Before experiments, complete Neurobasal media, ACM, supernatant, and EVs were thawed in a 37^{o}C water bath.

Primary neurons were cultured as per procedures in Chapter 2. Upon confluence, 100% of media in the cell culture was aspirated. The primary neuronal cultures were treated with complete Neurobasal media (sham), ACM (24 h Nx, 6 h OGD, 24 h OGD), supernatant (24 h Nx, 6 h OGD, 24 h OGD), and EVs (24 h Nx, 6 h OGD, 24

h OGD) for 6 h. The volume of ACM, supernatant, and EVs added to the neuronal cultures are described in Table 6.1. After this, primary neurons were subjected to 24 h reversion (100% media change with complete Neurobasal; and placed in a standard incubator with a humidified atmosphere containing 5% CO_2 at 37ºC). After 24 h, the media (100%) was aspirated and the cells were washed twice with glucose-free Neurobasal media and subjected to 6 h OGD insult (glucose-free Neurobasal media, purpose-built INVIVO$_2$ 400 humidified hypoxia workstation; 0.3% O_2, 5% CO_2, 94% N_2 at 37ºC) (Figure 6.2). Identical cultures were maintained in complete Neurobasal media throughout the experiment as a positive control (untreated control, C). Cell viability (MTT, LDH assay) and neuron morphology (MAP2) were assessed at the end of treatment. The expression of proteins (HIF1α, HIF2α, Lc3b, and p62) and hypoxic genes were studied in primary neurons subjected to complete Neurobasal media (untreated control, C) and whole ACM (Nx, 6 h OGD, and 24 h OGD). The materials and methods for cell viability (MTT and LDH assay; Section 2.5), IF imaging (MAP2; Section 2.8), gene expression (Section 2.6), and protein expression (Section 2.7) are described in Chapter 2.

Table 6.1. Volume of ACM used to treat neuronal cultures. On average, T175 flasks (~70-80% confluence) used for obtaining ACM consisted of an average of $16.3x10^6$ cells (S.D. $1.1x10^6$ cells, n=4). According to the neuronal seeding densities, an appropriate volume of ACM was added. Approximately, ACM from 2.7 astrocytes was used to treat each neuron (astrocyte: neuron ratio 2.7:1). Consistency was ensured across all replicates to mimic *in vivo* conditions and dose-response.

Plates / flasks	Neurons seeding density	Volume of ACM added	Approximate neuron: astrocyte ratio
96 well plate	3×10^4 cells	100 µL	1:2.7
24 well plate	1.5×10^5 cells	500 µL	1:2.7
T25 flask	1.5×10^6 cells	5 mL	1:2.7

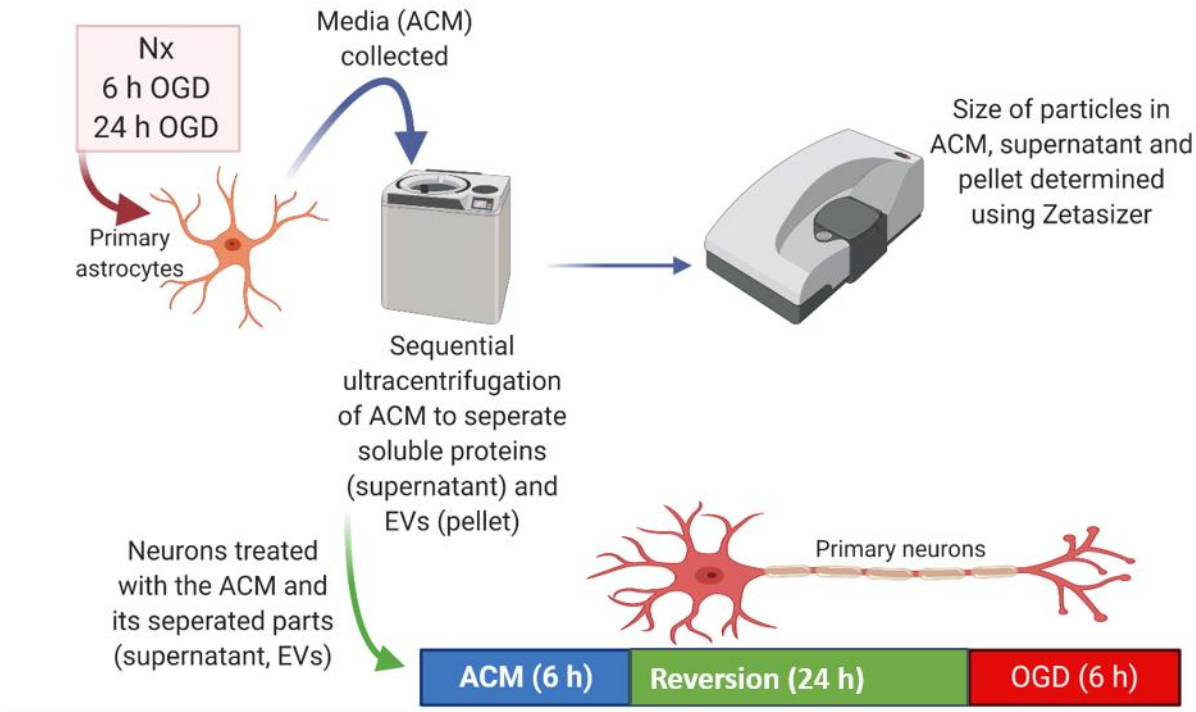

Figure 6.2. Timeline of treatment of primary neuronal cultures with ACM. Pure astrocytes were initially grown in D10 media and 50% changes were performed every 2 days until 70-80% confluence. Upon 70-80% confluence, the cultures were washed twice with D-PBS, switched to complete Neurobasal media, and maintained for 2 days. After 2 days, the media was aspirated and astrocytes were treated with Nx and OGD (6 h, 24 h). The media was collected from the astrocytes (ACM). The ACM (~15 mL) was ultracentrifuged to separate soluble proteins (supernatant) and EVs (pellet). The sizes of particles in complete Neurobasal media, ACM, supernatant, and EVs pellet were measured by Zetasizer and stored at -80^{o}C until required. Primary neuronal cultures were treated with all the parts of ACM for 6 h followed by 24 h reversion, and 6 h OGD insult. (Image produced using Biorender).

6.3 Results

6.3.1 Characterising primary rat astrocytes culture

High purity cultures of primary rat astrocytes were successfully derived, with 94.1 ± 6.6% of nuclei being associated with $GFAP^+$ expression (Figure 6.3). $GFAP^+$ cells exhibited typical astrocyte morphologies such as flat and stellate in structure with GFAP enriched cell bodies and processes with very few cells exhibiting pyknosis or other signs of poor health.

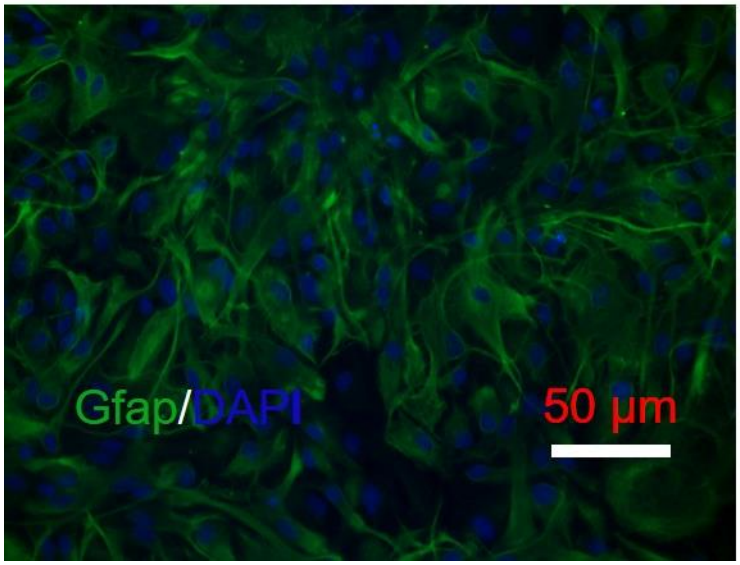

Figure 6.3. Fluorescence micrograph of typical healthy pure primary rat cortical astrocytes. Representative double merged (FITC labelled GFAP immunostaining (green) and DAPI stained nuclei) of healthy primary astrocytes. A typical culture consisted of 94.1 ± 6.6% $GFAP^+$ cells (Data represent mean ± S.D; n=5).

6.3.2 Responses of primary astrocytes to OD and OGD

Primary rat cortical astrocytes responses were studied in cells exposed to 6, 24, and 48 hours of OD and OGD versus Nx (same time point). The primary astrocytes responses were compared before and after 24 hours reperfusion using MTT, LDH assay, and GFAP intensity (IF staining) (Figure 6.1).

Compared to Nx (same time point), mitochondrial activity (Figure 6.4A) and LDH release (Figure 6.4B) were not altered by 6 h OD, 6 h OGD, and 24 h OD (before and after reperfusion). There was a significant reduction in mitochondrial activity and an increase in LDH release at 24 h OGD, 48 h OD, and 48 h OGD (before and after reperfusion) compared to Nx (same time point). The LDH release and mitochondrial activity at the end of 24 h OGD, 48 h OD, and 48 h OGD, and after a period of reperfusion were not significantly ($p>0.05$) different. Compared to 24 h OGD, the mitochondrial activity was significantly ($p<0.01$) lower and LDH release was significantly ($p<0.01$) higher at 48 h OGD.

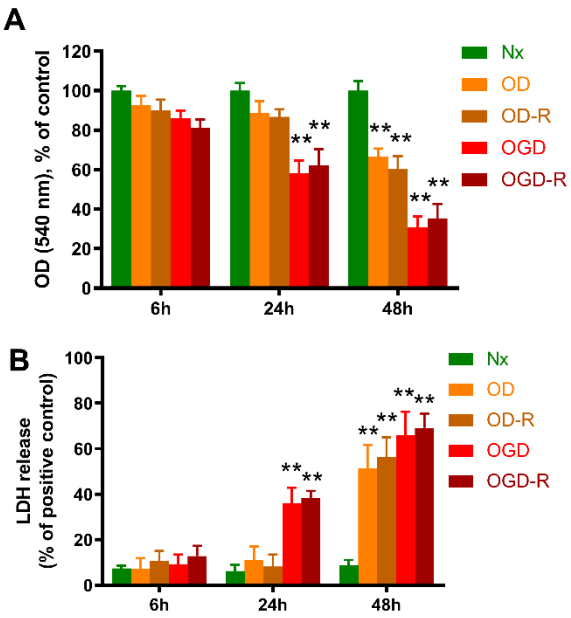

Figure 6.4. Responses of primary rat astrocytes to Nx, OD, and OGD. Bar graphs representing the viabilities of primary astrocytes in response to Nx, OD, and OGD (6 h, 24 h, and 48 h). The responses were compared before and after 24 h reperfusion (A) MTT assay revealed a significant reduction in mitochondrial activity by 24 hours OGD and 48 hours of OD and OGD (versus Nx, same time point). Compared to the end of treatment, there were no significant changes after 24 hours reperfusion. (B) LDH assay revealed a significant increase in LDH release at 24 hours OGD and 48 hours OD and OGD (versus Nx, same time point). Compared to the end of treatment, there were no significant changes after 24 hours reperfusion. *(For all graphs, ** represents $p < 0.01$ against Nx (same time point); two-way ANOVA followed by Tukey's post-hoc analysis; n=4).*

Morphological changes (GFAP staining) were evaluated in primary astrocytes subjected to Nx, OD, and OGD for 6 h, 24 h, and 48 h, both before and after reperfusion. Compared to Nx (same time point) treated astrocyte cultures, there were no significant changes in astrocyte morphology (Figure 6.5A) and GFAP intensity (Figure 6.5B) in 6 h OD, 6 h OGD, and 24 h OD (both before and after reperfusion) treated cultures. GFAP staining revealed astrocytes ($GFAP^+$ nuclei) with extended processes in cultures subjected to 6 h OGD (before and after reperfusion) compared to 6 h Nx treated cultures. There was a significant increase in GFAP intensity in cultures subjected to 24 h OGD, 48 h OD, and 48 h OGD (both before and after reperfusion) compared to Nx (same time point); similar to 6 h OGD cultures, the astrocytes ($GFAP^+$ nuclei) possessed extended processes. There was no significant difference in GFAP intensity between 24 h and 48 h OGD treated cultures. In line with LDH assay results, there was a significant reduction in cell densities ($GFAP^+$ nuclei / microscopic field) in 24 h OGD, 48 h OD, and 48 h OGD (both before and after reperfusion) treated cultures compared to Nx (same time point). The cell densities were significantly ($p<0.01$) lower at 48 h OGD compared to 24 h OGD (Figure 6.5C).

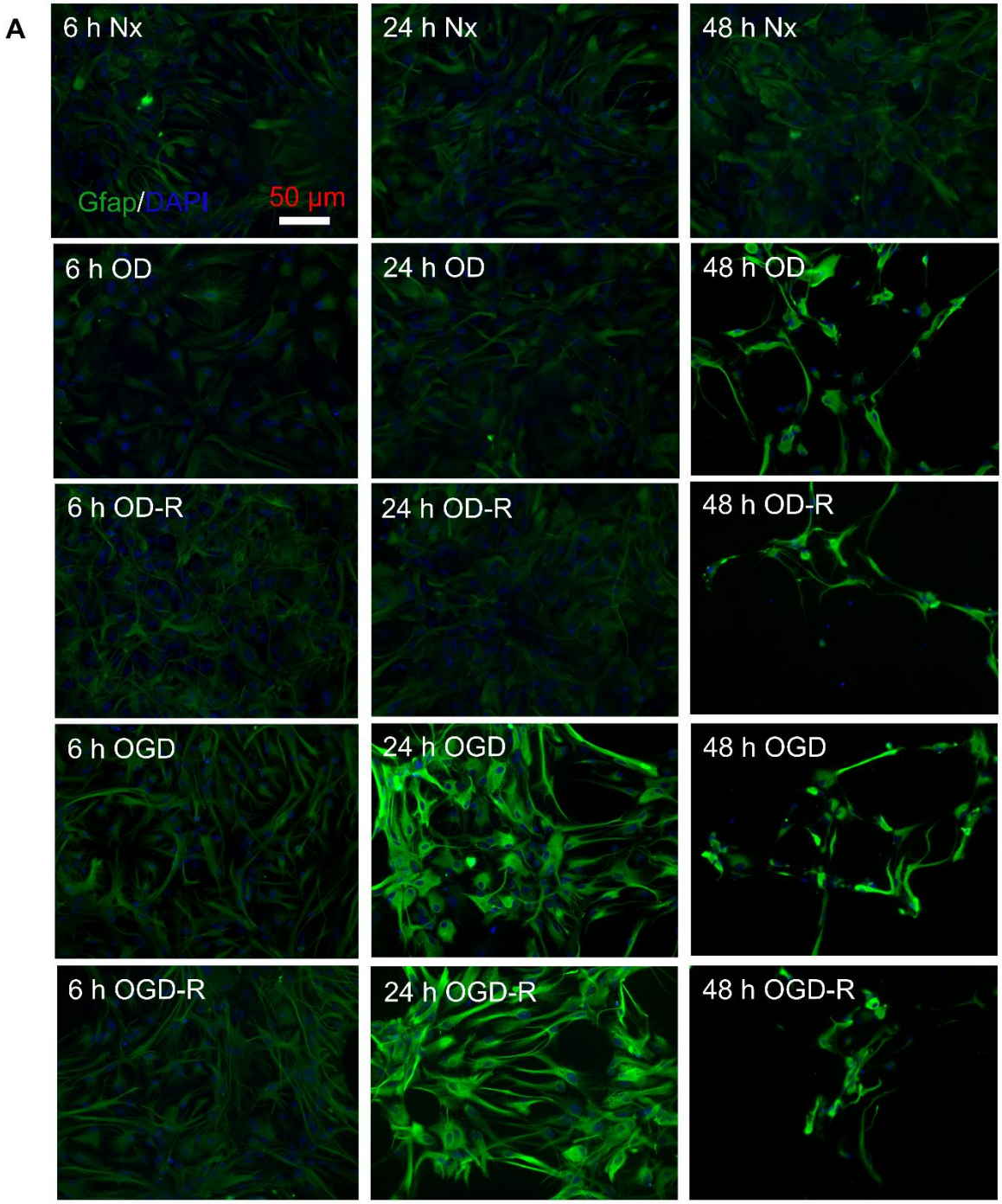
A
6 h Nx
24 h Nx
48 h Nx
Gfap/DAPI
50 µm
6 h OD
24 h OD
48 h OD
6 h OD-R
24 h OD-R
48 h OD-R
6 h OGD
24 h OGD
48 h OGD
6 h OGD-R
24 h OGD-R
48 h OGD-R

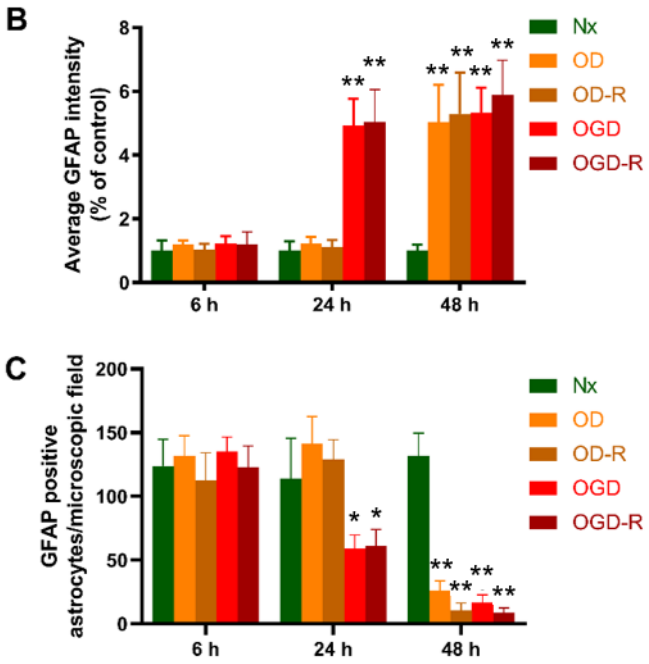

Figure 6.5. Fluorescence micrographs of primary cortical astrocytes subjected to Nx, OD, and OGD. Fluorescence micrograph representing astrocyte cultures subjected to Nx, OD, and OGD (6 h, 24 h, and 48 h). The responses were compared before and after 24 h reperfusion. (A) Representative double merged (FITC labelled astrocyte-specific GFAP and DAPI stained nuclei) of primary astrocytes ($GFAP^+$ cells) revealed astrocytes with extended processes at 6, 24 and 48 hours OGD and 48 hours OD. (B) Bar graph representing average GFAP intensity normalized to control (Nx). The GFAP intensity of five nuclei was obtained from each microscopic field. Compared to Nx (same time point), results revealed increased GFAP intensity at 24 h OGD and 48 h OD / OGD (both before and after reperfusion). There were no significant changes in GFAP intensity at the end of treatment and after 24 h reperfusion. (C) Bar graph representing $GFAP^+$ nuclei / microscopic field (cell densities). Compared to Nx (same time point), results revealed a significant reduction in cell densities in 24 h OGD, 48 h OD / OGD (both before and after

reperfusion). There were no significant changes in cell density at the end of treatment and after 24 h reperfusion. *(For all graphs,* * *represents* $p < 0.05$ and ** *represents* $p < 0.01$ *against Nx (same time point); two-way ANOVA followed by Tukey's post-hoc analysis; n=3).*

6.3.3 Effects of OD and OGD on HIF protein expression in primary astrocytes

The expression of HIF1α and HIF2α proteins were studied in primary astrocytes exposed to 6, and 24 hours of OD and OGD in comparison to Nx (same time point) (Figure 6.6). At 48 h OD and OGD, ~70-80% of the cells were dead yielding low protein concentration. Compared to Nx (same time point), HIF1α was significantly upregulated (~6.5-8.5 folds) by 6 h and 24 h OD and OGD. There were no significant ($p>0.05$) differences in HIF1α expression a 24 h (OD and OGD) compared to 6 h (OD and OGD). There was also no significant ($p>0.05$) difference in HIF1α expression in response to OD compared to OGD (same time point). Compared to Nx (same time point), HIF2α was significantly upregulated by 24 h (but not 6 h) OD (~5.7 folds) and OGD (~5.8 folds). There was no significant ($p>0.05$) difference in HIF2α expression in response to 24 h OD compared to 24 h OGD.

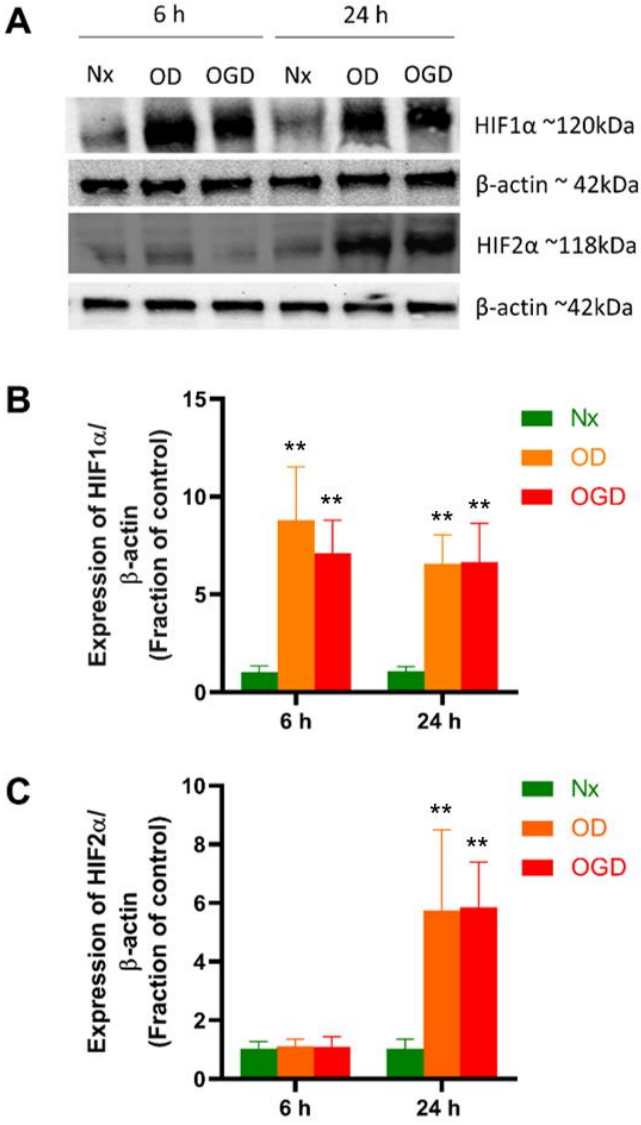

Figure 6.6. Effects of OD and OGD on HIF1α and HIF2α expression in primary rat cortical astrocytes. (A) Representative HIF1α and HIF2α immunoblots were shown with those for β-actin of primary astrocytes treated with 6 h and 24 h Nx, OD, and OGD. (B) Bar graph representing the normalised HIF1α expression. HIF1α was significantly upregulated by 6 h and 24 hours OD and OGD (versus Nx, same time point). (C) Bar graph representing the normalised HIF2α expression. HIF2α was significantly upregulated by 24 h OD and OGD (versus 24 h Nx). *(For all graphs, ** represents $p < 0.01$ against Nx (same time point); two-way ANOVA followed by Tukey's post-hoc analysis; n=3).*

6.3.4 Effects of OD and OGD on genes expression in primary astrocytes

The effects of 6 and 24 h OD and OGD were investigated on hypoxia gene expressions (*Hif1α*, *Hif2α, Epo, Glut1, Bnip3*, *Phd2*, *Vegf*, *Pfkfb1*, *Pfkfb3*, *and Ldha)* in primary astrocytes (Figure 6.7). Compared to Nx (same time point), both OD and OGD (6 h and 24 h) did not alter *Hif1α, Hif2α,* and *Pfkfb1* expression. *Phd2* was significantly upregulated by 6 h OD (~7 folds), 6 h OGD (~10 folds), 24 h OD (~12 folds), and 24 h OGD (~15 folds) compared to Nx (same time point). There was no significant difference in *Phd2* expression at 24 h compared to 6 h (by both OD and OGD). *Epo* was significantly upregulated by 24 h OD (~43 folds), and 24 h OGD (~68 folds) compared to Nx (same time point). *Vegf* was significantly upregulated by 6 h OD (~16 folds), 6 h OGD (~22 folds), 24 h OD (~25 folds), and 24 h OGD (~41 folds) compared to Nx (same time point). *Vegf* expression was significantly ($p<0.01$) higher at 24 h OGD compared to 6 h OGD. *Bnip3* was upregulated by 24 h OGD (~18 folds versus 24 h Nx). *Glut1* was significantly upregulated by 6 h OD (~14 folds), 6 h OGD (~29 folds), 24 h OD (~23 folds), and 24 h OGD (~42 folds) compared to Nx (same time point). There was no significant difference in *Glut1* expression at 24 h compared to 6 h (by both OD and OGD). *Ldha* was significantly upregulated by 6 h OD (~10 folds), 6 h OGD (~31 folds) compared to 6 h Nx. Both OD and OGD for 24 h did not upregulate *Ldha* expression compared to 24 h Nx. *Pfkfb3* was significantly upregulated by 6 h OD (~10 folds), 6 h OGD (~27 folds), 24 h OD (~18 folds), and 24 h OGD (~32 folds) compared to Nx (same time point). There was no significant difference in *Vegf* expression at 24 h compared to 6 h (by both OD and OGD).

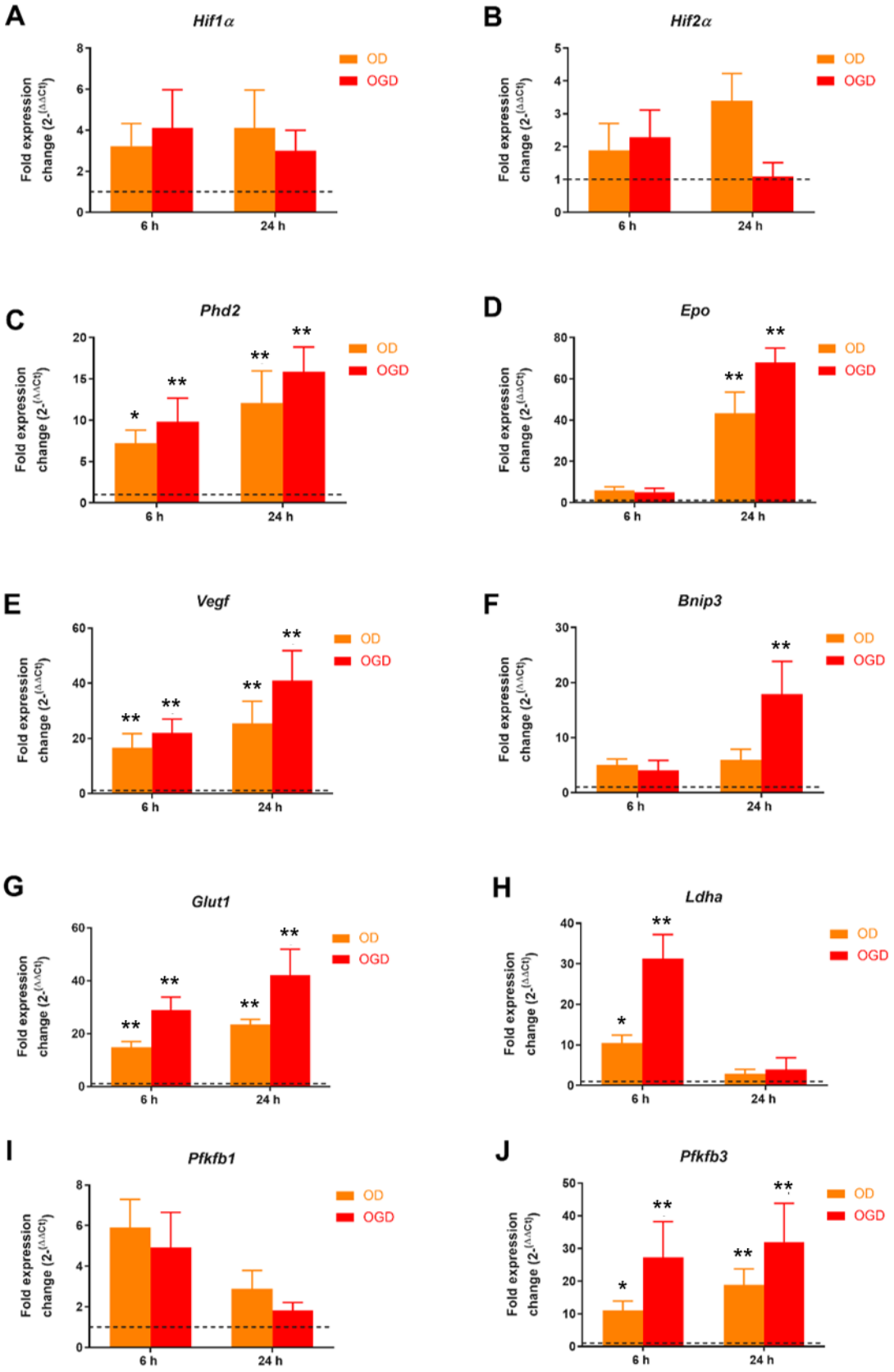
A
Hif1α
B
Hif2α
C
Phd2
D
Epo
E
Vegf
F
Bnip3
G
Glut1
H
Ldha
I
Pfkfb1
J
Pfkfb3
OD
OGD
Fold expression change (2-ΔΔCt)
6 h
24 h

Figure 6.7. Hypoxic and metabolic gene expression in response to OD and OGD in primary astrocytes. Bar graphs representing normalised gene expression in primary astrocytes in response to OD and OGD (6 h and 24 h). Compared to Nx (same time point), expression of (A) *Hif1α,* (B) *Hif2α,* and (J) *Pfkfb3* was not altered by OD and OGD (6 h and 24 h). (C) *Phd2*, (E) *Vegf*, (G) *Glut1*, and (J) *Pfkfb3* were significantly upregulated in response to 6 h and 24 h OD and OGD compared to Nx (same time point). (F) *Bnip3* was upregulated by 24 h OGD versus 24 h Nx. (D) *Epo* was significantly upregulated in response to 24 h OD and 24 h OGD (compared to 24 h Nx). (H) *Ldha* was upregulated by 6 h OD and OGD compared to 6 h Nx. The gene expression was measured against the housekeeping gene *β-actin* and normalised to Nx. The dotted line represents basal gene expression. *(For all graphs, * represents $p < 0.05$ and ** represents $p < 0.01$ against Nx (same time point); two-way ANOVA followed by Tukey's post-hoc analysis; n=3).*

6.3.5 Characterisation of extracellular vesicles (EVs)

ACM was collected from astrocytes subjected to Nx, 6 h OGD, and 24 h OGD (Figure 6.2). Following this, the ACM was separated into supernatant and EVs using sequential ultracentrifugation. The size distribution of particles was obtained using Malvern Zetasizer. Table 6.2 represents the particle size and % area (distribution) of the particles in ACM and EVs pellets. All the particles (~85%) in the EVs pellet were within ~20 to 200nm. ACM consisted of larger particle size distribution range (~7 to 4000nm range). The supernatant (Nx, 6 h OGD, 24 h OGD) and complete Neurobasal media did not contain any particles.

		ACM		
Nx	**Size (nm)**	2765.4±1304.4	328.2±207.3	20.9±13.3
	Area (%)	13.8±7.2	55.3±15.8	31.0±18.2
6 h OGD	**Size (nm)**	1810.8±1028.9	398.7±128.9	24.2±15.3
	Area (%)	16.2±9.8	46.0±12.1	33.7±12.9
24 h OGD	**nm**	2510.9±1101.9	311.0±198.3	26.8±14.1
	Area (%)	18.9±10.9	61.8±21.2	28.8±14.8
		EVs		
Nx	**nm**	135.5±35.3	29.0±10.5	7.1±1.6
	Area (%)	50.0±8.3	33.9±3.7	15.7±4.3
6 h OGD	**nm**	176.2±33.9	37.9±4.6	8.1±1.4
	Area (%)	46.7±4.3	31.8±2.6	20.9±1.3
24 h OGD	**nm**	149.4±36.8	31.4±11.8	7.2±1.2
	Area (%)	49.5±6.7	32.9±3.9	14.3±3.1

Table 6.2. Size and % of the area of peak of particles in ACM and extracellular vesicles (EVs). ACM (24 h Nx, 6 h OGD, and 24 h OGD) was collected from primary rat astrocytes. Sequential ultracentrifugation was performed to separate soluble proteins and EVs in the ACM. The particle size in nanometre (nm) and % distribution (area of peak) was obtained using Malvern Zetasizer. Values represent mean ± S.D.

6.3.6 Effect of ACM on primary rat neurons viabilities against ischaemic insult

Primary neurons were preconditioned with complete Neurobasal media (sham), whole ACM, and its separated parts: supernatant (soluble proteins), and pellet (EVs) for 6 h in normoxia. The ACM and its part were obtained from astrocytes subjected to Nx, 6 h OGD, and 24 h OGD. After preconditioning treatment, the neurons were subjected to 24 h reversion followed by 6 h OGD insults. Untreated control cultures (C) were maintained in normoxia (complete Neurobasal media) throughout (Figure 6.2). For all preconditioning treatments, insults resulted in significantly ($p<0.05$) reduced mitochondrial activity compared to untreated control (Figure 6.8A). Similarly, for all preconditioning treatments, 6 h OGD resulted in significantly ($p<0.05$) increased LDH release compared to untreated control, with the sole exception of 6 h OGD-ACM (whole) preconditioned cells (Figure 6.8B). Both the assays revealed that preconditioning with 6 h OGD-ACM (whole) and 6 h OGD-ACM (supernatant) provided some protection against these insults compared to sham-PC cells. MTT assay (but not LDH assay) revealed that 6 h OGD-ACM (whole) was significantly ($p<0.05$) more protective than 6 h OGD-ACM (supernatant).

Untreated control cultures consisted of $MAP2^+$ neurons surrounded by numerous dendrites (10.2±3.4 dendrites per neuron, with each dendrites measuring 29.6±6.8µm). For most preconditioning treatments, insults resulted in degradation of dendrites except 6 h OGD-ACM (whole: 9.3±4.5 dendrites per neurons, with each dendrites measuring 27.2±5.1µm) and 6 h OGD-ACM (supernatant: 7.1±5.2 dendrites per neurons, with each dendrites measuring 26.7±7.1µm) preconditioned groups (Figure 6.9). Both 6 h OGD-ACM (whole) and 6 h OGD-ACM (supernatant)

preconditioned cultures tolerated the ischaemic insult and consisted of healthier neurons (similar to untreated control).

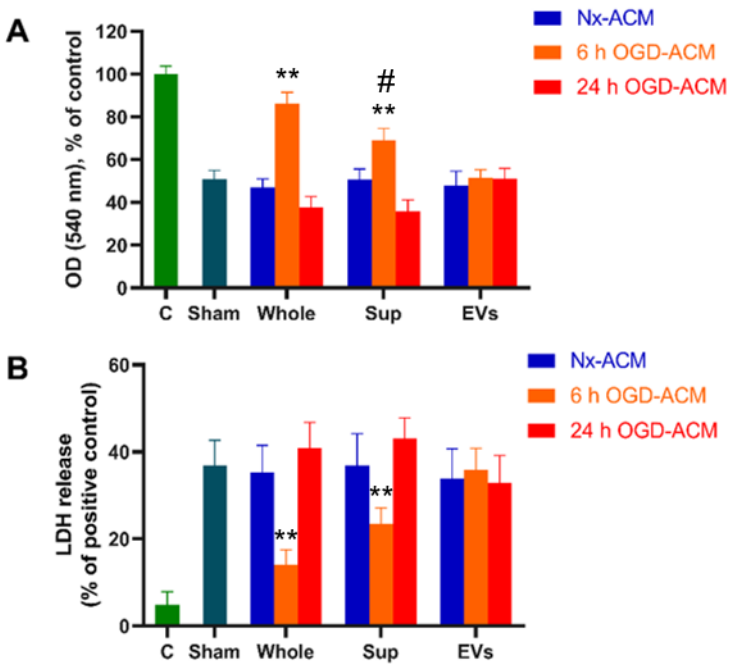

Figure 6.8. Effect of preconditioning with ACM followed by 24 hours reversion and 6 hours OGD insult on primary neurons. Primary neurons were preconditioned with complete media (sham), whole ACM, and its separated parts: supernatant (sup) and pellet (EVs) for 6 h (normoxia) followed by 24 h reversion and 6 h OGD insult. The ACM and its part were obtained from astrocytes subjected to Nx, 6 h OGD, and 24 h OGD. Untreated control (C) was maintained in normoxia throughout. (A) Bar graph representing MTT assay results. For all preconditioning treatments, 6 h OGD resulted in significantly ($p<0.05$) reduced mitochondrial activity compared to untreated control. The reductions in mitochondrial activity were significantly lower in 6 h OGD-ACM (whole), 6 h OGD-ACM (sup) but not 6 h OGD-ACM (EVs) preconditioned cells compared to sham-PC. 6 h OGD-ACM (whole) was significantly more protective than 6 h OGD-ACM (sup). (B) Bar graph representing LDH assay results. For all preconditioning treatments, insults resulted in significantly ($p<0.05$) increased LDH release compared to untreated control, with the sole exception of 6 h OGD-ACM (whole) preconditioned cells. The increase in LDH

release was significantly lower in 6 h OGD-ACM (whole), 6 h OGD-ACM (sup) but not 6 h OGD-ACM (EVs) preconditioned cells compared to sham-PC. *(For all graphs, ** represents $p < 0.01$ against sham-PC and $^{\#}$ represents $p < 0.05$ against whole ACM; two-way ANOVA followed by Tukey's post-hoc analysis; n=3).*

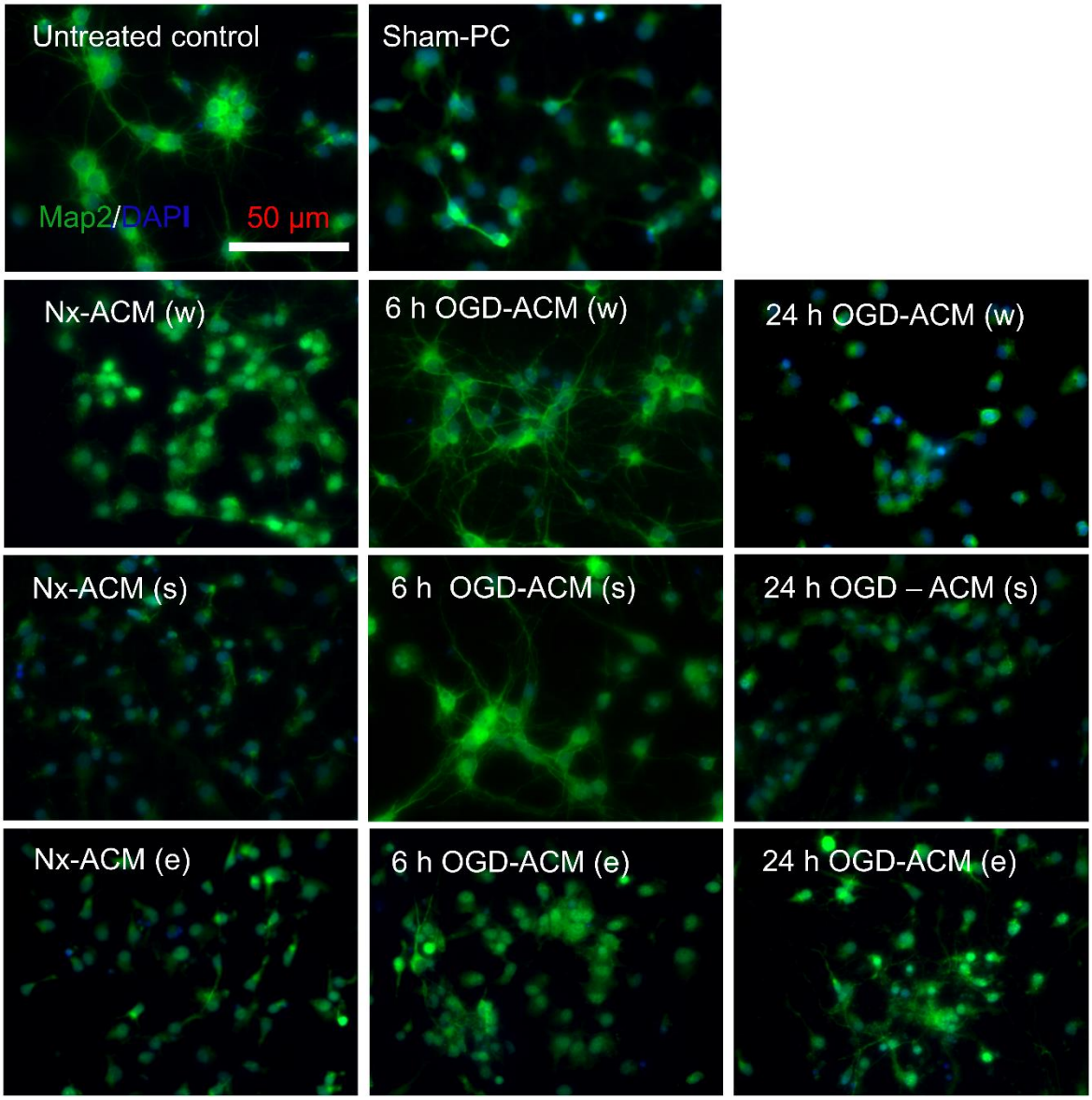

Figure 6.9. Fluorescence micrographs of primary neurons preconditioned with ACM followed by 24 h reversion and 6 h OGD insult. Representative double merged micrographs of MAP2 (FITC) and DAPI (blue) stained neuronal cultures preconditioned with complete media (sham), whole ACM, and separated parts: supernatant (sup) and pellet (EVs) for 6 h (normoxia) followed by 24 h reversion and 6 h OGD insult. The ACM and its part were obtained from astrocytes subjected to Nx, 6 h OGD, and 24 h OGD. Untreated control was maintained in normoxia throughout. (w) represents whole-ACM, (s) represents supernatant (soluble protein)

treatment, and (e) represents EVs preconditioning treatments. Untreated control cultures consisted of $MAP2^+$ neurons surrounded by numerous dendrites. For most preconditioning treatments, 6 h OGD resulted in degradation of dendrites except 6 h OGD-ACM and 6 h OGD-ACM preconditioned groups. Both 6 h OGD-ACM (whole) and 6 h OGD-ACM (supernatant) preconditioned cultures tolerated the ischaemic insult and consisted of healthier neurons (similar to untreated control).

6.3.7 The effect of ACM on HIF1α and HIF2α expression in primary rat neurons

HIF1α and HIF2α protein expression were studied in primary neurons subjected to untreated control (C) or ACM (Nx, 6 h, and 24 h OGD) for 6 h. Compared to untreated control, there were no significant changes in HIF1α and HIF2α expression in primary neurons treated with ACM (Nx, 6 h, and 24 h OGD).

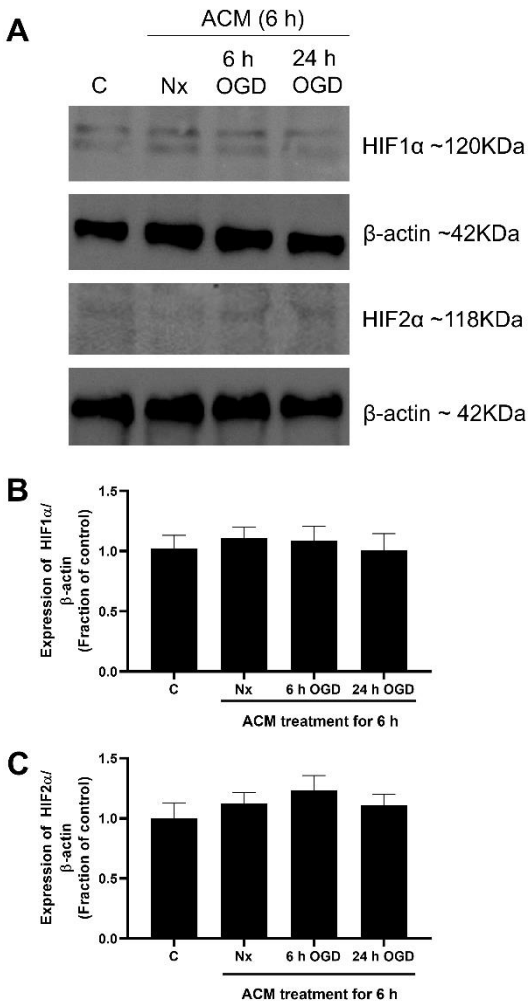

Figure 6.10. Effect of astrocyte conditioned media (ACM) on HIF1α and HIF2α proteins in primary rat neurons. (A) Representative HIF1α and HIF2α Western blots alongside β-actin of primary neurons treated with untreated control (C), Nx-ACM, 6 h OGD-ACM, and 24 h OGD-ACM. (B) Bar graph representing normalised HIF1α expression. There was no significant HIF1α expression in all treatment groups compared to untreated control. (C) Bar graph representing normalised HIF2α expression. There was no significant HIF2α expression in all treatment groups compared to untreated control. *(For all graphs, p>0.05; One-way ANOVA followed by Tukey's post-hoc analysis; n=3).*

6.3.8 The effect of ACM on autophagic proteins in primary rat neurons

The expression of autophagic markers: Lc3b and p62 were studied in primary rat neurons subjected to untreated control and ACM (Nx, 6 h OGD, 24 h OGD) for 6 h. Compared to untreated control, Lc3b-II was significantly upregulated in primary neurons subjected to 6 h OGD-ACM and 24 h OGD-ACM. Lc3b-II expression was significantly lesser in 24 h OGD-ACM compared to 6 h OGD-ACM treated cells. Compared to untreated control, p62 was significantly downregulated in primary neurons subjected to 6 h OGD-ACM and 24 h OGD-ACM. There was no significant difference in p62 expression between 6 h OGD-ACM and 24 h OGD-ACM treated cells. Compared to untreated control, Nx-ACM did not alter p62 and Lc3b-II expression (Figure 6.11).

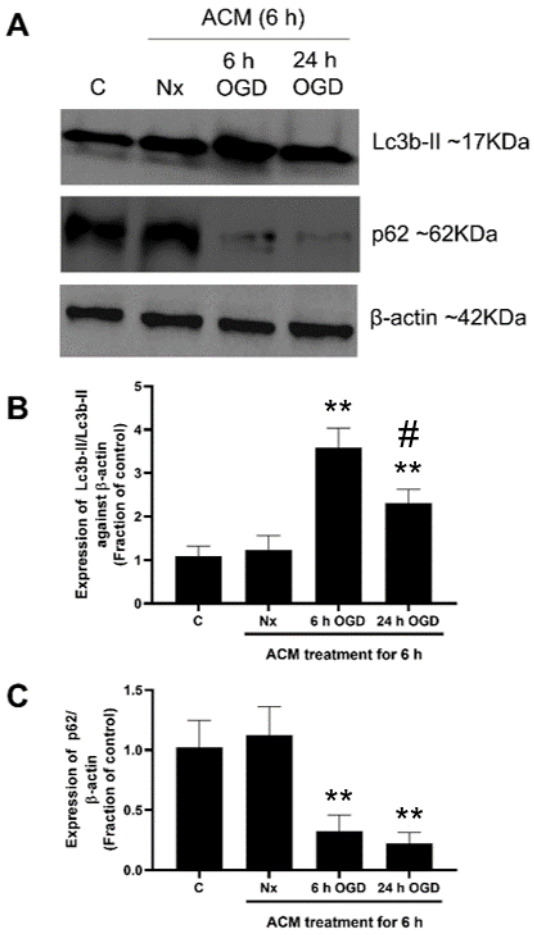

Figure 6.11. Effect of astrocyte conditioned media (ACM) on autophagic proteins in primary rat neurons. (A) Representative Lc3b and p62 Western blots alongside β-actin of primary neurons treated with untreated control (C), Nx-ACM, 6 h OGD-ACM, and 24 h OGD-ACM. (B) Bar graph representing normalised Lc3b-II / Lc3b-I ratio. Compared to untreated control, Lc3b-II was significantly upregulated by 6 h and 24 h OGD-ACM. Lc3b-II expression was significantly lower in 24 h OGD-ACM compared to 6 h OGD-ACM treated cells. (C) Bar graph representing normalised p62 expression. Compared to untreated control, p62 was significantly lower in 6 h and 24 h OGD-ACM treated cells. *(For all graphs, $^{+}$represents $p < 0.01$ against untreated control and $^{\#}$ represents $p < 0.05$ against 6 h OGD-ACM; two-way ANOVA followed by Tukey's post-hoc analysis; n=3).*

6.3.9 The effect of ACM on HIF downstream genes in primary rat neurons

Using qRT-PCR, the effect of ACM (Nx, 6 h OGD-ACM, and 24 h OGD-ACM; normalized to untreated control) was studied on hypoxia gene expressions (*Hif1α, Hif2α, Epo, Bnip3, Phd2, Vegf, Glut1, Pfkfb1, Pfkfb3, Ldha*) in primary rat neurons. Of all the genes studied, *Vegf* (~12 folds) was only upregulated in primary neurons subjected to 6 h OGD-ACM compared to untreated control (Figure 6.12). There were no significant changes in *Hif1α, Hif2α, Bnip3, Epo, Phd2, Glut1, Pfkfb1, Pfkfb3,* and *Ldha* expression in primary neurons subjected to ACM (Nx, 6 h OGD-ACM, and 24 h OGD-ACM).

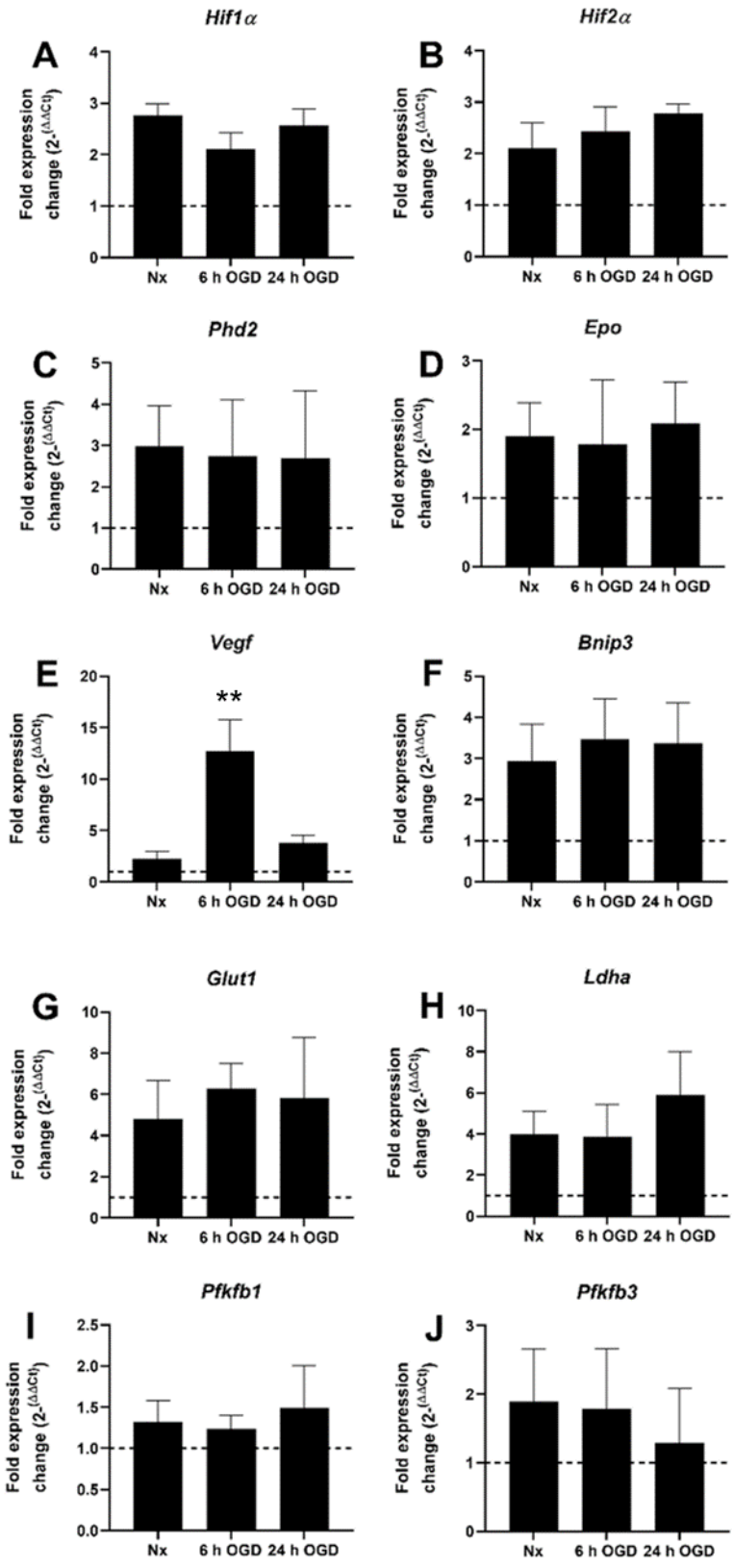
A
Hif1α
B
Hif2α
C
Phd2
D
Epo
E
Vegf
**
F
Bnip3
G
Glut1
H
Ldha
I
Pfkfb1
J
Pfkfb3
Fold expression change (2-[ΔΔCt])
Nx
6 h OGD
24 h OGD

Figure 6.12. Effect of astrocyte conditioned media (ACM) on hypoxic genes in primary rat neurons. Expression of hypoxia genes were evaluated in primary neurons treated with Nx-ACM, 6 h OGD-ACM, and 24 h OGD-ACM. There were no significant changes in (A) *Hif1α* (B) *Hif2α* (C) *Phd2* (E) *Bnip3* (F) *Epo* (G) *Glut1* (H) *Pfkfb1* (I) *Pfkfb3* (J) *Ldha* expression in all ACM treatment groups compared to untreated control. (D) *Vegf* was significantly upregulated in primary neurons subjected to 6 h OGD-ACM compared to untreated control. Each data point represents the mean and standard deviation of the relative fold change with respect to untreated control normalised to reference gene *β-actin* level. The dotted line represents basal gene expression. *(For all graphs, $^{+}$represents $p < 0.01$ against untreated control; One-way ANOVA followed by Tukey's post-hoc analysis; n=3).*

6.4 Discussion

Astrocytes play essential roles in normal and pathological CNS functioning (discussed in section 1.2.6). Astrocytes perform the following functions (i) formation and function of developing synapses by releasing molecules signals such as thrombospondin (ii) maintaining ion, fluid, pH and NT homeostasis (iii) regulating CNS blood flow and BBB (Barreto *et al.,* 2011; Sofroniew and Vinters, 2010). During ischaemia, astrocytes have been reported to be neuroprotective via anti-excitotoxicity effects such as uptake of excess glutamate, the release of antioxidants, provide neurons with healthy mitochondria, provide lactate to neurons, sequester free iron, modulate immune response, production of neurotrophic factors that promote angiogenesis, neurogenesis, synaptogenesis and axonal remodelling aiding recovery (Bylicky *et al*., 2018; Becerra-Calixto and Gomez, 2017).

In primary astrocytes, cell viability assays revealed a significant reduction in mitochondrial activity and an increase in LDH release by 24 h and 48 h OGD. There were no significant changes by 6 h OGD. This was in line with a study by Paquet *et al.,* (2013) that revealed that a significant reduction in primary rat cortical astrocytes viability and increased LDH release was observed from 12 h of OGD (0% O_2) onwards; there were no significant changes for up to 9 h OGD. Unlike results in primary neurons (chapter 3), there was no further reduction in mitochondrial activity or an increase in LDH release after 24 h reperfusion in primary astrocytes subjected to 24 h and 48 h OGD. Studies have previously shown that astrocytes have abilities to protect themselves and neurons against oxidative stress during I / R injury. Neuron co-cultures with astrocytes are less sensitive to oxidative stress than those cultured alone (Peng *et al.,* 2019). Astrocytes synthesize and release GSH, which

can minimize oxidative stress during and post ischaemia (Bylicky *et al.,* 2018). Astrocytes also release superoxide dismutase (SODs), a family of metal-containing proteins that catalyse the dismutation of superoxide radicals (Bylicky *et al.,* 2018; Ouyang *et al*., 2014).

Astrocytes consist of two subclasses: protoplasmic and fibrous. Protoplasmic are stellate in appearance and present in the grey matter; whereas fibrous are long, thin fibrocyte-like cells present in the white matter (Sofroniew and Winters, 2010). They have a distinct gene expression profile, but both express GFAP. GFAP is a prototypical marker for identifying astrocytes. GFAP is a sensitive, reliable, and most extensively studied marker that labels most reactive astrocytes that are responding to CNS injury. GFAP is an intermediate filament protein that serves largely the cell architectural functions (Barreto *et al.,* 2011; Sofroniew and Winters, 2010). Upon CNS injury, normal astrocytes are transformed into reactive astrocytes known as astrogliosis. The primary features of astrogliosis are increased GFAP expression, cellular hypertrophy, extended processes, and proliferation (Barreto *et al.,* 2011; Bylicky *et al.,* 2018). Within a few days post ischaemia, a glial scar is formed around the ischaemic core mainly generated by astrogliosis. The role of the glial scar is controversial. During recovery, it may obstruct axonal regeneration and reduce the functional outcome. On the other hand, it also secludes viable tissue from the injury site and protects the surrounding area from harmful substances in the ischaemic core (Becerra-Calixto and Gomez, 2017). Compared to astrocytes in healthy cultures (Nx treated), OD (48 h) and OGD (6 h, 24 h, and 48 h) treatment resulted in astrocytes with extended processes. Compared to Nx (same time point), GFAP intensity was upregulated in 24 h OGD, 48 h OD, and 48 h OGD treated cultures and

remained elevated after reperfusion. This was in-line with a study by Wang *et al.,* (2012) that revealed that OGD resulted in hypertrophic astrocytes with increased GFAP intensity and extended processes; which remains upregulated 24 h and 48 h after reperfusion. This was found as a characteristic of the glial scar, formed by astrogliosis post ischaemia. In line with LDH assay, cell densities ($GFAP^+$ nuclei / microscopic field) were significantly reduced in cultures subjected to 24 h OGD, 48 h OD, and 48 h OGD compared to Nx (same time point). The cell densities were significantly lower at 48 h OGD compared to 24 h OGD treated cultures.

Astrocytes were resistant to OD insult alone; no significant changes in mitochondrial activity, LDH release, or astrogliosis (GFAP intensity) were observed for up to 24 h. Several studies have shown that in the presence of glucose, astrocyte cultures were resistant to prolonged hypoxia (~24 h) (Vega *et al.,* 2006; Kelleher *et al.,* 1993; Callahan *et al.,* 1990). Astrocytes adapt to hypoxia by switching from oxidative phosphorylation to anaerobic glycolysis and produce lactate for energy. Astrocytes also mobilize their glycogen stores and provide ATP via glycogenolysis to neurons during hypoxia (Yu *et al*., 2005). In response to hypoxia, there is an increased expression of glucose transporters (GLUT1) on astrocytes to increase glucose uptake (Badawi *et al.,* 2012, Vega *et al.,* 2006; Yu *et al*., 2005). Studies have previously found that astrocytes and endothelial cells are more capable of withstanding hypoxic injury more than neurons and oligodendrocytes (Vega *et al.,* 2006). In astrocyte cultures, 48 h OD resulted in a significant reduction in mitochondrial activity, an increase in LDH release, and GFAP intensity. In the presence of glucose, astrocytes have abilities to survive in hypoxia, however, a drop in pH below 6.5 results in lactic acidosis and cytotoxicity (Badawi *et al.,* 2012).

HIF expression has not been as widely explored in astrocytes as in neurons (Hirayama *et al.,* 2015). HIF1α and HIF2α protect astrocytes during ischaemia by promoting the expression of various pro-survival genes (EPO, VEGF, HSPs, HO-1, glucose transporter, glycolytic enzymes) (Badawi *et al.,* 2012). HIF1α and HIF2α can also have a detrimental effect by exacerbating inflammatory response through activation of astrocyte-specific glial T-cell immunoglobulin and mucin domain protein (TIM-3) and upregulation of pro-inflammatory cytokines (Kim *et al*., 2019). In this study, we found both HIF1α and HIF2α were upregulated by 6 h and 24 h OD and OGD (versus Nx, same time point) in the primary rat astrocytes. This is consistent with studies on primary astrocytes. Chavez *et al.,* (2006) revealed that 4 h OGD (0.5% O_2) upregulated HIF1α and HIF2α in primary rat astrocytes, and HIF2α expression was more prominent in astrocytes than neurons. Liu and Alkayed (2005) showed that OD (1% O_2) for 6 h upregulated HIF1α primary cultured astrocytes. Hirayama *et al.,* (2015) found that P2X7 (an ion channel-forming ATP receptor) activation regulated HIF1α expression in astrocytes, resulting in a slow onset and long-lasting response. They found that HIF1α activation was abolished in P2X7 receptor KO mice subjected to hypoxia or ischaemia.

HIF mediates the expression of various downstream genes during hypoxia / ischaemia in the brain. Studies have suggested that in astrocytes, HIF1α regulates the expression of *Glut1*, *Vegf*, *Bnip3*, *Ldha*, and *Pfkfb3*; whereas HIF2α regulates the expression of *Epo* (Sun *et al.,* 2019; Singh *et al.,* 2018; Chavez *et al.,* 2006). In our study, there were no significant changes in *Hif1α* and *Hif2α* expression by OD and

OGD (6 h, 24 h) compared to Nx (same time point),. Obach *et al.,* (2004) revealed that HIF1α and HIF2α levels were regulated at the post-transcriptional level following hypoxia. We found that OD and OGD (6 h, 24 h) significantly upregulated *Phd2* compared to Nx (same time point). PHD2 is upregulated as a negative feedback response to HIF1α upregulation (Berra *et al.,* 2003). Only prolonged (24 h) OGD resulted in a ~24 folds increase in *Bnip3* gene expression compared to 24 h Nx. BNIP3 is a HIF1α target gene that is associated with cell death in astrocytes (Singh *et al.,* 2018). Following severe ischaemia, BNIP3 is upregulated inducing cell death by opening MPTP leading to loss of MMP and production in ROS in the mitochondria (Singh *et al.,* 2018).

During ischaemia / hypoxia, astrocytes are the main source of VEGF and EPO known to stimulate erythropoiesis, angiogenesis and inhibit apoptosis (Marti *et al.,* 2000). In our study, *Vegf* was significantly upregulated by OD and OGD (6 h, 24 h) compared to Nx (same time point) while *Epo* was significantly upregulated by 24 h OD and OGD in line with HIF1α protein upregulation in astrocytes. *Vegf* was upregulated by 6 h OD in primary astrocytes but not in primary neurons. *Vegf* expression in response to 6 h OGD was ~2 times higher in primary astrocytes compared to primary neurons. This was in-line with a study by Chavez *et al*., (2006), where significantly higher and more robust upregulation of *Epo* and *Vegf* mRNA was found in astrocytes compared to neurons exposed to similar ischaemic insult, indicating that astrocytes can provide trophic support for neurons.

HIF1α regulates the expression of several enzymes in the glycolytic pathway and expression of glucose transporter to mediate cellular glucose uptake in response to hypoxia or ischaemia (Choi *et al.,* 2018). We found *Glut1* was significantly upregulated by 6 h and 24 h of OD and OGD in astrocytes. GLUT1 is a glucose transporter mainly expressed on the plasma membrane to facilitate diffusion-type transport of glucose (Hocquette *et al.,* 1996). GLUT1 and GLUT3 are predominantly expressed in the brain, where GLUT1 is localized on astrocytes, oligodendrocytes and endothelial cells. GLUT3 is expressed on neurons and controls the uptake of glucose by neurons (Carreras *et al*., 2015). Studies have revealed that during anoxia, *Glut1* mRNA expression was significantly increased in astrocytes as an adaptive response since more glucose is required to maintain ATP levels by anaerobic glycolysis (Badawi *et al.,* 2012; Vega *et al.,* 2006).

In the absence of oxygen, anaerobic glycolysis is the main generator of ATP. LDHA is required to maintain anaerobic glycolysis by catalysing the conversion of pyruvate to lactate (Valvona *et al*., 2016). Lactate has traditionally been regulated as a waste product of glycolysis (Sofroniew and Vinters, 2010), however, studies have shown that it is an immediate energy source during hypoxia in the brain. Lactate is exported out of astrocytes (monocarboxylate transporter 1, MCT1) and taken up by neurons via the neuronal MCT2 transporter in the absence of oxygen (Valvona *et al*., 2016). In the neurons, lactate converted into pyruvate and consumed in the TCA cycle (Sofroniew and Vinters, 2010). In our study, we found *Ldha* was significantly upregulated by 6 h OD and OGD (versus 6 h Nx) in primary astrocytes. This is consistent with studies by Amaral *et al*., (2010) that revealed that *Ldha* was upregulated in primary astrocyte cultures following ischaemia.

PFKFB3 is a pro-glycolytic enzyme that is abundant in astrocytes. PFKFB3 is an allosteric regulator of glycolytic enzyme 6-phosphofructo-1-kinase (PFK1), which catalyses the conversion of fructose 6-phosphate to fructose-2, 6-bisphosphate; an essential step in anaerobic glycolysis (Burmistrova *et al.,* 2019; Valvona *et al*., 2016; Lv *et al*., 2015). We found *Pfkfb3* was significantly upregulated by OD and OGD (6 h, 24 h) compared to Nx (same time point) in primary astrocytes. This is consistent with a study by Minchenko *et al.,* (2003), where *Pfkfb3* mRNA was upregulated in rat cortical astrocytes in the absence of oxygen (6 h).

Samy *et al.,* (2018) suggested that HIF1α activation during hypoxia triggers the expression of various cytokines and chemokines in astrocytes, e.g. IFNγ, IFNβ, IL-1β, IL-6, IL-10, IL-17, TGFβ, TNFα, CCL2, CCL5, CCL20, CXCL8, CXCL10, CXCL12 and CX3CL1. However, the possibility of the involvement of other HIF1α independent mechanisms cannot be ruled out. Mojsilovic-Petrovic *et al.,* (2007) suggested that HIF1α induced transcriptional upregulation of inflammatory cytokines and chemokines during hypoxia, whereas NF-κB was involved in transcriptional regulation of these genes during reperfusion. Therefore, in addition to the genes studied, it would be interesting to study the effect of OD and OGD on the expression of astrocyte-specific cytokines and chemokines.

As discussed in Section 1.2.6, astrocytes are resistant to ischaemic insults compared to neurons and astrocytes secrete several neuroprotective and neurotoxic substances during an ischaemic stroke. It would be beneficial to modulate the

neuroprotective properties of astrocytes to protect neurons during ischaemia. Studies have previously focused on the protective effect of ACM as a whole, but the ACM consists of soluble factors and EVs (Hong *et al.,* 2018). Research in recent years has provided fundamental insight into the physiological roles of EVs (Li *et al.,* 2017). EVs can influence both physiological and pathological functions in human and animals (Hong *et al.,* 2018). In recent studies, EVs have been recognized to play roles in intercellular communication due to their capacity to transfer proteins, lipids and nucleic acids. Studies have implicated that EVs have several functions such as protein clearance, immunity, infection, signalling and cancer (Li *et al.,* 2017). In this study, the protective effect of supernatant (consisting of soluble factors) and EVs were evaluated separately.

Astrocytes are most abundant glial cells in the CNS. The ratio of astrocytes to neurons in brain varies between species and brain regions. In the human, glial outnumber neurons in all parts, except in the cerebellum where the neurons outnumber glia by 4.3:1 ratio. Throughout the rest of the CNS, the ratio of glia to neurons in human range from 1.7:1 in cerebral cortex to 11.4:1 in midbrain / hindbrain and 17:1 in thalamus (Herculano-Houzel, 2014). In rat brain cortex the ratio of neurons to astrocytes is between 1:2 to 1:3 (Herculano-Houzel, 2014). Therefore, ACM collected from one fold of astrocytes (e.g. 1 million) will be used to treat two folds of neurons (e.g. 2 million).

Various techniques for isolations of EVs such as ultracentrifugation, immunoaffinity capture-based techniques, flow cytometry, exosome precipitation, and microfluidic-

based techniques have been reported (Li *et al.,* 2017; Hong *et al.,* 2018). Ultracentrifugation based EVs isolation is considered the gold standard technique and is one of the most commonly used and reported techniques (~56% of all EV isolation reported techniques in research). It is easy to use, affordable and requires little technical expertise. Ultracentrifugation is widely classified into differential and density gradient ultracentrifugation. In this study, ACM was separated by differential ultracentrifugation. This involves a series of centrifugation cycles of different centrifugal forces and duration to isolate EVs based on density and size. Density ultracentrifugation involves the separation of EVs based on their mass, size, and density in a pre-constructed density gradient medium in a centrifuge tube with progressively decreased density from top to bottom (Li *et al.,* 2017).

EVs can be widely divided into exosomes (20 to 200 nm), microvesicles (200 to 1000nm), and apoptotic bodies (larger than 1000nm) (Hong *et al.,* 2018; Li *et al.,* 2017). In our study, the particle size range was large, from the smallest particles ~7nm up to ~3000-4000nm in the whole ACM. The majority of the particles (~60%) fell in ~100-500 nm range, ~30% were between ~20-40 nm and ~20% were between ~1800-4000 nm. The EVs pellet obtained from Nx-ACM, 6 h OGD-ACM, and 24 h OGD-ACM consisted of the majority of particles (~85%) in 20 to 200nm range; therefore classifying as exosomes. The pellet also consisted of ~15% of particles less than 20nm. It is clear that sequential ultracentrifugation eliminated the bigger particles (~1800-4000nm) and particles larger than ~200nm from the ACM. This is in line with the study by Pei *et al.,* (2019) that revealed that ~90% of particles obtained from sequential centrifugation of ACM were between 20-200nm i.e. exosomes. Studies have pointed out that the majority of the EVs obtained from astrocytes are

exosomes, with few microvesicles (Chaudhuri *et al.,* 2018; Jovičić and Gitler's, 2017). Additionally, sequential centrifugation followed by D-PBS wash performed in this study is commonly used to obtain pure exosomes; however, due to heterogeneity of exosomes and overlap in size of EVs, there is often some contamination and loss of material (Li *et al.,* 2017). Initially, the distribution of all particles in the centrifuge tube is homogenous due to which a portion of small particles inevitably co-sediments and are lost when large molecules are withdrawn. Additionally, a population of smaller exosomes avoid pelleting during ultracentrifugation due to relatively small densities and may be lost in the supernatant. Moreover, repeated centrifugation of the re-suspended pellet also increases the loss of material (Li *et al.,* 2017). Further characterisation of internal (Alix, TSG101) and external markers (CD9, CD63, CD81) of EVs (Pei *et al.,* 2019) using electron microscopy and Western blotting needs to be performed to validate these findings.

The most frequently used media for culturing primary astrocytes are DMEM, minimum essential medium (MEM), or Ham's F-12 medium. Astrocyte media is often supplemented with 10% FBS to fulfill metabolic requirements and promote astrocyte proliferation (Lange *et al.,* 2012). On the other hand, Neurobasal medium supplemented with serum-free B27 is the widely recommended medium for primary neuronal cultures (Brewer, 1995). Neurons are often cultures in serum-free media to avoid the proliferation of astrocytes (Lange *et al.,* 2012). In this study, astrocytes obtained from mixed glial cultures were initially grown and maintained in D10 media (DMEM containing 10% FBS) to aid their growth and proliferation. Before experiments to obtain ACM, the astrocytes were switched to Neurobasal media. This

was done to maintain comparable experimental conditions as the neurons were grown and treated with Neurobasal media. Additionally, FBS contains a large number of bovine EVs (Kornilov *et al.,* 2018), therefore serum-free media is suitable to exclusively analyse the astrocyte secreted EVs.

ACM was collected from primary rat astrocytes subjected to Nx, 6 h OGD, and 24 h OGD. ACM was separated into supernatant (soluble protein) and pellet (EVs). ACM (whole) and its separated parts were applied to primary rat neuronal cultures for 6 h followed by 24 h reversion and 6 h OGD insult. LDH, MTT assay, and MAP2 IF staining revealed that preconditioning neurons with 6 h OGD-ACM (whole) followed by 24 h reversion, provided significant cytoprotection against 6 h OGD insult compared to sham-PC. Nx-ACM and 24 h OGD-ACM (whole) were not cytoprotective compared to sham-PC. This is consistent with various studies (discussed in the introduction) that have shown that ACM induced tolerance in neurons against ischaemic insult (Dhandapani *et al.,* 2003; Becerra-Calixto and Gomez, 2017; Song *et al.,* 2019). Narayan and Perez-Pinzon (2017) also found that transferring IPC astrocytes to neurons was neuroprotective. ACM collected from cultures of primary retinal astrocytes subjected to metabolic stress reduced cell death in HT22 cell line and primary cortical neurons subjected to severe metabolic stress (Alqawlaq *et al.,* 2016). Several growth factors known to bind to receptor tyrosine kinases were found in the ACM (Alqawlaq *et al.,* 2016). Interestingly, 6 h OGD-ACM but not 24 h OGD-ACM was found protective in primary neurons. Our results indicated that 24 h OGD but not 6 h OGD was cytotoxic and increased GFAP intensity in primary astrocytes. Depending on the time, extent, and type (chronic versus acute) of ischaemic injury, the substances secreted by astrocytes can be

reparative or destructive (Buffo *et al.,* 2010; Lau and Yu, 2001). Studies have previously revealed that the secretory activity of reactive astrocytes can exacerbate tissue injury, for example, an increasing concentration of TNFα can inhibit neurite outgrowth. Astrocytes release several pro-inflammatory cytokines (TNFα, IL-1β, IL-6, IFNγ, TGFβ) in response to acute ischaemia; which triggers the production of secondary mediators such as arachidonic acid metabolites, nitric oxide, ROS and MMPs that promote neuronal degeneration and axonal demyelination (Buffo *et al.,* 2010). The factors secreted by astrocytes also act in an autocrine / paracrine fashion, thereby resulting in amplification in secretion, contributing to sustained astrogliosis and neurotoxicity (Trendelenburg and Dirnagl, 2005).

Initial results revealed that preconditioning neurons with whole ACM collected from astrocytes subjected to 6 h OGD was protective against OGD insult in neurons. For further studies, the whole ACM was separated into supernatant and EVs pellet. The supernatant and EVs pellet were separated and each of them was separately applied to primary neuronal cultures. Neurons subjected to the supernatant separated from 6 h OGD-ACM developed tolerance against subsequent 6 h OGD insults. Both MTT and LDH assay revealed that compared to sham-PC neuronal cultures, preconditioning with 6 h OGD-ACM (supernatant) followed by reversion provided significant cytoprotective against 6 h OGD insult. MTT assay (but not LDH assay) revealed that the whole 6 h OGD-ACM (whole) was significantly more protective than the supernatant alone. Previous studies have shown that several neurotrophic factors, such as VEGF, NGF, GDNF, BDNF, NT-3, and EPO are secreted by ischaemic astrocytes protect neurons from ischaemic damage both *in vitro* and *in vivo* (Barreto *et al.,* 2011). A study has reported that soluble factors such

as TNFα and TGFβ present in the ACM protected neurons against serum-deprivation induced cell death (Dhandapani *et al.,* 2003).

On the other hand, preconditioning with EVs (collected from Nx-ACM, 6 h OGD-ACM, and 24 h OGD-ACM) were not found protective against OGD in primary neurons. A study reported that preconditioning neurons with exosomes obtained from glial cells are protective during acute ischaemia (Venturini *et al*., 2019). It has been reported that glial cells transfer miRNA to neurons via exosomes targeting signaling pathways such as PI3K / AKT pathway, Hippo, MAPK, or mTOR. Exosomal content (such as miRNA) is reported to promote neurogenesis, axonal remodelling, vascular remodelling, and reducing neuroinflammation in neurons (Hong *et al.,* 2018). Li *et al.,* (2019) reported that astrocyte-derived exosomes suppress autophagy and ameliorate neuronal damage during ischaemic stroke. Another study by Hira *et al.,* (2018) reported astrocyte-derived exosome treated with semaphorin 3a inhibitor enhances stroke recovery via prostaglandin d2 synthase. Taylor *et al.,* (2007) reported that in response to oxidative stress, cultured astrocytes release elevated amounts of heat-shock protein 70 (HSP70) and synapsin 1 in association with exosomes. Although we have not found exosomes from ACM neuroprotective, further studies need to be conducted with prolonged periods of preconditioning treatment or increased concentration of EVs.

Besides proteins and cytokines, microRNA secreted by astrocytes could have roles in neuronal function following ischaemia. miR-92b-3p released from astrocytes subjected to OGD was associated with activation of the PI3K / AKT pathway and

ameliorated OGD-induced injury in neurons (Xu *et al.,* 2019). Viral vector expressing miR-124 was found to increase neurogenesis and promote neuroprotection against cerebral ischaemic *in vivo* (Yang *et al.,* 2017). Astrocytes also release the miR-17-92 cluster that promotes neurite elongation (Carlos *et al.,* 2016). Additionally, Hayakawa *et al.,* (2017) reported that during transient focal cerebral ischaemia in mice, astrocytes release functional mitochondria that enter into adjacent neurons and amplify cell survival signals.

Primary neurons subjected to ACM (Nx, 6 h OGD, and 24 h OGD) for 6 h did not upregulate HIF1α and HIF2α protein. Du *et al.,* (2011) reported that hyperthermia conditioned ACM upregulated HIF1α and protected neurons from ischaemic injury. Studies have not explored the effects of OGD conditioned ACM on HIF1α and HIF2α expression yet. Out of all the HIF1α and HIF2α downstream genes studies, 6 h OGD-ACM upregulated *Vegf* expression in neurons. Karar *et al.,* (2011) reported that activation of PI3K / Akt increased *Vegf* expression via both HIF dependent and independent mechanisms. Some of the cytokines (IL-6, IL-10, IL-1β, and TGFβ) secrete by astrocytes during ischaemia (Lau and Yu, 2001), which are known to promote angiogenesis. Cohen *et al.,* (1996) showed that *Vegf* was upregulated in various cell lines treated with IL-6. IL-1β increased *Vegf* mRNA expression in cultured neonatal rat cardiac myocytes (Tanaka *et al.,* 2000). Pro-inflammatory cytokines such as IL-1β and TNFα promoted neuron outgrowth and neurogenesis (Gougeon *et al.,* 2013). During ischaemic stroke, VEGF decreases the expression of caspase 3 and increases the expression of anti-apoptotic Bcl-2 protein (Sanchez *et al.,* 2011). VEGF promotes angiogenesis, axonal outgrowth, neuronal growth, and protects neurons against ischaemic injury (Patabendige *et al*., 2021; Sanchez *et al.,*

2011). VEGF also promotes neuron survival during ischaemic stroke indirectly, by interacting with other neurotrophic proteins such as pigment epithelium-derived factor (PEDF) (Sanchez *et al.,* 2011; Rosentein *et al.,* 2010).

Autophagic marker Lc3b-II was upregulated and p62 was downregulated in primary neurons subjected to ACM (6 h OGD and 24 h OGD) for 6 h, indicating autophagic induction. In a Huntingdon disease model, conditioned medium from primary glial culture resulted in Lc3b-II upregulation and p62 downregulation. It was postulated that Nrf2 overexpression in astrocytes promoted neuronal autophagy and protected against Huntingdon disease (Sung and Jimenez-Sanchez, 2019). Sun *et al.,* (2013) also reported that ACM induces PI3K / Akt signalling pathway in neurons. ACM from primary retinal astrocytes was neuroprotective in primary cortical neurons via PI3K / Akt signalling pathway (Alqawlaq *et al.,* 2016). PI3K / Akt pathway is known to modulate autophagy and promote survival in neurons during cellular stress (Heras-Sandoval *et al.,* 2014). Various soluble factors in the ACM such as VEGF (Sanchez *et al.,* 2011), IL-10 (Zhou *et al.,* 2010) have been reported to activate the PI3K / Akt pathway in neurons. TGFβ also activated autophagy in various cell models via Smad and non-Smad pathways (Zhang *et al.,* 2017; Alizadeh *et al.,* 2018; Ghavami *et al.,* 2015; Kiyono *et al.,* 2009). Although 24 h OGD-ACM promoted autophagy, it was not found protective in primary neurons. Studies have suggested that excessive and prolonged autophagy can result in cell death, whereas mild autophagy is neuroprotective (Kim *et al.,* 2018). The upregulation of *Vegf* and autophagy by 6 h OGD-ACM may be due to the PI3K / Akt pathways and warrants further investigation. In contrast, Madill *et al.,* (2017) showed that ACM derived from ALS patients reduced autophagy in the HEK293T cell line. Another study by Tripathi *et*

al., (2017) proposed that TGFβ1 released from reactive astrocytes resulted in mTOR activation and inhibited autophagy.

Key findings:

- Primary astrocyte cultures are more resistant to OGD insults compared to neuronal cultures.
- Primary astrocytes possess capabilities to stabilise HIF1α and HIF2α in response to OD and OGD.
- Media collected from astrocytes subjected to 6 h OGD insults (ACM) induced ischaemic tolerance in primary rat neurons.
- The soluble proteins but not the EVs in the ACM were involved in induction of ischaemic tolerance.
- Autophagy but not HIF1α plays an essential role in ACM induced ischaemic tolerance.

In conclusion, OD and OGD for 6 h were not cytotoxic in primary astrocytes but resulted in the upregulation of HIF1α and its downstream genes, while OGD (24 h) was cytotoxic. Additionally, HIF1α, HIF2α, and their downstream genes were upregulated in response to 24 h OGD. As astrocytes are comparatively less sensitive to OGD insults than neurons, therefore modulating astrocytes to protect neurons would be beneficial for ischaemic stroke therapeutics. Depending on the time and extent of ischaemic injury, the substances secreted by astrocytes can be protective or destructive. Preconditioning with ACM from astrocytes subjected to 6 h OGD but not 24 h OGD promoted ischaemic tolerance in primary neurons. ACM collected from ischaemic (6 h and 24 h OGD) astrocytes promoted autophagy in primary

neurons. In comparison to EVs pellet, the soluble proteins in the ACM (6 h OGD) played a vital role in ACM induced tolerance and warrants investigation into the exact protein profile.

Chapter 7.

General discussion and conclusion

7.1 Major finding

As shown in Figure 7.1. this study established *in vitro* ischaemic stroke models (OGD) using PC12 cells and primary rat neurons and evaluated the effects of OD, GD, OGD on cell viability, HIF1α and HIF2α protein expression as well as gene expressions of HIF downstream genes and metabolic genes at various time points. Upon determining the maximal non-lethal period of GD, OD, and OGD, the effectiveness of preconditioning with the sublethal conditions was studied against a subsequent OGD insult in PC12 cells and primary neurons. Thereafter, the effectiveness of pharmacological preconditioning induced tolerance was evaluated on the models using novel small molecule PHD inhibitors in the ischaemic tolerance models. These PHD inhibitors are pharmacological mimetics of hypoxia and are in phase 3 clinical trials / clinical use for anaemia treatment in patients with CKD. The effects of these molecules were studied on HIF1α / HIF2α proteins, autophagic proteins, and hypoxic genes in PC12 cells and primary neurons. Finally, the effects of OD and OGD (various time points) on astrocyte cell viability, GFAP expression, HIF1α / HIF2α protein expression, and HIF downstream genes were evaluated. Then studies were performed to determine the effectiveness of separable components i.e. soluble proteins and EVs of ACM collected from astrocytes subjected to OGD against OGD insult on primary neuronal cultures. The effect of the ACM was also studied on HIF1α / HIF2α proteins, autophagic proteins, and HIF downstream genes. Figure 7.1. Lists the major discoveries by this study.

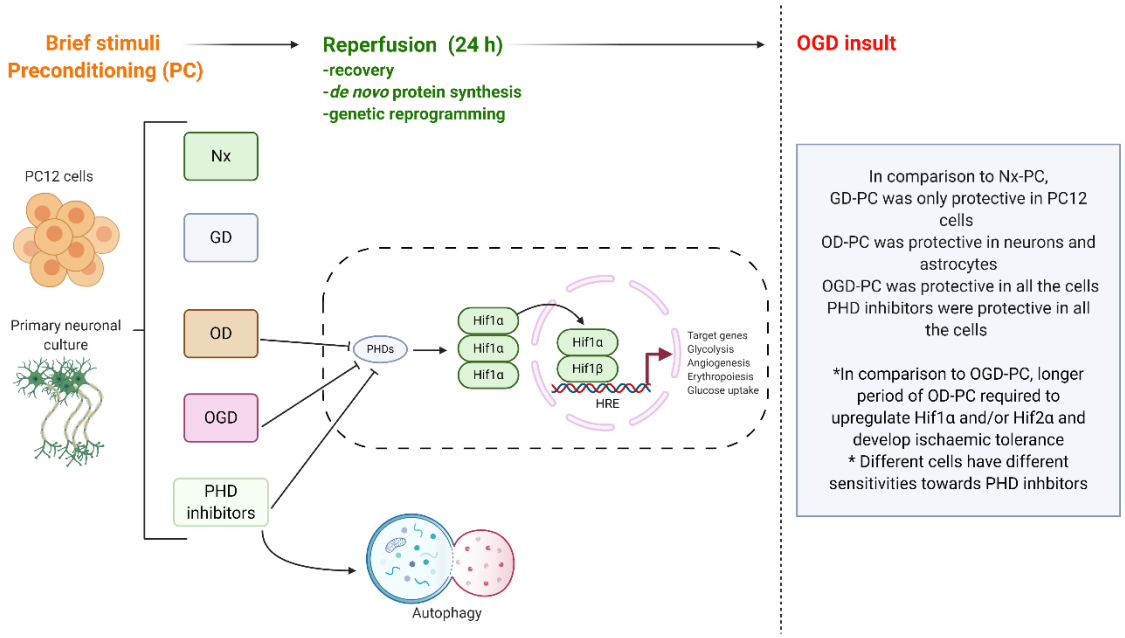

Figure 7.1. Summary of major findings. In PC12 cells, primary neuronal cultures and primary astrocytes, preconditioning with brief OD, OGD stimuli, and PHD inhibitors were protective against a subsequent OGD insult. GD-PC was protective in PC12 cells only. Reperfusion following brief preconditioning insult was essential for recovery, *de novo* protein synthesis, and genetic reprogramming. OD, OGD, and PHD inhibitors inhibit PHDs and upregulate HIF1α. HIF1α translocates to the nucleus and dimerizes with HIF1β, resulting in upregulation in various genes. PHD inhibitors also promote autophagy, but the link between HIF1 activation and autophagy needs further investigation. (Image produced using Biorender).

7.2 Establishing an *in vitro* model of stroke

Initial studies were performed to develop a suitable *in vitro* model of ischaemic stroke to evaluate the effectiveness of several treatment strategies and characterise their underlying mechanism. Ischaemic stroke models were developed using PC12 cells and primary neurons. Results revealed that in both PC12 cells and primary neurons, 6 h OGD resulted in significant cytotoxicity and was a suitable model for ischaemic insult. Reperfusion (24 h) further worsened 6 h OGD induced injury. OGD for 2 h and 4 h were not cytotoxic and therefore deemed sub-lethal. Alongside OGD, the effect of OD alone was evaluated on the cells. In PC12 cells, OD (6 h onwards) resulted in a significant reduction in mitochondrial activity and an increase in LDH release. In primary neurons, 6 h OD altered mitochondrial activity but did not elevate LDH release. The effect of GD alone was evaluated on PC12 cell viability. GD (12 h and 24 h) resulted in a significant increase in LDH release and reduction in mitochondrial activity.

In addition to cell viability, apoptosis was studied in PC12 cells using flow cytometric analysis (Annexin V and 7-AAD). GD, OD, or OGD for 24 h resulted in significant early apoptosis and necrosis which was worsened following reperfusion. Shorter periods of GD, OD, or OGD mainly resulted in early apoptosis, which was successfully reversed upon reperfusion. 6 h OGD insult resulted in significant early apoptosis, which was worsened following reperfusion.

HIF is a dimeric protein complex that plays an essential role in cellular responses to low oxygen levels. To evaluate the suitability of these cells as models of ischaemia *in*

vitro, the expression of HIF1α and HIF2α proteins were evaluated in PC12 cells and primary neurons. In PC12 cells, 4 h and 6 h OGD upregulated HIF1α and HIF2α; whereas a shorter period of OGD (2 h) was sufficient to upregulate HIF1α in primary neurons. The PC12 cells and primary neurons were less sensitive to OD, requiring 24 h and 6 h respectively to upregulate HIF1α and HIF2α. In PC12 cells, GD (24 h) upregulated HIF1α and HIF2α. Shorter periods of GD (2 h, 4 h and 6 h) did not upregulate HIF1α and HIF2α in PC12 cells.

Overall, results revealed that both PC12 cells and primary neurons respond similarly to OGD. HIF1α and HIF2α were upregulated in both PC12 cells and primary neurons during OD and OGD conditions, however, the time points slightly varied. The magnitude of HIF activation varied in the different cell types depending on the period of oxygen and / or glucose deprivation. The omission of both glucose and oxygen was found most effective in HIF activation. Both PC12 cells and primary neurons subjected to OGD are suitable *in vitro* models for ischaemic stroke for preliminary screening of several treatment strategies.

7.3 Preconditioning induced ischaemic tolerance

Ischaemic tolerance is a phenomenon whereby transient resistance to lethal ischaemia is gained due to prior exposure to sub-lethal noxious stimuli (i.e. preconditioning) (Hill, 2014). Upon characterising the timeline for sub-lethal ischaemia and ischaemic insult, the effectiveness of IPC and HPC were evaluated in PC12 cells and primary neurons. Sub-lethal GD, OD, or OGD (2, or 4 h) were applied to PC12 cells and primary neurons followed by a period of reperfusion and 6 h OGD insult. OGD-PC was the only strategy that was found protective in both the

cell types. The time point at which OGD-PC was protective, corresponded with the upregulation of HIF1α and / or HIF2α and its downstream gene.

OD-PC was cytoprotective in primary neurons but not in PC12 cells. Unlike OGD-PC (2, 4 h), a longer period of OD-PC (6 h) was required to generate sufficient cytoprotection in primary neurons. Similar to OGD-PC, the protective effect of OD-PC correlated with the upregulation of HIF1α and / or HIF2α and its downstream genes. GD-PC (4 h, 6 h) was only found protective in PC12 cells and the effect was HIF1α and HIF2α independent.

7.4 Pharmacological activation of HIF for neuroprotection in ischaemia

As OD-PC and OGD-PC were found protective in PC12 cells and primary neurons, the effectiveness of preconditioning with pharmacological hypoxia mimetics (i.e. PHD inhibitors) were evaluated in PC12 cells and primary neurons. In PC12 cells, novel PHD inhibitors (FG2216, FG4592, GSK1278863, and Bayer85-3934) were pursued along with non-specific and widely studied PHD inhibitor DMOG. In primary neurons, FG4592 was pursued as a representative of the novel class of PHD inhibitors, alongside a nonspecific HIF PHD inhibitor -- DMOG.

Preconditioning with DMOG (100μM) for 24 h followed by reversion was cytoprotective against 6 h OGD insults in PC12 cells and primary neurons, however, at this concentration HIF1α or HIF2α were not upregulated in PC12 cells. Preconditioning PC12 cells with the novel PHD inhibitors (100μM) for 24 h followed by reversion and 6 h OGD insult was found cytoprotective. In primary neurons, FG4592 (50 and 100μM) was protective against OGD insult. The novel PHD

inhibitors were found cytoprotective in PC12 cells and primary neurons at the concentrations HIF1α / HIF2α was upregulated.

In PC12 cells, 100μM of the novel PHD inhibitors resulted in significant HIF1α but not HIF2α upregulation. In contrast to PC12 cells, a lesser concentration of FG4592 (50μM) was sufficient to induce significant HIF1α upregulation. In both PC12 cells and primary neurons, HIF2α was not upregulated by the novel PHD inhibitors. Non-specific PHD inhibitor DMOG (100, 250 and 500 μM) upregulated both HIFα and HIF2α in primary neurons, however, in PC12 cells, a ten-times higher concentration of DMOG upregulated HIF1α (1mM) and HIF2α (2mM).

In addition to HIF expression, the effects of the PHD inhibitors were studied on autophagic proteins Lc3b-II and p62. In PC12 cells, PHD inhibitors: FG2216, FG4592, Bayer85-3934, and GSK1278863 significantly increased Lc3b-II expression and reduced p62 (i.e. promoted autophagy). In primary neurons, FG4592 (30, 50, and 100μM) promoted autophagy. In PC12 cells and primary neurons, independent of HIF1α upregulation, 100μM of DMOG was sufficient to promote autophagy. The variation in HIF1α / HIF2α expression and autophagy activation between PC12 cells and primary neurons by the PHD inhibitors is due to the differences in sensitivity and potency, resulting in a variation in the cytoprotective effect.

There are three human PHD isoforms due to which development of highly potent and selective PHD2 inhibitor is essential (Kenneth and Rocha, 2008). PHD inhibitors such as DMOG are non-specific and have effects on several 2-OG dioxygenases (~60 in human), therefore

they exert pleiotropic effects such as HIF induction, anti-oxidant, anti-inflammatory effects. The exact mechanism due to which these inhibitors exert protection is unknown and can also result in off-target effects. The novel PHD inhibitors (such as FG4592) are a stepping stone in stroke research because they are selective for PHDs over other 2-OG dependent enzymes. This minimizes off-target effects on other 2-OG dependent enzymes, however, it is essential to develop PHD isoform-specific inhibitors. Results have revealed that PHD2 inhibition was sufficient for protection in cerebral ischaemia, therefore the development of PHD2 specific inhibitors would be beneficial for stroke therapy.

Various PHD isoforms can hydroxylate HIF1α. PHD-2 is the primary regulator followed by PHD-3 that has comparatively lesser activity and PHD-1 having the least activity (Kenneth and Rocha, 2008). Studies have shown that inhibition of PHD-2 is sufficient for the upregulation of HIF-1α in various cell types (Karuppagounder and Ratan, 2012). Development of specific PHD-2 inhibitors and studying their effectiveness will be beneficial to minimize non-specific effects in different cells.

Similar to PHD, an asparaginyl hydroxylase known a FIH also controls HIF transcriptional activity in an oxygen-dependent manner (Yeh *et al*., 2017). Although PHD inhibitors have been widely studied on cerebral ischaemic models, FIH inhibitors have not been explored. It would be interesting to developing novel and specific FIH inhibitors and study their effectiveness in stroke. It would also be interesting to compare the differences in protein and gene expression profiles of PHD *versus* FIH inhibitors.

For clinical application, PHD inhibitors need to cross the BBB and have an effect on the neurons. The novel PHD inhibitors are small molecules and may cross the BBB. Li *et al*., 2018 revealed that FG4592 can partially cross the BBB and induce expression of HIF1α in mice brain tissue. Yeh *et al*., (2017) revealed that PHD inhibitor Bayer85-3934 partially crosses the BBB. With current advances in medicinal chemistry, the structures of the drugs can be altered to enhance lipid solubility promoting passive diffusion across the BBB.

Overall, the PHD inhibitors promoted autophagy as well as HIF1α and / or HIF2α upregulation, however, the link between HIF activation and autophagy remains unclear. Additionally, whether autophagy or HIF activation alone or together attribute to the pharmacological preconditioning induced tolerance, needs to be explored. Future studies should be directed towards understanding the link between autophagy and HIF activation. Most of the commercial HIF inhibitors such as 3-methyladenine or YC-1 are non-specific and inhibit autophagy too (Gunn *et al.,* 2018), therefore, HIF1α and / or HIF2α silencing using siRNA would be more effective to understand the role of HIF activation on autophagy and ischaemic tolerance.

In addition to the neuron, studying the effect of the novel PHD inhibitors on an *in vitro* BBB model (consisting of astrocytes, endothelial cells, neurons) would be beneficial to understand whether they can reduce ischaemic stroke potentiated cerebral oedema. The effect of the novel PHD inhibitors on membrane localisation of ZO-1,

claudins, and occludins in endothelial cells should be explored to evaluate the BBB integrity. HIF1α plays an important role in BBB disruption and oedema formation in the brain via pathways involving expression of AQP-4 water transporter, therefore, the effect of the novel PHD inhibitors on AQP-4 expression should be explored in primary astrocytes and endothelial cells.

7.5 Neuroglial interaction for ischaemic stroke treatment

Astrocytes are the main cells in the brain that are responsible to maintain homeostasis in the brain. Astrocytes interact and support neurons on several levels such as NT trafficking and recycling, ion homeostasis, energy metabolism and defence against oxidative stress (Carlos *et al.,* 2016). Astrocytes possess intrinsic neuroprotective properties that support and have abilities to protect neurons during stress. Therefore, it is essential to understand the innate mechanisms by which astrocytes protect neurons during ischaemia and translate these strategies into clinical applications (Bélanger, 2009).

Following studies in primary neurons, the effects of OGD were evaluated in primary astrocyte cultures. In primary astrocytes, there was no significant cytotoxicity by 6 h OGD, whereas 6 h OGD was found cytotoxic in primary neuronal cultures. In primary astrocytes, 24 h OGD resulted in significant cytotoxicity. Following 24 h reperfusion, the injury was not worsened, however, the astrocytes remained activated (elevated GFAP expression). Primary astrocytes were resistant to prolonged OD insults, 48 h OD resulted in significant cytotoxicity. In primary astrocytes, HIF1α and HIF2α were upregulated by 6 h and 24 h of OD and OGD. These results indicate that astrocytes are robust for ischaemia than neurons. Almeida *et al*., (2002) revealed that in

neuron-astrocyte co-culture models, astrocytes were more resistant to OGD than neurons. Neuronal death was observed within the first 90 minutes, whereas astrocytes remain viable for up to 4 to 6 h of injury. Similarly, an *in vivo* study by Gurer *et al.,* (2009) revealed that astrocytes remain viable for longer than neurons during focal cerebral ischaemia. Astrocytes were better preserved than neurons in the boundary zone to the infarct and even in the core region, astrocytes remain metabolically active and viable post focal cerebral ischaemia (Gurer *et al.,* 2009).

For preliminary studies, ACM was collected from astrocytes subjected to OGD (6 h, 24 h). The ACM was separated into EVs pellet and soluble proteins (supernatant) via sequential ultracentrifugation. Zetasizer detection revealed that ~85% of the particles in the EVs pellet were within the exosome size range (20-200 nm). The ACM and its separate parts (EVs and supernatant) were applied to primary neurons followed by reperfusion and 6 h OGD insult. Results revealed that the whole ACM (6 h OGD) as well as the supernatant only, were cytoprotective in primary neurons. 24 h OGD-ACM was not found protective. ACM (6 h OGD) also promoted autophagy and upregulated *Vegf* gene expression in primary neuronal cultures but did not upregulate HIF1α or HIF2α protein.

Although preliminary studies revealed no beneficial effect of EVs, recent studies have reported a protective effect of EVs in ischaemic stroke models. Therefore, studying the effectiveness of prolonged treatment (24 h) with EVs or higher concentrations of EVs should be explored. The EVs need to be further characterised by western blotting or electron microscopy using external (CD9, CD63, CD81) and

internal (TSG101, HSP70, Alix) exosomal markers (Hong *et al.,* 2018). The differences in the components in the EVs generated from astrocytes subjected to acute or chronic ischaemia should be studied using liquid chromatography-mass spectrometry (LC-MS) or flow cytometry.

In this thesis, a single marker of astrocyte activation (GFAP) was evaluated, however additional markers of astrocyte activation S100β (Yasuda *et al.,* 2004) and aldehyde dehydrogenase 1 family, memberL1 (Aldh1L1) gene (Matias *et al.,* 2019) need to be studied to validate the finding. The effect of OGD was only studied on a set of hypoxic genes in the astrocytes, however, *in vivo* studies have reported that astrocyte activation affects various astrocyte-specific genes such as Mmp2, Plaur, Mmp13, Axin2, Nes, Ctnnb1, Lcn2, Steap4, Gfap, Cxcl10, Timp1, S1pr3, and Serpina3n (Cohen and Torres, 2019). Hence, the expression of these genes in astrocytes *in vitro* and their role needs to be explored.

Preliminary results revealed that 6 h OGD-ACM but not 24 h OGD-ACM was protective in primary neurons, therefore, it would be interesting to explore the differences in the cytokines, chemokines, and growth factors (summarized in table 7.1) present in the ACM using LC-MS. Studies have reported that some molecules present in ACM such as IL-10, IFNβ, and EPO can confer resistance to ischaemic insults *in vivo* (Buffo *et al.,* 2010), therefore, determining the secretome profile would be beneficial to characterise the molecules essential to promote ischaemic tolerance and studying their effect on primary neuronal cultures individually. In addition to EVs and soluble factors, astrocytes also secrete healthy mitochondria (Hayakawa *et al.,*

2016) and miRNA (Carlos *et al.,* 2016). These need to be characterised using LC-MS, electron microscopy, or flow cytometry and their roles in ischaemic tolerance warrant further investigation. Studies in literature and preliminary findings (6 h OGD induced autophagy and *Vegf* gene upregulation) commonly pointed towards ACM affecting the PI3K / Akt / mTOR pathway. Further studies should be directed towards studying the effect of ACM on PI3K / Akt / mTOR pathway using knock out, and inhibitory studies and understanding its role on ischaemic tolerance.

Table 7.1. Lists the different cytokines, chemokines and neurotrophic factors that are secreted by astrocytes during ischaemia and their effects on neurons.

Cytokines	IFNγ	Neurotoxic
	IFNβ	Neuroprotective
	IL-1β	Neurotoxic
	IL-6	Neuroprotective
	IL-10	Neuroprotective
	IL-17	Neurotoxic / neurotoxic
	TGFβ	Neuroprotective
	TNFα	Neurotoxic
Chemokines	CCL2	Neurotoxic
	CCL5	Neuroprotective
	CCL20	Neurotoxic
	CXCL8	Neurotoxic
	CXCL10	Neurotoxic / neurotoxic
	CXCL12	Neuroprotective
	CX3CL1	Neuroprotective
Neurotrophic factors	EPO	Neuroprotective
	VEGF	Neuroprotective
	NGF	Neuroprotective
	GDNF	Neuroprotective
	BDNF	Neuroprotective
	NT-3	Neuroprotective

References: Buffo *et al.,* 2010; Barreto *et al.,* 2011

7.6 Conclusion

Through the several experiments carried out in this thesis, it was determined that the brain has endogenous protective mechanisms to cope with stress such as ischaemia and these mechanisms need to be well understood and modulated for clinical application. Ischaemic stroke was modelled *in vitro* in PC12 cells and primary neurons. Three different conditions GD, OD and OGD were evaluated on the cell models. During ischaemic stroke, a clot results in blockage of blood and oxygen supply to the brain, therefore, OGD (simultaneous omission of oxygen and glucose) most closely mimicked ischaemia *in vitro.* In PC12 cells and primary neurons, significant cytotoxicity was observed by 6 h OGD (0.3% O_2). OGD for 2 h and 4 h altered metabolic (MTT) activity of the cells but was not cytotoxic. The effects of reperfusion were dependent on the period of initial OGD insult. Reperfusion following short periods of OGD (2 h and 4 h) was protective in PC12 cells and primary neurons, however, following 6 h OGD it further propagated cytotoxicity. OGD upregulated oxygen-sensing HIF1α and HIF2α in PC12 cells and primary neurons, however, the magnitude of expression was time- and cell-dependent. In primary neurons, HIF1α commenced earlier (2 h) compared to PC12 cells (4 h). In both PC12 cells and primary neurons, HIF2α commenced later than HIF1α expression. Compared to OGD, both PC12 cells and primary neurons were resistant to GD and OD requiring prolonged exposure to initiate cytotoxicity and HIF1α / HIF2α upregulation.

Preconditioning (GD, OD and OGD) followed by reperfusion and 6 h OGD insult was evaluated as a treatment strategy in PC12 cells and primary neurons. Preconditioning with GD (4 h) followed by reperfusion was found protective in PC12

cells against 6 h OGD insult, however, there the cytoprotective effect was not HIF1α / HIF2α dependent. In PC12 cells, OD-PC was not found protective at the time points evaluated (2 h, 4 h and 6 h). In primary neurons, 6 h OD-PC was found protective against 6 h OGD insult. In both PC12 cells and primary neurons, OGD-PC exhibited significant cytoprotection; however, the effect was time-dependent and varied between these two cell types. In PC12 cells, 4 h (but not 2 h) OGD-PC was cytoprotective; whereas in primary neurons, both 2 h and 4 h of OGD-PC protected against 6 h OGD insult. In both PC12 cells and primary, the cytoprotective effect of OD-PC and OGD-PC corresponded with the time points for upregulation of HIF1α and / or HIF2α and their downstream genes.

Novel PHD inhibitors (FG2216, FG4592, GSK1278863, Bayer85-3934) were studied alongside non-specific DMOG in PC12 cells. In primary neurons, only FG4592 was pursued as a representative of novel PHD inhibitors. At 100μM, all the PHD inhibitors were not cytotoxic in PC12 cells and primary neurons. The PHD inhibitors at 100μM promoted autophagy in PC12 cells and so did FG4592 (30μM) and DMOG (100μM) in primary neurons. HIF1α was upregulated by all the PHD inhibitors at 100μM except for DMOG, which stabilised HIF1α at 1 mM. In primary neurons, HIF1α was upregulated by FG4592 (30μM) and DMOG (100μM). Overall, results indicated that the novel class of PHD inhibitors have higher potency than DMOG.

Preconditioning with 100μM of PHD inhibitors (DMOG, FG2216, FG4592, GSK1278863, Bayer85-3934) for 24 h followed by 24 h reversion significantly protected PC12 cells against 6 h OGD insult. Similar responses were observed in

neurons with FG4592 (50μM and100μM) and DMOG (100μM and 250μM). In PC12 cells, DMOG showed a neuroprotective effect at 100μM, but HIF1α was not upregulated. This is because DMOG exerts effects on several pathways that coordinate metabolic adaptation to energy crisis and oxidative stress such as AMPK signalling. Exposure to the PHD inhibitor followed by a period of reversion resulted in genetic reprogramming and development of ischaemic tolerance.

Primary astrocytes were comparatively more resistant to OGD or OD insult than neurons. OGD (6 h) was not cytotoxic in primary astrocytes but it upregulated HIF1α and HIF2α. Cytotoxicity was observed from 48 h OD and 24 h of OGD onwards in primary astrocytes. ACM collected from astrocytes subjected to 6 h but not 24 h OGD followed by reversion was found cytoprotective in primary neurons against 6 h OGD insult. The OGD-ACM (6 h) promoted autophagy and *Vegf* upregulation but not HIF1α or HIF2α stabilisation. The EVs pellet isolated from 6 h OGD-ACM were not found protective in ischaemic neurons, however, the soluble supernatant alone conferred significant cytoprotection.

Overall, all the neuroprotective interventions explored activated either HIF1α, HIF2α, and / or autophagy in the cells. The link between HIF activation, autophagy, and ischaemic tolerance needs to be further investigated. Ischaemic tolerance is an effective strategy that has shown great promise *in vitro* and needs to be explored further for application for clinical use.

7.7 Future perspectives

As with any body of work, addressing research problems sheds light on additional avenues of investigation based on outputs generated and experimental parameters. For the experiments carried out here, we have evaluated directions this work could take to make some things clearer and address new questions raised through experimentation.

As discussed in Section 3.4, current *in vitro* models of ischaemia stroke have several limitations and need improvement. Firstly, the oxygen levels in the normoxic incubator (for normoxia and reperfusion) are relatively higher than *in vivo*. Therefore, it would be ideal to culture the cells (normoxia) or return the cells back (reperfusion) to oxygen levels of around 3-5% to closely mimic the *in vivo* environment. This could be performed with an alternative hypoxia chamber set to around 3% O_2 or using a system that automatically regulates oxygen and glucose levels. In addition to the oxygen levels, the glucose levels *in vitro* are also very high, therefore to mimic glucose levels *in vivo*; a continuous perfusion system that delivers media and removes waste at a constant rate over an extended period would be most suitable. One of the limitations of *in vitro* models is the lack of intact blood vessels and leucocyte infiltration, therefore developing a suitable 3D ischaemic stroke model would be beneficial for stroke therapeutics. For example, a microfluidic 3D model with several layers of living cells (neurons, astrocytes, endothelial cells, and microglia) and luminal flow (for leucocyte infiltration) in a perfused chamber would be ideal. Additionally, the incorporation of blood vessels into the 3D model to study angiogenesis and erythropoiesis could also be beneficial. Over the past decade, there have been several efforts to develop microfluidics or hydrogel-based 3D

models of *in vitro* brain. These models aim to closely mimic the human tissue and provide reproducible results. Currently *in vitro* ischaemia models apply OGD to the entire cell culture and fail to mimic focal ischaemia (Jorfi *et al*., 2018). Thus developing experimental 3D models where hypoxia can be applied to a particular region of interest would be appropriate. It has been reported that cells grown in 3D environments exhibit distinct phenotypes (astrocytes maintained in resting state) and would be of greater physiological relevance (Holloway and Gavins, 2017).

Alongside neurons, NVU consists of several cell types such as astrocytes, microglia, endothelial cells, OPCs and pericytes. As the PHD inhibitors were found protective in primary neurons, it would be interesting to study the effects of non-specific PHD inhibitors *versus* novel PHD inhibitors on protein and gene expression on all the different cells that form the NVU. Furthermore, the effectiveness of these PHD inhibitors should be evaluated against *in vitro* OGD insults in all the different cells forming the NVU. In addition, it would be interesting to develop primary neuron and astrocyte co-cultures to mimic the ischaemic core and evaluate the effectiveness of novel PHD inhibitors on the co-culture model.

Preconditioning with the novel PHD inhibitors has shown promise *in vitro* ischaemic stroke models thus future studies should be directed towards studying their effectiveness *in vivo*. *In vivo* studies would be beneficial to study the overall effect of PHD inhibitors on all the different cell types and the brain as a whole. Although *in vitro* cell model systems are cheaper and simpler to procure, their major drawback is their failure to capture inherent organ complexity. Studying preconditioning *in vivo*

addresses these shortcomings and can evaluate safety, efficacy and toxicity on organ systems.

The occurrence of ischaemic stroke is unpredictable, therefore postconditioning is a much more preferential treatment protocol because it can be applied after ischaemic stroke. Postconditioning with novel PHD inhibitors was not found effective *in vitro*, however, studies in the past have revealed that postconditioning with PHD inhibitors such as DFO and DMOG was associated with reduced complications such as sensorimotor dysfunction (Mu *et al.,* 2005; Nagel *et al.,* 2011). It is difficult to study postconditioning *in vitro* because its effectiveness cannot be merely measured by cell viability studies. Other outcomes such as effects on sensorimotor dysfunction and size of brain oedema are immeasurable *in vitro*. The effectiveness of postconditioning with the novel PHD inhibitors should be explored *in vivo.*

Preliminary results revealed that ACM collected from astrocytes subjected to 6 h OGD (but not 24 h OGD) was protective in primary neurons, therefore, it would be interesting to explore the differences in the cytokines, chemokines, and growth factors present in the ACM using LC-MS at different time points. Upon identifying the molecules that play an essential role, the effectiveness of individual molecules in the ACM can be evaluated in ischaemic neurons. In addition, it would be interesting to study the dose-dependent effectiveness of ACM and EVs on ischaemic neurons.

Appendices

Recipes for preparation of reagents used for Western blotting

Table 1. TBS-T (10X) recipe. The reagents were dissolved in 700ml distilled water and the pH was adjusted to 7.4 with concentrated hydrochloric acid before making up to 1 L with distilled water. 1 L of 1 x TBS-T was prepared by diluting 10x TBS-T 1:10 in distilled water.

Reagent	Amount
Tris- Base	60.2 g
Sodium chloride	87.7 g
Tween 20	10 ml

Table 2. Mild stripping buffer recipe. The reagents were dissolved in 700 mL distilled water and the pH was adjusted to 2.2 with concentrated hydrochloric acid before making up to 1 L with distilled water.

Reagent	Amount
Glycine	15 g
SDS	1 g
Tween 20	10 ml

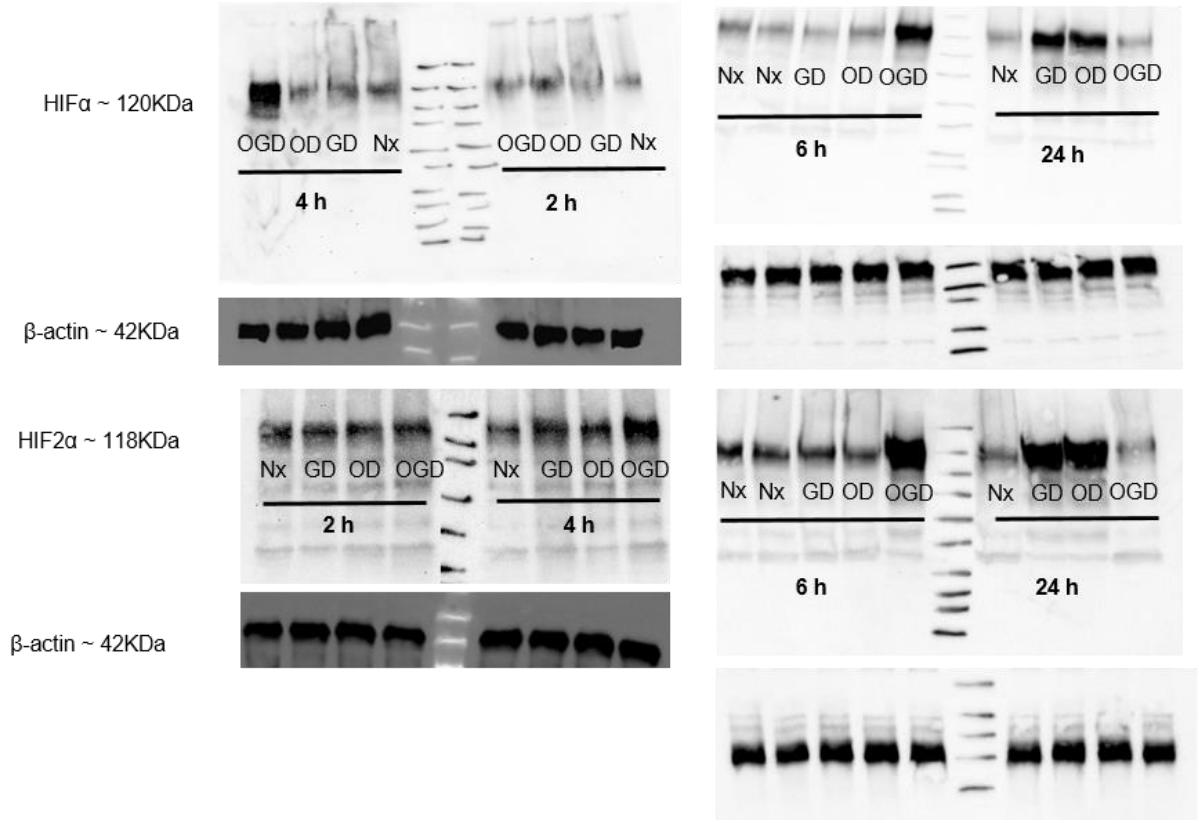

Figure 1. Representative western blot images Figure 3.6

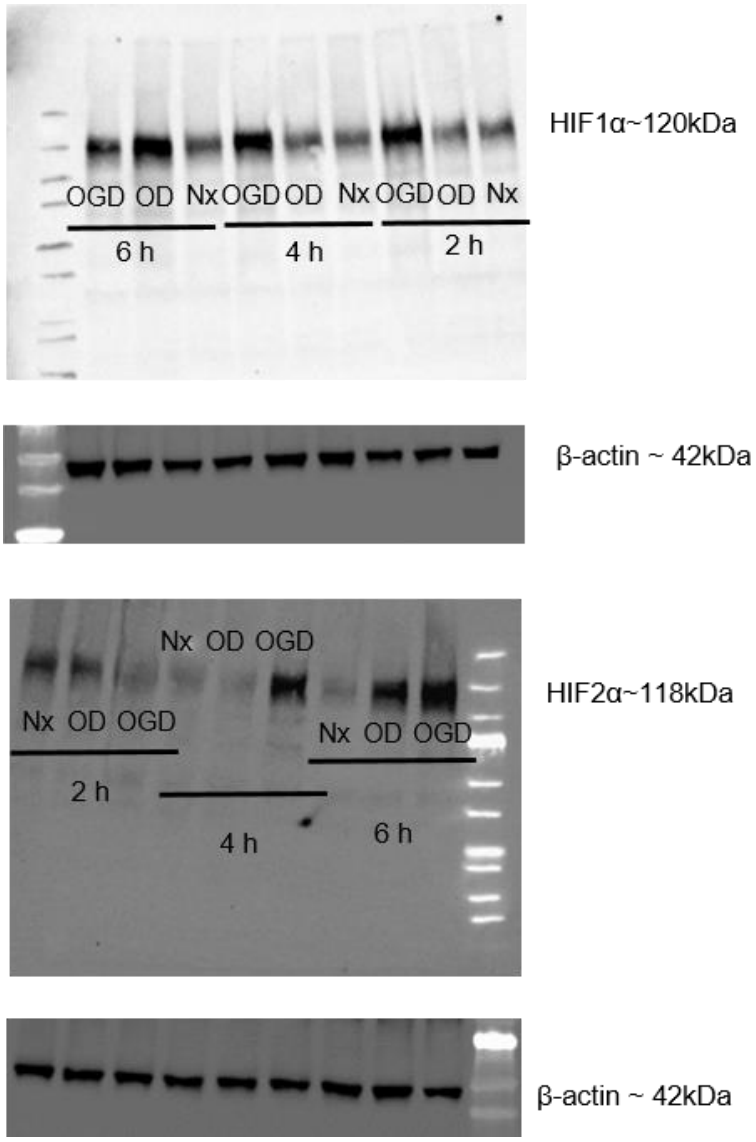

Figure 2. Representative western blot images for Figure 3.11

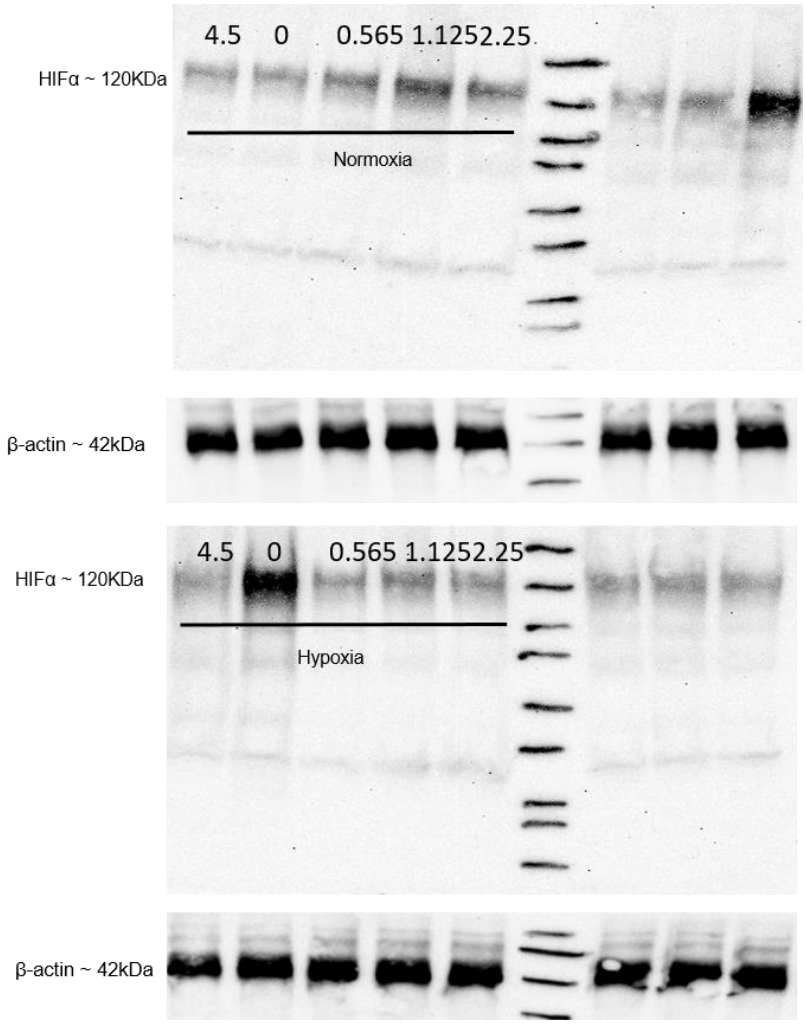

Figure 3. Representative western blot images for Figure 4.7

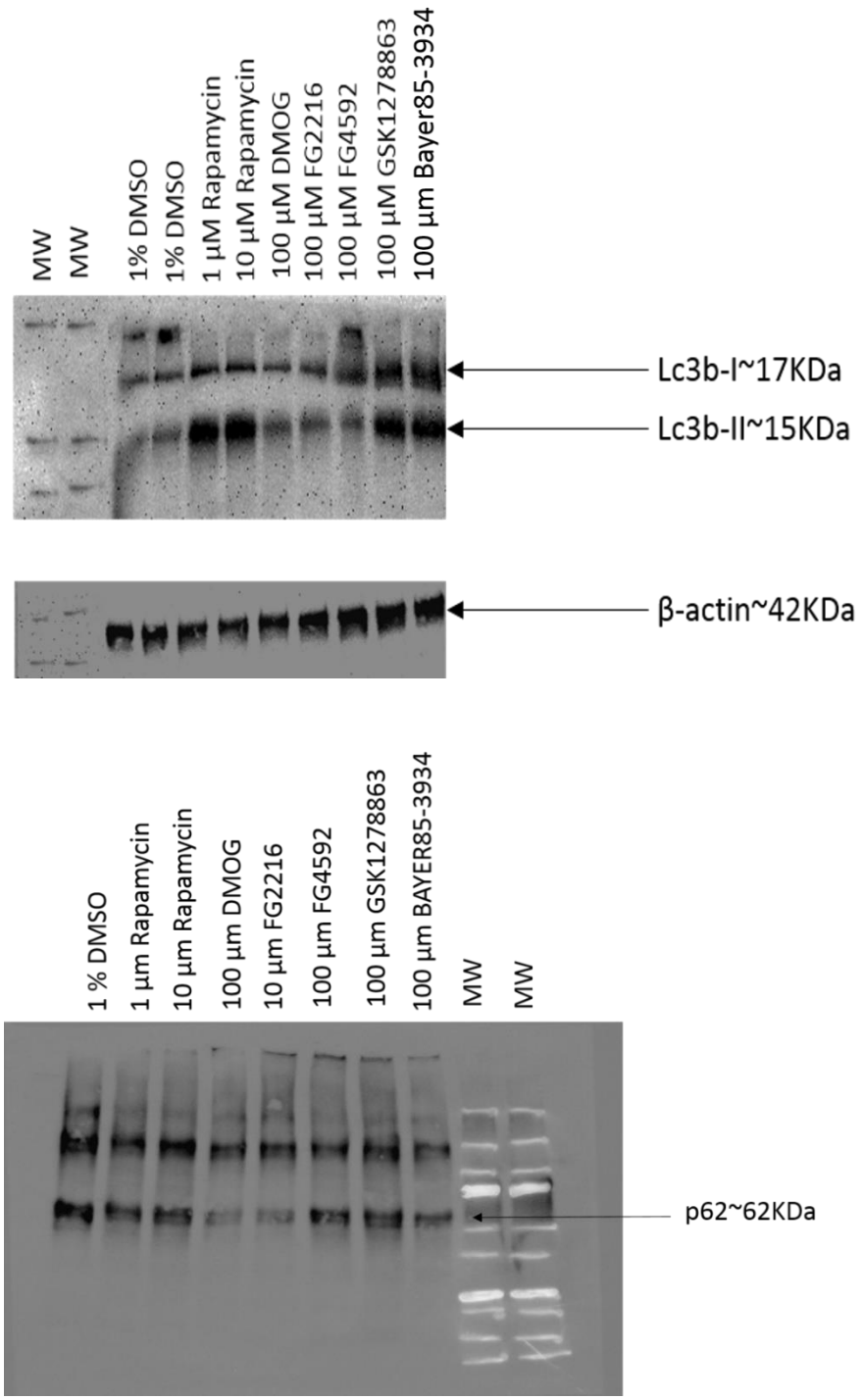
MW
MW
1% DMSO
1% DMSO
1 µM Rapamycin
10 µM Rapamycin
100 µM DMOG
100 µM FG2216
100 µM FG4592
100 µM GSK1278863
100 µm Bayer85-3934
Lc3b-I~17KDa
Lc3b-II~15KDa
β-actin~42KDa
1 % DMSO
1 µm Rapamycin
10 µm Rapamycin
100 µm DMOG
10 µm FG2216
100 µm FG4592
100 µm GSK1278863
100 µm BAYER85-3934
MW
MW
p62~62KDa

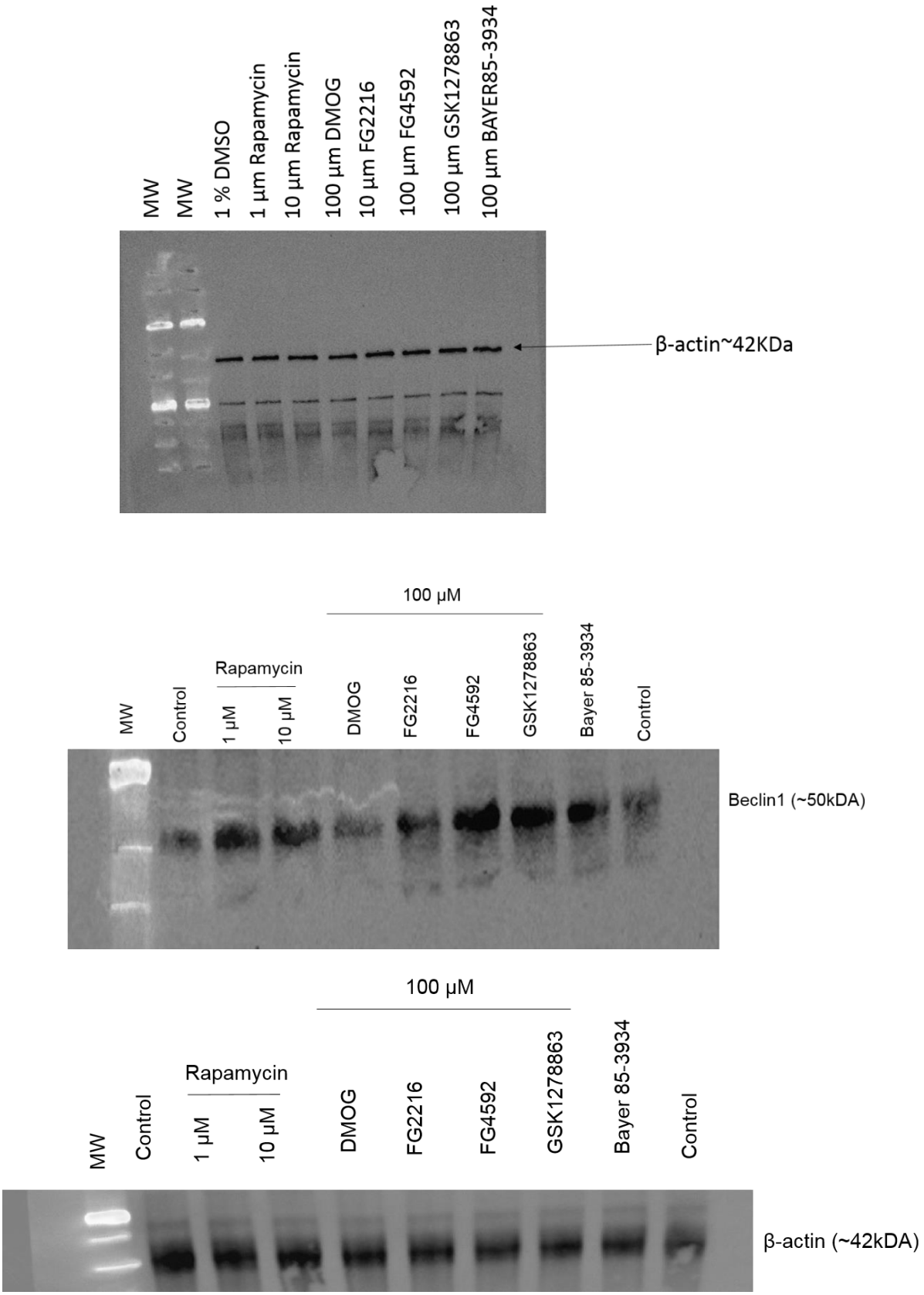

Figure 4. Representative western blot images for Figure 5.9

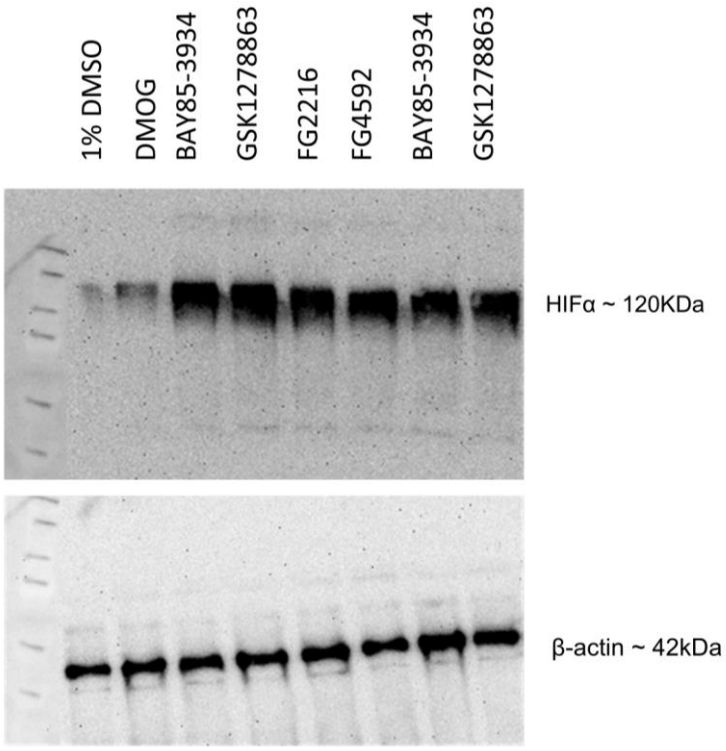

Figure 5. Representative western blot images for Figure 5.10.

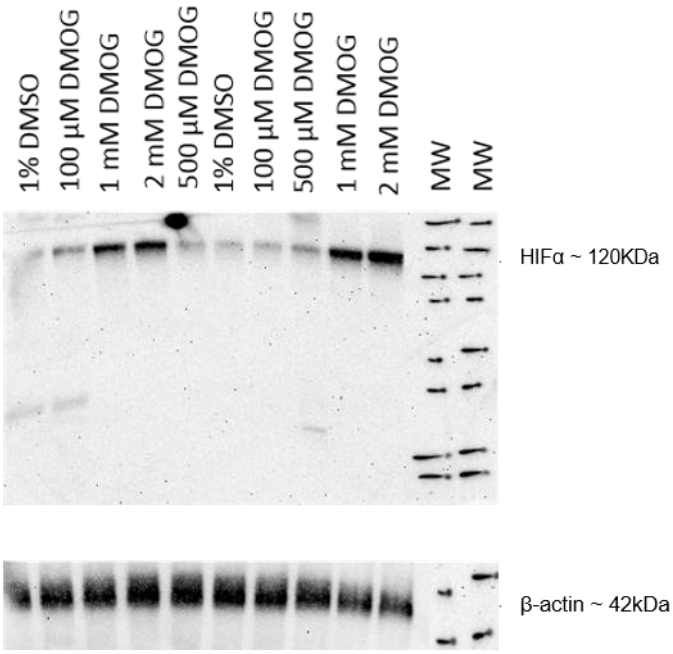

Figure 6. Representative western blot images for Figure 5.11.

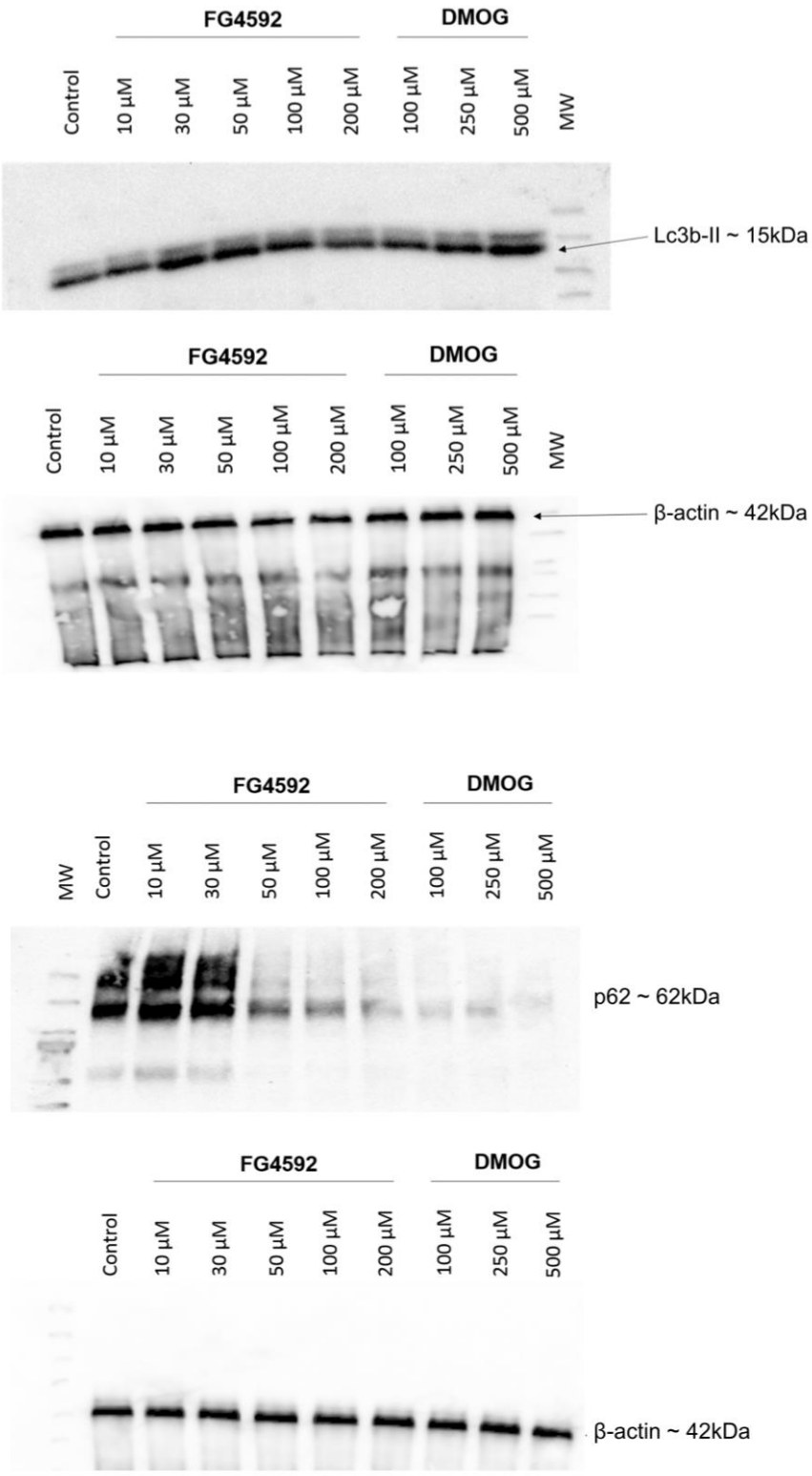

Figure 7. Representative western blot images for Figure 5.20.

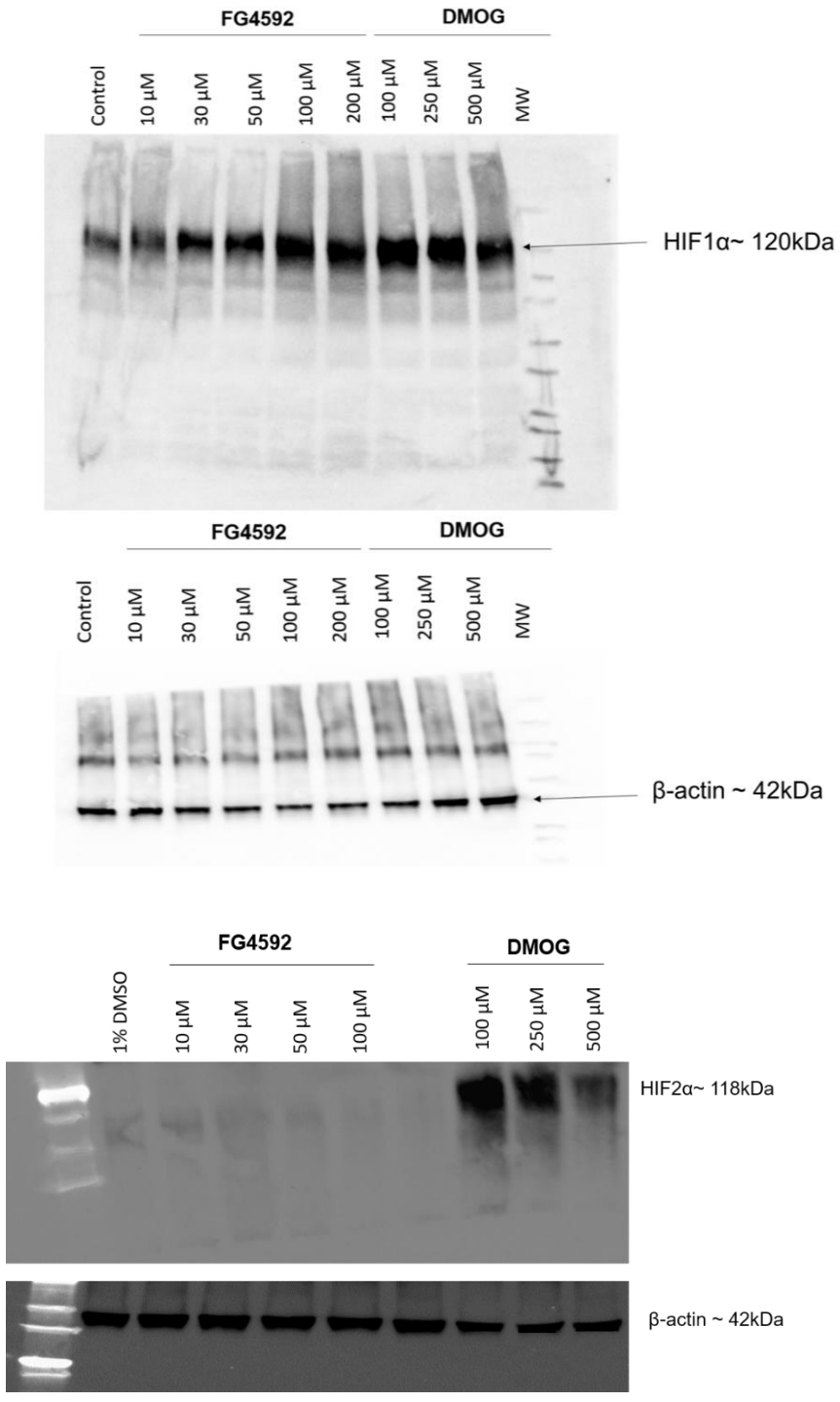

Figure 8. Representative western blot images for Figure 5.21.

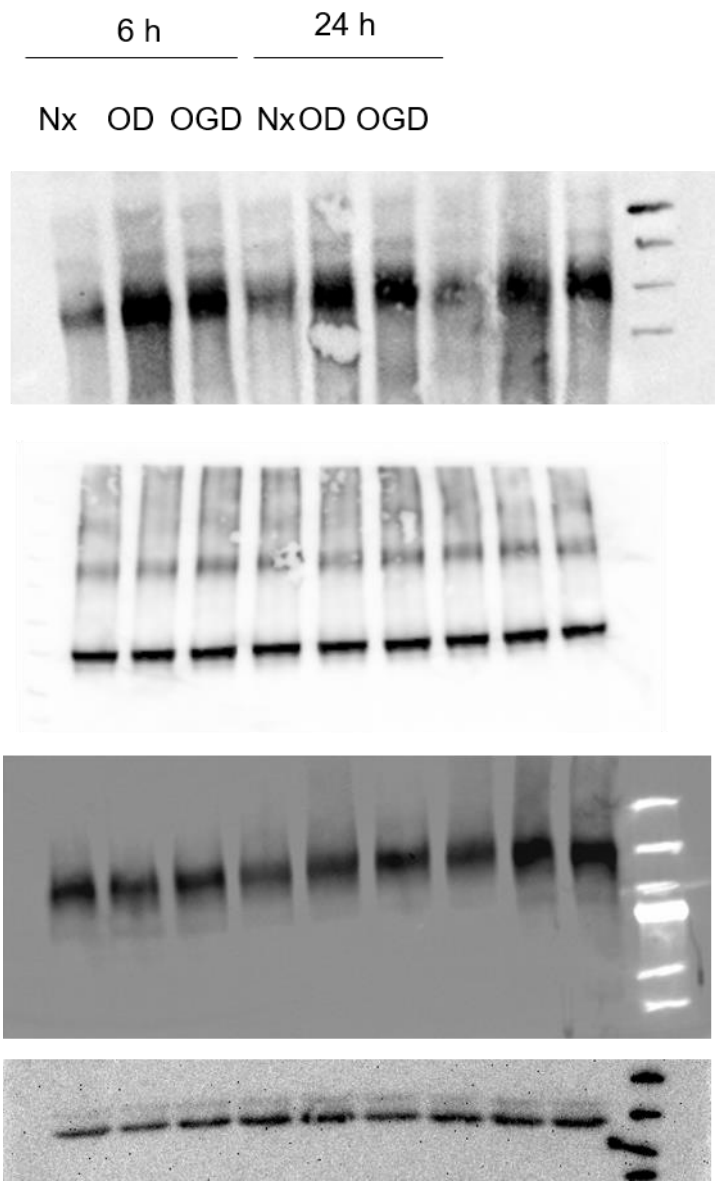

Figure 9. Representative western blot images for Figure 6.6.

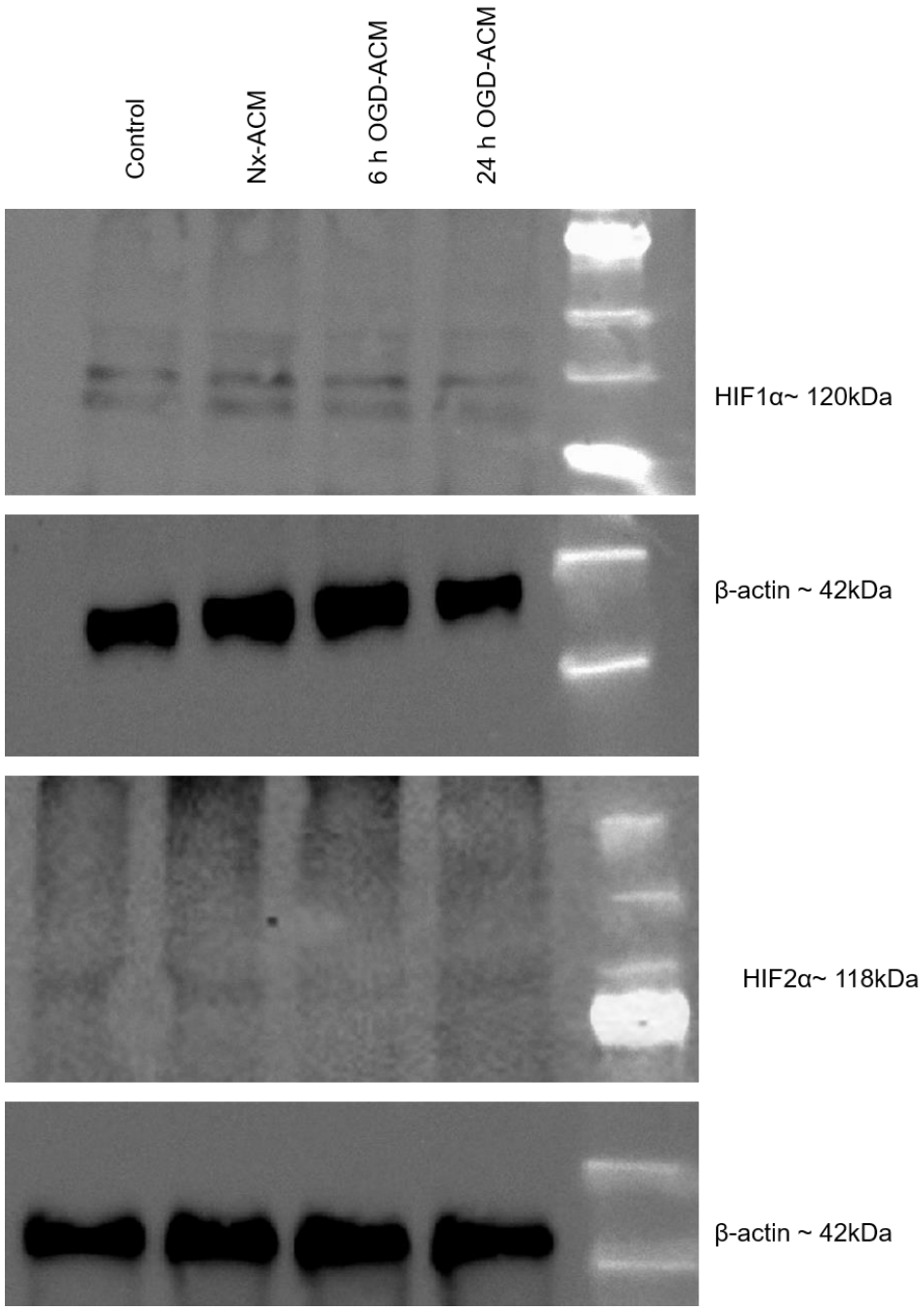

Figure 10. Representative western blot images for Figure 6.10.

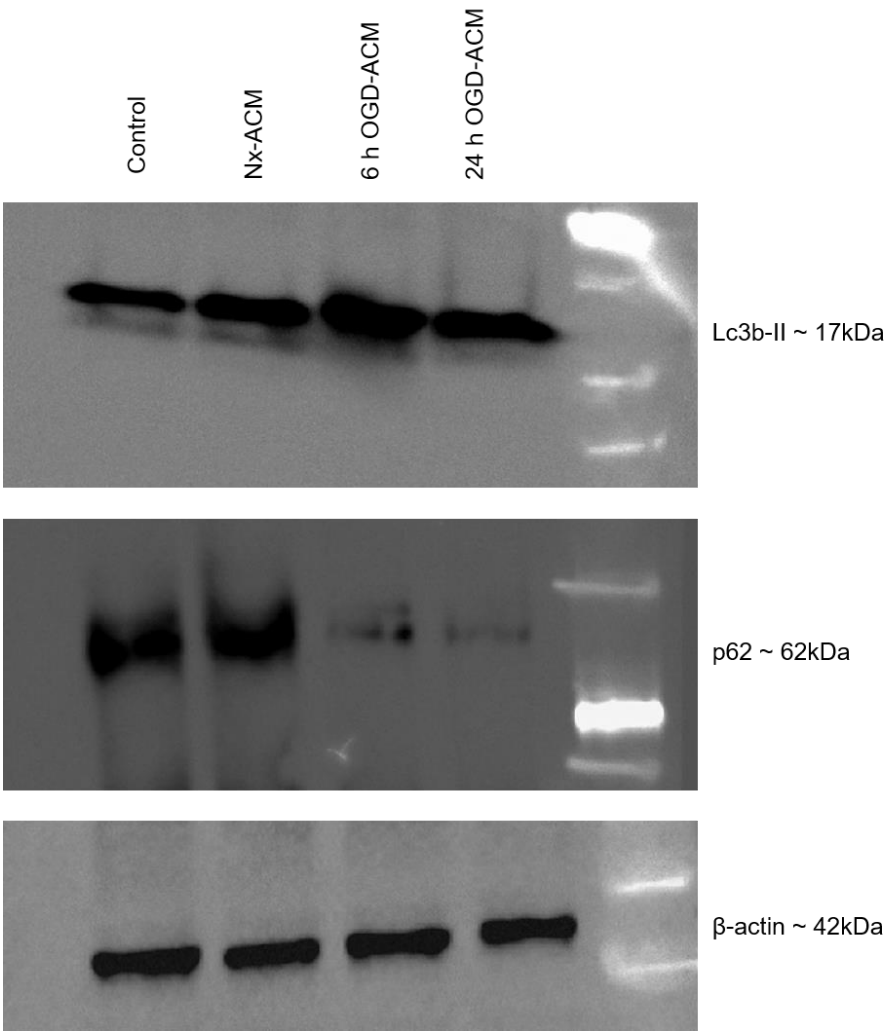

Figure 11. Representative western blot images for Figure 6.11.

References

ALIZADEH, J., GLOGOWSKA, A., THLIVERIS, J., KALANTARI, F., SHOJAEI, S., HOMBACH-KLONISCH, S., KLONISCH, T. and GHAVAMI, S., 2018. Autophagy modulates transforming growth factor beta 1 induced epithelial to mesenchymal transition in non-small cell lung cancer cells. *BBA - Molecular Cell Research,* **1865**(5), pp. 749-768.

ALMEIDA, A., DELGADO-ESTEBAN, M., BOLAÑOS, J.P. and MEDINA, J.M., 2002. Oxygen and glucose deprivation induces mitochondrial dysfunction and oxidative stress in neurones but not in astrocytes in primary culture. *Journal of neurochemistry,* **81**(2), pp. 207-217.

ALQAWLAQ, S., LIVINE-BAR, I., CHAN, D. and SIVAK, J.M., 2016. Retinal astrocytes protect neurons against metabolic stress by inducing the PI3K pathway. *Investigative opthalmology and visual science,* **57**(12), pp. 4213-4230.

AMARAL, A.I., TEIXEIRA, A.P., MARTENS, S., BERNAL, V., SOUSA, M.F.Q. and ALVES, P.M., 2010. Metabolic alterations induced by ischemia in primary cultures of astrocytes: merging 13C NMR spectroscopy and metabolic flux analysis. *Journal of neurochemistry,* **113**(3), pp. 735-748.

ANDERSEN, K.K., OLSEN, T.S., DEHLENDORFF, C. and KAMMERSGAARD, L.P., 2009. Hemorrhagic and ischemic strokes compared: stroke severity, mortality, and risk factors. *Stroke,* **40**(6), pp. 2068-2072.

ANTONIC, A., SENA, E., DONNAN, G. and HOWELLS, D., 2012. Human In Vitro Models of Ischaemic Stroke: a Test Bed for Translation. *Translational Stroke Research,* **3**(3), pp. 306-309.

ANTTILA, V., HAAPANEN, H., YANNOPOULOS, F., HERAJÄRVI, J., ANTTILA, T. and JUVONEN, T., 2016. Review of remote ischemic preconditioning: from laboratory studies to clinical trials. *Scandinavian Cardiovascular Journal: 50 Years Anniversary Issue,* **50**(5), pp. 355-361.

APPELHOFF, R.J., TIAN, Y., RAVAL, R.R., TURLEY, H., HARRIS, A.L., PUGH, C.W., RATCLIFFE, P.J. and GLEADLE, J.M., 2004. Differential Function of the Prolyl Hydroxylases PHD1, PHD2, and PHD3 in the Regulation of Hypoxia-inducible Factor. *The Journal of biological chemistry,* **279**(37), pp. 38458-38465.

ARIAZI, J.L., DUFFY, K.J., ADAMS, D.F., FITCH, D.M., LUO, L., PAPPALARDI, M., BIJU, M., DIFILIPPO, E.H., SHAW, T., WIGGALL, K. and ERICKSON-MILLER, C., 2017. Discovery and Preclinical Characterization of GSK1278863 (Daprodustat), a Small Molecule Hypoxia Inducible Factor–Prolyl Hydroxylase Inhibitor for Anemia. *The Journal of pharmacology and experimental therapeutics,* **363**(3), pp. 336-347.

ARTHUR, P.G., LIM, S.C.C., MELONI, B.P., MUNNS, S.E., CHAN, A. and KNUCKEY, N.W., 2004a. The protective effect of hypoxic preconditioning on cortical neuronal cultures is associated with increases in the activity of several antioxidant enzymes. *Brain Research,* **1017**(1), pp. 146-154.

ASLANTÜRK, O.S., 2018. *In Vitro Cytotoxicity and Cell Viability Assays: Principles, Advantages, and Disadvantages.* IntechOpen.

AWAN, M., MAKAULA, S., FORRESTI, S., SACK, M. and OPIE, L., 2000. Mechanisms whereby glucose deprivation triggers metabolic preconditioning in the isolated rat heart. *Molecular and Cellular Biochemistry,* **211**(1), pp. 111-121.

BADAWI, Y. and SHI, H., 2017. Relative Contribution of Prolyl Hydroxylase-Dependent and -Independent Degradation of HIF-1alpha by Proteasomal Pathways in Cerebral Ischemia. *Frontiers in neuroscience,* **11**, pp. 65-79

BADAWI, Y., RAMAMOORTHY, P. and SHI, H., 2012. Hypoxia-Inducible Factor 1 Protects Hypoxic Astrocytes against Glutamate Toxicity. *ASN neuro,* **4**(4), pp. 231-241.

BALLABH, P., BRAUN, A. and NEDERGAARD, M., 2004. The blood-brain barrier: an overview: structure, regulation, and clinical implications. *Neurobiology of disease,* **16**(1), pp. 1-13.

BARANOVA, O., MIRANDA, L.F., PICHIULE, P., DRAGATSIS, I., JOHNSON, R.S. and CHAVEZ, J.C., 2007. Neuron-specific inactivation of the hypoxia inducible factor 1 alpha increases brain injury in a mouse model of transient focal cerebral ischemia. *The Journal of neuroscience: the official journal of the Society for Neuroscience,* **27**(23), pp. 6320-6323.

BARRETO, G.E., GONZALEZ, J., TORRES, Y. and MORALES, L., 2011. Astrocytic-neuronal crosstalk: Implications for neuroprotection from brain injury. *Neuroscience Research,* **71**(2), pp. 107-113.

BARRETO, G.E., ROBIN E.W., YIBING O., LIJUN, X. and RONA G.G., 2011. Astrocytes: Targets for Neuroprotection in Stroke. *Central Nervous System Agents in Medicinal Chemistry,* **11**(2), pp. 164-173.

BARTECZEK, P., LI, L., ERNST, A., BÖHLER, L., MARTI, H.H. and KUNZE, R., 2017. Neuronal HIF-1α and HIF-2α deficiency improves neuronal survival and

sensorimotor function in the early acute phase after ischemic stroke. *Journal of Cerebral Blood Flow & Metabolism,* **37**(1), pp. 291-306.

BECERRA-CALIXTO, A. and CARDONA-GÓMEZ, G.P., 2017. The Role of Astrocytes in Neuroprotection after Brain Stroke: Potential in Cell Therapy. *Frontiers in molecular neuroscience,* **10**, pp. 88.

BECK, H., JESKE, M., THEDE, K., STOLL, F., FLAMME, I., AKBABA, M., ERGÜDEN, J., KARIG, G., KELDENICH, J., OEHME, F., MILITZER, H., HARTUNG, I.V. and THUSS, U., 2018. Discovery of Molidustat (BAY 85-3934): A Small-Molecule Oral HIF-Prolyl Hydroxylase (HIF-PH) Inhibitor for the Treatment of Renal Anemia. *, Medical Chemistry,* **13**(10), pp. 988-1003.

BÉLANGER, M., 2009. The role of astroglia in neuroprotection. *Dialogues in clinical neuroscience,* **11**(3), pp. 281-295.

BERGERON, M., GIDDAY, J.M., YU, A.Y., SEMENZA, G.L., FERRIERO, D.M. and SHARP, F.R., 2000. Role of hypoxia-inducible factor-1 in hypoxia-induced ischemic tolerance in neonatal rat brain. *Annals of Neurology,* **48**(3), pp. 285-296.

BERGERON, M., YU, A.Y., SOLWAY, K.E., SEMENZA, G.L. and SHARP, F.R., 1999. Induction of hypoxia-inducible factor-1 (HIF-1) and its target genes following focal ischaemia in rat brain. *European Journal of Neuroscience,* **11**(12), pp. 4159-4170.

BERNAUDIN, M., BELLAIL, A., MARTI, H.H., YVON, A., VIVIEN, D., DUCHATELLE, I., MACKENZIE, E.T. and PETIT, E., 2000. Neurons and astrocytes express EPO mRNA: Oxygen-sensing mechanisms that involve the redox-state of the brain. *Glia,* **30**(3), pp. 271-278.

BERNAUDIN, M., NEDELEC, A., DIVOUX, D., MACKENZIE, E.T., PETIT, E. and SCHUMANN-BARD, P., 2002. Normobaric Hypoxia Induces Tolerance to Focal Permanent Cerebral Ischemia in Association With an Increased Expression of Hypoxia-Inducible Factor-1 and Its Target Genes, Erythropoietin and VEGF, in the Adult Mouse Brain. *Journal of Cerebral Blood Flow & Metabolism,* **22**(4), pp. 393-403.

BERRA, E., ROUX, D., VOLMAT, V., BENIZRI, E., POUYSSÉGUR, J. and GINOUVÈS, A., 2003. HIF prolyl-hydroxylase 2 is the key oxygen sensor setting low steady-state levels of HIF-1α in normoxia. *The EMBO Journal,* **22**(16), pp. 4082-4090.

BHASIN, A., SRIVASTAVA, M.V.P., MOHANTY, S., VIVEKANANDHAN, S., SHARMA, S., KUMARAN, S. and BHATIA, R., 2016. Paracrine Mechanisms of Intravenous Bone Marrow-Derived Mononuclear Stem Cells in Chronic Ischemic Stroke. *Cerebrovascular diseases extra,* **6**(3), pp. 107-119.

BHUIYAN, M.I.H., KIM, H., KIM, S.Y. and CHO, K., 2011. The Neuroprotective Potential of Cyanidin-3-glucoside Fraction Extracted from Mulberry Following Oxygen-glucose Deprivation. *The Korean Journal of Physiology & Pharmacology,* **15**(6), pp. 353-361.

BICKLER, P.E., CLARK, J.P., GABATTO, P. and BROSNAN, H., 2015. Hypoxic preconditioning and cell death from oxygen / glucose deprivation co-opt a subset of the unfolded protein response in hippocampal neurons. *Neuroscience,* **310**, pp. 306-321.

BLANCO-SUAREZ, E., and HANLEY, J.G., 2014. Distinct Subunit-specific α-Amino-3-hydroxy-5-methyl-4-isoxazolepropionic Acid (AMPA) Receptor Trafficking

Mechanisms in Cultured Cortical and Hippocampal Neurons in Response to Oxygen and Glucose Deprivation. *The Journal of biological chemistry,* **289**(8), pp. 4644-4651.

BLUHMKI, E., CHAMORRO, Á, DÁVALOS, A., MACHNIG, T., SAUCE, C., WAHLGREN, N., WARDLAW, J. and HACKE, W., 2009. Stroke treatment with alteplase given 3·0–4·5 h after onset of acute ischaemic stroke (ECASS III): additional outcomes and subgroup analysis of a randomised controlled trial. *Lancet Neurology,* **8**(12), pp. 1095-1102.

BO, H., WEI, L., YULIN, S., LANPING, Z., YANG, X., and XIAOHANG, Z., 2014. A Prolyl-Hydroxylase Inhibitor, Ethyl-3,4-Dihydroxybenzoate, Induces Cell Autophagy and Apoptosis in Esophageal Squamous Cell Carcinoma Cells via Up-Regulation of BNIP3 and N-myc Downstream-Regulated Gene-1. *PLoS One,* **9**(9), pp. 107-114.

BONDE, C., NORABERG, J. and ZIMMER, J., 2002. Nuclear shrinkage and other markers of neuronal cell death after oxygen–glucose deprivation in rat hippocampal slice cultures. *Neuroscience letters,* **327**(1), pp. 49-52.

BOPP, S.K. and LETTIERI, T., 2008. Comparison of four different colorimetric and fluorometric cytotoxicity assays in a zebrafish liver cell line. *BMC pharmacology,* **8**(1), pp. 1-8.

BÖTTCHER, M., LENTINI, S., ARENS, E.R., KAISER, A., MEY, D., THUSS, U., KUBITZA, D. and WENSING, G., 2018. First-in-man–proof of concept study with molidustat: a novel selective oral HIF-prolyl hydroxylase inhibitor for the treatment of renal anaemia. *British Journal of Clinical Pharmacology,* **84**(7), pp. 1557-1565.

BREWER, G.J., 1995. Serum-free B27 / neurobasal medium supports differentiated growth of neurons from the striatum, substantia nigra, septum, cerebral cortex, cerebellum, and dentate gyrus. *Journal of Neuroscience Research,* **42**(5), pp. 674-683.

BRITISH NATIONAL FORMULARY, 2017. Atlepase. 72 edn. London: BMJ and Pharmaceutical Press,

BROUGHTON, B.R.S., REUTENS, D.C., and SOBEY, C.G., 2009. Apoptotic Mechanisms After Cerebral Ischemia. *Stroke,* **40**(5), pp. e331.

BRUICK, R.K. and MCKNIGHT, S.L., 2001. A Conserved Family of Prolyl-4-Hydroxylases That Modify HIF. *Science,* **294**(5545), pp. 1337-1340.

BUFFO, A., ROLANDO, C.M., and CERUTI, S., 2010. Astrocytes in the damaged brain: Molecular and cellular insights into their reactive response and healing potential. *Biochemical Pharmacology,* **79**(2), pp. 77-89.

BURMISTROVA, O., OLIAS-ARJONA, A., LAPRESA, R., JIMENEZ-BLASCO, D., EREMEEVA, T., SHISHOV, D., ROMANOV, S., ZAKURDAEVA, K., ALMEIDA, A., FEDICHEV, P.O. and BOLAÑOS, J.P., 2019. Targeting PFKFB3 alleviates cerebral ischemia-reperfusion injury in mice. *Scientific reports,* **9**(1), pp. 1670

BURR, S., COSTA, A.H., GRICE, G., TIMMS, R., LOBB, I., FREISINGER, P., DODD, R., DOUGAN, G., LEHNER, P., FREZZA, C. and NATHAN, J., 2016. Mitochondrial Protein Lipoylation and the 2-Oxoglutarate Dehydrogenase Complex Controls HIF1α Stability in Aerobic Conditions. *Cell Metabolism,* **24**(5), pp. 740-752.

BYLICKY, M.A., MUELLER, G.P. and DAY, R.M., 2018. Mechanisms of Endogenous Neuroprotective Effects of Astrocytes in Brain Injury. *Oxidative medicine and cellular longevity,* **2018**, pp. 650-666.

CALLAHAN, D.J., ENGLE, M.J. and VOLPE, J.J., 1990. Hypoxic Injury to Developing Glial Cells: Protective Effect of High Glucose. *Pediatric research,* **27**(2), pp. 186-190.

CARLOS, L., JUAN, P.P., ALEJANDRO, L., ANLLELY, F., and URSULA, W., 2016. MiRNAs in Astrocyte-Derived Exosomes as Possible Mediators of Neuronal Plasticity. *Journal of Experimental Neuroscience,* **2016**(Suppl. 1), pp. 1-9.

CARRERAS, F.J., ARANDA, C.J., PORCEL, D., RODRIGUEZ-HURTADO, F., MARTÍNEZ-AGUSTIN, O. and ZARZUELO, A., 2015. Expression of glucose transporters in the prelaminar region of the optic-nerve head of the pig as determined by immunolabeling and tissue culture. *PloS one,* **10**(6), pp. e018516.

CHAN, M.C., HOLT-MARTYN, J.P., SCHOFIELD, C.J. and RATCLIFFE, P.J., 2016. Pharmacological targeting of the HIF hydroxylases – A new field in medicine development. *Molecular Aspects of Medicine,* **47-48**, pp. 54-75.

CHAN, M.C., ILOTT, N.E., SCHÖDEL, J., SIMS, D., TUMBER, A., LIPPL, K., MOLE, D.R., PUGH, C.W., RATCLIFFE, P.J., PONTING, C.P. and SCHOFIELD, C.J., 2016. Tuning the Transcriptional Response to Hypoxia by Inhibiting Hypoxia-inducible Factor (HIF) Prolyl and Asparaginyl Hydroxylases. *The Journal of biological chemistry,* **291**(39), pp. 20661-20673.

CHAUDHURI, A.D., DASTGHEYB, R.M., YOO, S., TROUT, A., TALBOT, J., C Conover, HAO, H., WITWER, K.W. and HAUGHEY, N.J., 2018. TNFα and lL-1β

modify the miRNA cargo of astrocyte shed extracellular vesicles to regulate neurotrophic signaling in neurons. *Cell death & disease*, **9**(3), pp. 363-18.

CHAVEZ, J.C., BARANOVA, O., LIN, J. and PICHIULE, P., 2006. The Transcriptional Activator Hypoxia Inducible Factor 2 (HIF-2 / EPAS-1) Regulates the Oxygen-Dependent Expression of Erythropoietin in Cortical Astrocytes. *Journal of Neuroscience,* **26**(37), pp. 9471-9481.

CHEN, R., LAI, U.H., ZHU, L., SINGH, A., AHMED, M. and FORSYTH, N.R., 2018. Reactive Oxygen Species Formation in the Brain at Different Oxygen Levels: The Role of Hypoxia Inducible Factors. *Frontiers in cell and developmental biology,* **6**, pp. 132-144.

CHEN, C., HU, Q., YAN, J., LEI, J., QIN, L., SHI, X., LUAN, L., YANG, L., WANG, K., HAN, J., NANDA, A. and ZHOU, C., 2007. Multiple effects of 2ME2 and D609 on the cortical expression of HIF-1alpha and apoptotic genes in a middle cerebral artery occlusion-induced focal ischemia rat model. *Journal of neurochemistry,* **102**(6), pp. 1831-1844.

CHEN, H., LI, H., CAO, F., ZHEN, L., BAI, J., YUAN, S. and MEI, Y., 2012. 1,2,3,4,6-penta-O-galloyl-β-D-glucose protects PC12 Cells from MPP+-mediated cell death by inducing heme oxygenase-1 in an ERK- and Akt-dependent manner. *Journal of Huazhong University of Science and Technology [Medical Sciences],* **32**(5), pp. 737-745.

CHEN, N., QIAN, J., CHEN, J., YU, X., MEI, C., HAO, C., JIANG, G., LIN, H., ZHANG, X., ZUO, L., HE, Q., FU, P., LI, X., NI, D., HEMMERICH, S., LIU, C., SZCZECH, L., BESARAB, A., NEFF, T.B., YU, K.P. and VALONE, F.H., 2017. Phase 2 studies of oral hypoxia-inducible factor prolyl hydroxylase inhibitor FG-4592

for treatment of anemia in China. *Nephrology, Dialysis and Transplantation*, 32(8), pp. 1373-1386.

CHEN, R.L., OGUNSHOLA, O.O., YEOH, K.K., JANI, A., PAPADAKIS, M., NAGEL, S., SCHOFIELD, C.J. and BUCHAN, A.M., 2014. HIF prolyl hydroxylase inhibition prior to transient focal cerebral ischaemia is neuroprotective in mice. *Journal of Neurochemistry,* **131**(2), pp. 177-189.

CHEN, Q., MOULDER, K., TENKOVA, T., HARDY, K., OLNEY, J.W. and ROMANO, C., 1999. Excitotoxic Cell Death Dependent on Inhibitory Receptor Activation. *Experimental neurology,* **160**(1), pp. 215-225.

CHEN, W., OSTROWSKI, R.P., OBENAUS, A. and ZHANG, J.H., 2009. Prodeath or prosurvival: Two facets of hypoxia inducible factor-1 in perinatal brain injury. *Experimental Neurology,* **216**(1), pp. 7-15.

CHENG, B., CHEN, J., YANG, S., CHIO, C., LIU, S. and CHEN, R., 2017. Cobalt chloride treatment induces autophagic apoptosis in human glioma cells via a p53-dependent pathway. *International journal of oncology,* **50**(3), pp. 964-974.

CHOI, Y.K., PARK, J.H., YUN, J., CHA, J., KIM, Y., WON, M., KIM, K., HA, K., KWON, Y. and KIM, Y., 2018. Heme oxygenase metabolites improve astrocytic mitochondrial function via a Ca2+-dependent HIF-1α / ERRα circuit. *PloS one,* **13**(8), pp. 20-39.

CHU, K., JUNG, K., KIM, J., KIM, S.U., KIM, M., KIM, S., LEE, S.K., LEE, S., PARK, H., SONG, E. and ROH, J., 2008. Transplantation of human neural stem cells protect against ischemia in a preventive mode via hypoxia-inducible factor-1α stabilization in the host brain. *Brain Research,* **1207**, pp. 182-192.

COHEN, J. and TORRES, C., 2019. Astrocyte senescence: Evidence and significance. *Aging Cell,* **18**(3), pp. e12937.

COHEN, T., DORIT NAHARI, LEA WEISS CEREM, GERA NEUFELD and BEN-ZION LEVI, 1996. Interleukin 6 Induces the Expression of Vascular Endothelial Growth Factor. *Journal of Biological Chemistry,* **271**(2), pp. 736-741.

CONSTANTINO, L., BINDER, L., VANDRESEN-FILHO, S., VIOLA, G., LUDKA, F., LOPES, M., LEAL, R. and TASCA, C., 2018. Role of Phosphatidylinositol-3 Kinase Pathway in NMDA Preconditioning: Different Mechanisms for Seizures and Hippocampal Neuronal Degeneration Induced by Quinolinic Acid. *Neurotoxicity Research,* **34**(3), pp. 452-462.

DALGARD, C.L., LU, H., MOHYELDIN, A. and VERMA, A., 2004. Endogenous 2-oxoacids differentially regulate expression of oxygen sensors. *Biochemical journal,* **380**(Pt 2), pp. 419-424.

DANG, C.V. and SEMENZA, G.L., 1999. Oncogenic alterations of metabolism. *Trends in Biochemical Sciences,* **24**(2), pp. 68-72.

DAVE, K.R., SAUL, I., BUSTO, R., GINSBERG, M.D., SICK, T.J. and PÉREZ-PINZÓN, M.A., 2001. Ischemic Preconditioning Preserves Mitochondrial Function After Global Cerebral Ischemia in Rat Hippocampus. *Journal of Cerebral Blood Flow & Metabolism,* **21**(12), pp. 1401-1410.

DAVIS, C.K., JAIN, S.A., BAE, O., MAJID, A. and RAJANIKANT, G.K., 2018. Hypoxia Mimetic Agents for Ischemic Stroke. *Frontiers in cell and developmental biology,* **6**, pp. 175-182.

DESSI, F., CHARRIAUT-MARLANGUE, C. and BEN-ARI, Y., 1994. Glutamate-induced neuronal death in cerebellar culture is mediated by two distinct components: a sodium-chloride component and a calcium component. *Brain research,* **650**(1), pp. 49-55.

DHANDAPANI, K.M., HADMAN, M., DE SEVILLA, L., WADE, M.F., MAHESH, V.B. and BRANN, D.W., 2003. Astrocyte protection of neurons: role of transforming growth factor-beta signaling via a c-Jun-AP-1 protective pathway. *The Journal of biological chemistry,* **278**(44), pp. 43329-43339.

DIRNAGL, U., 2012. Pathobiology of injury after stroke: the neurovascular unit and beyond. *Annals of the New York Academy of Sciences,* **1268**(1), pp. 21-25.

DIRNAGL, U., IADECOLA, C. and MOSKOWITZ, M.A., 1999. Pathobiology of ischaemic stroke: an integrated view*. Trends in Neuroscience,* **22**(9), pp. 391-397

DIRNAGL, U., MD, BECKER, K., MD and MEISEL, A., MD, 2009. Preconditioning and tolerance against cerebral ischaemia: from experimental strategies to clinical use. *Lancet Neurology,* **8**(4), pp. 398-412.

DORWEILER, B., PRUEFER, D., ANDRASI, T., MAKSAN, S., SCHMIEDT, W., NEUFANG, A. and VAHL, C., 2007. Ischemia-Reperfusion Injury. *European Journal of Trauma and Emergency Surgery,* **33**(6), pp. 600-612.

DOWELL, J.A., JOHNSON, J.A. and LI, L., 2009. Identification of Astrocyte Secreted Proteins with a Combination of Shotgun Proteomics and Bioinformatics. *Journal of Proteome Research,* **8**(8), pp. 4135-4143.

DU, F., WU, X.M., GONG, Q., HE, X. and KE, Y., 2011. Hyperthermia conditioned astrocyte-cultured medium protects neurons from ischemic injury by the up-

regulation of HIF-1 alpha and the increased anti-apoptotic ability. *European Journal of Pharmacology,* **666**(1), pp. 19-25.

DURÁN, R.V., MACKENZIE, E.D., BOULAHBEL, H., FREZZA, C., HEISERICH, L., TARDITO, S., BUSSOLATI, O., ROCHA, S., HALL, M.N. and GOTTLIEB, E., 2013. HIF-independent role of prolyl hydroxylases in the cellular response to amino acids. *Oncogene*, **32**(38), pp. 4549-4556.

DURUKAN, A. and TATLISUMAK, T., 2007. Acute ischemic stroke: Overview of major experimental rodent models, pathophysiology, and therapy of focal cerebral ischemia. *Pharmacology, Biochemistry and Behavior,* **87**(1), pp. 179-197.

DURUKAN, A. and TATLISUMAK, T., 2010. Preconditioning-induced ischemic tolerance: a window into endogenous gearing for cerebroprotection. *Experimental & translational stroke medicine,* **2**(1), pp. 2-17.

EASTON, J.D., SAVER, J.L., ALBERS, G.W., ALBERTS, M.J., CHATURVEDI, S., FELDMANN, E., HATSUKAMI, T.S., HIGASHIDA, R.T., JOHNSTON, S.C., KIDWELL, C.S., LUTSEP, H.L., MILLER, E. and SACCO, R.L., 2009. Definition and Evaluation of Transient Ischemic Attack: A Scientific Statement for Healthcare Professionals From the American Heart Association/American Stroke Association Stroke Council; Council on Cardiovascular Surgery and Anesthesia; Council on Cardiovascular Radiology and Intervention; Council on Cardiovascular Nursing; and the Interdisciplinary Council on Peripheral Vascular Disease: The American Academy of Neurology affirms the value of this statement as an educational tool for neurologist. *Stroke,* **40**(6), pp. 2276-2293.

ELGENDY, I.Y., KUMBHANI, M.D., DHARAM. J., MAHMOUD, A., BHATT, A., and BAVRY, A.A., 2015. Mechanical Thrombectomy for Acute Ischemic Stroke. *Journal of the American College of Cardiology,* **66**(22), pp. 2498-2505.

ELKINS, J.M., HEWITSON, K.S., MCNEILL, L.A., SEIBEL, J.F., SCHLEMMINGER, I., PUGH, C.W., RATCLIFFE, P.J. and SCHOFIELD, C.J., 2003. Structure of Factor-inhibiting Hypoxia-inducible Factor (HIF) Reveals Mechanism of Oxidative Modification of HIF-1α. *The Journal of biological chemistry,* **278**(3), pp. 1802-1806.

ENGELHARDT, S., AL-AHMAD, A.J., GASSMANN, M. and OGUNSHOLA, O.O., 2014. Hypoxia Selectively Disrupts Brain Microvascular Endothelial Tight Junction Complexes Through a Hypoxia-Inducible Factor-1 (HIF-1) Dependent Mechanism. *Journal of Cellular Physiology,* **229**(8), pp. 1096-1105.

EPSTEIN, A.C.R., GLEADLE, J.M., MCNEILL, L.A., HEWITSON, K.S., O'ROURKE, J., MOLE, D.R., MUKHERJI, M., METZEN, E., WILSON, M.I., DHANDA, A., TIAN, Y., MASSON, N., HAMILTON, D.L., JAAKKOLA, P., BARSTEAD, R., HODGKIN, J., MAXWELL, P.H., PUGH, C.W., SCHOFIELD, C.J. and RATCLIFFE, P.J., 2001. C. elegans EGL-9 and Mammalian Homologs Define a Family of Dioxygenases that Regulate HIF by Prolyl Hydroxylation. *Cell,* **107**(1), pp. 43-54.

FAN, J., YI, L. and SHASHA, L., 2017. Nonhuman primate models of focal cerebral ischaemia. *Neural regeneration research,* **12**(2), pp. 321-328.

FIORELLA, P., FERDINANDO, R., and BARBARA C., 2011. Neuroprotection: The Emerging Concept of Restorative Neural Stem Cell Biology for the Treatment of Neurodegenerative Diseases. *Current Neuropharmacology,* **9**(2), pp. 313-317.

FRERET, T., VALABLE, S., CHAZALVIEL, L., SAULNIER, R., MACKENZIE, E.T., PETIT, E., BERNAUDIN, M., BOULOUARD, M., and SCHUMANN-BARD, P., 2006. Delayed administration of Deforoxamine reduces brain damage and promotes functional recovery after transient focal cerebral ischemia in the rat. *European Journal of Neuroscience,* **23**(7), pp. 1757-1765.

FUKUBA, H., TAKAHASHI, T., JIN, H.G., KOHRIYAMA, T. and MATSUMOTO, M., 2008. Abundance of aspargynyl-hydroxylase FIH is regulated by Siah-1 under normoxic conditions. *Neuroscience letters,* **433**(3), pp. 209-214.

GAO, C., CAI, Y., ZHANG, X., HUANG, H., WANG, J., WANG, Y., TONG, X., WANG, J. and WU, J., 2015. Ischemic Preconditioning Mediates Neuroprotection against Ischemia in Mouse Hippocampal CA1 Neurons by Inducing Autophagy. *PloS one,* **10**(9), pp. 137-146.

GÁSPÁR, T., KIS, B., SNIPES, J.A., LENZSÉR, G., MAYANAGI, K., BARI, F. and BUSIJA, D.W., 2006. Transient glucose and amino acid deprivation induces delayed preconditioning in cultured rat cortical neurons. *Journal of Neurochemistry,* **98**(2), pp. 555-565.

GEISERT, E.E. and FRANKFURTER, A., 1989. The neuronal response to injury as visualized by immunostaining of class III β-tubulin in the rat. *Neuroscience Letters,* **102**(2), pp. 137-141.

GHAVAMI, S., CUNNINGTON, R.H., GUPTA, S., YEGANEH, B., FILOMENO, K.L., FREED, D.H., CHEN, S., KLONISCH, T., HALAYKO, A.J., AMBROSE, E., SINGAL, R. and DIXON, I.M.C., 2015. Autophagy is a regulator of TGF-β1-induced fibrogenesis in primary human atrial myofibroblasts. *Cell death & disease,* **6**(3), pp.1696-1706.

GIDDAY, J.M., FITZGIBBONS, J.C., SHAH, A.R. and PARK, T.S., 1994. Neuroprotection from ischemic brain injury by hypoxic preconditioning in the neonatal rat. *Neuroscience Letters,* **168**(1), pp. 221-224.

GINSBERG, M.D., 2008. Neuroprotection for ischemic stroke: Past, present and future. *Neuropharmacology,* **55**(3), pp. 363-389.

GONZALEZ-PEREZ, O., LOPEZ-VIRGEN, V. and QUIÑONES-HINOJOSA, A., 2015. Astrocytes: everything but the glue. *Neuroimmunology and Neuroinflammation,* **2**(2), pp. 115-117.

GOUGEON, P., LOURENSSEN, S., HAN, T.Y., NAIR, D.G., ROPELESKI, M.J. and BLENNERHASSETT, M.G., 2013. The pro-inflammatory cytokines IL-1β and TNFα are neurotrophic for enteric neurons. *The Journal of neuroscience: the official journal of the Society for Neuroscience,* **33**(8), pp. 3339-3351.

GRAU, A.J., WEIMAR, C., BUGGLE, F., HEINRICH, A., GOERTLER, M., NEUMAIER, S., GLAHN, J., BRANDT, T., HACKE, W. and DIENER, H., 2001. Risk Factors, Outcome, and Treatment in Subtypes of Ischemic Stroke: The German Stroke Data Bank. *Stroke,* **32**(11), pp. 2559-2566.

GREENBERG, M, GREENE, L and ZIFF, B., 1985. Nerve growth factor and epidermal growth factor induce rapid transient changes in proto-oncogene transcription in PC12 cells. *Journal of Biological Chemistry,* **260**(26), pp. 14101.

GREIJER, A.E., 2004. The role of hypoxia inducible factor 1 (HIF-1) in hypoxia induced apoptosis. *Journal of Clinical Pathology,* **10**(57), pp. 1009.

GRISHCHUK, Y., GINET, V., TRUTTMANN, A.C., CLARKE, P.G.H. and PUYAL, J., 2011. Beclin 1-independent autophagy contributes to apoptosis in cortical neurons. *Autophagy,* **7**(10), pp. 1115-1131.

GRYSIEWICZ, R.A., THOMAS, K. and PANDEY, D.K., 2008. Epidemiology of Ischemic and Haemorrhagic Stroke: Incidence, Prevalence, Mortality, and Risk Factors. *Neurologic Clinics,* **26**(4), pp. 871-895.

GUNN, A., SINGH, A., DIAO, A. and CHEN, R., 2018. Pharmacological Modulation of Autophagy for Neuroprotection in Ischaemic Stroke. *Journal of Experimental Stroke & Translational Medicine,* **11**(1), pp. 87-92.

GURER, G., GURSOY-OZDEMIR, Y., ERDEMLI, E., CAN, A. and DALKARA, T., 2009. Astrocytes are More Resistant to Focal Cerebral Ischemia than Neurons and Die by a Delayed Necrosis. *Brain pathology (Zurich, Switzerland),* **19**(4), pp. 630-641.

GUO, H., KONG, S., CHEN, W., DAI, Z., LIN, T., SU, J., LI, S., XIE, Q., SU, Z., XU, Y. and LAI, X., 2014. Apigenin Mediated Protection of OGD-Evoked Neuron-Like Injury in Differentiated PC12 Cells. *Neurochemical Research,* **39**(11), pp. 2197-2210.

GUPTA, N. and WISH, J.B., 2017. Hypoxia-Inducible Factor Prolyl Hydroxylase Inhibitors: A Potential New Treatment for Anaemia in Patients With CKD. *American Journal of Kidney Diseases,* **69**(6), pp. 815-826.

GURUSWAMY, R. and ELALI, A., 2017. Complex Roles of Microglial Cells in Ischemic Stroke Pathobiology: New Insights and Future Directions. *International journal of molecular sciences,* **18**(3), pp. 496-502.

HAASE, V.H., 2017. HIF-prolyl hydroxylases as therapeutic targets in erythropoiesis and iron metabolism. *Hemodialysis International,* **21**(S1), pp. S110-S124.

HACKE. W., GEOFFREY. D., CESARE, F., MARKKU., K., and RUDIGER., V.K., 2004. Association of outcome with early stroke treatment: pooled analysis of ATLANTIS, ECASS, and NINDS rt-PA stroke trials. *The Lancet,* **363**(9411), pp. 768-774.

HACKE, W., KASTE, M., BLUHMKI, E., BROZMAN, M., DAVALOS, A., GUIDETTI, D., LARRUE, V., LEES, K.R., MEDEGHRI, Z., MACHNIG, T., SCHNEIDER, D., VON KUMMER, R., WAHLGREN, N., TONI, D. and ECASS INVESTIGATORS, 2008. Thrombolysis with Alteplase 3 to 4.5 Hours after Acute Ischemic Stroke. *The New England Journal of Medicine,* **359**(13), pp. 1317-1329.

HAHN, C.D., MANLHIOT, C., SCHMIDT, M.R., NIELSEN, T.T. and REDINGTON, A.N., 2011. Remote ischemic per-conditioning: a novel therapy for acute stroke? *Stroke,* **42**(10), pp. 2960-2962.

HALTERMAN, M.W., MILLER. C.C and FEDEROFF, H.J., 1999. Hypoxia inducibe factor 1 alpha mediates hypoxia-induced delayed neuronal death that involves p53. *The journal of neuroscience,* **19**(16), pp. 18-24.

HAMRICK, S.E.G., MCQUILLEN, P.S., JIANG, X., MU, D., MADAN, A. and FERRIERO, D.M., 2005. A role for hypoxia-inducible factor-1α in Desferrioxamine neuroprotection. *Neuroscience Letters,* **379**(2), pp. 96-100.

HANSON, L.R., ANNINA, R., PAULA, M.M., VALERIE, G.C., DONALD, C.S., RESHMA, J.R., DIANNE, L.M., JOHN, D, HOEKMAN, R.B., MATTHEWS, W.H., SCOTT, P., 2009. Intranasal Deforoxamine Provides Increased Brain Exposure and

Significant Protection in Rat Ischemic Stroke. *Journal of Pharmacology and Experimental Therapeutics,* **330**(3), pp. 679-686.

HARVEY, B.K., HOFFER, B.J. and WANG, Y., 2005. Stroke and TGF-β proteins: glial cell line-derived neurotrophic factor and bone morphogenetic protein. *Pharmacology and Therapeutics,* **105**(2), pp. 113-125.

HAYAKAWA, K., ESPOSITO, E., WANG, X., TERASAKI, Y., LIU, Y., XING, C., JI, X. and LO, E.H., 2016. Transfer of mitochondria from astrocytes to neurons after stroke. *Nature,* **535**(7613), pp. 551-555.

HELTON, R., CUI, J., SCHEEL, J.R., ELLISON, J.A., AMES, C., GIBSON, C., BLOUW, B., OUYANG, L., DRAGATSIS, I., ZEITLIN, S., JOHNSON, R.S., LIPTON, S.A. and BARLOW, C., 2005. Brain-specific knock-out of hypoxia-inducible factor-1alpha reduces rather than increases hypoxic-ischemic damage. *The Journal of neuroscience,* **25**(16), pp. 4099-4107.

HEPPONSTALL, M., IGNJATOVIC, V., BINOS, S., MONAGLE, P., JONES, B., CHEUNG, M.H.H., D'UDEKEM, Y. and KONSTANTINOV, I.E., 2012. Remote Ischemic Preconditioning (RIPC) Modifies Plasma Proteome in Humans. *PloS one,* **7**(11), pp. 482-484.

HERAS-SANDOVAL, D., PÉREZ-ROJAS, J.M., HERNÁNDEZ-DAMIÁN, J. and PEDRAZA-CHAVERRI, J., 2014. The role of PI3K / AKT / mTOR pathway in the modulation of autophagy and the clearance of protein aggregates in neurodegeneration. *Cellular Signalling,* **26**(12), pp. 2694-2701.

HERAVI, M., DARGAHI, L., PARSAFAR, S., TAYARANIAN MARVIAN, A., ALIAKBARI, F. and MORSHEDI, D., 2019. The primary neuronal cells are more

resistant than PC12 cells to α-synuclein toxic aggregates. *Neuroscience Letters,* **701**, pp. 38-47.

HERCULANO-HOUZEL, S., 2014. The glia / neuron ratio: How it varies uniformly across brain structures and species and what that means for brain physiology and evolution. *Glia,* **62**(9), pp. 1377-1391.

HESS, D.C., Prof, WECHSLER, L.R., Prof, CLARK, W.M., Prof, SAVITZ, S.I., Prof, FORD, G.A., Prof, CHIU, D., Prof, YAVAGAL, D.R., Prof, UCHINO, K., Prof, LIEBESKIND, D.S., Prof, AUCHUS, A.P., Prof, SEN, S., Prof, SILA, C.A., Prof, VEST, J.D., PhD and MAYS, R.W., PhD, 2017. Safety and efficacy of multipotent adult progenitor cells in acute ischaemic stroke (MASTERS): a randomised, double-blind, placebo-controlled, phase 2 trial. *Lancet neurology,* **16**(5), pp. 360-368.

HIGASHIDA, T., KREIPKE, C.W., RAFOLS, J.A., PENG, C., SCHAFER, S., SCHAFER, P., DING, J.Y., DORNBOS, D., LI, X., GUTHIKONDA, M., ROSSI, N.F. and DING, Y., 2011. The role of hypoxia-inducible factor-1α, aquaporin-4, and matrix metalloproteinase-9 in blood-brain barrier disruption and brain oedema after traumatic brain injury. *Journal of Neurosurgery,* **114**(1), pp. 92-101.

HILL, M.D., 2014. Alteplase in acute ischaemic stroke: the need for speed. *Lancet,* **384**(9958), pp. 1904-1906.

HILLION, J.A., LI, Y., MARIE, D., TAKANOHASHI, A., KLIMANIS, D., BARKER, J.L. and HALLENBEEK, J.M., 2006. Involvement of Akt in preconditioning-induced tolerance to ischemia in PC12 cells. *Journal of Cerebral Blood Flow & Metabolism,* **26**(10), pp. 1323-1331.

HILLION, J.A., TAKAHASHI, K., MARIC, D., RUETZLER, C., BARKER, J.L. and HALLENBECK, J.M., 2005. Development of an ischemic tolerance model in a PC12 cell line. *Journal of Cerebral Blood Flow & Metabolism,* **25**(2), pp. 154-162.

HIRA, K., UENO, Y., TANAKA, R., MIYAMOTO, N., YAMASHIRO, K., INABA, T., URABE, T., OKANO, H. and HATTORI, N., 2018. Astrocyte-Derived Exosomes Treated With a Semaphorin 3A Inhibitor Enhance Stroke Recovery via Prostaglandin D2 Synthase. *Stroke,* **49**(10), pp. 2483-2494.

HIRAYAMA, Y., IKEDA-MATSUO, Y., NOTOMI, S., ENAIDA, H., KINOUCHI, H. and KOIZUMI, S., 2015. Astrocyte-Mediated Ischemic Tolerance. *The Journal of neuroscience,* **35**(9), pp. 3794-3805.

HISHAM, N.F. and BAYRAKTUTAN, U., 2013. Epidemiology, pathophysiology, and treatment of hypertension in ischaemic stroke patients. *Journal of stroke and cerebrovascular diseases,* **22**(7), pp. 4-14.

HOCQUETTE, J., BALAGE, M. and FERRÉ, P., 1996. Facilitative glucose transporters in ruminants. *Proceedings of the Nutrition Society,* **55**(1B), pp. 221-236.

HOLLOWAY, P. and GAVINS, F., 2016. Modeling Ischemic Stroke In Vitro: Status Quo and Future Perspectives. *Stroke,* **47**(2), pp. 561-569.

HOLMQUIST-MENGELBIER, L., FREDLUND, E., LÖFSTEDT, T., NOGUERA, R., NAVARRO, S., NILSSON, H., PIETRAS, A., VALLON-CHRISTERSSON, J., BORG, A., GRADIN, K., POELLINGER, L. and PÅHLMAN, S., 2006. Recruitment of HIF-1alpha and HIF-2alpha to common target genes is differentially regulated in neuroblastoma: HIF-2alpha promotes an aggressive phenotype. *Cancer cell,* **10**(5), pp. 413-423.

HONG, S., YANG, H., MANAENKO, A., LU, J., MEI, Q. and HU, Q., 2019. Potential of Exosomes for the Treatment of Stroke. *Cell Transplantation*, **28**(6), pp. 662-667

HU, S., DONG, H., ZHANG, H., WANG, S., HOU, L., CHEN, S., ZHANG, J. and XIONG, L., 2012. Non-invasive limb remote ischemic preconditioning contributes neuroprotective effects via activation of adenosine A1 receptor and redox status after transient focal cerebral ischemia in rats. *Brain Research,* **1459**, pp. 81-90.

HUANG, L.E., GU, J., SCHAU, M. and BUNN, H.F., 1998. Regulation of Hypoxia-Inducible Factor 1α is Mediated by an O2-dependent Degradation Domain via the Ubiquitin-Proteasome Pathway. *Proceedings of the National Academy of Sciences - PNAS,* **95**(14), pp. 7987-7992.

HUBER, G. and MATUS, A., 1984. Differences in the cellular distributions of two microtubule-associated proteins, MAP1 and MAP2, in rat brain. *Journal of Neuroscience,* **4**(1), pp. 151-160.

HUMMITZSCH, L., ZITTA, K., BERNDT, R., WONG, Y.L., RUSCH, R., HESS, K., WEDEL, T., GRUENEWALD, M., CREMER, J., STEINFATH, M. and ALBRECHT, M., 2019. Remote ischemic preconditioning attenuates intestinal mucosal damage: insight from a rat model of ischemia-reperfusion injury. *Journal of translational medicine,* **17**(1), pp. 136-144.

HUNG, C., LIOU, Y., LU, S., TSENG, L., KAO, C., CHEN, S., CHIOU, S. and CHANG, C., 2010. Stem cell-based neuroprotective and neurorestorative strategies. *International journal of molecular sciences,* **11**(5), pp. 2039-2055.

ISAACS, J.S., JUNG, Y.J., MOLE, D.R., LEE, S., TORRES-CABALA, C., CHUNG, Y., MERINO, M., TREPEL, J., ZBAR, B., TORO, J., RATCLIFFE, P.J., LINEHAN,

W.M. and NECKERS, L., 2005. HIF overexpression correlates with biallelic loss of fumarate hydratase in renal cancer: Novel role of fumarate in regulation of HIF stability. *Cancer cell,* **8**(2), pp. 143-153.

JAILLARD, A., CORNU, C., DURIEUX, A., MOULIN, T., BOUTITIE, F., LEES, K.R. and HOMMEL, M., 1999. Haemorrhagic transformation in acute ischemic stroke (The MAST-E study). *Stroke,* **30**(7), pp. 1326-1332.

JANG, M., PARK, R., KIM, H., NAMKOONG, S., JO, D., HUH, Y.H., JANG, I., LEE, J.I. and PARK, J., 2018. AMPK contributes to autophagosome maturation and lysosomal fusion. *Scientific reports,* **8**(1), pp. 12637-10.

JAUCH, E.C., SAVER, J.L., ADAMS, J., Harold P, BRUNO, A., CONNORS, J.J.B., DEMAERSCHALK, B.M., KHATRI, P., MCMULLAN, J., Paul W, QURESHI, A.I., ROSENFIELD, K., SCOTT, P.A., SUMMERS, D.R., WANG, D.Z., WINTERMARK, M. and YONAS, H., 2013. Guidelines for the early management of patients with acute ischemic stroke: a guideline for healthcare professionals from the American Heart Association / American Stroke Association. *Stroke; a journal of cerebral circulation,* **44**(3), pp. 870-881.

JONES, N.M. and BERGERON, M., 2001. Hypoxic Preconditioning Induces Changes in HIF-1 Target Genes in Neonatal Rat Brain. *Journal of Cerebral Blood Flow & Metabolism,* **21**(9), pp. 1105-1114.

JONES, N.M., KARDASHYAN, L., CALLAWAY, J.K., LEE, E.M. and BEART, P.M., 2008. Long-term functional and protective actions of preconditioning with hypoxia, cobalt chloride, and Desferrioxamine against hypoxic-ischemic injury in neonatal rats. *Paediatric research,* **63**(6), pp. 620-624.

JONES, N.M., LEE, E.M., BROWN, T.G., JARROTT, B. and BEART, P.M., 2006. Hypoxic preconditioning produces differential expression of hypoxia-inducible factor-1α (HIF-1α) and its regulatory enzyme HIF prolyl hydroxylase 2 in neonatal rat brain. *Neuroscience Letters,* **404**(1), pp. 72-77.

JONES, S.M., ELLIOTT, J.P. and NOVAK, A.E., 2013. The role of HIF in cobalt-induced ischemic tolerance. *Neuroscience,* **252**, pp. 420-430.

JORFI, M., D'AVANZO, C., KIM, D.Y. and IRIMIA, D., 2018. Three-Dimensional Models of the Human Brain Development and Diseases. *Advanced Healthcare Materials,* **7**(1), pp. 1700-1723.

JOVIČIĆ, A. and GITLER, A.D., 2017. Distinct repertoires of microRNAs present in mouse astrocytes compared to astrocyte-secreted exosomes. *PloS one,* **12**(2), pp. e0171418.

JURCOVICOVA, J., 2014. Glucose transport in brain – effect of inflammation. *Endocrine regulations,* **48**(1), pp. 35-48.

KACHOIE, P., POURGHOLAMI, M.H., BAHRAMI-B, F., BADAR, S. and MORRIS, D.L., 2015. Minocycline attenuates hypoxia-inducible factor-1α expression correlated with modulation of p53 and AKT / mTOR / p70S6K / 4E-BP1 pathway in ovarian cancer: in vitro and in vivo studies. *American journal of cancer research,* **5**(2), pp. 575-588.

KAELIN, W.G. and RATCLIFFE, P.J., 2008. Oxygen Sensing by Metazoans: The Central Role of the HIF Hydroxylase Pathway. *Molecular Cell,* **30**(4), pp. 393-402.

KANG, R., ZEH, H.J., LOTZE, M.T., and TANG, D., 2011. The Beclin 1 network regulates autophagy and apoptosis. *Cell Death and Differentiation,* **18**(4), pp. 571-580.

KARAR, J. and MAITY, A., 2011. PI3K / AKT / mTOR Pathway in Angiogenesis. *Frontiers in Molecular Neuroscience,* **4**, pp. 51-62.

KARUPPAGOUNDER, S.S. and RATAN, R.R., 2012. Hypoxia-Inducible Factor Prolyl Hydroxylase Inhibition: Robust New Target or Another Big Bust for Stroke Therapeutics? *Journal of Cerebral Blood Flow & Metabolism,* **32**(7), pp. 1347-1361.

KEASEY, M., SCOTT, H., BANTOUNAS, I., UNEY, J. and KELLY, S., 2016. MiR-132 Is Upregulated by Ischemic Preconditioning of Cultured Hippocampal Neurons and Protects them from Subsequent OGD Toxicity. *Journal of Molecular Neuroscience,* **59**(3), pp. 404-410.

KELLEHER, J.A., CHAN, P.H., CHAN, T.Y. and GREGORY, G.A., 1993. Modification of hypoxia-induced injury in cultured rat astrocytes by high levels of glucose. *Stroke,* **24**(6), pp. 855-863.

KENNETH, N.S. and ROCHA, S., 2008. Regulation of gene expression by hypoxia. *The Biochemical journal,* **414**(1), pp. 19-32.

KHATRI, R., MCKINNEY, A.M., SWENSON, B. and JANARDHAN, V., 2012. Blood-brain barrier, reperfusion injury, and haemorrhagic transformation in acute ischemic stroke. *Neurology,* **79**(13), pp. 52-54.

KIM, K., SHIN, D., KIM, J., SHIN, Y., RAJANIKANT, G.K., MAJID, A., BAEK, S. and BAE, O., 2018. Role of Autophagy in Endothelial Damage and Blood-Brain Barrier Disruption in Ischemic Stroke. *Stroke,* **49**(6), pp. 1571-1579.

KIM, Y., PARK, J. and CHOI, Y.K., 2019. The Role of Astrocytes in the Central Nervous System Focused on BK Channel and Heme Oxygenase Metabolites: A Review. *Antioxidants (Basel, Switzerland),* **8**(5), pp. 121-128.

KITAGAWA, K., MATSUMOTO, M., TAGAYA, M., HATA, R., UEDA, H., NIINOBE, M., HANDA, N., FUKUNAGA, R., KIMURA, K., MIKOSHIBA, K. and KAMADA, T., 1990. 'Ischemic tolerance' phenomenon found in the brain. *Brain Research,* **528**(1), pp. 21-24.

KINTNER, D.B., WANG, Y. and SUN, D., 2007. Role of membrane ion transport proteins in cerebral ischemic damage. *Frontiers in bioscience,* **12**(1), pp. 762-770.

KIYONO, K., SUZUKI, H.I., MATSUYAMA, H., MORISHITA, Y., KOMURO, A., KANO, M.R., SUGIMOTO, K. and MIYAZONO, K., 2009. Autophagy is activated by TGF-beta and potentiates TGF-beta-mediated growth inhibition in human hepatocellular carcinoma cells. *Cancer research,* **69**(23), pp. 8844-8852.

KONTANI, S., NAGATA, E., UESUGI, T., MORIYA, Y., FUJII, N., MIYATA, T. and TAKIZAWA, S., 2013. A Novel Prolyl Hydroxylase Inhibitor Protects Against Cell Death After Hypoxia. *Neurochemical Research,* **38**(12), pp. 2588-2594.

KORNILOV, R., PUHKA, M., MANNERSTRÖM, B., HIIDENMAA, H., PELTONIEMI, H., SILJANDER, P., SEPPÄNEN-KAIJANSINKKO, R. and KAUR, S., 2018. Efficient ultrafiltration-based protocol to deplete extracellular vesicles from fetal bovine serum. *Journal of Extracellular Vesicles,* **7**(1), pp. 1422-1434.

KOSZEGI, Z., FIUZA, M. and HANLEY, J.G., 2017. Endocytosis and lysosomal degradation of GluA2 / 3 AMPARs in response to oxygen / glucose deprivation in hippocampal but not cortical neurons. *Scientific reports,* **7**(1), pp. 12312-12318.

KOTHARI, R., SAUERBECK, L., JAUCH, E., BRODERICK, J., BROTT, T., KHOURY, J. and LIU, T., 1997. Patients' Awareness of Stroke Signs, Symptoms, and Risk Factors. *Stroke,* **28**(10), pp. 1871-1875.

KRISTENSEN, B., MALM, J., CARLBERG, B., STEGMAYR, B., BACKMAN, C., FAGERLUND, M. and OLSSON, T., 1997. Epidemiology and Etiology of Ischemic Stroke in Young Adults Aged 18 to 44 Years in Northern Sweden. *Stroke,* **28**(9), pp. 1702-1709.

Lin, L., Wang, X., and Yu, Z., 2016. Ischemia-reperfusion Injury in the Brain: Mechanisms and Potential Therapeutic Strategies. *Biochemistry & pharmacology: open access,* **5**(4),.

LAHIANI, A., ZAHAVI, E., NETZER, N., OFIR, R., PINZUR, L., RAVEH, S., ARIEN-ZAKAY, H., YAVIN, E. and LAZAROVICI, P., 2015. Human placental expanded (PLX) mesenchymallike adherent stromal cells confer neuroprotection to nerve growth factor (NGF)-differentiated PC12 cells exposed to ischemia by secretion of IL-6 and VEGF. *BBA - Molecular Cell Research*, **1853**(2), pp. 422-430.

LAKHAN, S.E., KIRCHGESSNER, A., TEPPER, D. and LEONARD, A., 2013. Matrix metalloproteinases and blood-brain barrier disruption in acute ischemic stroke. *Frontiers in neurology,* **4**, pp. 32-40.

LANGE, S., BAK, L., WAAGEPETERSEN, H., SCHOUSBOE, A. and NORENBERG, M., 2012. Primary Cultures of Astrocytes: Their Value in Understanding Astrocytes in Health and Disease. *Neurochemical Research,* **37**(11), pp. 2569-2588.

LAU, L.T. and YU, A.C., 2001. Astrocytes Produce and Release Interleukin-1, Interleukin-6, Tumor Necrosis Factor Alpha and Interferon-Gamma Following Traumatic and Metabolic Injury. *Journal of Neurotrauma,* **18**(3), pp. 351-359.

LEE, S., SHAFE, A.C.E. and COWIE, M.R., 2011. UK stroke incidence, mortality and cardiovascular risk management 1999-2008: time-trend analysis from the General Practice Research Database. *BMJ open,* **1**(2), pp. 269-274.

LEGGE, S., KOCH, G., DIOMEDI, M., STANZIONE, P. and SALLUSTIO, F., 2012. Stroke prevention: managing modifiable risk factors. *Stroke Research and Treatment,* **2012**, pp. 391-398.

LEVY, M., CRAWFORD, J., DIB, N., VERKH, L., TANKOVICH, N. and CRAMER, S., 2019. Phase I/II Study of Safety and Preliminary Efficacy of Intravenous Allogeneic Mesenchymal Stem Cells in Chronic Stroke. *Stroke (1970),* **50**(10), pp. 2835-2841.

LI, C., LIAO, P., YANG, Y., HUANG, S., LIN, C., CHENG, Y. and KANG, J., 2014. Minocycline accelerates hypoxia-inducible factor-1 alpha degradation and inhibits hypoxia-induced neovasculogenesis through prolyl hydroxylase, von Hippel–Lindau-dependent pathway. *Archives of Toxicology,* **88**(3), pp. 659-671.

LI, H., GAO, A., FENG, D., WANG, Y., ZHANG, L., CUI, Y., LI, B., WANG, Z. and CHEN, G., 2014. Evaluation of the Protective Potential of Brain Microvascular Endothelial Cell Autophagy on Blood–Brain Barrier Integrity During Experimental Cerebral Ischemia–Reperfusion Injury. *Translational Stroke Research,* **5**(5), pp. 618-626.

LI, H., WU, J., SHEN, H., YAO, X., LIU, C., PIANTA, S., HAN, J., BORLONGAN, C.V. and CHEN, G., 2018. Autophagy in hemorrhagic stroke: Mechanisms and clinical implications. *Progress in Neurobiology,* **163-164**, pp. 79-97.

LI, J., ZHANG, S., LIU, X., HAN, D., XU, J. and MA, Y., 2018. Neuroprotective effects of leonurine against oxygen-glucose deprivation by targeting Cx36 / CaMKII in PC12 cells. *PloS one,* **13**(7), pp. 20-28.

LI, P., KASLAN, M., LEE, S.H., YAO, J. and GAO, Z., 2017. Progress in Exosome Isolation Techniques. *Theranostics,* **7**(3), pp. 789-804.

LI, X., CUI, X., CHEN, Y., WU, T., XU, H., YIN, H. and WU, Y., 2018. Therapeutic Potential of a Prolyl Hydroxylase Inhibitor FG-4592 for Parkinson's Diseases in Vitro and in Vivo : Regulation of Redox Biology and Mitochondrial Function. *Frontiers in Aging Neuroscience,* **10**, pp. 121-130.

LI, Y., DING, S., XIAO, L., GUO, W. and ZHAN, Q., 2008. Desferrioxamine preconditioning protects against cerebral ischemia in rats by inducing expressions of hypoxia inducible factor 1[alpha] and erythropoietin. *Neuroscience Bulletin,* **24**(2), pp. 89-94.

LI, X., PRESCOTT, M., ADLER, B., JOHN, D., BOYCE, D., and RODNEY, J.D., 2013. Beclin 1 Is Required for Starvation-Enhanced, but Not Rapamycin-Enhanced, LC3-Associated Phagocytosis of Burkholderia pseudomallei in RAW 264.7 Cells. *Infection and Immunity,* **81**(1), pp. 271-277.

LI, Y., LU, Z., KEOGH, C.L., YU, S.P. and WEI, L., 2007. Erythropoietin-induced neurovascular protection, angiogenesis, and cerebral blood flow restoration after

focal ischemia in mice. *Journal of Cerebral Blood Flow & Metabolism,* **27**(5), pp. 1043-1054.

LI, Z., YANG, L., ZHEN, J., ZHAO, Y. and LU, Z., 2018. Nobiletin protects PC12 cells from ERS-induced apoptosis in OGD / R injury via activation of the PI3K / AKT pathway. *Experimental and therapeutic medicine,* **16**(2), pp. 1470-1476.

LIANG, W., LIN, C., YUAN, L., CHEN, L., GUO, P., LI, P., WANG, W. and ZHANG, X., 2019. Preactivation of Notch1 in remote ischemic preconditioning reduces cerebral ischemia-reperfusion injury through crosstalk with the NF-κB pathway. *Journal of Neuroinflammation,* **16**(1), pp. 1-16.

LIEB, M.E., MENZIES, K., MOSCHELLA, M.C., NI, R. and TAUBMAN, M.B., 2002. Mammalian EGLN genes have distinct patterns of mRNA expression and regulation. *Biochemistry and cell biology,* **80**(4), pp. 421-426.

LIN, H.W., THOMPSON, J.W., MORRIS, K.C. and PEREZ-PINZON, M.A., 2011. Signal Transducers and Activators of Transcription: STATs-Mediated Mitochondrial Neuroprotection. *Antioxidants & Redox Signalling,* **14**(10), pp. 1853-1861.

LIN, L. and WANG, X., 2016. Ischemia-reperfusion Injury in the Brain: Mechanisms and Potential Therapeutic Strategies. *Biochemistry & Pharmacology: Open Access,* **5**(4), pp. 11-23.

LIU, XQ., SHENG, R., and QIN, ZH., 2009. The neuroprotective mechanism of brain ischemic preconditioning. *Acta Pharmacology Sin,* **30**(8), pp. 1071-1080.

LIU, J., YUAN, C., PU, L. and WANG, J., 2017. Nutrient deprivation induces apoptosis of nucleus pulposus cells via activation of the BNIP3 / AIF signalling pathway. *Molecular Medicine Reports,* **16**(5), pp. 7253-7260.

LIU, Y., SPNG, X., LIU, W., TIAN-YI, Z. and JI, Z., 2003. Glucose deprivation induces mitochondrial dysfunction and oxidative stress in PC12 cell line. *Journal of cellular and molecular medicine,* **7**(1), pp. 49-56.

LIU, Z. and CHOPP, M., 2016. Astrocytes, therapeutic targets for neuroprotection and neurorestoration in ischemic stroke. *Progress in neurobiology,* **144**, pp. 103-120.

LOPEZ, A.D., MATHERS, C.D., EZZATI, M., JAMISON, D.T. and MURRAY, C.J., 2006. Global and regional burden of disease and risk factors, 2001: systematic analysis of population health data. *The Lancet (British edition),* **367**(9524), pp. 1747-1757.

LU, N., LI, X., TAN, R., AN, J., CAI, Z., HU, X., WANG, F., WANG, H., LU, C. and LU, H., 2018. HIF-1α / Beclin1-Mediated Autophagy Is Involved in Neuroprotection Induced by Hypoxic Preconditioning. *Journal of Molecular Neuroscience,* **66**(2), pp. 238-250.

LU, P., KAMBOJ, A., GIBSON, S.B. and ANDERSON, C.M., 2014. Poly(ADP-Ribose) Polymerase-1 Causes Mitochondrial Damage and Neuron Death Mediated by Bnip3. *The Journal of neuroscience : the official journal of the Society for Neuroscience,* **34**(48), pp. 15975-15987.

LU, X., AL-AREF, R., ZHAO, D., SHEN, J., YAN, Y. and GAO, Y., 2015. Astrocyte-conditioned medium attenuates glutamate-induced apoptotic cell death in primary cultured spinal cord neurons of rats. *Neurological Research,* **37**(9), pp. 803-808.

LUO, H., HUANG, J., LIAO, W., HUANG, Q. and GAO, Y., 2011. The antioxidant effects of garlic saponins protect PC12 cells from hypoxia-induced damage. *British Journal of Nutrition,* **105**(8), pp. 1164-1172.

LV, Y., ZHANG, B., ZHAI, C., QIU, J., ZHANG, Y., YAO, W. and ZHANG, C., 2015. PFKFB3-mediated glycolysis is involved in reactive astrocyte proliferation after oxygen-glucose deprivation / reperfusion and is regulated by Cdh1. *Neurochemistry International,* **91**, pp. 26-33.

MA, H., XIN, W., XINZHU, Q., LINLIN, J., WEI, S. and ZHENGPING, J., 2017. Tempol protects against hypoxia induced oxidative stress in PC12 cells. *International journal of experimental medicine,* **10**(4), pp. 6071-6080.

MA, Z., CHEN, C., TANG, P., ZHANG, H., YUE, J. and YU, Z., 2017. BNIP3 induces apoptosis and protective autophagy under hypoxia in esophageal squamous cell carcinoma cell lines: BNIP3 regulates cell death. *Diseases of the Esophagus,* **30**(9), pp. 1-8.

MADILL, M., MCDONAGH, K., MA, J., VAJDA, A., MCLOUGHLIN, P., O'BRIEN, T., HARDIMAN, O. and SHEN, S., 2017. Amyotrophic lateral sclerosis patient iPSC-derived astrocytes impair autophagy via non-cell autonomous mechanisms. *Molecular brain,* **10**(1), pp. 22-29.

MAJID, A., 2014. Neuroprotection in Stroke: Past, Present, and Future. *ISRN neurology,* **2014**, pp. 515-527.

MALHOTRA, S., NAGGAR, I., STEWART, M. and ROSENBAUM, D.M., 2011. Neurogenic pathway mediated remote preconditioning protects the brain from transient focal ischemic injury. *Brain Research,* **1386**, pp. 184-190.

MANG, J., MEI, C., WANG, J., LI, Z., CHU, T., HE, J. and XU, Z., 2013. Endogenous Protection Derived from Activin A / Smads Transduction Loop Stimulated via

Ischemic Injury in PC12 Cells. *Molecules (Basel, Switzerland),* **18**(10), pp. 12977-12986.

MARTI, H.H., 2004. Erythropoietin and the hypoxic brain. *Journal of Experimental Biology,* **207**(18), pp. 3233-3242.

MARTI, H.H., BERNAUDIN, M., PETIT, E. and BAUER, C., 2000. Neuroprotection and Angiogenesis: Dual Role of Erythropoietin in Brain Ischemia. *Physiology,* **15**(5), pp. 225-232.

MARTIN, R., YEATTS, S., HILL, M., MOY, C., GINSBERG, M. and PALESCH, Y., 2016. ALIAS (Albumin in Acute Ischemic Stroke) Trials: Analysis of the Combined Data From Parts 1 and 2. *Stroke,* **47**(9), pp. 2355-2359.

MARTÍN-ARAGÓN, B., MIGUEL, A.S., RAE, M.T., DARLISON, M.G., POOLE, A.V. and FRASER, J.A., 2017. Preferential activation of HIF-2α adaptive signalling in neuronal-like cells in response to acute hypoxia. *PloS one,* **12**(10), pp. 185-192.

MATIAS, I., MORGADO, J. and GOMES, F.C.A., 2019. Astrocyte Heterogeneity: Impact to Brain Aging and Disease. *Frontiers in aging neuroscience,* **11**, pp. 59-66.

MATSUYAMA, N., LEAVENS, J. E., MCKINNON, D., GAUDETTE, G. R., AKSEHIRLI, T. O., AND KRUKENKAMP, I. B., 2000. Ischemic but not pharmacological preconditioning requires protein synthesis. *Circulation,* **102**(19), pp. 1109-1111.

MEI, C., HE, J., MANG, J., ZHONGSHU, L., LIANG, W., XU, Z. and GIUHUA, X., 2011. Nerve growth factor (NGF) combined with oxygen glucose deprivation OGD induces neural ischemia tolerance in PC12 cells. *African Journal of Biochemistry Research*, **5**(10), pp. 315-320.

MILLER, B., PEREZ, R., SHAH, A., GONZALES, E., PARK, T. and GIDDAY, J., 2001. Cerebral protection by hypoxic preconditioning in a murine model of focal ischemia-reperfusion. *Neuroreport,* **12**(8), pp. 1663-1669.

MINCHENKO, A., LESHCHINSKY, I., OPENTANOVA, I., SANG, N., SRINIVAS, V., ARMSTEAD, V. and CARO, J., 2002. Hypoxia-inducible factor-1-mediated expression of the 6-phosphofructo-2-kinase / fructose-2,6-bisphosphatase-3 (PFKFB3) gene. Its possible role in the Warburg effect. *The Journal of biological chemistry,* **277**(8), pp. 6183-6187.

MINCHENKO, O., OPENTANOVA, I. and CARO, J., 2003. Hypoxic regulation of the 6-phosphofructo-2-kinase / fructose-2,6-bisphosphatase gene family (PFKFB-1–4) expression in vivo. *FEBS Letters,* **554**(3), pp. 264-270.

MIYAMOTO, O. and AUER, R.N., 2000. Hypoxia, hyperoxia, ischemia, and brain necrosis. *Neurology,* **54**(2), pp. 362-370.

MOHAMMAD, A.Z., SULE SUSO, J. and FORSYTH, N., 2015. Precision control of dissolved oxygen in mammalian cell culture media impacts on in situ volatile generation and promotes improved mesenchymal stem cell yield accompanied by reduced transcriptional variability. *Free Radical Biology and Medicine,* **86**, pp. 16-30.

MOJSILOVIC-PETROVIC, J., CALLAGHAN, D., CUI, H., DEAN, C., STANIMIROVIC, D.B. and ZHANG, W., 2007. Hypoxia-inducible factor-1 (HIF-1) is involved in the regulation of hypoxia-stimulated expression of monocyte chemoattractant protein-1 (MCP-1 / CCL2) and MCP-5 (Ccl12) in astrocytes. *Journal of neuroinflammation,* **4**(1), pp. 12-21.

MOKIN, M., ANSARI, S.A., MCTAGGART, R.A., BULSARA, K.R., GOYAL, M., CHEN, M. and FRASER, J.F., 2019. Indications for thrombectomy in acute ischemic stroke from emergent large vessel occlusion (ELVO): report of the SNIS Standards and Guidelines Committee. *Journal of NeuroInterventional Surgery,* **11**(3), pp. 215-220.

MOZAFFARIAN, D., BENJAMIN, E., GO, A., ARNETT, D., BLAHA, M., CUSHMAN, M., DAS, S., DE FERRANTI, S., DESPRÉS, J., FULLERTON, H., HOWARD, V., HUFFMAN, M., ISASI, C., JIMÉNEZ, M., JUDD, S., KISSELA, B., LICHTMAN, J., LISABETH, L., LIU, S., MACKEY, R., MAGID, D., MCGUIRE, D., MOHLER, I., Emile, MOY, C., MUNTNER, P., MUSSOLINO, M., NASIR, K., NEUMAR, R., NICHOL, G., PALANIAPPAN, L., PANDEY, D., REEVES, M., RODRIGUEZ, C., ROSAMOND, W., SORLIE, P., STEIN, J., TOWFIGHI, A., TURAN, T., VIRANI, S., WOO, D., YEH, R. and TURNER, M., 2016. Executive Summary: Heart Disease and Stroke Statistics—2016 Update: A Report From the American Heart Association. *Circulation,* **133**(4), pp. 447-454.

MU, D., CHANG, Y.S., VEXLER, Z.S. and FERRIERO, D.M., 2005. Hypoxia-inducible factor 1alpha and erythropoietin upregulation with Deforoxamine salvage after neonatal stroke. *Experimental neurology,* **195**(2), pp. 407-415.

NAGEL, S., PAPADAKIS, M., CHEN, R., HOYTE, L.C., BROOKS, K.J., GALLICHAN, D., SIBSON, N.R., PUGH, C. and BUCHAN, A.M., 2011. Neuroprotection by dimethyloxalylglycine following permanent and transient focal cerebral ischemia in rats. *Journal of Cerebral Blood Flow & Metabolism,* **31**(1), pp. 132-143.

NAGEL, S., TALBOT, N.P., MECINOVIĆ, J., SMITH, T.G., BUCHAN, A.M. and SCHOFIELD, C.J., 2010. Therapeutic Manipulation of the HIF Hydroxylases. *Antioxidants & redox signaling,* **12**(4), pp. 481-501.

NARAYANAN, S.V. and PEREZ-PINZON, M.A., 2017. Ischemic preconditioning treatment of astrocytes transfers ischemic tolerance to neurons. *Conditioning medicine,* **1**(1), pp. 2-8.

NATIONAL INSTITUTE OF NEUROLOGICAL DISORDERS AND STROKE, 2001-last update, Report of Stroke research review group. Available: https://www.ninds.nih.gov/About-NINDS/Strategic-Plans-Evaluations/Strategic-Plans/Stroke-Progress-Review-Group [14/03/2022].

NEWBY, D., MARKS, L. and LYALL, F., 2005. Dissolved oxygen concentration in culture medium: assumptions and pitfalls. *Placenta,* **26**(4), pp. 353-357.

NEUTSCH, L., KROLL, P., BRUNNER, M., PANSY, A., KOVAR, M., HERWIG, C. and KLEIN, T., 2018. Media photo-degradation in pharmaceutical biotechnology – impact of ambient light on media quality, cell physiology, and IgG production in CHO cultures. *Journal of chemical technology and biotechnology (1986),* **93**(8), pp. 2141-2151.

NICE CG 68, 2008-last update, Stroke and transient ischaemic attack in over 16s: diagnosis and initial management [Homepage of https: / / www.nice.org.uk / guidance / cg68 / chapter / 1-Guidance#pharmacological-treatments-for-people-with-acute-stroke], [Online] [14 / 12 / 2017].

NICE CKS, 2017-last update, Stroke and TIA. Available: https: / / cks.nice.org.uk / stroke-and-tia [14 / 12 / 2017].

NICE PATHWAYS, 2016a-last update, Atrial Fibrillation . Available: https: / / pathways.nice.org.uk / pathways / atrial fibrillation [14 / 12 / 2017].

NICE PATHWAYS, 2016b-last update, Hypertension. Available: https: / / pathways.nice.org.uk / pathways / hypertension [14 / 12 / 2017].

NICO, B., MANGIERI, D., CRIVELLATO, E., LONGO, V., DE GIORGIS, M., CAPOBIANCO, C., CORSI, P., BENAGIANO, V., RONCALI, L. and RIBATTI, D., 2007. HIF Activation and VEGF Overexpression are Coupled with ZO-1 Up-phosphorylation in the Brain of Dystrophic MDX Mouse. *Brain Pathology,* **17**(4), pp. 399-406.

NISHIMOTO, A., KUGIMIYA, N., HOSOYAMA, T., ENOKI, T., LI, T. and HAMANO, K., 2014. HIF-1α activation under glucose deprivation plays a central role in the acquisition of anti-apoptosis in human colon cancer cells. *International Journal of Oncology,* **44**(6), pp. 2077-2084.

NOUR, M., SCALZO, F. and LIEBESKIND, D.S., 2013. Ischemia-Reperfusion Injury in Stroke. *Interventional Neurology,* **1**(3-4), pp. 185-199.

NOVAK, A., SUSAN, J. and PAUL, E., 2019. Induction of the HIF pathway: Differential regulation by chemical hypoxia and oxygen glucose deprivation. *BioRxiv,* **261**(2), pp. 127-149

O'FLAHERTY, L., ADAM, J., HEATHER, L.C., ZHDANOV, A.V., CHUNG, Y., MIRANDA, M.X., CROFT, J., OLPIN, S., CLARKE, K., PUGH, C.W., GRIFFITHS, J., PAPKOVSKY, D., ASHRAFIAN, H., RATCLIFFE, P.J. and POLLARD, P.J., 2010. Dysregulation of hypoxia pathways in fumarate hydratase-deficient cells is

independent of defective mitochondrial metabolism. *Human molecular genetics,* **19**(19), pp. 3844-3851.

OBACH, M., NAVARRO-SABATÉ, À, CARO, J., KONG, X., DURAN, J., GÓMEZ, M., PERALES, J.C., VENTURA, F., ROSA, J.L. and BARTRONS, R., 2004. 6-Phosphofructo-2-kinase (pfkfb3) Gene Promoter Contains Hypoxia-inducible Factor-1 Binding Sites Necessary for Transactivation in Response to Hypoxia. *The Journal of biological chemistry,* **279**(51), pp. 53562-53570.

OGLE, M.E., GU, X., ESPINERA, A.R. and WEI, L., 2012. Inhibition of prolyl hydroxylases by dimethyloxaloylglycine after stroke reduces ischemic brain injury and requires hypoxia inducible factor-1α. *Neurobiology of disease,* **45**(2), pp. 733-762.

OLNEY, J.W., PRICE, M.T., SAMSON, L. and LABRUYERE, J., 1986. The role of specific ions in glutamate neurotoxicity. *Neuroscience letters,* **65**(1), pp. 65-71.

OUYANG, Y., XU, L., LIU, S. and GIFFARD, R.G., 2014. Role of astrocytes in delayed neuronal death: GLT-1 and its novel regulation by MicroRNAs. *Advances in neurobiology,* **11**, pp. 171-188.

OZAKI, T., NAKAMURA, H. and KISHIMA, H., 2019. Therapeutic strategy against ischemic stroke with the concept of neurovascular unit. *Neurochemistry International,* **126**, pp. 246-251.

PATABENDIGE, A., SINGH, A., JENKINS, S., SEN, J. and CHEN, R., 2021. Astrocyte Activation in Neurovascular Damage and Repair Following Ischaemic Stroke. *International journal of molecular sciences,* **22**(8), pp. 4280.

PAN, J., KONSTAS, A., BATEMAN, B., ORTOLANO, G. and PILE-SPELLMAN, J., 2007. Reperfusion injury following cerebral ischemia: pathophysiology, MR imaging, and potential therapies. *Neuroradiology,* **49**(2), pp. 93-102.

PAQUET, M., RIBEIRO, F.M., GUADAGNO, J., ESSELTINE, J.L., FERGUSON, S.S.G. and CREGAN, S.P., 2013. Role of metabotropic glutamate receptor 5 signaling and homer in oxygen glucose deprivation-mediated astrocyte apoptosis. *Molecular brain,* **6**(1), pp. 9-21.

PARK, H., CHU, K., JUNG, K., LEE, S., LEE, S.K., BAHN, J., KIM, M. and ROH, J., 2009. Autophagy is involved in the ischemic preconditioning. *Neuroscience Letters,* **451**(1), pp. 16-19.

PATEL, A.R., RITZEL, R., MCCULLOUGH, L.D. and LIU, F., 2013. Microglia and ischemic stroke: a double-edged sword. *International Journal of Physiology, Pathophysiology and Pharmacology,* **5**(2), pp. 73-81.

PEI, X., LI, Y., ZHU, L. and ZHOU, Z., 2019. Astrocyte-derived exosomes suppress autophagy and ameliorate neuronal damage in experimental ischemic stroke. *Experimental Cell Research,* **382**(2), pp. 111-124.

PENG, L., ZHAO, Y., LI, Y., ZHOU, Y., LI, L., LEI, S., YU, S. and ZHAO, Y., 2019. Effect of DJ-1 on the neuroprotection of astrocytes subjected to cerebral ischemia / reperfusion injury. *Journal of Molecular Medicine,* **97**(2), pp. 189-199.

PICKARD, M.R., JENKINS, S.I., KOLLER, C.J., FURNESS, D.N. and CHARI, D.M., 2011. Magnetic Nanoparticle Labeling of Astrocytes Derived for Neural Transplantation. *Tissue engineering. Part C, Methods,* **17**(1), pp. 89-99.

PLACE, T.L., DOMANN, F.E. and CASE, A.J., 2017. Limitations of oxygen delivery to cells in culture: An underappreciated problem in basic and translational research. *Free Radical Biology and Medicine,* **113**, pp. 311-322.

POSADA-DUQUE, R.A., BARRETO, G.E. and CARDONA-GOMEZ, G.P., 2014. Protection after stroke: cellular effectors of neurovascular unit integrity. *Frontiers in cellular neuroscience,* **8**, pp. 231-242.

POTTER, M., NEWPORT, E. and MORTEN, K.J., 2016. The Warburg effect: 80 years on. *Biochemical Society transactions,* **44**(5), pp. 1499-1505.

PRABAL, D., SHARMA, S. and HASSAN, K.M., 2010. Pathophysiologic mechanisms of acute ischemic stroke: An overview with emphasis on therapeutic significance beyond thrombolysis. *Pathophysiology,* **17**(3), pp. 197-218.

PRASS, K., RUSCHER, K., KARSCH, M., ISAEV, N., MEGOW, D., PRILLER, J., SCHARFF, A., DIRNAGL, U. and MEISEL, A., 2002. Desferrioxamine Induces Delayed Tolerance against Cerebral Ischemia in Vivo and in Vitro. *Journal of Cerebral Blood Flow & Metabolism,* **22**(5), pp. 520-525.

QUAEGEBEUR, A., SEGURA, I., SCHMIEDER, R., VERDEGEM, D., DECIMO, I., BIFARI, F., DRESSELAERS, T., EELEN, G., GHOSH, D., DAVIDSON, S.M., SCHOORS, S., BROEKAERT, D., CRUYS, B., GOVAERTS, K., DE LEGHER, C., BOUCHÉ, A., SCHOONJANS, L., RAMER, M., HUNG, G., BOSSAERT, G., CLEVELAND, D., HIMMELREICH, U., VOETS, T., LEMMENS, R., BENNETT, C. ., ROBBERECHT, W., DE BOCK, K., DEWERCHIN, M., GHESQUIÈRE, B., FENDT, S. and CARMELIET, P., 2016. Deletion or Inhibition of the Oxygen Sensor PHD1 Protects against Ischemic Stroke via Reprogramming of Neuronal Metabolism. *Cell Metabolism,* **23**(2), pp. 280-291.

RADAK, D., NIKI KATSIKI, IVANA RESANOVIC, ALEKSANDRA JOVANOVIC, EMINA SUDAR-MILOVANOVIC, SONJA ZAFIROVIC, SHAKER A. MOUSAD and ESMA R. ISENOVIC, 2017. Apoptosis and Acute Brain Ischemia in Ischemic Stroke. *Current Vascular Pharmacology,* **15**(2), pp. 115-122.

RATCLIFFE, P.J., O'ROURKE, J.F., MAXWELL, P.H. and PUGH, C.W., 1998. Oxygen sensing, hypoxia-inducible factor-1 and the regulation of mammalian gene expression. *Journal of Experimental Biology,* **201**(8), pp. 1153-1162.

REISCHL, S., LI, L., WALKINSHAW, G., FLIPPIN, L.A., MARTI, H.H. and KUNZE, R., 2014. Inhibition of HIF prolyl-4-hydroxylases by FG-4497 reduces brain tissue injury and edema formation during ischemic stroke. *PloS one,* **9**(1), pp. e84767.

ROSENSTEIN, J.M., KRUM, J.M. and RUHRBERG, C., 2010. VEGF in the nervous system. *Organogenesis,* **6**(2), pp. 107-114.

ROSSI, D.J., BRADY, J.D. and MOHR, C., 2007. Astrocyte metabolism and signaling during brain ischemia. *Nature Neuroscience,* **10**(11), pp. 1377-1386.

ROTHMAN, S.M., 1985. The neurotoxicity of excitatory amino acids is produced by passive chloride influx. *The Journal of neuroscience,* **5**(6), pp. 1483-1489.

RUSCHER, K., ISAEV, N., TRENDELENBURG, G., WEIH, M., IURATO, L., MEISEL, A. and DIRNAGL, U., 1998. Induction of hypoxia inducible factor 1 by oxygen glucose deprivation is attenuated by hypoxic preconditioning in rat cultured neurons. *Neuroscience Letters,* **254**(2), pp. 117-120.

RYOU, M. and MALLET, R.T., 2018. An In Vitro Oxygen-Glucose Deprivation Model for Studying Ischemia-Reperfusion Injury of Neuronal Cells. *Methods in molecular biology (Clifton, N.J.),* **1717**, pp. 229-235.

SAMY, Z.A., AL-ABDULLAH, L., TURCANI, M., CRAIK, J. and REDZIC, Z., 2018. Rat astrocytes during anoxia: Secretome profile of cytokines and chemokines. *Brain and Behavior,* **8**(7), pp.13-27.

SANCHEZ, A., WADHWANI, S. and GRAMMAS, P., 2010. Multiple neurotrophic effects of VEGF on cultured neurons. *Neuropeptides,* **44**(4), pp. 323-331.

SANTORE, M.T., DAVID, S., MCCLINTOCK, V.Y., LEE, G.R., SCOTT, B., and NAVDEEP S.C., 2002. Anoxia-induced apoptosis occurs through a mitochondria-dependent pathway in lung epithelial cells. *American Journal of Physiology - Lung Cellular and Molecular Physiology,* **282**(4), pp. 727-734.

SCHMID, T., ZHOU, J. and BRÜNE, B., 2004. HIF-1 and p53: communication of transcription factors under hypoxia. *Journal of Cellular and Molecular Medicine,* **8**(4), pp. 423-431.

SCHOFIELD, C.J. and RATCLIFFE, P.J., 2004. Oxygen sensing by HIF hydroxylases. *Nature Reviews Molecular Cell Biology,* **5**(5), pp. 343-354.

SELAK, M.A., ARMOUR, S.M., MACKENZIE, E.D., BOULAHBEL, H., WATSON, D.G., MANSFIELD, K.D., PAN, Y., SIMON, M.C., THOMPSON, C.B. and GOTTLIEB, E., 2005. Succinate links TCA cycle dysfunction to oncogenesis by inhibiting HIF-α prolyl hydroxylase. *Cancer cell,* **7**(1), pp. 77-85.

SEMENZA, G., BING-HUA JIANG, SANDRA W. LEUNG, ROSA PASSANTINO, JEAN-PAUL CONCORDET, PASCAL MAIRE and AGATA GIALLONGO, 1996. Hypoxia Response Elements in the Aldolase A, Enolase 1, and Lactate Dehydrogenase A Gene Promoters Contain Essential Binding Sites for Hypoxia-inducible Factor 1. *Journal of Biological Chemistry,* **271**(51), pp. 32529-32537.

SEMENZA, G.L., 2000. HIF-1 and human disease: one highly involved factor. *Genes & development,* **14**(16), pp. 1983-1997.

SEMENZA, G.L., 2001. *HIF-1 and mechanisms of hypoxia sensing.* England: Elsevier Ltd.

SENTINEL STROKE NATIONAL AUDIT PROGRAMME, 2021-last update, National Clinical Audit reports. Available: https://www.strokeaudit.org/results/Clinical-audit/National-Results.aspx [14/03/2022].

SHARP, F., RAN, R., LU, A., TANG, Y., STRAUSS, K., GLASS, T., ARDIZZONE, T. and BERNAUDIN, M., 2004. Hypoxic preconditioning protects against ischemic brain injury. *Neurotherapeutics,* **1**(1), pp. 26-35.

SHENG, R., ZHANG, L., HAN, R., LIU, X., GAO, B. and QIN, Z., 2010. Autophagy activation is associated with neuroprotection in a rat model of focal cerebral ischemic preconditioning. *Autophagy,* **6**(4), pp. 482-494.

SHENG, R., ZHANG, T., FELICE, V.D., QIN, T., QIN, Z., SMITH, C.D., SAPP, E., DIFIGLIA, M. and WAEBER, C., 2014. Preconditioning Stimuli Induce Autophagy via Sphingosine Kinase 2 in Mouse Cortical Neurons. *The Journal of biological chemistry,* **289**(30), pp. 20845-20857.

SIDDIQ, A., AMINOVA, L.R., TROY, C.M., SUH, K., MESSER, Z., SEMENZA, G.L. and RATAN, R.R., 2009. Selective Inhibition of Hypoxia-Inducible Factor (HIF) Prolyl-Hydroxylase 1 Mediates Neuroprotection against Normoxic Oxidative Death via HIF- and CREB-Independent Pathways. *Journal of Neuroscience,* **29**(27), pp. 8828-8838.

SIDDIQ, A., AYOUB, I.A., CHAVEZ, J.C., AMINOVA, L., SHAH, S., LAMANNA, J.C., PATTON, S.M., CONNOR, J.R., CHERNY, R.A., VOLITAKIS, I., BUSH, A.I., LANGSETMO, I., SEELEY, T., GUNZLER, V. and RATAN, R.R., 2005. Hypoxia-inducible factor prolyl 4-hydroxylase inhibition. A target for neuroprotection in the central nervous system. *The Journal of biological chemistry,* **280**(50), pp. 41732-41743.

SINGH, A., AZAD, M., SHYMKO, M.D., HENSON, E.S., KATYAL, S., EISENSTAT, D.D. and GIBSON, S.B., 2018. The BH3 only Bcl-2 family member BNIP3 regulates cellular proliferation. *PloS one,* **13**(10), pp. e0204792.

SINGH, G., SIDDIQUI, M.A., KHANNA, V.K., KASHYAP, M.P., YADAV, S., GUPTA, Y.K., PANT, K.K. and PANT, A.B., 2009. Oxygen Glucose Deprivation Model of Cerebral Stroke in PC-12 Cells: Glucose as a Limiting Factor. *Toxicology Mechanisms and Methods,* **19**(2), pp. 154-160.

SOFRONIEW, M., SOFRONIEW, M., VINTERS, H. and VINTERS, H., 2010. Astrocytes: biology and pathology. *Acta Neuropathologica,* **119**(1), pp. 7-35.

SOLTANI, M.H., PICHARDO, R., SONG, Z., SANGHA, N., CAMACHO, F., SATYAMOORTHY, K., SANGUEZA, O.P. and SETALURI, V., 2005. Microtubule-Associated Protein 2, a Marker of Neuronal Differentiation, Induces Mitotic Defects, Inhibits Growth of Melanoma Cells, and Predicts Metastatic Potential of Cutaneous Melanoma. *The American Journal of Pathology,* **166**(6), pp. 1841-1850

SOMMER, C.J., 2017. Ischemic stroke: experimental models and reality. *Acta neuropathologica,* **133**(2), pp. 245-261.

SONG, C., WU, Y., YANG, Z., KALUEFF, A., TSAO, Y., DONG, Y. and SU, K., 2019. Astrocyte-Conditioned Medium Protects Prefrontal Cortical Neurons from Glutamate-Induced Cell Death by Inhibiting TNF-α Expression. *Neuroimmunomodulation,* **26**(1), pp. 33-42.

SOUCEK, T., CUMMING, R., DARGUSCH, R., MAHER, P. and SCHUBERT, D., 2003. The Regulation of Glucose Metabolism by HIF-1 Mediates a Neuroprotective Response to Amyloid Beta Peptide. *Neuron,* **39**(1), pp. 43-56.

STAGLIANO, N.E., PÉREZ-PINZÓN, M.A., MOSKOWITZ, M.A. and HUANG, P.L., 1999. Focal Ischemic Preconditioning Induces Rapid Tolerance to Middle Cerebral Artery Occlusion in Mice. *Journal of Cerebral Blood Flow & Metabolism,* **19**(7), pp. 757-761.

STEVEN, J.C., REBEKAH, S.V., NICOLE, M.A., ANDY, H. and K ULRICH BAYER, 2011. CaMKII in cerebral ischemia. *Acta Pharmacology Sinica B,* **32**(7), pp. 861-872.

STEVENS, S., VARTANIAN, K. and STENZEL-POORE, M., 2014. Reprogramming the Response to Stroke by Preconditioning. *Stroke,* **45**(8), pp. 2527-2531.

STONE, L.L., GRANDE, A. and LOW, W.C., 2013. Neural repair and neuroprotection with stem cells in ischemic stroke. *Brain sciences,* **3**(2), pp. 599-614.

STRANDGAARD, S. and PAULSON, O.B., 1989. Cerebral blood flow and its pathophysiology in hypertension. *American journal of hypertension,* **2**(6 Pt 1), pp. 486-492.

STRAUSS, M.H. and HALL, A., 2009. Angiotensin Receptor Blockers Should Be Regarded as First-Line Drugs for Stroke Prevention in Both Primary and Secondary Prevention Settings. *Stroke,* **40**(9), pp. 3161-3170.

STROKE ASSOCIATION, 2017. State of the nation- Stroke statistics 2017. UNITED KINGDOM: STROKE ASSOCIATION.

SULSER, P., PICKEL, C., GÜNTER, J., LEISSING, T.M., CREAN, D., SCHOFIELD, C.J., WENGER, R.H. and SCHOLZ, C.C., 2020. HIF hydroxylase inhibitors decrease cellular oxygen consumption depending on their selectivity. *The FASEB Journal,* **34**(2), pp. 2344-2358.

SUN, Y., LIN, S., LIN, H., HUNG, C., WANG, C., LIN, Y., HUNG, K., LIEN, C., KUAN, C. and LEE, Y., 2013. Cell Type-Specific Dependency on the PI3K / Akt Signaling Pathway for the Endogenous Epo and VEGF Induction by Baicalein in Neurons versus Astrocytes. *PloS one,* **8**(7), pp. 69-79.

SUN, Y., ZHU, W., ZHOU, S., WANG, Z., CHEN, X. and JIA, L., 2017. Exploring the model of PC12 apoptosis induced by OGSD / R through in vitro experiments. *Oncotarget,* **8**(52), pp. 90176-90184.

SUN, Y., ZHU, Y., ZHONG, X., CHEN, X., WANG, J. and YING, G., 2019. Crosstalk Between Autophagy and Cerebral Ischemia. *Frontiers in neuroscience,* **12**, pp. 1022-1035.

SUN, Z., HU, W., YIN, S., LU, X., ZUO, W., GE, S. and XU, Y., 2017. NGF protects against oxygen and glucose deprivation-induced oxidative stress and apoptosis by up-regulation of HO-1 through MEK / ERK pathway. *Neuroscience Letters,* **641**, pp. 8-14.

SUNG, K. and JIMENEZ-SANCHEZ, M., 2020. Autophagy in Astrocytes and its Implications in Neurodegeneration. *Journal of Molecular Biology,* **432**(8), pp. 2605-2621 .

SÜNWOLDT, J., BOSCHE, B., MEISEL, A. and MERGENTHALER, P., 2017. Neuronal Culture Microenvironments Determine Preferences in Bioenergetic Pathway Use. *Frontiers in molecular neuroscience,* **10**(1), pp. 305-321.

SUTHERLAND, B.A., MINNERUP, J., BALAMI, J.S., ARBA, F., BUCHAN, A.M. and KLEINSCHNITZ, C., 2012. Neuroprotection for ischaemic stroke: Translation from the bench to the bedside. *International Journal of Stroke,* **7**(5), pp. 407-418.

SWEETLOVE, L.J., BEARD, K.F.M., NUNES-NESI, A., FERNIE, A.R. and RATCLIFFE, R.G., 2010. Not just a circle: flux modes in the plant TCA cycle. *Trends in Plant Science,* **15**(8), pp. 462-470.

TABAKMAN, R., JIANG, H., SHAHAR, I., ARIEN-ZAKAY, H., LEVINE, R.A. and LAZAROVICI, P., 2005. Neuroprotection by NGF in the PC12 in vitro OGD model: involvement of mitogen-activated protein kinases and gene expression. *Annals of the New York Academy of Sciences,* **1053**(1), pp. 84-96.

TAHIR, R. and PABANEY, A., 2016. Therapeutic hypothermia and ischemic stroke: A literature review. *Surgical Neurology International,* **7**(15), pp. 381.

TANAKA, T., KANAI, H., SEKIGUCHI, K., AIHARA, Y., YOKOYAMA, T., ARAI, M., KANDA, T., NAGAI, R. and KURABAYASHI, M., 2000. Induction of VEGF Gene Transcription by IL-1 β is Mediated Through Stress-activated MAP Kinases and Sp1 Sites in Cardiac Myocytes. *Journal of Molecular and Cellular Cardiology,* **32**(11), pp. 1955-1967.

TANG, Y., PACARY, E., FRÉRET, T., DIVOUX, D., PETIT, E., SCHUMANN-BARD, P. and BERNAUDIN, M., 2006. Effect of hypoxic preconditioning on brain genomic

response before and following ischemia in the adult mouse: Identification of potential neuroprotective candidates for stroke. *Neurobiology of Disease,* **21**(1), pp. 18-28.

TAUSKELA, J., ERIC, B., ROBERT, M., TANYA, C., and PAUL, M., 2003. Preconditioning of cortical neurons by oxygen-glucose deprivation: tolerance induction through abbreviated neurotoxic signalling. *American Journal of Physiology - Cell Physiology,* **285**(4), pp. 899-911.

TAYLOR, A.R., ROBINSON, M.B., GIFONDORWA, D.J., TYTELL, M. and MILLIGAN, C.E., 2007. Regulation of heat shock protein 70 release in astrocytes: Role of signaling kinases. *Developmental Neurobiology,* **67**(13), pp. 1815-1829.

TENG, K.K., ANGELASTRO, J.M., CUNNINGHAM, M.E. and GREENE, L.A., 2006. Chapter 21 - Cultured PC12 Cells: A Model for Neuronal Function, Differentiation, and Survival. *Cell Biology,* **4**(3), pp. 171-176.

THRIFT, A.G., CADILHAC, D.A., THAYABARANATHAN, T., HOWARD, G., HOWARD, V.J., ROTHWELL, P.M. and DONNAN, G.A., 2014. Global Stroke Statistics. *International Journal of Stroke,* **9**(1), pp. 6-18.

TIAN, T., ZENG, J., ZHAO, G., ZHAO, W., GAO, S. and LIU, L., 2018. Neuroprotective effects of orientin on oxygen-glucose deprivation / reperfusion-induced cell injury in primary culture of rat cortical neurons. *Experimental biology and medicine,* **243**(1), pp. 78-86.

TRENDELENBURG, G. and DIRNAGL, U., 2005. Neuroprotective role of astrocytes in cerebral ischemia: Focus on ischemic preconditioning. *Glia,* **50**(4), pp. 307-320.

TRIPATHI, P., RODRIGUEZ-MUELA, N., KLIM, J.R., DE BOER, A.S., AGRAWAL, S., SANDOE, J., LOPES, C.S., OGLIARI, K.S., WILLIAMS, L.A., SHEAR, M.,

RUBIN, L.L., EGGAN, K. and ZHOU, Q., 2017. Reactive Astrocytes Promote ALS-like Degeneration and Intracellular Protein Aggregation in Human Motor Neurons by Disrupting Autophagy through TGF-β1. *Stem Cell Reports,* **9**(2), pp. 667-680.

VAGHEFI, H. and NEET, K.E., 2004. Deacetylation of p53 after nerve growth factor treatment in PC12 cells as a post-translational modification mechanism of neurotrophininduced tumor suppressor activation. *Oncogene*, **23**(49), pp. 8078-8087.

VALVONA, C.J., FILLMORE, H.L., NUNN, P.B. and PILKINGTON, G.J., 2016. The Regulation and Function of Lactate Dehydrogenase A: Therapeutic Potential in Brain Tumor. *Brain Pathology,* **26**(1), pp. 3-17.

VÉGA, C., R. SACHLEBEN, L., GOZAL, D. and GOZAL, E., 2006. Differential metabolic adaptation to acute and long-term hypoxia in rat primary cortical astrocytes. *Journal of Neurochemistry,* **97**(3), pp. 872-883.

VENTURINI, A., PASSALACQUA, M., PELASSA, S., PASTORINO, F., TEDESCO, M., CORTESE, K., GAGLIANI, M.C., LEO, G., MAURA, G., GUIDOLIN, D., AGNATI, L.F., MARCOLI, M. and CERVETTO, C., 2019. Exosomes From Astrocyte Processes: Signaling to Neurons. *Frontiers in pharmacology,* **10**, pp. 1452-1466.

VILLA, P., BIGINI, P., MENNINI, T., AGNELLO, D., LARAGIONE, T., CAGNOTTO, A., VIVIANI, B., MARINOVICH, M., CERAMI, A., COLEMAN, T.R., BRINES, M. and GHEZZI, P., 2003. Erythropoietin Selectively Attenuates Cytokine Production and Inflammation in Cerebral Ischemia by Targeting Neuronal Apoptosis. *Journal of Experimental Medicine,* **198**(6), pp. 971-975.

VOSLER, P., BRENNAN, C. and CHEN, J., 2008. Calpain-Mediated Signaling Mechanisms in Neuronal Injury and Neurodegeneration. *Molecular Neurobiology,* **38**(1), pp. 78-100.

WANG, L., ZHANG, Z., WANG, Y., ZHANG, R. and CHOPP, M., 2004. Treatment of Stroke With Erythropoietin Enhances Neurogenesis and Angiogenesis and Improves Neurological Function in Rats. *Stroke,* **35**(7), pp. 1732-1737.

WANG, P., GUAN, Y., DU, H., ZHAI, Q., SU, D. and MIAO, C., 2012. Induction of autophagy contributes to the neuroprotection of nicotinamide phosphoribosyltransferase in cerebral ischemia. *Autophagy,* **8**(1), pp. 77-87.

WANG, P., SHAO, B., DENG, Z., CHEN, S., YUE, Z. and MIAO, C., 2018. Autophagy in ischemic stroke. *Progress in Neurobiology,* **163-164**, pp. 98-117.

WANG, R., ZHANG, X., ZHANG, J., FAN, Y., SHEN, Y., HU, W. and CHEN, Z., 2012. Oxygen-Glucose Deprivation Induced Glial Scar-Like Change in Astrocytes. *PloS one,* **7**(5), pp. 375-381.

WAPPLER, E.A., INSTITORIS, A., DUTTA, S., KATAKAM, P.V.G. and BUSIJA, D.W., 2013. Mitochondrial Dynamics Associated with Oxygen-Glucose Deprivation in Rat Primary Neuronal Cultures. *PloS one,* **8**(5), pp. 206-215.

WENGER, R.H., KVIETIKO, I., ROLFS, A., GASSMANN, M. and MARTI, H.H., 1997. Hypoxia-inducible factor-1α is regulated at the post-mRNA level. *Kidney International,* **51**(2), pp. 560-563.

WESTERINK, R.H.S. and EWING, A.G., 2008. The PC12 cell as model for neurosecretion. *Acta Physiologica,* **192**(2), pp. 273-285.

WICK, A., WICK, W., WALTENBERGER, J., WELLER, M., DICHGANS, J. and SCHULZ, J.B., 2002. Neuroprotection by Hypoxic Preconditioning Requires Sequential Activation of Vascular Endothelial Growth Factor Receptor and Akt. *Journal of Neuroscience,* **22**(15), pp. 6401-6407.

WIENER, C.M., BOOTH, G. and SEMENZA, G.L., 1996. In Vivo Expression of mRNAs Encoding Hypoxia-Inducible Factor 1. *Biochemical and Biophysical Research Communications,* **225**(2), pp. 485-488.

WILKINS, S.E., ABBOUD, M.I., HANCOCK, R.L. and SCHOFIELD, C.J., 2016. Targeting Protein-Protein Interactions in the HIF System. *Medicinal Chemistry,* **11**(8), pp. 773-786.

WINKLER, E.A., NISHIDA, Y., SAGARE, A.P., REGE, S.V., BELL, R.D., PERLMUTTER, D., SENGILLO, J.D., HILLMAN, S., KONG, P., NELSON, A.R., SULLIVAN, J.S., ZHAO, Z., MEISELMAN, H.J., WENDY, R.B., SOTO, J., ABEL, E.D., MAKSHANOFF, J., ZUNIGA, E., VIVO, D.C. and ZLOKOVIC, B.V., 2015. GLUT1 reductions exacerbate Alzheimer's disease vasculoneuronal dysfunction and degeneration. *Nature Neuroscience,* **18**(4), pp. 521-530.

WOODRUFF, T.M., THUNDYIL, J., TANG, S., SOBEY, C.G., TAYLOR, S.M. and ARUMUGAM, T.V., 2011. Pathophysiology, treatment, and animal and cellular models of human ischemic stroke. *Molecular neurodegeneration,* **6**(1), pp. 11.

WORLD HEALTH ORGANISATION, 2017-last update, STROKE. Available: http: / / www.who.int / topics / cerebrovascular_accident / en / [14 / 12 / 2017].

WU, L.Y., MA, Z.M., FAN, X.L., ZHAO, T., LIU, Z.H., HUANG, X., LI, M.M., XIONG, L., ZHANG, K., ZHU, L.L., and FAN, M., 2010. The anti-necrosis role of hypoxic

preconditioning after acute anoxia is mediated by aldose reductase and sorbitol pathway in PC12 cells. *Cell Stress & Chaperones,* **15**(4), pp. 387-394.

XIAN, J., CHOI, A., LAU, C., LEUNG, W., NG, C., and CHAN, C., 2016. Gastrodia and Uncaria (tianma gouteng) water extract exerts antioxidative and antiapoptotic effects against cerebral ischemia in vitro and in vivo*. Journal of Chinese Medicine*, **11**(27), e-collections2016

XU, L., CAO, H., XIE, Y., ZHANG, Y., DU, M., XU, X., YE, R. and LIU, X., 2019. Exosome-shuttled miR-92b-3p from ischemic preconditioned astrocytes protects neurons against oxygen and glucose deprivation. *Brain Research,* **1717**, pp. 66-73.

YAN, J., BO ZHOU, SAEID TAHERI and HONGLIAN SHI, 2011. Differential Effects of HIF-1 Inhibition by YC-1 on the Overall Outcome and Blood-Brain Barrier Damage in a Rat Model of Ischemic Stroke. *PLoS One,* **6**(11), pp. e27798.

YAN, W., HAOPENG, B., XIAOGUANG, L., YAN, D., and HAILONG, X., 2011. Autophagy activation is involved in neuroprotection induced by hyperbaric oxygen preconditioning against focal cerebral ischemia in rats. *Brain Research,* **1402**, pp. 109-121.

YANG, F., ZHOU, L., WANG, D., WANG, Z. and HUANG, Q., 2015. Minocycline ameliorates hypoxia-induced blood-brain barrier damage by inhibition of HIF-1α through SIRT-3 / PHD-2 degradation pathway. *Neuroscience,* **304**, pp. 250-259.

YANG, J., ZHANG, X., CHEN, X., WANG, L. and YANG, G., 2017. Exosome Mediated Delivery of miR-124 Promotes Neurogenesis after Ischemia. *Molecular Therapy - Nucleic Acids,* **7**(C), pp. 278-287.

YASUDA, Y., TATEISHI, N., SHIMODA, T., SATOH, S., OGITANI, E. and FUJITA, S., 2004. Relationship between S100beta and GFAP expression in astrocytes during infarction and glial scar formation after mild transient ischemia. *Brain research,* **1021**(1), pp. 20-29.

YEH, S., OU, L., GEAN, P., HUNG, J. and CHANG, W., 2011. Selective Inhibition of Early—but Not Late—Expressed HIF-1α Is Neuroprotective in Rats after Focal Ischemic Brain Damage. *Brain Pathology,* **21**(3), pp. 249-262.

YEH, T., LEISSING, T.M., ABBOUD, M.I., THINNES, C.C., ATASOYLU, O., HOLT-MARTYN, J.P., ZHANG, D., TUMBER, A., LIPPL, K., LOHANS, C.T., LEUNG, I.K.H., MORCRETTE, H., CLIFTON, I.J., CLARIDGE, T.D.W., KAWAMURA, A., FLASHMAN, E., LU, X., RATCLIFFE, P.J., CHOWDHURY, R., PUGH, C.W. and SCHOFIELD, C.J., 2017. Molecular and cellular mechanisms of HIF prolyl hydroxylase inhibitors in clinical trials. *Chemical science,* **8**(11), pp. 7651-7672.

YEH, W., LU, D., LIN, C., LIOU, H. and FU, W., 2007. Inhibition of hypoxia-induced increase of blood-brain barrier permeability by YC-1 through the antagonism of HIF-1alpha accumulation and VEGF expression. *Molecular pharmacology,* **72**(2), pp. 440-457.

YU, S., ZHAO, T., GUO, M., FANG, H., MA, J., DING, A., WANG, F., CHAN, P. and FAN, M., 2005. Hypoxic preconditioning up-regulates glucose transport activity and glucose transporter (GLUT1 and GLUT3) gene expression after acute anoxic exposure in the cultured rat hippocampal neurons and astrocytes. *Brain Research,* **1211**, pp. 22-29.

YUAN, J., ZENG, L., SUN, Y., WANG, N., SUN, Q., CHENG, Z. and WANG, Y., 2018. SH2B1 protects against OGD / R-induced apoptosis in PC12 cells via

activation of the JAK2 / STAT3 signaling pathway. *Molecular Medicine Reports,* **18**(3), pp. 2613-2620.

ZAMAN, K., RYU, H., HALL, D., O'DONOVAN, K., LIN, K., MILLER, M.P., MARQUIS, J.C., BARABAN, J.M., SEMENZA, G.L. and RATAN, R.R., 1999. Protection from Oxidative Stress-Induced Apoptosis in Cortical Neuronal Cultures by Iron Chelators Is Associated with Enhanced DNA Binding of Hypoxia-Inducible Factor-1 and ATF-1 / CREB and Increased Expression of Glycolytic Enzymes, p21waf1 / cip1, and Erythropoietin. *Journal of Neuroscience,* **19**(22), pp. 9821-9830.

ZHANG, C., ZHANG, X., XU, R., HUANG, B., CHEN, A., LI, C., WANG, J. and LI, X., 2017. TGF-[beta]2 initiates autophagy via Smad and non-Smad pathway to promote glioma cells' invasion. *Journal of Experimental & Clinical Cancer Research,* **36**(1), pp. 117-131.

ZHANG, J., QIAN, H., ZHAO, P., HONG, S. and XIA, Y., 2006b. Rapid Hypoxia Preconditioning Protects Cortical Neurons From Glutamate Toxicity Through δ-Opioid Receptor. *Stroke,* **37**(4), pp. 1094-1099.

ZHANG, L., QU, Y., YANG, C., TANG, J., ZHANG, X., MAO, M., MU, D. and FERRIERO, D., 2009. Signaling pathway involved in hypoxia-inducible factor-1α regulation in hypoxic-ischemic cortical neurons in vitro. *Neuroscience Letters,* **461**(1), pp. 1-6.

ZHANG, X., DEGUCHI, K., YAMASHITA, T., OHTA, Y., SHANG, J., TIAN, F., LIU, N., PANIN, V.L., IKEDA, Y., MATSUURA, T. and ABE, K., 2010. Temporal and spatial differences of multiple protein expression in the ischemic penumbra after transient MCAO in rats. *Brain Research,* **1343**, pp. 143-152.

ZHANG, Y., YANG, K., WANG, T., LI, W., JIN, X. and LIU, W., 2017. Nrdp1 Increases Ischemia Induced Primary Rat Cerebral Cortical Neurons and Pheochromocytoma Cells Apoptosis Via Downregulation of HIF-1α Protein. *Frontiers in cellular neuroscience,* **11**, pp. 293-310.

ZHANG, Z., YANG, X., ZHANG, S., MA, X. and KONG, J., 2007. BNIP3 Upregulation and EndoG Translocation in Delayed Neuronal Death in Stroke and in Hypoxia. *Stroke,* **38**(5), pp. 1606-1613.

ZHANG, Z.G., MD and CHOPP, M., PhD, 2009. Neurorestorative therapies for stroke: underlying mechanisms and translation to the clinic. *Lancet Neurology, The,* **8**(5), pp. 491-500.

ZHAO, S., CHEN, M., LI, S., ZHANG, M., LI, B., DAS, M., BEAN, J.C., KONG, J., ZHU, X. and GAO, T., 2009. Mitochondrial BNIP3 upregulation precedes endonuclease G translocation in hippocampal neuronal death following oxygen-glucose deprivation. *BMC neuroscience,* **10**(1), pp. 113-130.

ZHAO, Y. and REMPE, D.A., 2011. Prophylactic neuroprotection against stroke: low-dose, prolonged treatment with deferoxamine or deferasirox establishes prolonged neuroprotection independent of HIF-1 function. *Journal of Cerebral Blood Flow & Metabolism,* **31**(6), pp. 1412-1423.

ZHDANOV, A.V., OKKELMAN, I.A., COLLINS, F.W.J., MELGAR, S. and PAPKOVSKY, D.B., 2015. A novel effect of DMOG on cell metabolism: direct inhibition of mitochondrial function precedes HIF target gene expression. *BBA - Bioenergetics,* **1847**(10), pp. 1254-1266.

ZHOU, J., JIE LI, DANIEL M ROSENBAUM, JIAN ZHUANG, CARRIE POON, PU QIN, KATRINA RIVERA, JOHN LEPORE, ROBERT N WILLETTE, ERDING HU and FRANK C BARONE, 2017. The prolyl 4-hydroxylase inhibitor GSK360A decreases post-stroke brain injury and sensory, motor, and cognitive behavioral deficits. *PLoS One,* **12**(9), pp. 184-192.

ZHOU, Z., PENG, X., INSOLERA, R., FINK, D.J. and MATA, M., 2009. Interleukin-10 provides direct trophic support to neurons. *Journal of Neurochemistry,* **110**(5), pp. 1617-1627.

ZOPPO, G.J. and HALLENBECK, J.M., 2000. Advances in the Vascular Pathophysiology of Ischemic Stroke. *Thrombosis Research,* **98**(3), pp. 73-81.